

**Establishment of cell lines expressing erythrocyte
membrane protein 1 (PfEMP1) variants of choice to study
Plasmodium falciparum cytoadherence associated functions**

-Dissertation-

with the aim of achieving a doctoral degree at the Faculty of
Mathematics, Informatics and Natural Sciences

Department of Biology

University of Hamburg

submitted by

Jakob Johannes Cronshagen

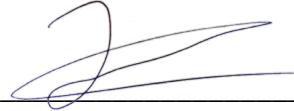
Hamburg, 2024

Ich versichere, dass dieses gebundene Exemplar der Dissertation und das in elektronischer Form eingereichte Dissertationsexemplar (über den Docata-Upload) und das bei der Fakultät (zuständiges Studienbüro bzw. Promotionsbüro Physik) zur Archivierung eingereichte gedruckte gebundene Exemplar der Dissertationsschrift identisch sind.

I, the undersigned, declare that this bound copy of the dissertation and the dissertation submitted in electronic form (via the Docata upload) and the printed bound copy of the dissertation submitted to the faculty (responsible Academic Office or the Doctoral Office Physics) for archiving are identical.

Hamburg, 08.05.2024

City, Date



Signature

Day of oral defense: 03.05.2024

1. Dissertation reviewer: Dr. Tobias Spielmann

2. Dissertation reviewer: Prof. Dr. Tim Gilberger

Member of the examination committee: Prof. Dr. Iris Bruchhaus

Chair of the examination committee: Prof. Dr. Julia Kehr

LANGUAGE CERTIFICATE

I am a native speaker, have read the present PhD thesis and hereby confirm that it complies with the rules of the English language.

Hamburg, 08.03.2024
City, Date

 Isabelle Henshall
Signature

DECLARATION ON OATH

I hereby declare upon oath that I have written the present dissertation independently and have not used further resources and aids than those stated in the dissertation.

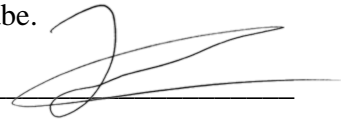
Hamburg, 08.03.2024
City, Date


Signature

EIDESSTATTLICHE ERKLÄRUNG

Hiermit erkläre ich an Eides statt, dass ich die vorliegende Dissertationsschrift selbst verfasst und keine anderen als die angegebenen Quellen und Hilfsmittel benutzt habe.

Hamburg, 08.03.2024
Ort, Datum


Unterschrift

SUMMARY

Malaria, caused by a unicellular eukaryotic apicomplexan parasite of the genus *Plasmodium*, remains a leading cause of morbidity and mortality globally. The pathological most relevant species for humans is *Plasmodium falciparum* which is responsible for almost all of the malaria related deaths. The symptoms of the disease are exclusively caused by the asexual stages of the parasite's life cycle, during which the parasites multiply in erythrocytes of the host. Erythrocytes infected with *P. falciparum* can cytoadhere to various host receptors and ligands on the endothelium to evade the removal of the infected erythrocytes in the spleen. This can lead to blockage and inflammation of blood vessels, cutting off tissue from oxygen support, and resulting in severe forms of the disease, such as cerebral malaria. The interaction of infected erythrocytes with the host's endothelium is mediated by a large parasite encoded transmembrane protein presented on the erythrocyte surface termed *Plasmodium falciparum* erythrocyte membrane protein 1 (PfEMP1). PfEMP1 variants possess differing binding properties and are expressed by a multigene family, the *var* genes. The expression of *var* genes in the parasite is mutually exclusive so that a parasite expresses only a single *var* gene. Furthermore, the parasites can switch their *var* gene expression over time, enabling the parasites to persistently evade the host's immune system, facilitating long lasting infections. PfEMP1 is considered a key factor for the parasite's virulence and survival, rendering it as the main virulence factor of *P. falciparum* parasites. However, the study of specific PfEMP1 variants and *var* genes has been hampered by PfEMP1s large size and the fact that parasite in vitro cultures are a mix of parasites expressing different PfEMP1s, making them inaccessible to genetic manipulation and molecular analysis.

In this thesis, selection linked integration (SLI) was exploited to generate cell lines that express a single HA-tagged PfEMP1 of choice in the entire population of parasites in an *in vitro* culture. The predominant expression of targeted *var* genes were validated for transgenic 3D7 and IT4 (formerly FCR3) lab strains by bulk RNA sequencing. The trackability of the HA-tagged PfEMP1s in the cell was demonstrated with immunofluorescence assays. Trypsin cleavage assays confirmed the surface presentation of the targeted PfEMP1 variant in most cases. SLI modified 3D7 and IT4 parasites expressing VAR2CSA or a CD36-binding PfEMP1 variant on the erythrocyte surface were tested and compared for binding against corresponding ligands. This provided empirical evidence that the IT4 strain is superior for the study of PfEMP1-mediated binding while 3D7 parasites only showed poor binding. To increase binding assay

throughput and comparability, a semi-automated pipeline was developed for standardized evaluation of binding assays.

Furthermore, PfEMP1 variants were activated in IT4 parasites that showed specific binding against the major endothelial cell receptors CD36, ICAM-1 and EPCR, validating the feasibility of this approach. These cell lines are expected to facilitate the study of the binding properties of different PfEMP1 variants without the need to subject the parasites to elaborate receptor or antibody selection procedures. This will enable the comparison of binding capacities and to explore potentially novel interacting receptors of specific PfEMP1 variants.

The trackability of the HA-tagged PfEMP1 was further exploited to study PfEMP1 transport into the host cell in 3D7 parasites. In order to do this, an approach to conditionally block protein transport through PTEX, the translocon pumping exported proteins into the host cell, was chosen. When PTEX was blocked, PfEMP1 was no longer exported. The timing of this approach in the parasite blood cycle was chosen in a way to minimize the effect of accessory factors needed for PfEMP1 transport which would indirectly lead to a failure of PfEMP1 export. Overall, these experiments indicated that PfEMP1 is transported by PTEX into the host cell.

Next, BioID experiments were conducted to determine the proximiome of PfEMP1 in living parasites. For this the biotin ligase BirA* was fused to three distinct positions of PfEMP1, resulting in three different cell lines. Testing of the cell lines expressing the PfEMP1-BirA* fusions showed that the modified PfEMP1s were predominantly expressed in the parasite cultures and functionally presented on the host cells surface, exhibiting binding against the expected receptors. Large scale BioID experiments with subsequent mass spectrometry analysis of biotinylated proteins identified proteins shown to be important for PfEMP1s transport and function as well as previously characterized and uncharacterized proteins of the Maurer's clefts, erythrocyte membrane and other host cell structures. The proximiome of the three positions showed marginal differences to each other, indicating that PfEMP1 is not transported as an integral membrane protein. Furthermore, only partial overlap with a Maurer's clefts proximiome indicated the detected hits were PfEMP1-specific. Notably six exported proteins with unknown function previously not linked to cytoadherence were identified and termed PfEMP1-interacting candidate 1-6 (EMPIC1-6).

Subsequently, a modified version of SLI, SLI2, was utilized to introduce a second endogenous modification to the cell lines harboring a SLI-activated *var* gene. This was used to disrupt candidate proteins identified in the proximiome to evaluate their role in PfEMP1-mediated cytoadherence. The evaluation of PfEMP1 presentation and function with trypsin cleavage

assays and binding assays led to the discovery of two novel proteins that are needed for the efficient cytoadherence of *P. falciparum* parasites despite the fact that their disruption did not ablate PfEMP1 surface transport.

In summary, this thesis -by utilizing SLI techniques - successfully generated and validated cell lines expressing specific PfEMP1 variants, which is expected to substantially aid studies on the interaction between these proteins and host cell receptors, *var* gene switching mechanisms and transport of PfEMP1. This work not only advances our understanding of *P. falciparum*'s main virulence factor but also opens new avenues to illuminate the cellular mechanisms that enable cytoadherence, leading to a better understanding of the parasite-host interactions.

ZUSAMMENFASSUNG

Malaria wird durch einen einzelligen eukaryotischen *Apicomplexa*-Parasiten der Gattung *Plasmodium* verursacht und bleibt weltweit eine führende Ursache für Morbidität und Mortalität. Die für den Menschen pathologisch relevanteste Spezies ist *Plasmodium falciparum*, welche für fast alle Malaria-bedingten Todesfälle verantwortlich ist. Die Symptome der Krankheit werden ausschließlich durch die asexuellen Stadien des Lebenszyklus des Parasiten verursacht. Während dieser vermehrt sich der Parasiten in den Erythrozyten des Wirts. Erythrozyten, die mit *P. falciparum* infizierte sind, können an verschiedene Rezeptoren und Liganden des Wirts auf den Endothelzellen zytoadhärieren, wodurch diese der Zerstörung durch die Milz entgehen. Dies kann zu Entzündungen bis hin zum Verschluss der Blutgefäße führen, wodurch Gewebe von der Sauerstoffversorgung abgeschnitten wird. Dies führt zu schweren Formen wie zum Beispiel Malaria, einer der schwersten Komplikationen dieser Infektion. Die Interaktion infizierter Erythrozyten mit den Endothelzellen des Wirts wird durch ein großes auf der Oberfläche der Erythrozyten präsentiertes Parasite-Transmembranprotein hervorgerufen, bekannt als *P. falciparum* erythrocyte membrane protein 1 (PfEMP1). Verschiedene PfEMP1-Varianten besitzen unterschiedliche Bindungseigenschaften und werden von einer Multigenfamilie, den *var*-Genen, kodiert. Die Expression von *var*-Genen im Parasiten ist sich gegenseitig ausschließend, das heißt, dass ein Parasit jeweils nur ein einzelnes *var*-Gen exprimiert. Außerdem verändern die Parasiten ihre *var*-Gene expression über die Zeit. Dies ermöglicht es den Parasiten, dauerhaft dem Immunsystem des Wirts zu entgehen und langanhaltende Infektionen zu manifestieren. PfEMP1 wird deshalb als Schlüsselfaktoren für die Virulenz und das Überleben des Parasiten angesehen, weshalb dieser als Hauptvirulenzfaktor von *P. falciparum*-Parasiten bezeichnet werden. Die Untersuchung spezifischer PfEMP1-Varianten und *var*-Gene wird durch die große Größe von PfEMP1 sowie durch die Tatsache erschwert, dass Parasiten in *In-vitro*-Kulturen eine Mischung von *var*-Genen exprimieren. Dies macht sie für genetische Manipulationen und molekulare Analysen schwer zugänglich.

In dieser Dissertation wurde das Selection Linked Integration (SLI)-System genutzt, um Zelllinien zu generieren, die in der gesamten Parasitenpopulation einer *in-vitro*-Kultur ein einzelnes erwünschtes HA-markiertes PfEMP1 exprimieren. Die Expression der Ziel-*var*-Gene wurde für transgene SLI-Parasitenpopulationen durch Bulk-RNA-Sequenzierung validiert. Die HA-markierten PfEMP1s konnte in der Zelle mit Immunfluoreszenzexperimenten lokalisiert werden und der Oberflächenproteinverdau mit Trypsin bestätigte für die meisten Zelllinien die

Oberflächenpräsentation der modifizierten PfEMP1-Variante. Es wurden zwei *P. Falciparum* Laborstämme mit SLI-modifiziert, 3D7 und IT4 (ehemals FCR3), die VAR2CSA oder eine CD36-bindende PfEMP1-Variante auf der Oberfläche der Erythrozyten exprimierten, wurden auf ihre Bindungseigenschaften verglichen, indem ihre Bindung gegenüber entsprechenden Liganden getestet wurden. Dies lieferte empirische Hinweis dafür, dass der IT4-Parasitenstamm für die Untersuchung von PfEMP1-Bindungen geeigneter ist als der 3D7-Parasitenstamm, welcher lediglich schwache Bindung zeigte. Um den Durchsatz und die Vergleichbarkeit von Bindungsexperimenten zu verbessern, wurde eine semi-automatisierte Pipeline für eine standardisierte Auswertung von Bindungsexperimenten entwickelt.

Darüber hinaus wurden in IT4-Parasiten PfEMP1-Varianten aktiviert, welche eine spezifische Bindung gegen die prominentesten interagierenden Zellrezeptoren, CD36, ICAM-1 und EPCR zeigten. Dies validierte die Zuverlässigkeit des SLI-Systems für diese Anwendungen. Es ist zu erwarten, dass diese Zelllinien die Erforschung der Bindungseigenschaften verschiedener PfEMP1-Varianten vereinfachen, da diese Parasiten ohne Rezeptor- oder Antikörperselektion generiert wurden. Dies ermöglicht den Vergleich der Bindungskapazitäten und die Erforschung potenzieller neuer interagierender Rezeptoren spezifischer PfEMP1-Varianten.

Des Weiteren wurde die Möglichkeit das HA-markierten PfEMP1 in der Zelle zu lokalisieren genutzt, um den Transport von PfEMP1 in die Wirtszelle bei 3D7-Parasiten zu untersuchen. Zu diesem Zweck wurde der Proteinexport durch das PTEX-Translocon, welches exportierte Proteine in die Wirtszelle transloziert, induzierbar blockiert. Bei einer Blockierung von PTEX, wurde PfEMP1 nicht mehr in die Wirtszelle exportiert. Der Zeitpunkt der Blockierung wurde im asexuellen Zyklus so induziert, dass früh exportierte Proteine, die potenziell für den PfEMP1-Transport benötigt werden, nicht beeinflusst wurden, da diese indirekt den Export von PfEMP1 beeinflussen könnten. Insgesamt deuten die Ergebnisse dieser Experimente darauf hin, dass PfEMP1 durch PTEX in die Wirtszelle transloziert wird.

Außerdem wurden BioID-Experimente durchgeführt, um Proteine in der Umgebung (Proxiom) von PfEMP1 in lebenden Parasiten zu identifizieren. Dafür wurde die Biotin-Ligase BirA* an drei unterschiedliche Positionen von PfEMP1 fusioniert, wodurch drei verschiedenen Zelllinien hergestellt wurden. Für diese Zelllinien wurde gezeigt, dass die PfEMP1-Varianten mit dem fusionierten BirA* prädominant in der Parasitenkulturen exprimiert und auf der Oberfläche der Wirtszellen präsentiert wurden. Des Weiteren wurden die Bindung der modifizierten PfEMP1 gegen die erwarteten Rezeptoren gezeigt. BioID-Experimente im großen Maßstab mit anschließender Massenspektrometrie-Analyse der biotinylierten Proteine identifizierten

Proteine, die für den Transport und die Funktion von PfEMP1 relevant sind. Darüber hinaus wurden zuvor charakterisierte und nicht charakterisierte Proteine der Maurer'schen Spalten, der Erythrozytenmembran und anderer Strukturen der Wirtszelle detektiert. Das Proxiom der drei Positionen zeigte nur kleine Unterschiede zueinander, was darauf hinweist, dass PfEMP1 nicht als integrales Membranprotein transportiert wird. Darüber hinaus deutete eine nur teilweise Überlappung mit einem Proxiom der Maurer'schen Spalten darauf hin, dass die detektierten Proteine PfEMP1-spezifisch waren. Dadurch wurden sechs exportierte Proteine mit unbekannter Funktion, die zuvor nicht mit Zytoadhärenz in Verbindung gebracht wurden, identifiziert und als PfEMP1-Interacting Candidate 1-6 (EMPIC1-6) benannt.

Des Weiteren wurde eine modifizierte Version von SLI, SLI2, angewandt, um eine zweite endogene Modifikation in den Zelllinien einzubringen, die bereits ein SLI-aktiviertes *var*-Gene beherbergten. Dies wurde verwendet, um die Funktion von Kandidatenproteine, die im Proxiom identifiziert wurden, zu trunkieren und deren Rolle im Transport und Oberflächenpräsentation von PfEMP1 zu ermitteln. Dies führte zur Identifizierung von zwei neuen Proteinen, die in Oberflächenproteinverdau- und Bindungsexperimenten zeigten, dass diese Kandidaten relevant für die effiziente Zytoadhärenz von *P. falciparum*-Parasiten sind. Jedoch wurde der Transport von PfEMP1 an die Oberfläche durch die Disruption der Kandidatenproteine nicht beeinflusst.

Zusammenfassend hat diese Dissertation - durch die Nutzung von SLI-Techniken - erfolgreich Zelllinien generiert und validiert, die spezifische PfEMP1-Varianten exprimieren. Es ist zu erwarten, dass dies die Studien über die Interaktion dieser Proteine mit Wirtszellrezeptoren, *var*-Gen-Expressionsmechanismen und den Transport von PfEMP1 erheblich vereinfachen wird. Diese Arbeit erweitert nicht nur unser Verständnis des Hauptvirulenzfaktors von *P. falciparum*, sondern eröffnet auch neue Wege, um die zellulären Mechanismen der Zytoadhärenz zu beleuchten, was dabei helfen wird, die Parasiten-Wirt-Interaktion besser zu verstehen.

TABLE OF CONTENTS

Language certificate	ii
Affidavit	iii
Eidesstattliche Erklärung.....	iv
Summary	v
Zusammenfassung.....	viii
Table of contents	xi
Abbreviations	xvii
List of figures	xx
List of tables	xxii
1 Introduction	1
1.1 Malaria.....	1
1.2 Biology of the malaria parasite <i>P. falciparum</i>	3
1.2.1 Life cycle of <i>P. falciparum</i>	4
1.2.1.1 Mosquito stages.....	4
1.2.1.2 Liver stages.....	5
1.2.1.3 Invasion	6
1.2.1.4 Intracellular Blood stages.....	7
1.2.1.4.1 Ring stage	7
1.2.1.4.2 Trophozoite stage	7
1.2.1.4.3 Schizont stage.....	8
1.2.1.4.4 Sexual development	9
1.2.2 Cellular biology of <i>P. falciparum</i> parasites	10
1.2.2.1 Organelles.....	10
1.2.2.1.1 Apical complex, dense granules and inner membrane complex	11
1.2.2.1.2 Apicoplast.....	12
1.2.2.1.3 Food vacuole	13

1.2.2.2	Parasitophorous vacuole.....	13
1.2.2.3	Export.....	14
1.2.2.4	Host cell modification.....	17
1.2.2.4.1	Maurer’s clefts.....	18
1.2.2.4.2	Plasmodial surface anion channel.....	19
1.2.2.4.3	Knobs.....	20
1.3	Cytoadherence.....	21
1.3.1	<i>var</i> genes.....	22
1.3.2	PfEMP1.....	25
1.3.2.1	Structure.....	25
1.3.2.2	Extracellular binding domains.....	25
1.3.2.3	Cellular biology of PfEMP1.....	29
1.3.2.3.1	PfEMP1 transport.....	29
1.3.2.3.2	Proteins influencing cytoadherence.....	30
1.3.2.4	Challenges to study PfEMP1.....	31
1.4	Aims.....	31
2	Material and Methods.....	33
2.1	Material.....	33
2.1.1	Technical devices.....	33
2.1.2	Chemicals.....	35
2.1.3	Labware and disposables.....	39
2.1.4	Kits.....	40
2.1.5	DNA and protein ladders.....	40
2.1.6	Solutions, buffers and media.....	41
2.1.6.1	Media, solution and drugs.....	41
2.1.6.1.1	Drugs.....	41
2.1.6.1.2	Media and solution for cell culture and binding assays.....	42
2.1.6.1.3	Bacterial culture.....	46
2.1.6.2	Solutions and buffers for biochemical analysis.....	47
2.1.6.2.1	Gel electrophoresis.....	47
2.1.6.2.2	Other buffers and solutions.....	48

2.1.7	Mammalian cell, <i>E. coli</i> and <i>P. falciparum</i> strains	51
2.1.8	Enzymes	52
2.1.9	Antibodies	53
2.1.9.1	Primary antibodies.....	53
2.1.9.2	Secondary antibodies.....	54
2.1.10	Primers	54
2.1.10.1	Standard primers for diagnostic PCRs	55
2.1.10.2	General Primers.....	55
2.1.11	Plasmids	55
2.1.12	Computer software, bioinformatic tools and data bases	55
2.2	Methods.....	57
2.2.1	Molecular methods.....	57
2.2.1.1	Polymerase chain reation (PCR)	57
2.2.1.2	Agarose gel electrophoresis.....	57
2.2.1.3	Purification of PCR products	57
2.2.1.4	Enzymatic DNA digestion.....	58
2.2.1.5	DNA ligation with T4 ligase or Gibson assembly	58
2.2.1.6	Colony PCR screen	58
2.2.1.7	Preparation plasmid DNA	59
2.2.1.8	Sanger sequencing.....	59
2.2.1.9	DNA precipitation	59
2.2.2	Microbiological methods.....	60
2.2.2.1	Transformation of compenent <i>E.coli</i> cells	60
2.2.2.2	Freezing of transgenic <i>E. coli</i> cells	60
2.2.2.3	Preparation of competent <i>E. coli</i> cells.....	60
2.2.3	Cell culture methods.....	61
2.2.3.1	Culturing of mammlian cells.....	61
2.2.3.2	<i>P. falciparum</i> cell culture	61
2.2.3.3	Blood smears	62
2.2.3.4	Freezing and thawing of parasite cultures.....	62
2.2.3.5	Synchronization of ring stage parasites.....	62
2.2.3.6	Isolation of trophozoite and schizont stage parasites	63

2.2.3.7	Transfection of <i>P. falciparum</i> schizont stage parasites	63
2.2.3.8	Introducing genomic modifications via SLI.....	64
2.2.3.9	Plaque assay	64
2.2.3.10	Enrichment of knobby parasites	65
2.2.3.11	PTEX co-block assay	65
2.2.4	Fluorescence Microscopy	65
2.2.4.1	Immunofluorescence and streptavidin-fluorescence assay	66
2.2.5	Binding assays.....	66
2.2.5.1	Static binding assays against mammalian cells or decorin.....	66
2.2.5.2	Automated scoring of binding assays.....	68
2.2.6	RNA sequencing	68
2.2.7	BioID and mass spectrometry	69
2.2.8	Biochemical methods	70
2.2.8.1	Trypsin cleavage assay	70
2.2.8.2	Western blot	70
2.2.9	Quantification, statistical analysis and figure construction.....	71
3	Results	72
3.1	Exploiting SLI-generated <i>var</i> gene cell lines	72
3.1.1	SLI strategy	72
3.1.2	SLI-modified <i>var</i> genes are predominantly expressed.....	73
3.1.3	Copenhagen 3D7 cell line shows defect in mutually exclusive expression.....	75
3.1.4	Evidence that PfEMP1 is exported through the PTEX channel.....	77
3.1.5	Establishment of a pipeline for automated evaluation of binding assays.....	79
3.1.6	3D7 show poor binding phenotypes.....	83
3.1.7	Generation of a collection of IT4 lines with different activated <i>var</i> genes.....	87
3.1.7.1	<i>IT4var02</i>	89
3.1.7.2	<i>IT4var03</i>	90
3.1.7.3	<i>IT4var08</i>	92
3.1.7.4	<i>IT4var16</i>	92
3.1.7.5	<i>IT4var19</i>	94

3.1.7.6	<i>IT4var20</i> and <i>IT4var22</i>	97
3.1.8	DBL β 12 in <i>IT4var19</i> shows similarities to ICAM-1-binding DBL β 5 domain....	100
3.2	Identification and characterization of proxime of a functional PfEMP1	102
3.2.1	Fusion of BirA* to endogenous PfEMP1 in three positions	102
3.2.1.1	Characterization of the BioID cell lines	104
3.2.1.2	Fusion of miniTurbo and FKBP to PfEMP1	108
3.2.2	Identification of biotinylated proteins proximal to PfEMP1	111
3.2.3	SLI2 enables characterization of PfEMP1 interactors	117
3.2.4	Characterization of interacting candidates of PfEMP1	119
3.2.4.1	TryThrA.....	120
3.2.4.2	PTEF.....	123
3.2.4.3	EMPIC3.....	125
3.2.4.4	PeMP2	128
3.2.4.5	EMPIC5.....	130
3.2.4.6	PTP7	131
3.2.4.7	TryThrA and EMPIC3 are relevant for efficient cytoadherence of <i>P.</i> <i>falciparum</i> parasites	134
4	Discussion	136
4.1	Activation of <i>var</i> genes with SLI	136
4.1.1	Expression of targeted <i>var</i> genes	136
4.1.2	Improving binding assays.....	140
4.1.3	3D7 is not suitable for binding studies.....	142
4.1.4	Surface presentation and binding of HA-tagged PfEMP1 variants.....	144
4.1.5	<i>IT4var19</i> contains an ICAM-1 binding domain.....	146
4.1.6	PfEMP1 is likely translocated via PTEX	148
4.2	Proxiome of PfEMP1	150
4.2.1	Is the proxime of PfEMP1 its global interactome?	150
4.2.2	Identification of PfEMP1 interactors relevant for cytoadherence.....	153

4.3 Conclusion.....	156
References	158
Appendix	191
Publications	209
Danksagung.....	210

ABBREVIATIONS

α	Anti
2A/T2A	Peptides derived from the 2A region in the genome of virus
4D	Four-dimensional
aa	Amino acids
ACT	Artemisinin combination therapy
AMA-1	Apical membrane antigen 1
AP2-G	Transcription factor
ATS	Acidic terminal segment
BioID	Proximity-dependent biotin identification
Biotinylerizer	BirA*-containing constructs inducible recruited to FKBP
BirA*	<i>E. coli</i> promiscuous biotin ligase
bp	Base pair
BSD	Blasticidin S
BSD-R	Blasticidin S resistance conferring gene
CD	Cluster of differentiation
CHO	Chinese hamster ovary
CIDR	Cysteine-rich interdomain region
CLAG	Cytoadherence linked asexual gene
COVID19	Coronavirus SARS-CoV-2
CRISPR	Clustered regularly interspaced short palindromic repeats
CSA	Chondroitin sulfate
DAPI	4',6-diamidino-2-phenylindole
DBL	Duffy binding-like
DC	Domain cassette
DDT	Dichlorodiphenyltrichlorethan
DHE	Dihydroethidium
DHFR	Dihydrofolate reductase
DHODH	Dihydroorotate dehydrogenase
DIC	Differential interference contrast
DiQ-BioID	Dimerization-induced quantitative BioID
DMSO	Dimethyl sulfoxide
DNA	Deoxyribonucleic acid
dNTP	Desoxynucleotide
DPBS	Dulbecco's Phosphate-Buffered Saline
DSM1	5-Methyl-N-(2-naphthyl)[1,2,4]triazolo[1,5-a]pyrimidin-7-amine
DTT	1,4-dithiothreitol
<i>E. coli</i>	<i>Escherichia coli</i>
EBL	Erythrocyte binding-like
ECL	Enhanced chemiluminescence
EDTA	Ethylenediaminetetraacetic Acid
EMPIC	EMP1 interacting candidate
EPCR	Endothelial protein C receptor
EPIC	Exported protein-interacting Complex
ER	Endoplasmic reticulum
et al.	et alii/et aliae
ETRAMP	Early transcribed membrane protein
EXP	Exported protein
FACS	Fluorescence-Activated Cell Sorting
FIKK	Serine/threonine kinase family
FKBP	FK506 binding protein
FRB	FKBP12-rapamycin binding domain
FV	Food vacuole
fw	Forward
G418	Geneticin 418
GBP	Glycophorin binding protein
gC1qR	Globular C1q receptor
GDV1	Gametocyte development 1
GEXP	Gametocyte exported protein

GFP	Green fluorescence protein
h	hours
HA	Hemagglutinin
HBEC-5i	Primary brain cells
HEPES	4-(2-Hydroxyethyl)-1-piperazineethanesulfonicacid
HP1	Heterochromatin protein 1
hpi	Hours post invasion
HR	Homology region
HRP	Horseradish peroxidase
HSP	Heat shock protein
ICAM-1	Intercellular adhesion molecule 1
ICC	Intraclass correlation coefficient
iE	Infected erythrocyte
IFA	Immunofluorescence assay
IgG	Immunglobulin G
IMC	Inner membrane complex
J-Dot	Mobile structures in the <i>P. falciparum</i> -infected erythrocyte
KAHRP	Knob-associated histidine-rich protein
kDa	Kilodalton
LB	Lysogeny broth
LC-MS	Label free quantitative liquid chromatography-mass spectrometry
Log	Logarithmic
LyMP	Lysine-rich membrane-associated PHISTb
lysoPC	Lysophosphatidylcholine
m	minute
MAHRP	Membrane associated histidine-rich protein
MC	Maurer's clefts
mCherry	Red fluorescent protein of the mFruits family
mScarlet	Red fluorescent protein
MEED	Mutually exclusive expression defect
MFS	Malaria freezing solution
MSP	Merozoite surface protein
MSRP6	MSP-7 related protein 6
MTS	Malaria thawing solution
Mw	Molecular weight
NCBI	National Center for Biotechnology Information
Neo R	Neomycin resistance conferring gene
NPP	New permeability pathways
NTS	N-terminal segment
ori	Original locus
<i>P. falciparum</i>	<i>Plasmodium faciparum</i>
PBS	Phosphate buffer solution
PCR	Polymerase chain reaction
PECAM-1	Platelet endothelial cell adhesion molecule 1
PeMP	Peripheral Maurer's clefts protein
PEXEL	<i>Plasmodium</i> export element
Pf332	<i>P. falciparum</i> protein 332
PfEMP1	<i>P. falciparum</i> erythrocyte membrane protein 1
pH	Potential of hydrogen
PHIST	<i>Plasmodium</i> helical interspersed subtelomeric
pI	Isoelectric point
PlasmoDB	Plasmodium database
PNEP	PEXEL negative exported protein
PPM	Parasite plasma membrane
Proxiome	Proximal proteome
PSAC	<i>Plasmodium</i> surface anion channel
PTEF	<i>P. falciparum</i> translation enhancing factor
PTEX	<i>Plasmodium</i> translocon of exported proteins
PTP	PfEMP1 transport protein
PV	Parasitophorous vacuole
PVM	Parasitophorous vacuole membrane

qPCR	Quantitative Polymerase Chain Reaction
RBL	Reticulocyte binding-like
REX1	Ring exported protein
RFP	Red fluorescence protein
RhopH	High molecular weight rhoptry protein
RMSD	Root-mean-square deviation
RNA	Ribonucleic Acid
RON3	Rhoptry neck protein 3
Rpm	Rounds per minute
RPMI	Roswell Park Memorial Institute (medium)
RT	Room temperature
rv	Reverse
SBP1	Skeleton binding protein 1
SD	Standard deviation
SDS	Sodium dodecyl sulfate
SDS-PAGE	Sodium dodecyl sulfate polyacrylamide gel electrophoresis
SEMP	Small exported proteins
SERA	Serine repeat antigen
SLI	Selection linked integration
SP	Signal peptide
STARP	Sporozoite threonine and asparagine-rich protein
SUB1	Subtilisin-like protease 1
SURFIN	Protein transcribed by surface-associated interspersed gene
TAE	TRIS-acetat-EDTA-Puffer
TE	Tris-EDTA
TGD	Targeted gene disruption
TM	Transmembrane domain
TPCK	L-1-Tosylamido-2-Phenylethylchloromethylketon
TPM	Transcripts per million
TRX	Thioredoxin-2 enzyme
TryThrA	Tryptophan-threonine-rich antigen
TVN	Tubovesicular network
UIS2	Unregulated infected sporozoite 2
UPS	5' upstream
VSA	Variant surface antigens
WHO	World health organization

LIST OF FIGURES

Figure 1: Countries with indigenous malaria cases in 2000 and their status in 2021.....	1
Figure 2: Life cycle of <i>P. falciparum</i>	4
Figure 3: Invasion and formation of the parasitophorous vacuole.	6
Figure 4: Asexual blood stages.	8
Figure 5: Gametocyte stages.	9
Figure 6: Organelles of <i>P. falciparum</i> parasites.....	11
Figure 7: Export and nutrient uptake from the host cell cytosol across the PV..	16
Figure 8: Host cell modifications.	18
Figure 9: Cytoadherence of infected erythrocytes.....	22
Figure 10: <i>var</i> gene groups location on the chromosomes.....	23
Figure 11: PfEMP1 structure, binding domains and interacting receptors.....	27
Figure 12: Integration strategy for the activation of a specific <i>var</i> gene.	73
Figure 13: Confirmation of predominant expression of specific <i>var</i> genes modified with SLI in 3D7.	74
Figure 14: 3D7 ^{MEED} shows a defect in mutually exclusive expression.	76
Figure 15: Export of PfEMP1 is prevented by blocking PTEX at the onset of the trophozoite stage.....	78
Figure 16: Establishment of an automated pipeline for the evaluation of binding assay images.	80
Figure 17: Confirmation of SLI-activation of two <i>var</i> genes in IT4.	84
Figure 18: Comparison of the cytoadherence properties of 3D7 and IT4 parasites.	86
Figure 19: Characterization of the activation of <i>var02</i> in IT4 parasites.....	90
Figure 20: Characterization of the activation of <i>var03</i> in IT4 parasites.....	91
Figure 21: Characterization of the activation of <i>var08</i> in IT4 parasites.....	92
Figure 22: Characterization of the activation of <i>var16</i> in IT4 parasites.....	94
Figure 23: Characterization of the activation of <i>var19</i> in IT4 parasites.....	96
Figure 24: Attempted activation of <i>var20</i> and <i>var22</i>	98
Figure 25: DBLβ12 shows structural similarities to ICAM-1-binding DBLβ5.	100
Figure 26: SLI-strategy for fusion of BirA* to <i>var01</i> in IT4.	102
Figure 27: BirA*-fused PfEMP1s are functional and able to biotinylate.....	105
Figure 28: Generation of PfEMP1-miniTurbo cell lines.	108
Figure 29: Attempt to establish DiQ-BioID for PfEMP1.....	109
Figure 30: MS analysis of biotinylated proteins enriched in the BioID cell lines.....	113
Figure 31: Comparison of the PfEMP1 proximiomes with each other and a general Mauer's cell's proximiome.	115
Figure 32: Second endogenous modification in cell line with a SLI-activated <i>var</i> gene.	118
Figure 33: Characterization of TryThrA.	121
Figure 34: Characterization of PTEF.	124
Figure 35: Characterization of EMPIC3.	126
Figure 36: Characterization of PeMP2.....	129
Figure 37: Characterization of EMPIC5..	131
Figure 38: Characterization of PTP7.....	132
Figure 39: TryThrA and EMPIC3 are relevant for cytoadherence.....	134

Figure 40: Exploring key processes in cytoadherence using SLI-activated *var* gene cell lines. 157

LIST OF TABLES

Table 1: List of technical devices.....	33
Table 2: List of chemicals.....	35
Table 3: List of labware and disposables	39
Table 4: List of kits	40
Table 5: List of DNA and protein ladders.....	40
Table 6: List of drugs for parasite culture	41
Table 7: List of media and solutions for parasite culture	42
Table 8: List of solutions for bacterial culture	46
Table 9: List of solutions for gel electrophoresis	47
Table 10: List other buffers and solutions.....	48
Table 12: List of mammalian, <i>E. coli</i> and <i>P.falciparum</i> strains.....	51
Table 13: List of enzymes.....	52
Table 14: List of primary antibodies	53
Table 15: List of secondary antibodies	54
Table 16: List of standard primers	55
Table 17: List of general primers	55
Table 18: List of <i>var</i> genes chosen for the activation in IT4 parasites.....	87

1 INTRODUCTION

1.1 MALARIA

It is likely that malaria has accompanied humanity since its origin. Historical records tracing as far back as the 2700 BC, including those from ancient civilizations in China, Egypt, Mesopotamia, and Greece, already described symptoms of the disease (Cox, 2010). There is evidence that numerous historical figures, including Julius Caesar (Ridley, 2000), several members of the Medici dynasty (Maixner et al., 2023; Sommi Picenardi, 1888), and the Egyptian pharaoh Tutankhamun (Hawass et al., 2010) were plagued by malaria, illustrating the long-standing impact on humanity.

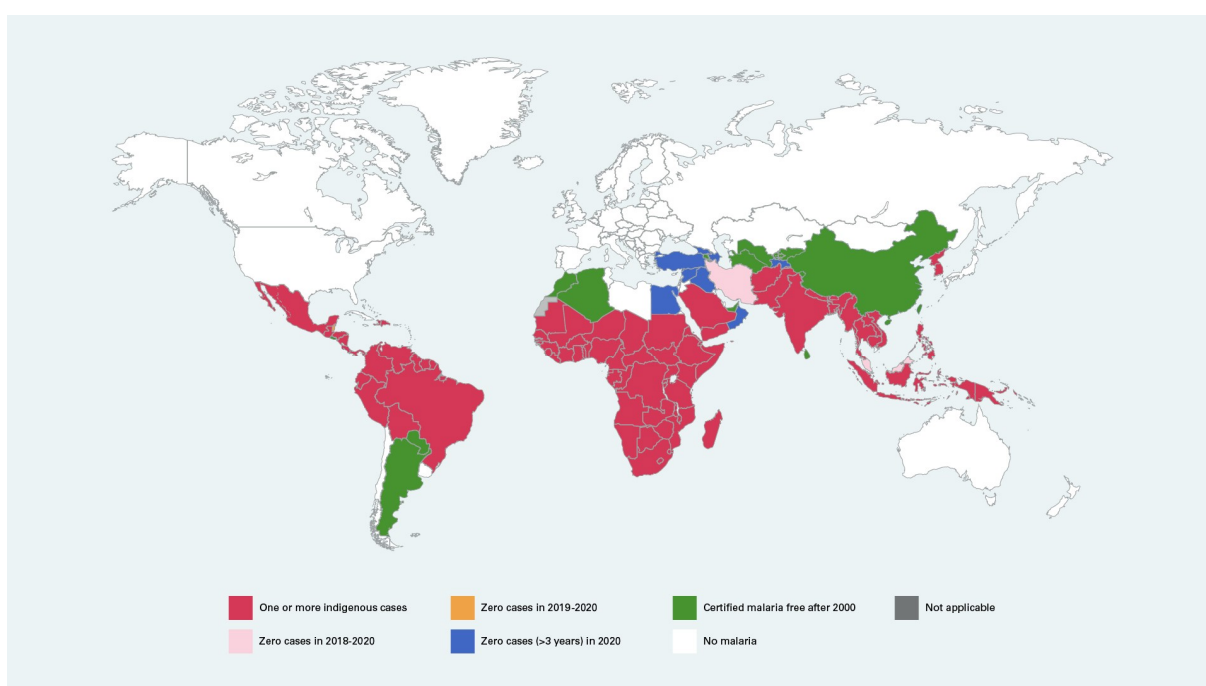


Figure 1: Countries with indigenous malaria cases in 2000 and their status in 2021. Red indicates countries with indigenous cases of malaria in 2021; Orange, green, pink, blue and white indicate malaria free countries that previously registered malaria cases (figure from WHO, 2020).

For centuries the disease was attributed to bad air in the swamps and in medieval Italy was termed "mala aria" (bad air). The paradigm shifted with Louis Pasteur's germ theory of disease in the 1860s, laying the groundwork for the microbial origin of diseases. However, only in 1880 Alphonse Laveran, a young military doctor in Algeria, observed malaria parasites in the blood of patients for the first time. He proposed that a protozoan parasite was responsible for the disease, a postulate that was broadly accepted a decade later. Laveran already hypothesized about the role of mosquitoes in the transmission of these parasites. This was later confirmed by

Sir Ronald Ross in 1897 on avian malaria and by Giovanni Battista Grassi in 1898 on human malaria parasites. Only Ross and Laveran were honored with the Nobel prize, Ross in 1902 and Laveran in 1907 (reviewed in Cox, 2010).

Malaria's clinical symptoms vary from asymptomatic to severe, including nausea, fever, anemia, and neurological complications (Marsh et al., 1995). The World Health Organization (WHO) reported over 200 million malaria infections and 600,000 fatalities in 2021, with an increase from the previous year attributed to the exacerbation of the disease burden due to the COVID-19 pandemic disrupting malaria control services. The vast majority of malaria cases occur in sub-Saharan Africa, often affecting the poorest and youngest individuals (Figure 1) (WHO, 2023).

The WHO has the goal to reduce malaria cases by 90 % by 2030 (WHO, 2023). However, these aims are hampered by increased resistances of the parasites to the currently available antimalarials. Antimalarial medication like quinine were already used in the 16th hundreds (Achan et al., 2011). Today, the frontline antimalarial drug is artemisinin and derivatives used in combination with other antimalarials, so called ACTs (artemisinin combination therapies). However, reduced susceptibility of parasites to artemisinins are now widespread in Southeast Asia (Dondorp et al., 2009; Noedl et al., 2008) and was also reported for Africa (Stokes et al., 2021; Uwimana et al., 2021, 2020) South America (Mathieu et al., 2020) and Papua New Guinea (Miotto et al., 2020).

Preventive strategies implemented by the WHO focus on vector control, with insecticide-treated bed nets and the elimination of mosquito breeding grounds are among the most effective in preventing malaria transmission (WHO, 2023). Furthermore, DDT was used in large scale eradication programs to diminish mosquito populations (Sadasivaiah et al., 2007). In Sri Lanka for example, malaria cases were reduced from one million per year to 18 in 1963 before numbers rose again when the program was stopped (Karunaweera et al., 2014). The appreciation of the effect of DDT on the environment drastically reduced the use of DDT. Currently only small quantities are used for indoor spraying.

Malaria continues to be a major global health challenge, remaining one of the top causes of mortality in low-income countries (WHO, 2020). This disease not only poses a significant threat to public health but also imparts a substantial economic burden. Its persistence highlights the critical need for enhanced preventive strategies and stronger healthcare interventions.

1.2 BIOLOGY OF THE MALARIA PARASITE *P. FALCIPARUM*

Malaria is caused by unicellular eucaryotic parasites of the genus *Plasmodium* which belong to the *Apicomplexa* phylum in the *Alveolata* clade. Other well-known representatives of the *Apicomplexans* are *Toxoplasma* and *Cryptosporidium*, the causative agents of toxoplasmosis and cryptosporidiosis. The genus *Plasmodium* comprises around 200 species that can infect a wide range of mammals, birds, and reptiles (Martinsen and Perkins, 2013). Only five of these species are known to regularly infect the human as a host, *P. falciparum*, *P. vivax*, *P. knowlesi*, *P. ovale* and *P. malariae* (Lalremruata et al., 2017). While *P. vivax* is the most prevalent outside African countries, *P. falciparum* is by far the deadliest of the human malaria species that is responsible for nearly all of the malaria related death (WHO, 2023).

P. falciparum is the only human infecting malaria parasite that belongs to the subgroup of *Laverania* (Bray, 1958). The *Laverania* subgenus comprises *Plasmodium* species that infect gorillas and chimpanzees and most likely derived from bird infecting malaria parasites. *P. falciparum* probably arose from an ancestral *Laverian* parasite that used gorillas as their hosts, *P. praefalciparum*. *P. falciparum* therefore differs from the other human malaria parasites like *P. vivax* and is a rather distant relative of these (reviewed in Escalante et al., 2022) with higher virulence and unique properties such as the capacity to bind to the host endothelium (section 1.3).

The second host of all the *Plasmodium* species are mosquitoes of the genus *Anopheles* in which the parasites mate and migrate between vertebrate hosts (Figure 2). Of the 140 *Anopheles* species only 20 are known to transmit malaria (Hay et al., 2000; Sinka et al., 2012, 2010).

through very rapid DNA replication, the fastest DNA replications in any eucaryotic organism (Matthews et al., 2018), to produce eight microgametes (1n) within 15 min (Janse et al., 1986; Kawamoto et al., 1991). The female gametocytes develop into a single larger macrogamete (1n) (Guttery et al., 2012). The haploid micro- and macrogametes then lyse the erythrocytes and are released into the midgut. Microgametes undergo exflagellation (Billker et al., 2004; Laveran, 1880) and subsequently fertilize the macrogametes to form a diploid zygote (2n). The zygote undergoes DNA replication and meiosis to transform into a motile ookinete (4n) that migrates through the midgut epithelium into the basal lamina where it transforms into an ookinete. The developmental transition from initial ingestion to ookinete formation within the mosquito's midgut takes approximately 19 to 36 hours. In the next 10-12 days the ookinete develops into an oocyst in which sporozoites are formed by sporogonic replication (reviewed in Aly et al., 2009). The motile sporozoites are then released into the body cavity of the mosquito and reach the salivary glands where they are ready to infect the following human host during another bite of the mosquito (Figure 2).

1.2.1.2 LIVER STAGES

Once injected into the human host the sporozoites migrate to reach the bloodstream from the injection side in the dermis. Only 70 % of the sporozoites make it to the blood stream, the rest ends up in the lymphatic system where they are degraded (Amino et al., 2006). Once in the bloodstream the sporozoites are transported to the liver (Dobrowolski and Sibley, 1996). In the liver the sporozoites adhere to the endothelial cells (Kori et al., 2018) and proceed to reach hepatocytes via multiple routes, including direct penetration through endothelial cells, migration through interstitial gaps between discontinuous endothelial cells (Ishino et al., 2004) or traversal through Kupffer cells (Pradel and Frevert, 2001). The sporozoites then transmigrate several hepatocytes before settling in a single hepatocyte (Rankin et al., 2010). In the next 5-7 days the parasite goes through hepatic schizogony to multiply and form thousands of merozoites (Bartoloni and Zammarchi, 2012). The merozoites are released into the bloodstream by budding off merozoite filled merosomes from the infected hepatocyte (Sturm et al., 2006). These merosomes rupture and release the merozoites in the blood stream (Baer et al., 2007) (Figure 2).

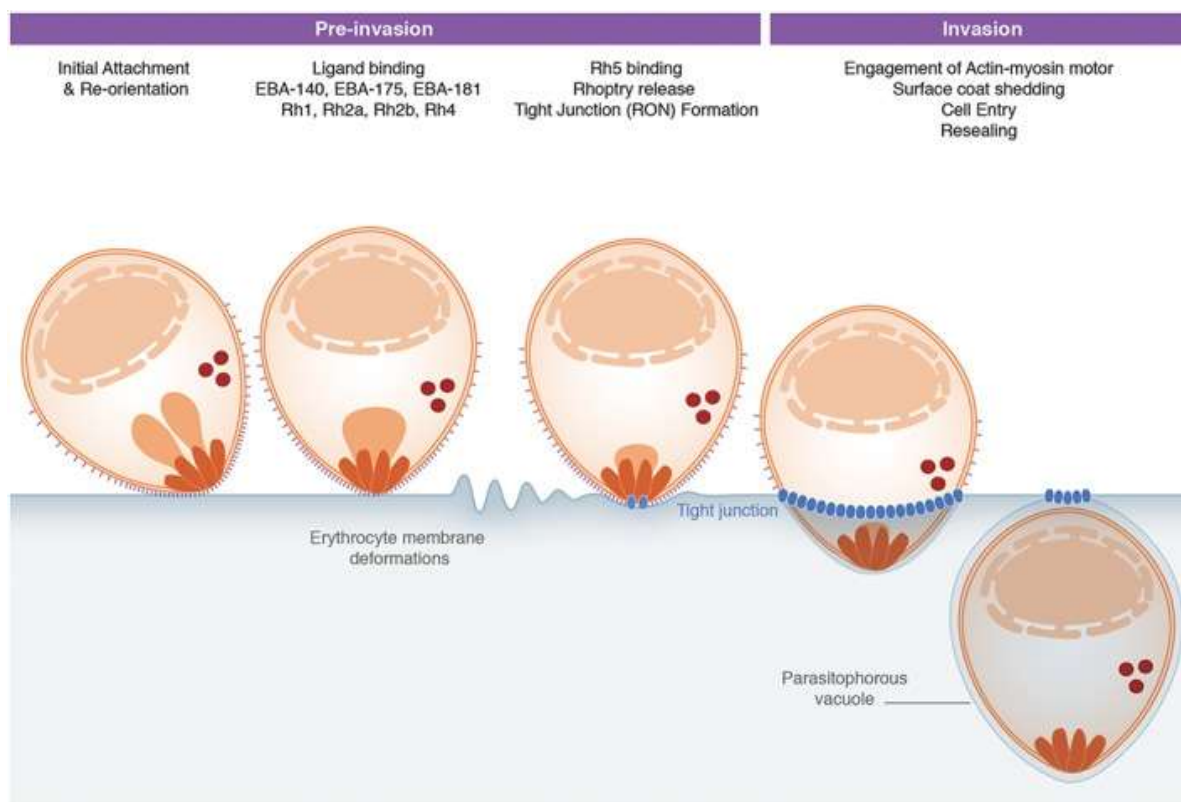


Figure 3: Invasion and formation of the parasitophorous vacuole. Illustration showing simplified scheme of the invasion process. EBA: Erythrocyte binding antigen; Rh: reticulocyte binding-like protein; RON: Rhoptry Neck Proteins; light blue background; erythrocyte; white background extracellular space (figure from Koch and Baum, 2016).

1.2.1.3 INVASION

Despite some evasion mechanisms, merozoites in the bloodstream are exposed and vulnerable to the immune system as they are the only free-living form of the blood stages (Hill et al., 2013). Therefore, merozoites swiftly invade red blood cells (within 30 seconds) to avoid prolonged exposure to the serum (Gilson and Crabb, 2009). The invasion process can be classified into multiple steps: attachment, strong binding, reorientation, entry and sealing (different steps are sometimes used in the literature) (Cowman et al., 2017; Dvorak et al., 1975; Gilson and Crabb, 2009). Initially, the merozoite binds to the erythrocyte, likely through a weak interaction involving the merozoite surface proteins (MSPs) and the erythrocyte surface (attachment) (Sanders et al., 2005). This interaction triggers members of the erythrocyte binding-like (EBL), reticulocyte binding-like (RBL) families, and apical membrane antigen 1 (AMA-1) that mediate strong attachment (strong binding) (Besteiro et al., 2011; Cowman et al., 2017; Lopaticki et al., 2011). Guided by these proteins, the merozoite then repositions its apical end toward the erythrocyte (reorientation) and establishes a tight junction. Subsequently the merozoite enters the erythrocyte by causing the host cell membrane to invaginate (entry). The invasion process

is finalized by the sealing of the invaginated erythrocyte membrane, followed by echinocytosis and subsequent restoration of the erythrocyte's shape (sealing) (Figure 3; reviewed in Cowman et al., 2017). During this process the erythrocyte membrane forms a second membrane around the parasite, the parasitophorous vacuole membrane (PVM), creating the parasitophorous vacuole (PV), separating the parasite from the host cell cytosol (section 1.2.2.2).

1.2.1.4 INTRACELLULAR BLOOD STAGES

Erythrocytes present a unique ecological niche for the malaria parasites with specific advantages and disadvantages. To overcome these disadvantages the parasite has developed sophisticated strategies which are linked to great expenses for the parasite (section 1.2.2.4). During the intraerythrocytic stages, the parasite's primary functions are proliferation and transitioning to its sexual stage, and subsequent uptake by *Anopheles* mosquitoes, thereby ensuring propagation and survival (Figure 2).

1.2.1.4.1 RING STAGE

The first stage after invasion into an erythrocyte is termed the ring stage which comprises the first 18 hours after invasion (Grüring et al., 2011) (Figure 4). During this stage, the parasite can be observed in a circular form or adopt an amoeboid shape. On the molecular level, ring stage parasites modify their host cell by exporting a large number of proteins into the host cell (section 1.2.2.3 and 1.2.2.4). The ring stage is superseded by the trophozoite stage, distinguishable morphologically by the formation of a hemozoin containing food vacuole.

1.2.1.4.2 TROPHOZOITE STAGE

The trophozoite stage is characterized by the uptake of hemoglobin from the host cell and nutrients from the bloodstream (section 1.2.2.4.2) by the parasite and takes until ~32 hour after invasion (Grüring et al., 2011) (Figure 4). Hemoglobin is digested and the by-product heme is transformed to hemozoin and stored in the food vacuole (section 1.2.2.1.3) which is visible and a distinctive feature of the malaria parasite (Figure 4). Concurrently, the parasite dramatically increases in size. Trophozoites have a more spherical shape with a fixed position in the host cell than ring stages (Sachanonta et al., 2011). To achieve this the parasite heavily relies on the foundational host cell modifications instigated during the preceding ring stage.

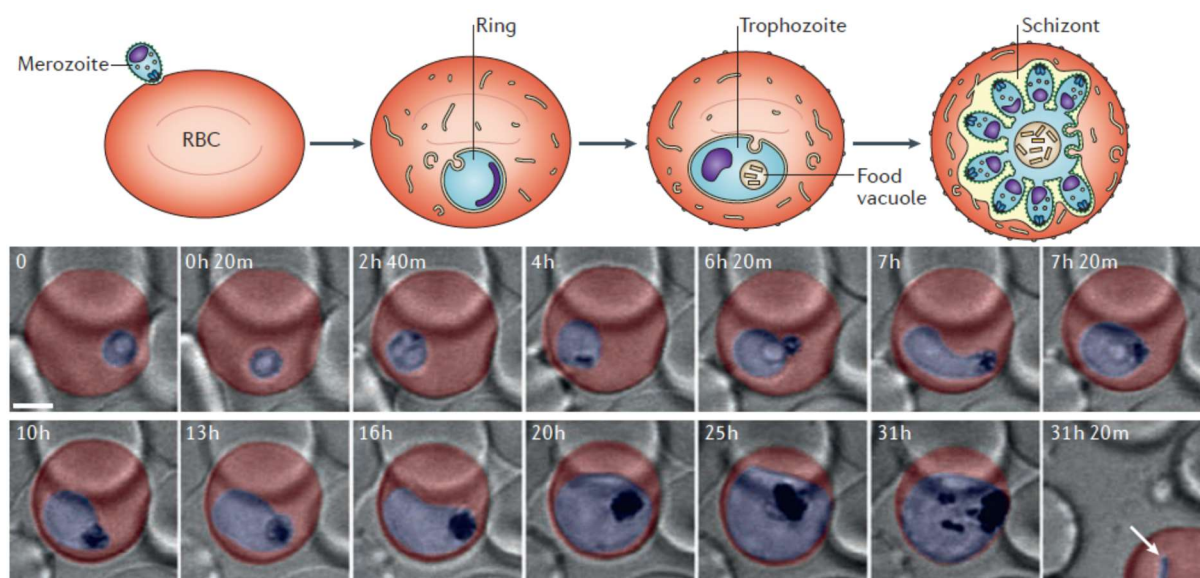


Figure 4: Asexual blood stages. Top Panel: Schematic illustration of the *P. falciparum* asexual erythrocytic cycle, depicting the progression through the key blood stages: ring, trophozoite and schizont with the generation of merozoites. Bottom Panel: A detailed single differential interference contrast (DIC) z-section from a series constituting four-dimensional (4D) confocal microscopy imaging, capturing the dynamic development of a *P. falciparum* parasite during the erythrocytic stage. Selected time-lapse frames, captured at 20-minute intervals and artificially colored for contrast enhancement, are presented. The elapsed time since the onset of imaging is indicated for each frame. Initial imaging (time point 0) reveals a parasite in the late ring stage, with subsequent times therefore not aligned with the typical post-invasion timeline. White Arrow (at time point 31h20m): Denotes a newly invaded ring stage parasite; red: erythrocyte membrane; blue: *Plasmodium* parasite body; black: hemozoin (pigment) in the parasite's food vacuole; h: Hours post-initiation of imaging; m: Minutes post-initiation of imaging; Scale bar, 2 μm . (Modified from De Niz et al., 2017).

1.2.1.4.3 SCHIZONT STAGE

After the increased energy and nutrient consumption, the parasite prepares to enter the schizont stage heralded by the first nuclear division, approximately 32 hpi. The nuclear division during schizogony is asynchronous (endodyogeny) without the formation of plasma membranes around the newly formed nuclei (Klaus et al., 2022; Read et al., 1993). Only after the nuclear division is completed new cells are formed within the parent through the invagination of plasma membrane and give rise to 16-32 daughter cells (Figure 4). In this stage the schizonts are often referred to as segmenters. Furthermore, the inner membrane complex (IMC) and apical complexes (section 1.2.2.1.1) form which are essential for invasion of merozoites into new erythrocytes (Voß et al., 2023). The release of daughter cells occurs 48 hpi in a rapid and highly orchestrated egress process (Abkarian et al., 2011). Egress is initiated when subtilisin-like protease 1 (SUB1) is secreted into the PV activating egress effectors (Suarez et al., 2013; Tawk et al., 2013) of the merozoite surface protein-1 (MSP-1) (Koussis et al., 2009; Yeoh et al., 2007) and serine repeat antigen (SERA) families (Collins et al., 2017; Ruecker et al., 2012; Stallmach et al., 2015; Thomas et al., 2018). This activates the breakdown of the PVM and erythrocyte

membrane (Blackman and Carruthers, 2013) and enables the escape of merozoites into the bloodstream. This coordinated sequence of events ends one round of the continuous asexual life cycle of *P. falciparum* parasites (Figure 2).

1.2.1.4.4 SEXUAL DEVELOPMENT

During asexual reproduction in the blood, a small population of *Plasmodium* parasites undergoes sexual commitment, giving rise to gametocyte progeny and initiating the sexual stage of the life cycle. This pivotal process is initiated by gametocyte development 1 (GDV1) which activates heterochromatin protein 1 (HP1) (Filarsky et al., 2018) followed by de-repression of the transcription factor AP2-G (Kafsack et al., 2014; Sinha et al., 2014). This process is controlled by the exogenous host serum lipid lysophosphatidylcholine (lysoPC). Depletion of lysoPC leads to increased sexual commitment of the parasites (Brancucci et al., 2017). The conversion rates in clinical isolates range from 3.3% to 12.2% of the parasites. Notably, conversion rates *in vitro* can drop to 0% in parasites lacking the *gdv1* gene, with non-sense mutations in the *ap2g* gene or lost chromosome ends (Eksi et al., 2012; Kafsack et al., 2014; Stewart et al., 2022; Tibúrcio et al., 2021). In controlled *in vitro* conditions, the induction of this conversion is attainable through the conditional depletion of *hpl1* (Brancucci et al., 2014) and conditional overexpression of *gdv1* (Boltryk et al., 2021; Usui et al., 2019) or *ap2-g* (Kent et al., 2018; Llorà-Batlle et al., 2020).

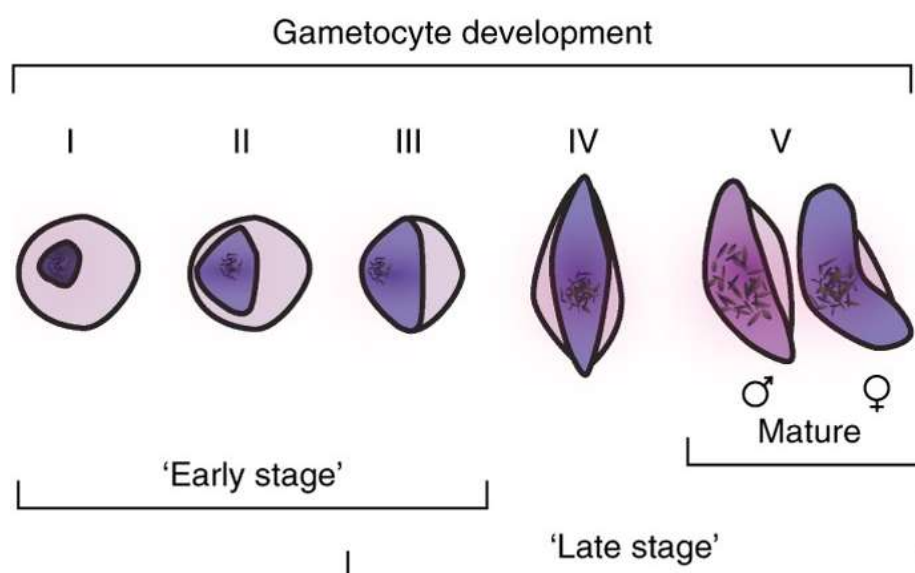


Figure 5: Gametocyte stages. Simplified illustration of the morphology of the gametocyte stages I–V. Stages I–III are categorized as early stages. Stages III–V categorized as late stages. The banana-like shape characteristic for gametocytes appears in stage V. Stage V shows sex specific differences (male and female gametocytes). (Figure modified from (from Delves et al., 2016).

Once a schizont is sexually committed, all merozoites of that parasite develop into either male or female gametocytes after they invaded a new erythrocyte (Silvestrini et al., 2000). The maturation of gametocytes spans a period of 10-12 days in *P. falciparum* and is categorized into five stages (Stages I-V; Figure 5) (Josling and Llinás, 2015). Stage I gametocytes lack morphological distinctions to asexual trophozoites. Only in stage II the gametocytes take on a form unique to sexually committed parasites. Stage V gametocytes assume a distinctive banana-shaped morphology and occupy most of the host erythrocyte (Figure 5). Early- and late-stage as well as male and female gametocytes can be reliably distinguished from one another and from asexual stages using molecular markers (Alano, 2007; Russell et al., 2023). In the peripheral blood of patients only stage I and stage V gametocytes are detectable. Stages II - IV are sequestered within the bone marrow and spleen to evade splenic clearance (De Niz et al., 2016; Joice et al., 2014; Lee et al., 2018; Obaldia et al., 2018). Mature stage V gametocytes are ingested by *Anopheles* mosquitoes and enter gametogenesis (Figure 2).

It is noteworthy that gametocytes display limited susceptibility to antimalarial treatments (Bradley et al., 2019; Delves et al., 2016) and thereby can persist in the patient after otherwise successful antimalarial therapy.

1.2.2 CELLULAR BIOLOGY OF *P. FALCIPARUM* PARASITES

1.2.2.1 ORGANELLES

P. falciparum parasites possess the typical eukaryotic organelles such as the ER, nucleus, Golgi apparatus, lysosome-like organelle and mitochondria. Additionally, malaria parasites possess highly specialized organelles to invade the erythrocytes (apical complex; section 1.2.2.1.1), digest hemoglobin in a lysosome-like organelle (food vacuole; section 1.2.2.1.3) and produce essential precursors for biochemical pathways in a plastid (apicoplast; section 1.2.2.1.2) (Figure 6). Parasite-induced compartments in the host cell are summarized in 1.2.2.4.1 (Maurer's clefts) and the compartment the parasite is residing in the host cell in 1.2.2.2 (Figure 6).

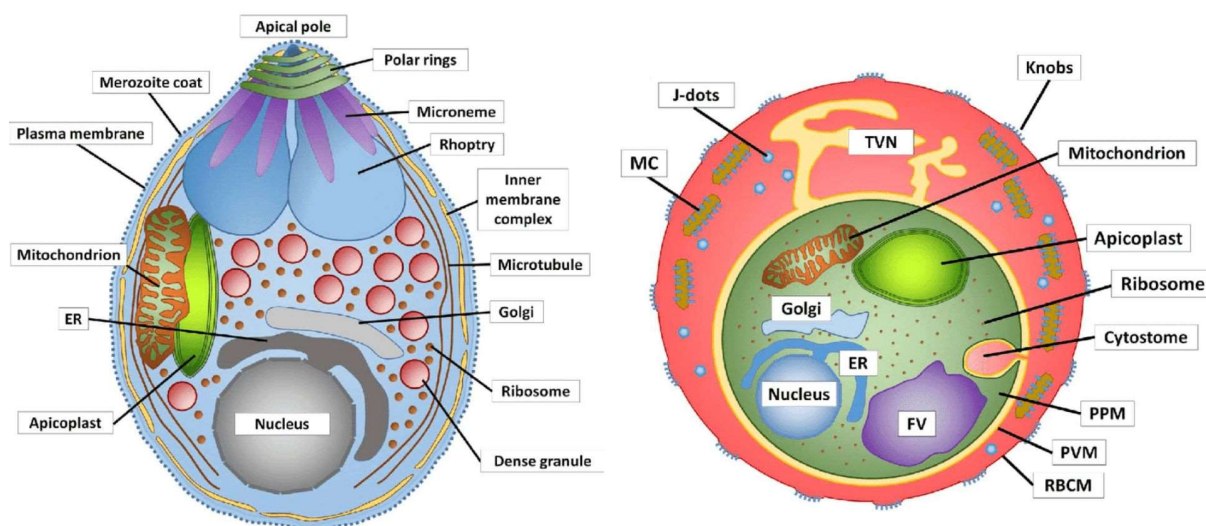


Figure 6: Organelles of *P. falciparum* parasites. (A) Illustration of the organelles in a *P. falciparum* merozoite. Red: Host cell cytosol; Yellow: PV lumen; Darker green: Parasite cytosol. (B) Illustration of the organelles in a *P. falciparum* trophozoite stage parasite. IMC: inner membrane complex; ER: Endoplasmic reticulum; MC: Maurer's cleft; FV: Food vacuole; PPM: Parasite plasma membrane; PVM: Parasitophorous vacuole membrane; RBCM: red blood cell membrane; TVN: tubovesicular network. (Figure modified from Flammersfeld et al., 2018).

1.2.2.1.1 APICAL COMPLEX, DENSE GRANULES AND INNER MEMBRANE COMPLEX

P. falciparum merozoites possess three specialized secretory organelles orchestrating secretion of proteins for the invasion of erythrocyte and formation of the PVM. Two of these organelles are in the apical complex, which is situated at the parasite's apex. The third secretory organelle, the dense granules are scattered throughout the cytosol (Bannister et al., 2003) (Figure 6, left). The apical complex consists of the apical ring, micronemes, and rhoptries (Martinez et al., 2022). The rhoptries are prominent, bulbous, electron-dense structures that taper towards the apex and are accompanied by the slender, filamentous micronemes (Figure 6, left). The invasion mechanism (section 1.2.1.3) is orchestrated through a finely regulated spatial and temporal interplay between these organelles. The exocytosis of micronemes, largely driven by calcium signaling, initiates prior to merozoite egress from the host cell (Bisio et al., 2019; Farrell et al., 2012). However, *in vitro* studies suggest that microneme exocytosis may be dispensable for egress (Farrell et al., 2012). Micronemes are pivotal for the parasite's gliding motility in *P. berghei* sporozoites (Fréchal et al., 2017). The parasite's gliding motility is a movement process important for invasion and sporozoite migration (Beyer et al., 2021; Yahata et al., 2021).

The interaction between the merozoite and the erythrocyte, facilitated by microneme exocytosis, likely instigates the release of rhoptries. Proteins from the rhoptries are then discharged, contributing to the establishment of a moving junction (Guérin et al., 2017) between

merozoite and host cell. A second wave of exocytosis of rhoptry proteins occurs during the formation of the PVM (Håkansson et al., 2001).

The electron-dense dense granules, which are also involved in the secretion during invasion, release their contents only after the parasite is inside the erythrocyte, contributing proteins to the PVM and the erythrocyte surface. Notably, proteins such as exported protein 2 (EXP2) and the RhopH complex are stored within these granules during the schizont stage (section 1.2.2.3 and 1.2.2.4.2) (Bullen et al., 2012; Maier et al., 2008) to facilitate protein export and nutrient import right after invasion.

During schizogony a new membrane, termed the inner membrane complex (IMC), is formed *de novo* beneath the plasma membrane of newly forming merozoites. This membrane likely derived from Golgi material (Bannister et al., 2000) and eventually underlies the plasma membrane of the merozoite, leading to flat membranous cisternae underneath the plasma membrane of the merozoites (Figure 6, left). The IMC, which is a discontinuous structure (Hanssen et al., 2013; Riglar et al., 2013), is thought to provide a structural framework for gametocytes (Dearnley et al., 2012; Parkyn Schneider et al., 2017; Sinden, 1982) and during merozoite formation (Kono et al., 2012). Furthermore, it is integral to gliding motility by anchoring the actin-myosin machinery of the glideosome (Gaskins et al., 2004; Jones et al., 2006; Keeley and Soldati, 2004). Post-invasion, the IMC is swiftly dismantled within approximately 15-60 minutes (Riglar et al., 2013). The composition and function in invasion of the IMC is a field of active research (Ferreira et al., 2021; Qian et al., 2022; Wichers et al., 2021).

1.2.2.1.2 APICOPLAST

The apicoplast, a non-photosynthetic plastid, is ubiquitous among the *Apicomplexa* phylum with the notable exception of *Cryptosporidium* *ssp.* (Zhu et al., 2000) and *Gregarina niphandrodes* (Toso and Omoto, 2007). This remarkable organelle originated from a secondary endosymbiotic process, probably involving a red algae, which intrinsically contained a prokaryotic symbiont, leading to an organelle encased by four distinct membranes (Fast et al., 2001; Köhler et al., 1997). Despite containing different kinds of approximately 500 proteins, the apicoplast's genome just encodes a mere 10% of these, with the majority transcribed in the nucleus and transported to the apicoplast via a specialized targeting sequence (McFadden and Yeh, 2017).

Given its prokaryotic heritage and critical metabolic functions, the apicoplast has been identified as a pivotal vulnerability - the “Achilles' heel” - of *Plasmodium spp.* (Soldati, 1999). Experiments utilizing specific antibiotics (e.g., Chloramphenicol, Doxycycline, etc.) resulted in the eradication of the apicoplast (Dahl et al., 2006), leading to the parasite's demise during the subsequent asexual proliferation cycle, a phenomenon described as a “delayed death phenotype”. However, the exogenous supply of a single precursor involved in isoprenoid biosynthesis, isopentenyl pyrophosphate, can rescue blood stage parasites lacking an apicoplast (Yeh and DeRisi, 2011). This underscores the apicoplast's essential role for the parasite in the isoprenoid synthesis pathway during its blood stages.

1.2.2.1.3 FOOD VACUOLE

An essential part of the parasite's survival is the degradation of hemoglobin. The parasite degrades around 80% of the hemoglobin of the host cell within an intraerythrocytic cycle. The host cell cytosol is taken up in bulk without the need for receptors to discriminate what is internalized (Spielmann et al., 2020). The internalized cytosol is transported to an acidic lysosomal-like compartment, the food vacuole. Several proteases in the food vacuole help to break down hemoglobin (Banerjee et al., 2002; Francis et al., 1997). One of the key products of this digestion is free radical producing ferriprotoporphyrin IX (α -hematin) which is toxic for the parasite (Goldberg et al., 1991, 1990). The α -hematin is polymerized in the food vacuole which results in the accumulation of non-toxic crystallized hemozoin, also known as the “malaria pigment”. This pigment builds up in the parasite's food vacuole and becomes a noticeable feature of parasites that conducted endocytosis (Ehlgen et al., 2012).

1.2.2.2 PARASITOPHOUS VACUOLE

The PV and PVM are formed during the invasion process by invagination of the host cells membrane and lipids from the rhoptries (section 1.2.1.3). Host proteins are excluded (Aikawa et al., 1981; Atkinson et al., 1988; Dluzewski et al., 1989; McLaren et al., 1977), and parasite proteins and lipids are integrated into the newly formed PVM (Bannister and Dluzewski, 1990; Dluzewski et al., 1992; Joiner, 1991; Lauer et al., 2000; Mikkelsen et al., 1988; Murphy et al., 2006). It is poorly understood how the *Plasmodium* parasites contribute to the PVM formation (Goldberg and Zimmerberg, 2020; Lingelbach and Joiner, 1998; Spielmann et al., 2012). However, in *Toxoplasma gondii* the formation of the PVM is supported by the secretion of the rhoptries and dense granules (Mercier et al., 2005) (section 1.2.2.1.1).

The PVM separates the host cells cytosol from the parasite and must be crossed for nutrient influx, waste disposal and export of parasite proteins. An important mediator for this is EXP2, a channel forming integral membrane protein. Depending also on exported protein 1 (EXP1), a nutrient channel is formed for molecules up to 1.4 kDa (Desai et al., 1993; Desai and Rosenberg, 1997; Garten et al., 2018) to promote nutrient influx (Figure 7.4). Additionally, EXP2 together with other proteins can form a complex that functions as a translocon in the PVM for protein export (Figure 7.2; section 1.2.2.3). Furthermore, rhoptry neck protein 3 (RON3) seems to be important for the formation of the nutrient channel and protein export (Low et al., 2019). For the intake of larger molecules (especially hemoglobin), the parasite forms a cytostome at the PVM to accomplish endocytosis, involving invagination of both, the PVM and PPM (Aikawa et al., 1966; Lazarus et al., 2008; Spielmann et al., 2020). It was discovered only recently that the Kelch 13 complex is located at the sites of cytostome formation where it functions in endocytosis and plays a major role in artemisinin resistance (Birnbaum et al., 2020).

Other proteins of the PVM worth mentioning are members of the early transcribed membrane protein (ETRAMP) family (Spielmann et al., 2003). The functions of ETRAMPs are still unknown (Cronshagen, 2020; Spielmann et al., 2012) even though these proteins are found in the PVM in extremely high quantities (Spielmann et al., 2006a). Knockouts of several *etramps* did not show an effect on the parasite's growth *in vitro* (Cronshagen, 2020).

1.2.2.3 EXPORT

Parasite proteins, unlike those from intracellular organisms without a PV/PVM, must traverse an additional membrane to enter the host cell. Initially, all exported proteins undergo secretion into the PV before they are exported (Figure 7.1). *Plasmodium*'s secretion mechanism parallels that of other organisms (Beck and Ho, 2021). Proteins targeted for secretion contain a signal peptide sequence (SP) in their N-terminal region that mediates insertion into the ER and directs them to the secretory system. After a processing step cleaving off the SP, the mature exported proteins are transported from the ER to the Golgi apparatus from where they get transported to the PV. The PV is believed to be the default destination and no extra sorting information is needed for a protein to reach that compartment (Adisa et al., 2003; Waller et al., 2000). In the PV resident proteins remain whereas proteins destined for the host cell are translocated beyond the PVM (Figure 7.2).

Most known proteins destined for export contain a *Plasmodium* export element (PEXEL) (a pentameric motif (RxLxE/Q/D)) usually found ~20 residues after a frequently recessed signal

peptide for ER entry (Hiller et al., 2004; Marti et al., 2004). In the ER, the PEXEL motif is recognized and cleaved after the leucine prior to N-terminal acetylation by the aspartic protease plasmepsin V (Boddey et al., 2013; Chang et al., 2008; Russo et al., 2010). However, some exported proteins do not contain a PEXEL motif and are termed PEXEL-negative exported proteins (PNEPs) (Heiber et al., 2013; Spielmann et al., 2006b). The majority of the PNEPs contain a transmembrane domain at the N-terminus and some even lack a SP, presumably using the transmembrane domain as an ER entry signal. Initially, the number of PNEP proteins was predicted to be rather small and only an exception to the more common PEXEL proteins (Spielmann and Gilberger, 2010). But more and more proteins are discovered that are exported and do not contain a PEXEL motif (Heiber et al., 2013). Furthermore, proteins were identified that contain a PEXEL motif but are not exported like unregulated infected sporozoite 2 (UIS2) (Fierro et al., 2023; Fréville et al., 2024; Khosh-Naucke et al., 2018; Schnider et al., 2018; van Ooij et al., 2008). How PEXEL and PNEP proteins are recognized and sorted within the secretion pathway is not clear, but there may be differences to other proteins already during ER entry (Marapana et al., 2018) while otherwise brefeldin A sensitive (Wickham et al., 2001) default transport to the PV may be used.

Exported proteins within the PV are unfolded prior to translocation to the host cell (Figure 7.2). Reporter proteins, that were fused to the mouse dihydrofolate reductase (mDHFR), a domain that upon addition of a ligand (WR) prevents its unfolding (Eilers and Schatz, 1986), were blocked in transport and not exported to the host cell (Gehde et al., 2009; Grüning et al., 2012; Heiber et al., 2013; Mesén-Ramírez et al., 2016). After unfolding, exported proteins are translocated to the host cell via the *Plasmodium* translocon of exported proteins (PTEX) (Beck et al., 2014; de Koning-Ward et al., 2009; Elsworth et al., 2014; Ho et al., 2018) and subsequently folded in the host cell (Figure 7.3).

The synthesis of PTEX components primarily happens in the trophozoite and schizont stage and are stored in the secretory organelles. Right after or during invasion PTEX is deposited into the PVM by the discharge of dense granules (Bullen et al., 2012). Hence, the parasite is capable of exporting proteins immediately after invasion, at the beginning of the ring stage.

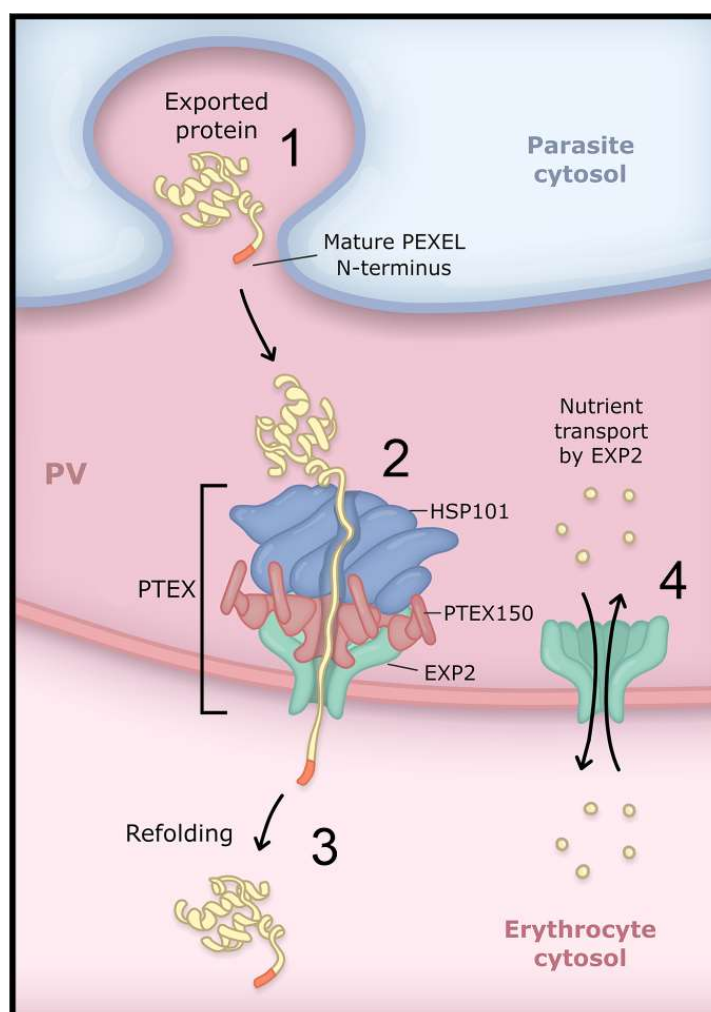


Figure 7: Export and nutrient uptake from the host cell cytosol across the PV. (1-3) Illustration of the export of a PEXEL protein. (1) Exported proteins reach the PV in vesicle via the secretory pathway. (2) The mature N-terminus of a PEXEL protein is recognized and fed to the PTEX channel and translocated to the host cells cytosol. Proteins are unfolded for the translocation and (3) refolded in the host cell cytosol. PTEX complex formed by HSP101, PTEX150 and EXP2. (4) Nutrient import from the host cells cytosol to the PV through the nutrient channel formed by EXP2. PEXEL: *Plasmodium* export element; PV: parasitophorous vacuole; HSP101: Heat shock protein 101; PTEX150: *Plasmodium* translocon of exported proteins 150; EXP2: Exported protein 2. (Figure modified from (figure from Beck and Ho, 2021).

A key component of the PTEX translocon is the pore forming single pass transmembrane protein EXP2 (de Koning-Ward et al., 2009). The C-terminus of EXP2 projects into the cytosol of the infected erythrocyte and the N-terminus into the PV lumen (Ho et al., 2018; Sanders et al., 2019). Another structurally important component for PTEX is PTEX150 which forms a stable complex with EXP2 and interacts with HSP101, the third important component (Bullen et al., 2012). HSP101 is a ClpB-like AAA⁺ ATPase that probably unfolds the exported protein before passage through the pore and feeds it to the EXP2-PTEX150 funnel. The three components form the PTEX complex in a 6:7:7 ratio (HSP101:EXP2:PTEX150) (Ho et al., 2018). Recent work suggests that the subcomplex formation of EXP2 and PTEX150 is HSP101-

independent and that HSP101 has a dual localization in the PV and the ER, possibly recruiting the cargo for export already in the ER (Elsworth et al., 2016; Gabriela et al., 2022). Furthermore, the PTEX complex contains the accessory proteins TRX2, a thioredoxin that could help in unfolding of the proteins and PTEX88, a novel protein with no homologies outside of the *Plasmodium* genus (de Koning-Ward et al., 2009). TRX2 and PTEX88 are not essential for protein export but might contribute to virulence and cytoadherence (Chisholm et al., 2016; Matz et al., 2015). Proteins destined for export are funneled into the PTEX channel, subsequently being translocated into the cytosol of the host cell to effectuate or facilitate remodeling processes. A further complex termed Exported Protein-Interacting Complex (EPIC) was recently identified in the PV (Batinovic et al., 2017) and postulated to be important for the transport of PfEMP1 (section 1.3.2.3.1).

1.2.2.4 HOST CELL MODIFICATION

The erythrocyte is a unique habitat for an intracellular parasitic organism. It lacks the organelles with the accompanying molecular machinery for protein and lipid synthesis and transport (Moras et al., 2017) that could be hijacked for the parasite's use. Also, the erythrocyte membrane has suboptimal permeability properties to permit the import of the nutrients the parasite needs for its proliferation (Dhangadamajhi et al., 2010). For this reason, the parasites must spend a significant amount of their energy and proteome into remodeling the erythrocyte. Around 10 % of the proteins encoded in the genome of *P. falciparum* is exported and contributes to the modification of the host cell (Spielmann and Gilberger, 2015). Exported proteins orchestrate the generation of the Maurer's clefts (section 1.2.2.4.1), membranous structures believed to organize proteins to then form the knobs at the host cell membrane (section 1.2.2.4.1) that likely have the sole purpose to concentrate and present variant surface antigens (VSAs) (section 1.3) on the erythrocyte's surface and increase nutrient influx (section 1.2.2.4.2). For the latter, proteins are organized for the parasite's increased erythrocyte's membrane permeability by the generation of a new permeability pathway to promote the influx of nutrients from the host blood plasma (section 1.2.2.4.2).

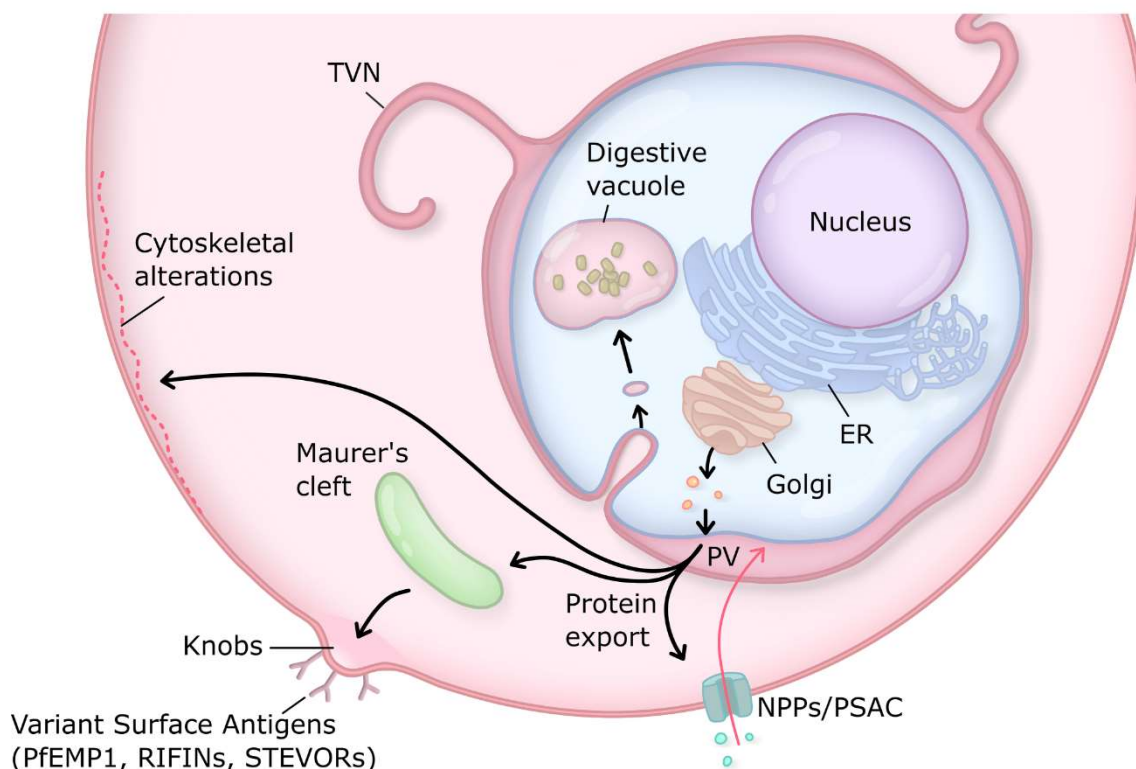


Figure 8: Host cell modifications. Illustration shows a trophozoite parasite with host cell modifications. Exported proteins during the ring stage modify the erythrocyte cytoskeleton, generate Maurer's clefts, the PSAC channel and knob. Variant surface antigens are presented at the knobs. Black arrows outwards: Protein secretion and export; Black arrows towards the digestive vacuole: Endocytosis pathway; ER: Endoplasmatic reticulum; PV: Parasitophorous vacuole; TVN: Tubovesicular network; NPP: New permeability pathways; PSAC: Plasmoidal surface anion channel. (Figure modified from Beck and Ho, 2021).

1.2.2.4.1 MAURER'S CLEFTS

Maurer's clefts were already described in 1902 by Georg Maurer (Maurer, 1902) since these can be detected in Giemsa stained infected erythrocytes in thin blood smears. Maurer's clefts are comparably large membranous structures in the host cells cytosol often proximal to the erythrocyte membrane (Figure 8; Figure 6) (Hanssen et al., 2008). More than a century after their discovery, the exact function of the Maurer's clefts and the proteins localized to them are still unresolved. Most likely Maurer's clefts are sorting centers for exported proteins to direct them to their final destination in the host cell and possibly they may serve to pre-assemble functional complexes (Mundwiler-Pachlatko and Beck, 2013).

Maurer's clefts are formed early in the ring stage surrounded by a single membrane (Grüning et al., 2011; Hanssen et al., 2008). In thin sections, they appear as slender flattened or circular structures with an electron dense coat that in three dimensions were revealed as flattened circular disks (Henrich et al., 2009; Langreth et al., 1978). The Maurer's clefts may originate from the PVM (Aikawa et al., 1975; Atkinson et al., 1987; Kara et al., 1988). Morphology and

number of Maurer's clefts differ in different parasite strains: 3D7 mostly shows long and slender Maurer's clefts while in D10, Dd2, HB3, NF54, and FCQ-27 strains multiple stacked lamellae can be observed (Mundwiler-Pachlatko and Beck, 2013). Connections of the Maurer's clefts to other Maurer's clefts, PVM and erythrocyte membrane have been observed, named tethers, (Hanssen et al., 2008; Pachlatko et al., 2010; Wickert et al., 2004, 2003) which tether the Maurer's clefts to the erythrocyte membrane (Pachlatko et al., 2010). Other work suggested a connection of the Maurer's clefts to host cell actin (Cyrklaff et al., 2011; Rug et al., 2014). The Maurer's clefts remain constant in number from the point they can be detected with markers (1.5 hpi) and are highly mobile until they become fixed in position during the transition to the trophozoite stage (Grüning et al., 2011). This fixed position coincides with the presentation of PfEMP1 and cytoadherence of the infected erythrocytes (section 1.3) (Kriek et al., 2003; McMillan et al., 2013).

Many exported proteins are localized to or pass through the Maurer's clefts. Ring exported protein 1 (REX1) is exported and localized to the host cell shortly after invasion (~2 hpi), followed by the skeleton binding protein 1 (SBP1) and membrane associated histidine rich protein 1 (MAHRP1) shortly after (Grüning et al., 2011; McMillan et al., 2013). REX1 is relevant for the structural integrity of the Maurer's clefts (Dixon et al., 2008). Examples of proteins that do not directly localize to the Maurer's clefts are membrane associated histidine rich protein 2 (MARHP2) (Pachlatko et al., 2010) which is localized proximal to the Maurer's clefts at the tethers, HSP40 and HSP70x which is located in foci termed J-dots (Petersen et al., 2016) and the soluble ring exported protein 3 (REX3) in the host cells cytosol (Spielmann et al., 2006b). Proteins such as the knob resident knob-associated histidine-rich protein (KAHRP) and the VSAs transiently localize to the Maurer's clefts before further transport to the host cell membrane (Wickham et al., 2001).

1.2.2.4.2 PLASMODIAL SURFACE ANION CHANNEL

Around 14 hours after infection the erythrocytes membrane increases the permeability for nutrients (Beck and Ho, 2021; Desai, 2014; Desai et al., 2000; Elford et al., 1985; Ginsburg et al., 1985; Homewood and Neame, 1974). Thereby, the parasites obtain increased access to nutrients in the extracellular space of the infected erythrocytes (*in vitro*: medium; *in vivo*: blood plasma). While permeability for anions and antimalarials are increased, the cation (Ca^{2+} , Na^{+}) permeability is not altered to prevent osmotic lysis (Cohn et al., 2003; Henshall and Spielmann, 2023). The plasmodial surface anion channel (PSAC) was identified as an important component for this increased permeability of the host cells membrane (Desai, 2014; Desai et al., 2000).

However, as it is unclear whether PSAC is the only parasite derived channel in the host cells membrane or not, the increased permeability is sometimes more generally referred to as the new permeability pathway (NPP).

One contributor to PSAC activity is CLAG3 which is mutually exclusively expressed from two copies in the genome (*clag3.1* and *clag3.2*) and is integrated into the host cell membrane (Nguitrugool et al., 2011). The proteins RhopH2 and RhopH3 form a complex with CLAG3 and participate in PSAC activity (Counihan et al., 2017; Ito et al., 2017; Sherling et al., 2017). It was shown that these three proteins are trafficked in a soluble complex (termed RhopH complex), with RHopH2 and RhopH3 (Ho et al., 2021; Schureck et al., 2021) (Beck and Ho, 2021). However, none of these proteins individually or taken together seem to have the typical characteristics to form functional ion-channels (Alkhalil et al., 2004; Gupta et al., 2020; Henshall and Spielmann, 2023). Nevertheless, the export and function of these proteins is to be essential for the parasite's nutrient acquisition. Interestingly, knockout of the *clag3* genes did not lead to the parasite's death *in vitro*, possibly due to the high concentrations of nutrients in the culture medium (Gupta et al., 2020). While the amino acid uptake of erythrocytes is negligible (Kirk and Saliba, 2007), the glucose permeability of infected erythrocytes is primary through the human glucose transporter 1 (hGLUT1) (Kirk et al., 1996; Roth, 1987). How the active PSAC channel is constituted and organized in the erythrocyte membrane remains unsolved.

1.2.2.4.3 KNOBS

Early ultrastructural investigations of *P. falciparum* parasites, small protrusions on the surface of infected erythrocytes were discovered and termed knobs (Trager et al., 1966). The knobs are cup-shaped structures with a diameter of 50 to 120 nm and a height of 2 to 20 nm (Gruenberg et al., 1983; Quadt et al., 2012) and evenly distributed on the membrane of the infected erythrocytes (Rug et al., 2006) (Figure 6 and Figure 8). The knobs are formed around 24 hpi (Looker et al., 2019). A significant portion of the proteins exported by *P. falciparum* parasites appears to be primarily dedicated to enable the transport and presentation of the main virulence factor PfEMP1 (section 1.3.2) on these knobs. This specialized property may explain the larger repertoire of exported proteins in *P. falciparum* compared to other *Plasmodium* species, which show no or lower levels of cytoadherence (Craig et al., 2012) (section 1.3).

The PEXEL-positive knob-associated histidine-rich protein (KAHRP) is present in high concentrations in the knobs (Kilejian, 1979) and is responsible for the physical knob structure and essential for their formation (Rug et al., 2006). Furthermore, KAHRP alters the rigidity of

the erythrocytes (Glenister et al., 2002). Parasites that lack KAHRP do not form knobs and cannot cytoadhere under flow conditions (Crabb et al., 1997; Rug et al., 2006). An electron dense spiral scaffold that underlies the knobs that connects to the cytoskeleton of the erythrocyte was discovered using electron microscopy (Watermeyer et al., 2016) but KAHRP does not seem to constitute this spiral scaffold but rather coats it (Looker et al., 2019). It was suggested that KAHRP is anchored to the host cell protein as interactions have been shown to actin, spectrin and ankyrin (Kilejian et al., 1991; Magowan et al., 2000; Pei et al., 2005; Weng et al., 2014).

Two additional proteins have been shown to contribute to the knob formation, a PHIST domain protein (PF3D7_0424600) and Hsp40-like DNAJ Type IV protein (Maier et al., 2008). Furthermore, the PHIST domain proteins PF3D7_0532400 (Oberli *et al.*, 2014) and PF3D7_0936800 (Mayer et al., 2012), knob-associated Hsp40 (KAHSP40) (Acharya et al., 2012), Pf332 (Hinterberg et al., 1994), a SURFIN (Winter et al., 2005) and PfEMP3 (Waterkeyn et al., 2000) were shown to localize to the knobs. The PHIST protein PF3D7_0532400 is important for cytoadherence but not for the formation of the knobs (Proellocks et al., 2014). Recently the proximiome of KAHRP was identified using PerTurboID (Davies et al., 2023) and supported the interaction with most of these proteins including PF3D7_0532400, PF3D7_0936800, KAHSP40, Pf332 and PfEMP3.

There remains a gap in knowledge both in terms of completely identifying the protein constituents of these knobs and in fully elucidating the precise functional roles of the proteins that have been identified. This area represents a significant opportunity for further research to unravel the molecular mechanisms underlying knob formation and function.

1.3 CYTOADHERENCE

Erythrocytes infected by *P. falciparum* exhibit cytoadherent properties mediated by binding to various receptors on endothelial cells (Figure 9). This is believed to be the cause of binding of infected erythrocytes to the wall of blood vessels, a property of post-ring stage blood stage parasites and a diagnostic feature of *P. falciparum* infections that show only ring stages in peripheral circulation (Bachmann et al., 2009). Cytoadherence avoids the splenic clearance of the more rigid post ring stage infected erythrocytes, as erythrocytes normally undergo filtering in the spleen's narrow passages (Bachmann et al., 2009; Cranston et al., 1984; Hommel et al., 1983). An increase in rigidity which happens to infected erythrocytes would lead to their removal and destruction (Langreth and Peterson, 1985; Miller et al., 1994). The sequestration

of infected erythrocytes in the microvasculature can precipitate severe consequences for the host, including localized inflammation and deprived tissue-oxygen supply. In cases where this occurs in venules in the brain, it can lead to cerebral malaria, the most severe form of the disease (Newton et al., 2000).

Additionally, the phenomenon that infected erythrocytes adhere to infected and non-infected erythrocytes (Figure 9) has been documented and is known as autoagglutination and rosetting (Rowe et al., 1997). However, the actual occurrence and biological significance of autoagglutination and rosetting remain topics of dispute (Goel et al., 2015; Wang and Hviid, 2015).

The adherence to endothelial cell receptors is attributed to a large transmembrane protein, *P. falciparum* erythrocyte membrane protein 1 (PfEMP1) (section 1.3.2), displayed at the knobs on the host cell's (Baruch et al., 1995; Leech et al., 1984; Smith et al., 1995; Su et al., 1995) which is encoded by a multigene family, the *var* genes (section 1.3.1).

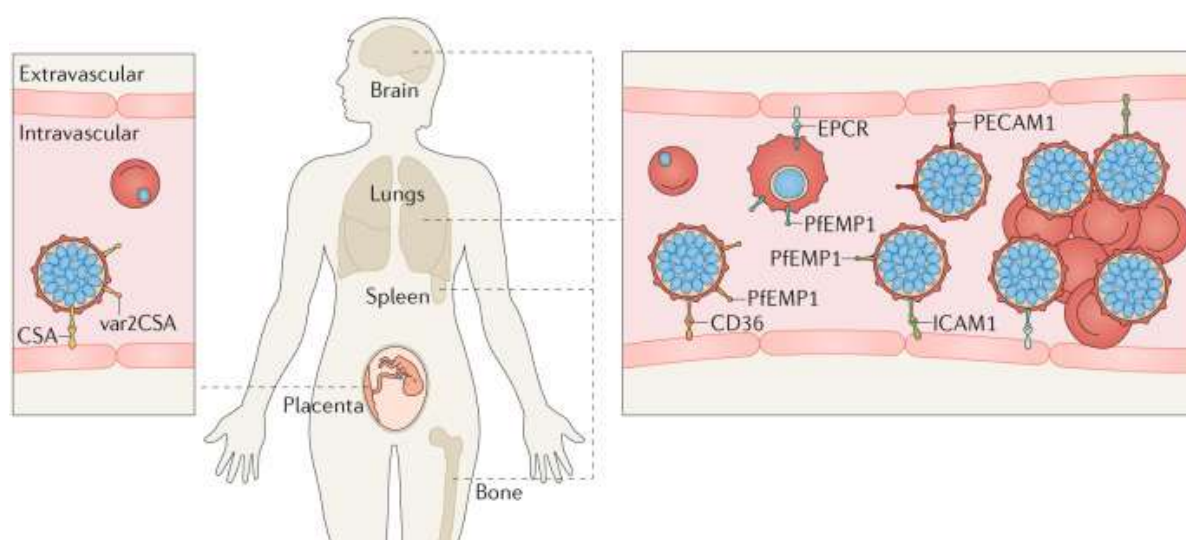


Figure 9: Cytoadherence of infected erythrocytes. Illustration of infected erythrocytes cytoadhering to receptors and CSA of endothelial cells. (Left) Binding of VAR2CSA presented on the surface of trophozoite and schizont infected erythrocytes to CSA in the placenta. (Right) Binding of PfEMP1 variants presented on the surface of trophozoite and schizont infected erythrocytes to EPCR, PECAM1, CD36 and ICAM-1 presented on endothelial cells in the brain, lungs, spleen and bone marrow and to other infected erythrocytes and erythrocytes, leading to blockage of the microvasculature. CD36: cluster of differentiation 36; ICAM-1: Intercellular Adhesion Molecule 1; EPCR: Endothelial Protein C Receptor; PECAM-1: platelet endothelial cell adhesion molecule, CSA: chondroitin sulfate A (figure from Venugopal et al., 2020).

1.3.1 VAR GENES

The *var* genes are the most important family of VSAs in *P. falciparum*. While there are other VSAs such as *rifs* and *stevors*, their roles are less clear but are speculated to also be associated with binding of infected erythrocytes to the endothelium or other erythrocytes, but this is more

uncertain than for *vars* (Wahlgren et al., 2017). Each *P. falciparum* isolate contains around 60 *var* genes in their genome, which are highly susceptible to recombination during the sexual stages (Freitas-Junior et al., 2000), resulting in a vast number of *var* genes observed in natural populations (Otto et al., 2019). The *var* genes contain two exons separated by an intron, while exon 1 is highly variable, exon 2 is more conserved between different *var* genes.



Figure 10: *var* gene groups location on the chromosomes. *var* genes in subtelomeric region transcribed towards the centromere of the chromosome are upsB. *var* genes in the subtelomeric region transcribed towards the telomere are upsA and upsE. *var* genes located at centromeric region of the chromosome are upsB and upsC (Figure modified from Andradi-Brown et al., 2024).

To categorize the countless *vars* they can be classified based on their upstream region (homology in DNA sequence), direction of transcription and chromosomal location into four major types of *var* genes: upsA (group A), upsB (group B), upsC (group C), and upsE (group E) (Figure 10), the latter encompassing only a single *var* gene (*var2csa*). Furthermore, some *var* genes show intermediate characteristics and are grouped into group A/B and group B/C (Gardner et al., 2002; Lavstsen et al., 2003; Mercereau-Puijalon et al., 2002; Voss et al., 2000). Group E, A and B *var* genes can be found in subtelomeric regions transcribed in opposite directions. The central chromosome regions contain upsB and upsC *var* genes. *var1csa* (also sometimes termed *var1*), *var2csa* and *var3* are the only *var* gene conserved across strains (Dimonte et al., 2020; Rowe et al., 2002; Salanti et al., 2003, 2002; Sander et al., 2009; Trimnell et al., 2006) of which only *var2csa* was shown to be functionally expressed. It is expressed in female patients with pregnancy malaria, mediating binding of infected erythrocytes to CSA, abundant in the placenta (Duffy et al., 2005; Elliott et al., 2005; Gamain et al., 2005; Salanti et al., 2004, 2003; Viebig et al., 2007). *var1csa* is often conserved as a pseudogene (e.g. IT4 strain: premature stop codon; disrupted ATS domain) which does not reach the erythrocyte's surface (Kyes et al., 2003). *var3*, classified into group A, is a very short and unusual *var* gene with unknown binding properties (Zhang et al., 2014).

The expression of *vars* is mutually exclusive, meaning that at a given time an individual parasite expresses only a single *var* gene while the rest of the *var* genes are transcriptionally silenced (Kyes et al., 2007; Voss et al., 2006). How the mutually exclusive expression of *var* genes is regulated appears to be a complex, multi-layered mechanism that is still subject to research. It

is suspected that cis-acting DNA elements and non-coding RNA transcripts as well as epigenetic modifications and subnuclear organization play a role in the orchestration of mutually exclusive expression (Deitsch and Dzikowski, 2017). It was shown that active *var* genes are found in less electron dense regions of the nucleus, while the other *vars* stay in the periphery of the nucleus with electron-dense heterochromatin (Kyes et al., 2007). Furthermore, in patients there is a predominant expression of a single *var* gene in the parasite population due to selective pressure of the immune system (Bachmann et al., 2019, 2016; Barry et al., 2007; Bull et al., 1998; Bull and Marsh, 2002; Wang et al., 2009; Warimwe et al., 2009).

This intricate expression mechanism utilized by the parasite is an evolutionary strategic response to the vulnerability created by presenting its protein, PfEMP1, on the surface of the erythrocyte. This exposure necessitates the parasite's ability to express a range of antigenically distinct PfEMP1 variants from its *var* gene repertoire. When the host immune system identifies and begins targeting a specific PfEMP1 variant, the parasite shifts to expressing a different PfEMP1 variant from its *var* gene repertoire. In theory, this strategy allows continuous evasion of the host's antibody-mediated immune defenses although the *in vivo* situation is often more complex and classical waves of single antigenic types such as those originally thought to occur in *Trypanosoma* (but now have turned out to also be more complex) (McCulloch et al., 2017), are even less obvious in natural malaria parasites infections (Bachmann et al., 2019). To prevent premature exhaustion of the *var* gene repertoire switching of *var* genes happens with a rather low rate (Horrocks et al., 2004; Roberts et al., 1992; Ye et al., 2015). Thereby, long lasting infections of a single parasite isolate can be maintained (Ashley and White, 2014). Interestingly, *var* gene switching was shown to follow a loose hierarchy rather than a strict sequence of *var* genes (Bachmann et al., 2011; Recker et al., 2011).

Initial infection with *P. falciparum* in malaria-naive individuals shows broad expression of *var* genes, primarily group B, but shifts toward group A or A/B in severe disease (Bachmann et al., 2019). In individuals with recurrent exposures to the disease *var* gene expression seems to shift towards group C. This expression pattern, influenced by host immunity, affects disease severity and parasite transmission, with changes in expression types and adherence properties occurring over the course of infection. In instances of severe malaria, particularly among individuals with no previous exposure to the disease, there is a notable prevalence of group A *var* genes (reviewed in Bachmann et al., 2022). *In vitro* nevertheless, *var* gene expression is more heterogenous as there is no selection for specific antigenic phenotypes and group A *var* genes are rarely transcribed due to higher switching rates (Fastman et al., 2012; Janes et al., 2011).

1.3.2 PfEMP1

1.3.2.1 STRUCTURE

PfEMP1 is a rather large protein with a molecular mass ranging between 200 to 350 kDa, depending on the variant (Baruch et al., 1995). Its considerable size contributes to the complexity of studying this molecule. The protein features a highly conserved Acidic Terminal Segment (ATS) domain located at the C-terminus, which is encoded by exon 2 of the *var* gene (Kraemer and Smith, 2006) (Figure 11). While the precise function of the ATS domain remains elusive, it is hypothesized to play a critical role in anchoring PfEMP1 to the knobs (Crabb et al., 1997; Mayer et al., 2012). Although PfEMP1 and KAHRP both localize within these knobs, leading to the initial speculation of their interaction (Crabb et al., 1997). It is possible that KAHRP, which is essential for proper knob formation (Looker et al., 2019; Rug et al., 2006; Wickham et al., 2001), may be needed for generating the knob but that PfEMP1 is anchored to different proteins within the overall knob structure.

Exon 1 of *var* genes encodes a transmembrane domain that extends across the erythrocyte membrane, a semi-conserved N-terminal segment (NTS) and a succession of highly variable extracellular domains, which are referred to as binding domains (Figure 11). Notably, the NTS domain does not feature a SP but includes a PEXEL-like sequence (RNVLE) and appears to be structurally significant for the protein's most N-terminal binding domain (Juillerat et al., 2011). In line with that idea, it was shown that the PEXEL-like motif is not processed by plasmepsin V and PfEMP1 were therefore re-classified as PNEPs (Boddey et al., 2013). The diverse extracellular domains of PfEMP1 exhibit distinct binding affinities, which enable the protein to attach to endothelial receptors within the host's vascular system.

1.3.2.2 EXTRACELLULAR BINDING DOMAINS

While the scientific literature contains reports of a broad range of receptors as potential interaction partners for PfEMP1, concrete evidence of binding is limited to a relatively small number. These experimentally well-established PfEMP1 interacting receptors, include cluster of differentiation 36 (CD36) (Robinson et al., 2003), intercellular adhesion molecule 1 (ICAM-1) (Bengtsson et al., 2013; Smith et al., 2000), endothelial protein C receptor (EPCR) (Turner et al., 2013), platelet endothelial cell adhesion molecule 1 (PECAM-1) (Joergensen et al., 2010), and the globular C1q receptor (gC1qR) (Biswas et al., 2007). Below only the first three of these

receptors are addressed as well as the glycoprotein CSA that only VAR2CSA binds to (Figure 9), as their interaction with PfEMP1 is the best studied.

Due to the high recombination rates of *var* genes, PfEMP1's extracellular regions display a large repertoire of domain structures and combinations (Otto et al., 2019; Rask et al., 2010). These domains are composed of Duffy binding-like (DBL) domains and cysteine-rich interdomain region (CIDR) domains (Kraemer *et al.*, 2006). DBL domains are divided into seven main categories: α , β , γ , δ , ϵ , ζ and PAM. Similarly, CIDR domains are classified into five major types: α , β , γ , δ , and PAM (Gardner et al., 2002; Rask et al., 2010; Smith et al., 2000). These domains were subcategorized further in the past decades, distinguished by numbers (e.g. $\alpha 1.1$). In smaller PfEMP1 variants, DBL and CIDR domains appear exclusively in tandems, while in larger variants, multiple tandem pairs are accompanied by an additional DBL domain (Rask et al., 2010; Smith, 2014) (Figure 11A).

Certain extracellular domains are recurrently found together in different PfEMP1 variants (Rask et al., 2010). The organization of these binding domains in PfEMP1 can be grouped into specific configurations known as domain cassettes that seem to stay together during recombination events and could act as breaking points for these. To this day, 22 domain cassettes have been identified (Bengtsson et al., 2013; Rask et al., 2010). Notable examples include DC8 and DC13, which are commonly observed in patients suffering from severe malaria and were experimentally shown to bind to EPCR (Avril et al., 2016; Turner et al., 2013).

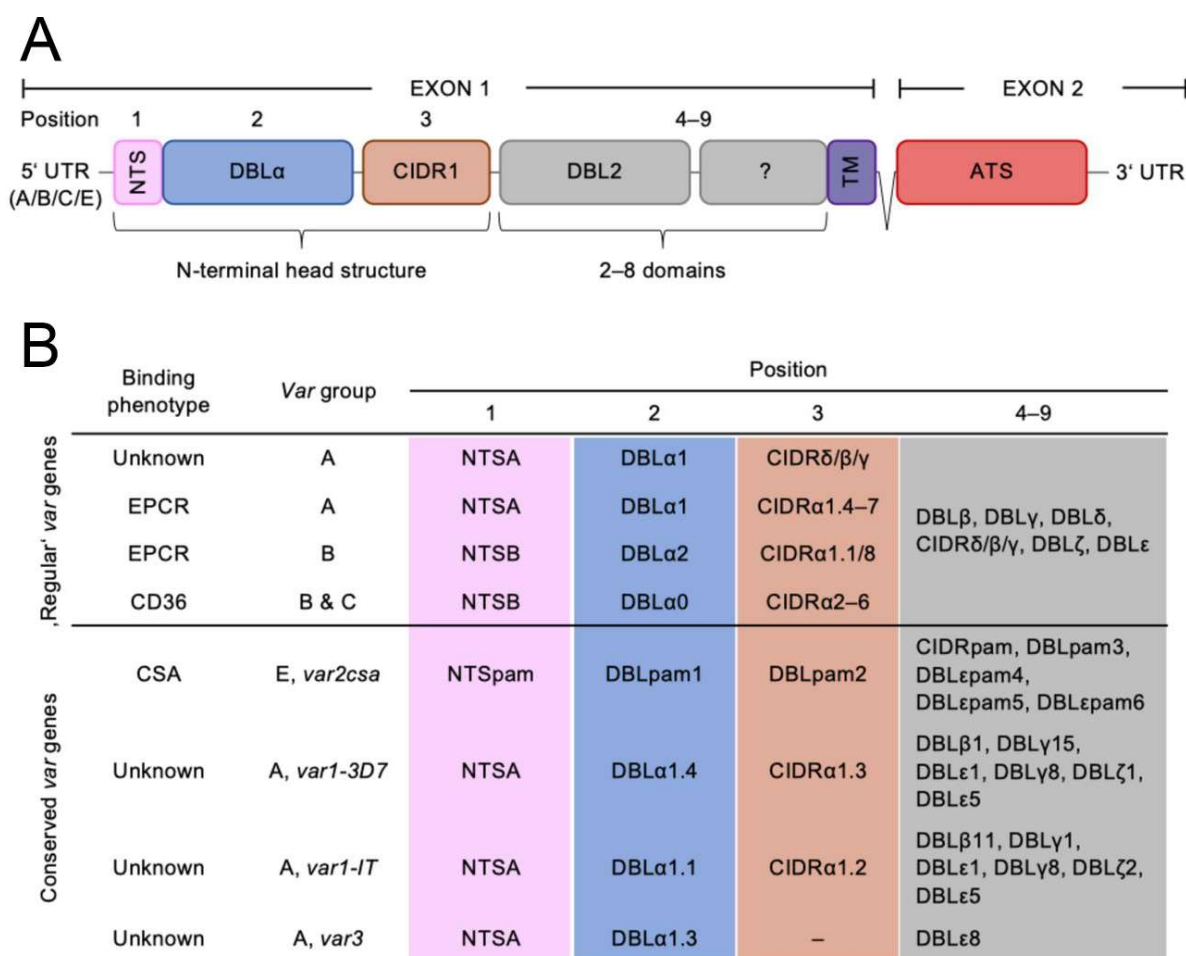


Figure 11: PfEMP1 structure, binding domains and interacting receptors. (A) Structure of PfEMP1. Exon 1: Position 1: NTS domain; Position 2-3: Domains in the head structure; Position 4-9: Domains after the head structure (number varies); TM: Transmembrane domain. Exon 2: Intracellular ATS domain. (B) Table shows binding phenotypes of “regular” and conserved *var* genes with the concurrent domains in position 1-9. NTS: N-terminal segment; TM: Transmembrane domain; ATS: Intracellular c-terminal domain; DBL: Duffy Binding-Like; CIDR: cysteine-rich interdomain region. (Figure modified from Andradi-Brown et al., 2024).

Shortly after the discovery of PfEMP1, it was observed that erythrocytes infected by the malaria parasite in pregnant women specifically bind to CSA in the placenta (Buffet et al., 1999; Fried and Duffy, 1996; Salanti et al., 2004). *In vitro* studies, where parasites were selected for binding to CSA, consistently showed an upregulated expression of a single *var* gene, *var2csa* (Scherf et al., 1998). This gene is unique in its conservation across different *P. falciparum* strains and contains distinct binding domains, named DBLpam and CIDRpam, which exclusively bind to CSA (Figure 11B). This selective binding reflects a particular adaptation of the malaria parasite to the placental environment in pregnant women.

The common binding target for CIDR domains, specifically those in group B and C PfEMP1s, is CD36 which makes up the majority of PfEMP1 variants. Between 75-80% of PfEMP1 variants contain a CIDR α 2-6 domain that promotes CD36 binding and typically appear in

tandem with a DBL α 0 domain (Figure 11B). Group B and C PfEMP1s that bind to CD36 are more present in patients with mild malaria. The large number of CD36-binding PfEMP1 variants could be due to a potential benefit for binding this receptor for both the parasite and host. These variants enable the parasite to bind effectively to host cells and avoid immune detection, while also regulating the host's immune response and cytokine production, leading to a balance that allows parasite survival and transmission without severely harming the host (reviewed in Bachmann et al., 2022).

Only in the last decade it was discovered that there are PfEMP1 variants that can bind to EPCR. The domains identified to bind EPCR are CIDR α 1.1/1.4-8 (Bachmann et al., 2022; Turner et al., 2013). These domains can be found in group A and B PfEMP1s and appear in tandem with DBL α domains in the head structure of the PfEMP1 (Figure 11B), found among others in DC8 and DC13 domain cassettes. Other members of group A PfEMP1s accommodate CIDR β / γ / δ domains with unknown binding interactors (Figure 11B) but also are present in patients with severe cases of malaria (Jensen et al., 2004).

CD36 binding domains in group B and C and EPCR binding domains in group A can co-occur with ICAM-1 binding domains resulting in dual binding properties (Figure 11B). Especially dual binding of EPCR and ICAM-1 seems to increase the binding under shear stress (Bernabeu et al., 2019; Lennartz et al., 2017). ICAM-1 binding is predominantly facilitated by DBL β domains located after the tandem head structure, primarily by DBL β 5 in group B and C PfEMP1s and DBL β 3 in group A PfEMP1s (Bengtsson et al., 2013; Howell et al., 2008; Lennartz et al., 2019, 2017; Oleinikov et al., 2009; Smith et al., 2000). The position of the ICAM-1 binding domains further away from the head structure can be explained by the relatively large size of ICAM-1. ICAM-1 reaches further out of the glycocalyx than, e.g. CD36 and therefore may be more accessible to the domains in position 4 and 5 (Figure 11A, B). The binding of PfEMP1 variants to EPCR and ICAM-1 has been associated with the severest manifestations of malaria, including cerebral malaria.

In summary, while the diverse domain structures and combinations in PfEMP1 variants illustrate the complex molecular mechanism underlying malaria pathogenesis, the precise binding properties, and the roles of the associated domains, remain elusive. This complexity underscores the intricate and still not fully understood interactions between the malaria parasite and its human host. A key problem, besides the difficulties in obtaining insights into the *in vivo* situation, is the fact that it is difficult to obtain parasites expressing only one particular PfEMP1 to study its exact binding properties. Furthermore, parasites expressing different PfEMP1 and

regular switching prevent targeted modification of the genome to generate modified PfEMP1 to pinpoint binding properties to specific domain.

1.3.2.3 CELLULAR BIOLOGY OF PfEMP1

The activation of *var* gene transcription occurs in the ring stage, reaching maximum transcript levels approximately 12 hours post invasion (Kyes et al., 2000). Approximately 16 hours after invasion, PfEMP1 is detectable at the Maurer's clefts, where it appears alongside REX1 and SBP1 that are already present in these structures before PfEMP1 (Gardner et al., 1996; Grüning et al., 2011; McMillan et al., 2013). The small disparity in timing between the peak of *var* gene transcript levels and the surface appearance of PfEMP1 on infected erythrocytes suggests a gradual process for the expression and transport of PfEMP1 to the erythrocyte. However, the delay in protein synthesis after the peak of RNA expression was shown for numerous *P. falciparum* proteins and is relatively small for PfEMP1 compared to other proteins (Foth et al., 2011). Interestingly, the amount of PfEMP1 on the surface increases drastically between 16-20 hours post invasion and stagnates afterwards, without being replenished if digested off from the surface (Kriek et al., 2003). A significant PfEMP1 population stays at the Maurer's clefts and only a very small proportion of the total protein population is presented on the surface of the erythrocyte. It was calculated that only approximate three PfEMP1 molecules are presented per knob (Sanchez et al., 2019). Solubilization of the erythrocyte membrane followed by trypsin treatment resulted in the digestion of the C-terminus of PfEMP1, whereas the N-terminus remained unaffected. This pattern suggests that prior to its localization in the knob structures of the infected erythrocyte, PfEMP1 is integrated into the membrane in such a way that the N-terminus is shielded from enzymatic degradation (Kriek et al., 2003).

1.3.2.3.1 PfEMP1 TRANSPORT

The transport and mechanisms of surface display of PfEMP1 are still unclear. The pathway of PfEMP1's transport into the host cell, its subsequent transport to the Maurer's clefts within the host cell's cytosol, and its eventual conveyance to the knob structures followed by display on the host cell surface, remain mostly elusive. A fundamental question revolves around the integration of PfEMP1 into the cellular membrane: is it transported as an integral membrane protein or is it inserted into a membrane later during its transport, possibly only once it arrives at the knobs, i.e. embedded directly at its destination?

It is also unclear if PfEMP1 is exported via the PTEX pathway, paralleling the translocation mechanism observed for other known exported proteins. Inactivation of PTEX components prevents PfEMP1 trafficking, which could indicate that this is the case (Beck et al., 2014; Elsworth et al., 2014). However, as this also blocks transport of many proteins needed for PfEMP1 transport, such as SBP1 and REX1 (Mesén-Ramírez et al., 2016), this could also be a secondary effect. It was also observed that PfEMP1 resides in regions of the PVM that do not overlap with PTEX (Riglar et al., 2013) and a complex termed EPIC was proposed to be involved in PfEMP1 transport in the PV (Batinovic et al., 2017). It is therefore at present unclear whether PfEMP1 is transported via PTEX or not and underscores the need for further investigation into the molecular logistics governing PfEMP1's journey and functional deployment within the host cell.

It has been proposed that PfEMP1 is transported not as an integral membrane protein but in a soluble form, being inserted into the membrane only upon reaching its final destination (Batinovic et al., 2017; Marti and Spielmann, 2013; Papakrivovs et al., 2005; Petersen et al., 2016). J-Dots, mobile structures within the host cell, are implicated in this transport process, potentially serving as intermediate transporters that facilitate the transport of PfEMP1 to Maurer's clefts and/or erythrocyte membrane (Petersen et al., 2016). Proteins residing in these structures have been identified to influence cytoadherence, underscoring their significance in the efficient surface transport of PfEMP1 (Charnaud et al., 2017; Külzer et al., 2012).

Some work on the transport of PfEMP1 was done with episomally expressed chimeric mini-PfEMP1s (Batinovic et al., 2017; McMillan et al., 2013; Melcher et al., 2010) 7). This was a valuable approach at that time but likely does not fully reflect the properties of the much larger endogenous PfEMP1. The overexpression and chimeric product can lead to incorrect localization patterns, e.g. a necklace-bead-like localization of the mini-PfEMP1 was observed in the PV which was not detected by other publications (McMillan et al., 2013).

1.3.2.3.2 PROTEINS INFLUENCING CYTOADHERENCE

Some exported proteins have been detected that are essential for the transport of PfEMP1 to the erythrocyte surface and/or PfEMP1-mediated binding. The knockout of the prominent Maurer's clefts resident SBP1 ablated PfEMP1 surface presentation and cytoadherence (Cooke et al., 2006; Maier et al., 2007). Knockout of REX1 leads to severe defects in Maurer's cleft morphology with stacked cisternae (Hawthorne et al., 2004). Furthermore, PfEMP1 surface presentation and binding was reduced in Δ REX1 parasites (McHugh et al., 2015). Also MAHRP1 knockout parasites showed a defect in PfEMP1 surface transport and CD36-binding

(Spycher et al., 2008). Furthermore, an extensive study by Maier *et al.* (2008) identified a PHIST protein (PF3D7_0424600) and six exported proteins that upon disruption reduced PfEMP1-mediated binding and hence were termed PfEMP1 transport proteins 1-6 (PTP1-6). Additionally, the knockout of these proteins influenced PfEMP1 surface presentation and the rigidity of the host cell. The best characterized of these proteins is PTP1. Its knockout led to full depletion of PfEMP1 from the surface, changed Maurer's clefts morphology and had an effect on actin remodeling (Rug et al., 2014). Recently, PTP7 has been identified as a further Maurer's clefts resident that is essential for PfEMP1 presentation (Carmo et al., 2022). The disruption of PTP7 ablates PfEMP1 surface presentation and leads to vesicle-like structures proximal to the Maurer's clefts that contain PfEMP1.

Additionally, it was shown that cytoadherence of infected erythrocytes is influenced by the PHIST protein LyMP (PF3D7_0532400) (Oberli et al., 2016; Proellocks et al., 2014), the J-Dot proteins HSP70x (PF3D7_0831700) and HSP40s (PF3D7_0113700) which might form a complex with PfEMP1 during transport (Charnaud et al., 2017; Diehl et al., 2021; Külzer et al., 2012) and PfEMP3 (Waterkeyn et al., 2000).

1.3.2.4 CHALLENGES TO STUDY PFEMP1

Studying *var* genes and PfEMP1, is challenging due to their complex genetic regulation, high variability, and antigenic variation. *In vitro* research is especially complicated by mixed *var* gene expression or *in vitro* parasite populations, obscuring functional insights and trackability of individual PfEMP1s. Additionally, the large size of PfEMP1 and the poorly understood function and organization of other exported proteins influencing PfEMP1 function present major obstacles in understanding the intracellular transport and surface presentation of PfEMP1.

1.4 AIMS

This thesis aims to address challenges associated with studying *var* genes and PfEMP1 by employing selection linked integration (SLI) (Birnbaum et al., 2017) to generate culture parasites all expressing a PfEMP1 of choice that can be tracked using a small epitope tag. This will then be exploited to assess the binding properties of particular PfEMP1s and to generate modified PfEMP1 expressed in all parasites to study its transport.

The second part of this thesis aims to identify the interactome of functional, endogenously expressed PfEMP1 within living cells. By testing various biotinylation techniques such as BioID, miniTurbo, and DiQ-BioID, PfEMP1 proximal proteins will be biotinylated and identified via mass spectrometry. The resultant analysis of proximal proteins is expected to reveal new PfEMP1 interactors needed for its function. These newly identified interactors will then be subjected to functional disruption using a second version of SLI, termed SLI2, which allows for additional endogenous modifications in the parasite lines expressing a specific PfEMP1 variant and characterization of the interacting candidate.

This thesis is expected to generate tools facilitating PfEMP1 research, providing novel tools and insights into the most important virulence factor of the parasite.

2 MATERIAL AND METHODS

2.1 MATERIAL

2.1.1 TECHNICAL DEVICES

Table 1: List of technical devices

Device	Specification	Brand
Agarose gel chamber	Sub Cell GT basic	Bio-Rad, München
Analytical Balance	870	Kern
Bacterial incubator	Thermo function line	Heraeus, Hannover
Bioanalyser	Agilent 2100	Agilent Technologies
Cell culture incubator	Binder Incubator BD 400	Binder GmbH, Tuttlingen
	Heratherm IGS400	Thermo Scientific, Langenselbold
	Function Line	Heraeus, Hannover
Centrifuges	Megafuge 1.0R	Heraeus, Hannover
	J2- HS Ultracentrifuge	
	JA-12	
	Avanti J-26S XP Rotor	Beckman Coulter, Krefeld
	JA-14	
	5415D	Eppendorf, Hamburg
	Butterfly	Thermo Scientific, Schwerte
Counting chamber	Neubauer Imp. 0,1mm	Roth
Fluorescence Microscope	Axioscope M1, M2	Zeiss, Jena
Gel imaging system	ChemiDoc XRS imaging system	Bio-Rad, München

Device	Specification	Brand
Ice machine	EF 156 easy fit	Scotsmann, Vernon Hills/USA
Inversed microscope	EVOS XL	Thermo Fisher Scientific
Laboratory scale	Atilon	Acculab Sartorius, Göttingen
Light Microscope	Axio Lab A1	Zeiss, Jena
Mass spectrometer	Orbitrap Fusion	Thermo Fisher Scientific
Microscope digital camera	Orca C4742-95	Hamamatsu Phototonics K.K., Japan
Microwave	Micro 750W	Whirlpool, China
Nano-flow	Easy-nLC 1000	Thermo Fisher Scientific
PCR Mastercycler	EP gradient	Eppendorf, Hamburg
pH-meter	SevenEasy	Mettler-Toledo, Gießen
Photometer	NanoDrop 2000	Thermo Scientific
Pipettes	1-10/200/1000 µl	Gilson, Middleton, USA
Pipettor	Pipetboy acu	IBS
Power supply	EV31 Power Source 300 V	VWR, Taiwan
Roller mixer	STR6	Stuart
SDS-PAGE and Western blot equipment:	Mini Protean Tetra Cell System: 12-well comb Blot device Casting frames Casting gel stuff Casting plates	Bio-Rad, München

Device	Specification	Brand
	Casting stand	
	Cooling unit	
	Foam pads	
	Electrode assembly	
	Gel holder cassettes	
Sequencer	NextSeq 550 system	Illumina, USA
Shaking incubator	Max Q4000	Barnstead, Iowa/ USA
	Innova 40	New Brunswick scientific, Edison, USA
Sterile laminar flow bench	Steril Gard III Advance	Baker, Stanford USA
Table centrifuge	Eppendorf 5415 D	Eppendorf, Hamburg
	Nucleofector II	Bio-Rad, München
	AAD-1001N	
Thermoblock	Thermomixer compact	Eppendorf, Hamburg
Vacuum pump	BVC Control	Vacuubrand, Sigma-Aldrich, Deutschland
Vortex	Genie 2	Scientific Industries, USA
Water bath	1083	GFL, Burgwedel
Water purification system	Milli-Q	Merck, Darmstadt

2.1.2 CHEMICALS

Table 2: List of chemicals

Chemical	Brand/ Distributor
(4-(2-Hydroxyethyl)-1-piperazineethanesulfonicacid) HEPES	Roche, Mannheim

Chemical	Brand/ Distributor
1,4,-dithiothreitol (DTT)	Biomol, Hamburg
4',6-diamidino-2-phenylindole (DAPI)	Roche, Mannheim
Acrylamide/Bisacrylamide solution (40 %)	Roth, Karlsruhe
Agar LB (Lennox)	Roth, Karlsruhe
Agarose	Invitrogen, USA
AlbumaxII	Gibco, Life Technologies, USA
Albumin bovine Fraction V (BSA)	Biomol, Hamburg
Ammonium persulfate (APS)	Applichem, Darmstadt
Ampicillin	Roche, Mannheim
Biotin	Sigma Aldrich, Steinheim
Blasticidin S	Invitrogen, USA
Bromophenol blue	Roth, Karlsruhe
Chloroform	Roth, Karlsruhe
CV-Mount	Leica, Wetzlar
Dako	Sigma Aldrich, Steinheim
ddH ₂ O (Ampuwa)	Fresenius Kabi, Bad Homburg
Desoxynucleotides (dNTPs)	Thermo Scientific, Lithuania
D-Glucose	Merck, Darmstadt
Dimethyl sulfoxide (DMSO)	Sigma Aldrich, Steinheim
Dipotassium phosphate	Merck, Darmstadt

Chemical	Brand/ Distributor
Disodium phosphate	Roth, Karlsruhe
Dulbecco's Phosphate Buffered Saline (DPBS)	PAN, Biotech, Aidenbach
Ethanol	Roth, Karlsruhe
Ethidium bromide	Sigma Aldrich, Steinheim
Ethylenediaminetetraacetic acid (EDTA)	Biomol, Hamburg
Gentamicin (40 mg/ml)	Ratiopharm, Ulm
Giemsa's azure, eosin, methylene blue solution	Merck, Darmstadt
Glucose (water-free)	Roth, Karlsruhe
Glutaraldehyde (25%)	Merck, Darmstadt
Glycerol	Merck, Darmstadt
Hoechst 33342	Chemodox, Switzerland
Hydrochloric acid (HCl)	Merck, Darmstadt
Hypoxanthine	Sigma Aldrich, Steinheim
Hypoxanthine (9636)	Sigma Aldrich, Steinheim
Isopropanol	Roth, Karlsruhe
Magnesium chloride	Merck, Darmstadt
Methanol	Roth, Karlsruhe
Milk powder	Roth, Karlsruhe
N, N, N, N-Tetramethylethylenediamin (TEMED)	Merck, Darmstadt
Percoll	GE Healthcare, Sweden

Chemical	Brand/ Distributor
Phenylmethylsulfonylfluorid (PMSF)	Sigma Aldrich, Steinheim
Potassium chloride	Merck, Darmstadt
Protease inhibitor cocktail (Complete Mini)	Roche, Mannheim
RPMI (Roswell Park Memorial Institute)-Medium	Applichem, Darmstadt
Saponin	Sigma Aldrich, Steinheim
Sodium acetate	Merck, Darmstadt
Sodium bicarbonate	Sigma Aldrich, Steinheim
Sodium chloride	Gerbu, Gaiberg
Sodium dihydrogen phosphate	Roth, Karlsruhe
Sodium dodecyl sulfate (SDS)	Applichem, Darmstadt
Sodium hydroxide	Merck, Darmstadt
Sorbitol	Sigma Aldrich, Steinheim
Soybean trypsin inhibitor (STI)	Sigma Aldrich, Steinheim
Streptavidin Sepharose	GE Healthcare, Germany
TEMED	Merck, Darmstadt
Trichloroacetic acid	Roth, Karlsruhe
Tris base	Roth, Karlsruhe
Triton X-100	Biomol, Hamburg
Trizol	Life Technologies, USA
Tween20	Roth, Karlsruhe

2.1.3 LABWARE AND DISPOSABLES

Table 3: List of labware and disposables

Labware and disposables	Specification	Manufacturer
Blotting membrane	Nitrocellulose Amersham 0,45 μm	GE Healthcare, Germany
Conical Falcon tubes	50 / 15 ml Material	Sarstedt, Nümbrecht
Conical falcon tubes	15 ml, 50 ml	Sarstedt, Nümbrecht
Coverslips	13 mm	Sarstedt, Nümbrecht
Cryo tubes	1.6 ml	Sarstedt, Nümbrecht
Culture flask	T75 (250 ml), T25 (50 ml)	Sarstedt, Nümbrecht
Culture plates	24-well, flat bottom	Sarstedt, Nümbrecht
Diagnostic microscope slides for IFAs	10-wells 6.7 mm	Thermo Scientific, USA
Disposable pipette tips	1-10/ 20-200/ 100-1000 μl	Sarstedt, Nümbrecht
Electroporation Cuvettes	0.2 cm-gap sterile electroporation cuvette	Bio-Rad, München
Eppendorf Reaction Tubes	1.5 ml / 2 ml	Sarstedt, Nümbrecht
Filter tips	1-10/ 20-200/ 100-1000 μl	Sarstedt, Nümbrecht
Glass cover slips	24 X 65 mm Thickness 0.13-0.16	R. Langenbrinck, Emmendingen
Glass slides		Engelbrecht, Edermünde
Parafilm	Amersham 0.45 μm	GE Healthcare, Germany
Parafilm		Bemis, USA
Pasteur pipette		
PCR Reaction tubes	Multiply- μStrip Pro 8- Strip	Sarstedt, Nümbrecht
PCR reaction tubes	multiply- μStrip per 8-Strip	Sarstedt, Nümbrecht
Petri dishes	5 ml/ 10 ml	Sarstedt, Nümbrecht

Labware and disposables	Specification	Manufacturer
Plastic pipettes	5/ 10/ 25 ml	Sarstedt, Nümbrecht
Protran® Nitrocellulose Membranes		Whatman
Reaction tubes	1.5/2 ml	Bio-Rad, München
Sterile filter	0.22 µm	Sarstedt, Nümbrecht
Transfection cuvettes	0.2 cm	Bio-Rad, München
Vacuum Filter	Millipore Stericup	Merck, Darmstadt

2.1.4 KITS

Table 4: List of kits

Name	Manufacturer
Monarch Genomic DNA Purification Kit	NEB, Ipswich, USA
NextSeq 500/550 Mid Output Kit v2.5	Illumina, USA
NucleoSpin, Gel and PCR clean-up	Macherey-Nagel, Düren
NucleoSpin, Plasmid	Macherey-Nagel, Düren
PureYield™ Plasmid Midiprep System	Promega, Walldorf, Germany
QIAamp DNA Mini Kit	Qiagen, Hilden
QIAGEN Plasmid Midi Kit	Thermo Scientific, Schwerte
QIAseq FastSelect RNA Removal Kit	Qiagen, Hilden
QIAseq Stranded mRNA Library Kit	Qiagen, Hilden
Western Blot ECL-Clarity Detection Kit	Bio-Rad, USA

2.1.5 DNA AND PROTEIN LADDERS

Table 5: List of DNA and protein ladders

Name	Manufacturer
------	--------------

GeneRuler™1000 bp ladder	Thermo Scientific, Schwerte
PageRuler™ prestained protein ladder 26619	Thermo Scientific, Schwerte

2.1.6 SOLUTIONS, BUFFERS AND MEDIA

2.1.6.1 MEDIA, SOLUTION AND DRUGS

2.1.6.1.1 DRUGS

Table 6: List of drugs for parasite culture

Name	Composition
DSM1 stock solution	187.5 mM DSM1 in DMSO
DSM1 working solution	100 µl DSM1 stock solution ad 5 ml 95% DMSO/5% 1x PBS
WR99210 (WR) working solution	20 µM WR99210 (in DMSO) in RPMI complete medium, sterile filtered
Blasticidin S (BSD) working solution	5 mg/ml BSD in RPMI complete medium, sterile filtered
G418 working solution	50 mg/ml G418 in RPMI complete medium, sterile filtered
Zeocin solution	100mg/ml in solution (InvivoGen)

2.1.6.1.2 MEDIA AND SOLUTION FOR CELL CULTURE AND BINDING ASSAYS

Table 7: List of media and solutions for parasite culture

Name	Composition/Provider
10x PBS	1,37 M NaCl 28,6 mM KCl 80,6 mM Na ₂ HPO ₄ (water-free) 14,7 mM KH ₂ PO ₄ In .ddH ₂ O; pH 7,4
1x PBS	10% 10x PBS 90% ddH ₂ O
RPMI complete medium	1.587% (w/v) RMPI 1640 12 mM NaHCO ₃ 6 mM D-Glucose 0.5% (v/v) Albumax II 0.2 mM Hypoxanthine 0.4 mM Gentamycin pH 7.2 in dH ₂ O, sterile filtered
10% Giemsa solution	10 ml Giemsa's Azure, Eosin, Methylene blue solution 90 ml dH ₂ O
Synchronization solution	5% D-Sorbitol (w/v)

Name	Composition/Provider
	in dH ₂ O, sterile filtered
Amaxa transfection buffer	90 mM NaPO ₄ 5 mM KCl 0.15 mM CaCl ₂ 50 mM HEPES pH 7.3 in dH ₂ O, sterile filtered
Cytomix transfection buffer	120 mM KCl 150 μM CaCl ₂ 2 mM EGTA 5 mM MgCL ₂ 10 mM K ₂ HPO ₄ /KH ₂ PO ₄ 25 mM HEPES pH 7.6 sterile filtered
Malaria freezing solution (MFS)	4.2% D-Sorbitol 0.9% NaCl 28% Glycerol in dH ₂ O, sterile filtered
Malaria thawing solution (MTS)	3.5% NaCl

Name	Composition/Provider
	in dH ₂ O, sterile filtered
Human erythrocytes	sterile concentrate bloodtype 0+ Blood bank of Universitätsklinikum Eppendorf (UKE), Hamburg
Parasite lysis buffer	4% SDS 0.5% Triton X-100 0.5x PBS in dH ₂ O
Percoll stock solution	90% Percoll (v/v) 10% 10x PBS (v/v)
80% Percoll solution	8.9 ml 90% Percoll stock solution 1.1 ml RPMI complete medium 0.8 g Sorbitol sterile filtered
60% Percoll solution	6.7 ml 90% Percoll stock solution 3.3 ml RPMI complete medium 0.8 g Sorbitol sterile filtered

Name	Composition/Provider
64% Percoll solution	12 ml 80% Percoll solution 8 ml 40% Percoll solution
40% Percoll solution	4.4 ml 90% Percoll stock solution 5.6 ml RPMI complete medium 0.8 g Sorbitol sterile filtered
Saponin solution	0.03% Saponin (w/v) in dPBS
DHE stock solution (10x)	5 mg DHE in 1 ml DMSO
DHE working solution (1x)	0.5 mg DHE in 1 ml DMSO
Hoechst 33342 stock solution (10x)	4.5 mg Hoechst 33342 in 1 ml DMSO
Hoechst 33342 working solution (1x)	0.45 ml Hoechst 33342 in 1 ml DMSO

Name	Composition/Provider
Binding medium	16,4 g/l RPMI-HEPES 1640 20 g/l Glucose (wasserfrei) in 1 liter dest. H ₂ O; pH 7,2
RPMI glucose-free medium	16,4 g/l RPMI-HEPES 1640 0,05 g/l hypoxanthine 30 ml /l NaHCO ₃ (7,5 %) 250 µl/l gentamycin in 1 liter dest. H ₂ O; pH 7,2
Gelatin solution for knob enrichment	1% gelatin in RPMI glucose-free medium
Ham's F12 Medium mit L-Glutamin und 25 mM HEPES	PAN-Biotech
Inactivated fetal bovine serum	Capricorn
Dulbecco's Modified Eagle Medium	Gibco/Thermo Fisher,

2.1.6.1.3 BACTERIAL CULTURE

Table 8: List of solutions for bacterial culture

Name	Composition
10x Lysogeny broth (LB) medium stock solution	10% NaCl 5% Peptone 10% Yeast extract in dH ₂ O

LB medium working solution (1x)	1% NaCl (w/v) 0.5% Peptone (w/v) 1% Yeast extract (w/v) in dH ₂ O
Ampicillin stock solution LB-Amp	100 mg/ml in 70% ethanol
LB-Amp working solution	0.1% ampicillin in LB medium working solution (1x)
LB Agar plate solution	1.5% Agar-Agar 1x LB medium
Glycerol freezing solution	50% Glycerol (v/v) in 1x LB medium

2.1.6.2 SOLUTIONS AND BUFFERS FOR BIOCHEMICAL ANALYSIS

2.1.6.2.1 GEL ELECTROPHORESIS

Table 9: List of solutions for gel electrophoresis

Name	Composition
50x TAE buffer	2 M Tris base 1 M pure Acetic acid 50 mM EDTA pH 8.5 in dH ₂ O

6x Loading buffer	40% Glycerol (v/v)
	2.5% Xylene cyanol (w/v)
	2.5% Bromophenol blue
	in dH ₂ O

2.1.6.2.2 OTHER BUFFERS AND SOLUTIONS

Table 10: List other buffers and solutions

Name	Composition/Provider
10x Running buffer	250 mM Tris base 1.92 M Glycine 1% SDS
Ammonium persulfate (APS)	10% in dH ₂ O (w/v)
Separating gel buffer	1.5 M Tris-HCl pH 8.8 in dH ₂ O
Stacking gel buffer	1 M Tris-HCl pH 6.8 in dH ₂ O
Stacking gel (for two gels, 5%)	0.75 ml stacking gel buffer 4.35 ml dH ₂ O 0.75 ml Acryl amide (40%) 60 µl SDS (10%) 60 µl APS (10%)

Name	Composition/Provider
	6 μ l TEMED
Separating gel (for two gels, 12%)	2.5 ml running gel buffer 4.2 ml dH ₂ O 3 ml Acryl amide (40%) 100 μ l SDS (10%) 100 μ l APS (10%) 4 μ l TEMED
6x SDS sample buffer	375 mM Tris-HCl, pH 6.8 12% SDS (w/v) 60% Glycerol (v/v) 0.6 M DTT 0.06% Bromophenol blue (w/v)
10x Western Blot transfer buffer	250 mM Tris base 1.92 M Glycerol 0.1% SDS (w/v) in dH ₂ O
1x Western Blot transfer buffer	10% 10x Western blot transfer buffer 20% Methanol in dH ₂ O

Name	Composition/Provider
Blocking solution	5% milk powder (w/v) in 1x TBS
10x T4 – Ligasebuffer	ThermoFisher
Gibson buffer	5x isothermaler Reaktionspuffer T5 exonuclease (10U/ μ l) Phusion DNA Polymerase (2 U/ μ l) Taq DNA ligase (40 U/ μ l)
5x isothermaler Reaktionspuffer	1M TrisHCl in H ₂ O, pH 7,5 2M MgCl ₂ in H ₂ O 400mM dNTP in H ₂ O 1M DTT in H ₂ O 100mM NAD in H ₂ O PEG-8000
5x Phusion HF reaction buffer	NEB, Ipswich, USA
BioID lysis buffer	50 nM Tris-HCL pH7.5 500 mM NaCl 1 % Triton-X-100 1mM DTT 1 mM PMSF 1x protein inhibitor cocktail

Name	Composition/Provider
	in ddH ₂ O
Triethylammonium bicarbonate buffer	Sigma Aldrich, Steinheim
ECL solutions	<p>Solution A:</p> <p>Tris-HCl in dest. H₂O</p> <p>Luminol</p> <p>pH 8,6</p> <p>0,1 M</p> <p>0,025 %</p> <p>Solution B:</p> <p>p-Coumarinsäure</p> <p>in DMSO</p> <p>6,7 mM</p> <p>Solution C:</p> <p>H₂O₂</p>
ECL working solution	<p>5 ml Solution A</p> <p>500 µl Solution B</p> <p>1,5 µl Solution C</p>

2.1.7 MAMMALIAN CELL, *E. COLI* AND *P. FALCIPARUM* STRAINS

Table 11: List of mammalian, *E. coli* and *P.falciparum* strains

Name	Provider
------	----------

Chinese hamster ovary cells (CHO-745) expressing GFP, CD36 or ICAM-1	Metwally et al., 2017
Chinese hamster ovary cells (CHO-K1) expressing EPCR	Kindly provided by Thomas Lavstsen
<i>E. coli</i> XL-10 Gold	NEB, Ipswich/USA
HBEC-5i primary brain cells	Wassmer et al., 2006
<i>P. falciparum</i> strain 3D7	Clone of NF54 isolated from an airport malaria patient, near Schiphol Airport, Amsterdam, Netherlands
<i>P. falciparum</i> strain IT4	Jensen and Trager, 1978

2.1.8 ENZYMES

Table 12: List of enzymes

Type	Enzyme	Provider
Ligases	T4 DNA-Ligase [3 U/μl]	NEB, Ipswich, USA
	Taq DNA ligase (40.000U/ml)	NEB, Ipswich, USA
Polymerases	FirePol DNA Polymerase [5 U/μl]	Solis Biodyne, Taipei, Taiwan
	Phusion High-Fidelity DNA Polymerase [2 U/μl]	NEB, Ipswich, USA
	KAPA HiFi HotStart DNA Polymerase	Roche, Mannheim, Germany
Restriction enzymes	AvrII	NEB, Ipswich, USA
	MluI	
	NotI	
	Sall	
	SpeI	
	XhoI	

	Xmal	
Exonuclease	T5 exonuclease (10.000 U/ml)	NEB, Ipswich, USA

2.1.9 ANTIBODIES

2.1.9.1 PRIMARY ANTIBODIES

Table 13: List of primary antibodies

Antigen	Organism	Dilution		Source
		WB	IFA	
GFP	Mouse		1:500	Roche, Mannheim
	Rabbit		1:500	Thermo Fisher
RFP	Rat		1:1000	Chromotek
Hemagglutinin (HA)	Rat	1:1000	1:2000	Roche, Mannheim
	Rabbit		1:1000	Cell Signaling Technology
SBP1-N	Rabbit	1:4000		Struck et al., 2010
SBP1-C	Rabbit		1:2500	Mesén-Ramírez et al., 2016
REX1	Rabbit		1:10000	Mesén-Ramírez et al., 2016

Aldolase	Rabbit	1:4000		Mesén-Ramírez et al., 2016
KAHRP	Rabbit		1:500	Kind gift of Prof. Brian Cooke
Ty1-tag	Mouse		1:20000	Sigma Aldrich

2.1.9.2 SECONDARY ANTIBODIES

Table 14: List of secondary antibodies

Antigen	Organism	Conjugate	Dilution	Application	Source
Mouse	Goat	Alexa-488	1:2000	IFA	Life Technologies, USA
Rabbit	Donkey	HRP	1:2500	Western blot	Dianova, Hamburg
		Alexa-488	1:2000	IFA	Invitrogen, Molecular Probes Leiden
		Alexa-594	1:2000	IFA	Life Technologies, USA
		Alexa-647	1:2000	IFA	Invitrogen, Molecular Probes Leiden
Rat	Goat	HRP	1:3000	Western blot	Dianova, Hamburg
		Alexa-488	1:2000	IFA	Invitrogen, Molecular Probes Leiden
		Alexa-594	1:2000	IFA	Invitrogen, Molecular Probes Leiden

2.1.10 PRIMERS

All primers were synthesized by Sigma-Aldrich (Steinheim) (0.025 μmol , desalt, in TE, 100 μM). The stock solution was diluted 1:10 in Ampuwa H₂O before being used for PCRs. Primer sequences are in Appendix A1, 2.

2.1.10.1 STANDARD PRIMERS FOR DIAGNOSTIC PCRS

Table 15: List of standard primers

Name	Indication	Sequence
GFP 85 rv	P8	ACCTTCACCCTCTCCACTGAC
pARL 55 fw	P3/P7	GGAATTGTGAGCGGATAACAATTCACACAGG
Neo 40 rv	P2	CGAATAGCCTCTCCACCCAAG
Ty1 rv	P8	GTGGATCTTGATTTGTATGC

2.1.10.2 GENERAL PRIMERS

Table 16: List of general primers

Name	Sequence
FKBP 276 fw	CAGGCCATCCTGGCATCATC
FRB 42 rv	AAACGAGATGCCTCTTCCAG
FRB 76 rv	TCAAACATGCCTTTCACGTTCC
GFP 85 rv	ACCTTCACCCTCTCCACTGAC
Neo 40 rv	CGAATAGCCTCTCCACCCAAG
pARL minus	CAGTTATAAATACAATCAATTGG
pARL sense 55	GGAATTGTGAGCGGATAACAATTCACACAGG

2.1.11 PLASMIDS

pSLI-TGD (Birnbaum et al., 2017)

pSLI2-DHOD (Birnbaum et al., 2017)

pARL-*mal7*-SBP1-mDHFR-GFP-2A-KAHRP-mScarlet (Mesén-Ramírez et al., 2016)

2.1.12 COMPUTER SOFTWARE, BIOINFORMATIC TOOLS AND DATA BASES

ApE - A plasmid Editor (<http://biologylabs.utah.edu/jorgensen/wayned/ape>)

Axio Vision 40 V 4.7.0.0, Zeiss, Jena

bioinfokit (version 2.1.2)

BLAST (<http://blast.ncbi.nlm.nih.gov/Blast.cgi>)

CellProfiler (version 4.2.1) (Stirling et al., 2021)

ColabFold v1.5.5: AlphaFold2 using MMseqs2 (<https://colab.research.google.com/github/sokrypton/ColabFold/blob/main/AlphaFold2.ipynb#scrollTo=G4yBrceuFbf3>)

Compute pI/Mw (http://web.expasy.org/compute_pi/)

CorelDraw Graphics Suite (version 2021)

featureCounts (version 2.0.4)

Fiji - ImageJ (version 2.15.0) (Schindelin et al., 2012)

GOR4 (https://npsa-prabi.ibcp.fr/cgi-bin/npsa_automat.pl?page=/NPSA/npsa_gor4.html)

GraphPad Prism (version 9), GraphPad Software, La Jolla, USA

hisat2 (version 2.2.1)

Ilastik (version 1.3.3post3) (Berg et al., 2019)

ImageLab (version 5.2)

IUPRED2A (<https://iupred2a.elte.hu/>)

matplotlib (version 3.7.2)

Perseus software (Tyanova et al., 2016)

PlasmoDB (<http://plasmodb.org/plasmo/>)

PubMed (<http://www.ncbi.nlm.nih.gov/pubmed>)

Pymol (version 2)

Python3 (version 3.11.4)

samtools (version 1.17)

Translate tool (<http://web.expasy.org/translate/>)

TMHMMv2.0 (<https://services.healthtech.dtu.dk/services/TMHMM-2.0/>)

VarDom 1.0 (<https://services.healthtech.dtu.dk/services/VarDom-1.0/>)

2.2 METHODS

2.2.1 MOLECULAR METHODS

2.2.1.1 POLYMERASE CHAIN REACTION (PCR)

DNA sequences were amplified from *P. falciparum* 3D7 or IT4 genomic DNA, plasmid DNA, or synthesized genes obtained from GenScript Biotech (USA), utilizing the Phusion High Fidelity DNA polymerase or KAPA HiFi HotStart for PCRs that need proofreading capabilities. For diagnostic PCRs testing the correct integration of the SLI or SLI2 plasmid into the genome (Birnbaum et al., 2017), colony-PCR screening (section 2.2.1.6) and hard to obtain DNA amplifications, the FIREPol DNA polymerase was employed. The primers utilized were acquired from Sigma Aldrich (Steinheim, Germany) and are detailed in Appendix A1 and A2. Analysis of the PCR products was carried out using agarose gel electrophoresis as described in section 2.2.1.2.

2.2.1.2 AGAROSE GEL ELECTROPHORESIS

To separate DNA fragments by size the charged backbone of DNA is exploited to separate in an electric field applied to a gel containing DNA (Garoff and Ansorge, 1981). To perform this, a 1% agarose gel was prepared by dissolving agarose powder in 1x TAE buffer, heating the mixture in a microwave, occasionally shaking, until fully dissolved. Ethidium bromide was added to a final concentration of 1 µg/ml after the solution cooled down and the solution was poured into a gel casting tray. Combs were used to create the pockets where the DNA is loaded into. Once set, the gel was fully emerged in an electrophoresis tank filled with 1x TAE buffer. PCR-products were mixed with 6x DNA loading dye corresponding to the volume, and 5 µl of the mixture was loaded into the wells of the gel. The "GeneRuler™ 1 kb" (Thermo Scientific) served as a DNA ladder. Electrophoresis was conducted at 130V or 80V, depending on the chamber used, for 25-35 minutes. The gel was then imaged using the ChemiDoc™ XRS+ molecular imager. Resulting images were processed in ImageLab 5.2 software.

2.2.1.3 PURIFICATION OF PCR PRODUCTS

PCR products that were successfully amplified and intended for ligation, plasmid DNA that had been digested with restriction enzymes (section 2.1.8) or PCR products separated with agarose gel electrophoresis (section 2.2.1.2) were purified using the "NucleoSpin Gel and PCR Clean-up" Kit (Macherey-Nagel), as described in the protocol of the kit. The purified DNA was then eluted from the column in 10-30 µl elution buffer supplied with the kit.

2.2.1.4 ENZYMATIC DNA DIGESTION

Purified PCR products used for T4-ligation and plasmid vectors underwent digestion with various restriction enzymes (section 2.1.8), facilitating subsequent ligation processes. In scenarios where T4 DNA ligase was utilized for ligation (section 2.2.1.5), both the PCR amplicons and the target vectors were subjected to restriction enzyme digestion. Conversely, for ligation using the Gibson DNA assembly method (section 2.2.1.5), only the target vectors were digested with restriction enzymes and the PCR amplicons remained undigested. The digestion reactions were incubated at 37°C for approximately 1-3 hours or overnight.

2.2.1.5 DNA LIGATION WITH T4 LIGASE OR GIBSON ASSEMBLY

PCR-products were either ligated into target vectors using T4 DNA ligase or Gibson DNA assembly (Gibson et al., 2009). For ligations utilizing T4 DNA ligase, digested plasmid vector and digested PCR product was mixed in a molar ratio of 1:5 in 1X T4 DNA-Ligase-Puffer and H₂O. Subsequently, the mixture was incubated at room temperature for 1 hour or overnight.

For Gibson DNA assembly method, digested plasmid vector was mixed with one or multiple undigested PCR-products which contained overhangs overlapping the ligation sites. The digested plasmid and inserts were added in a 2-3 fold molar excess of each insert to 8µl of Gibson assembly buffer. The reaction was then incubated at 50°C for 1 hour. The ligated plasmids were subsequently transformed into XL10 Gold *E. coli* (section 2.2.2.1).

2.2.1.6 COLONY PCR SCREEN

Following the transformation of competent *E. coli* cells with plasmid DNA, a colony-PCR screen was conducted on the bacterial clones to pinpoint clones harboring plasmids with the correct insert. This was achieved by picking clones from the LB-agar plate using a small pipette tip and transferring them individually into PCR reaction tubes filled with 10-20 µl of FIREpol PCR solution. Prior to adding the clones to the PCR reaction, bacterial clones selected for the screening were transferred to a master plate which was incubated at 37 °C overnight, for subsequent use of positive clones. The utilized primers bound to the insert and proximal to the insert on the plasmid. Occasionally primers were used that flanked the insert and the integration of the insert was validated by size. The PCR products from these screenings were then subjected to analysis via agarose gel electrophoresis (section 2.2.1.2). Clones tested positive in the colony PCR screenings underwent mini plasmid preparation (section 2.2.1.7) for sequencing 2.2.1.8.

2.2.1.7 PREPARATION PLASMID DNA

Clones validated by colony PCR (section 2.2.1.6) or sequencing (section 2.2.1.8) were selected and either inoculated in 5 ml LB-Medium for a mini preparation (mini) or 150 ml LB-Medium for a midi preparation (midi). The culture was subsequently incubated shaking at 37 °C for ~16 hours (mini) or ~20 hours (midi). The bacteria were pelleted by centrifugation at 2000 rpm for 5 min at RT (mini) or 6000 rpm for 15 min at 4 °C (midi). The plasmid DNA was extracted from the bacteria using the NucleoSpinPlasmid Kit (mini), QIAGEN Plasmid Midi Kit (midi), or PureYield™ Plasmid Midiprep (midi) following the instructions provided by the manufacturer. Plasmid DNA was dissolved in 50 µl (mini) or 600 µl (midi) TE-buffer provided in the kits. The plasmids obtained by mini preparation were usually used sequencing (section 2.2.1.8) or subsequent cloning. The plasmids obtained by midi preparation were used for transfections of the *P. falciparum* parasites (section 2.2.3.7).

2.2.1.8 SANGER SEQUENCING

To sequence plasmids and rule out mutations in relevant regions sanger sequencing was employed. For that, 100-200 µg of plasmid DNA from a clone that was verified via colony PCR screen (section 2.2.1.6) was mixed with 3µl of an appropriate sequencing primer, ideally binding 30-60 bp upstream or downstream of the targeted sequence depending on primer direction and was filled up with H₂O to a final volume of 15 µl. The solutions were sent to Seqlab (Göttingen, Germany) for overnight sequencing. Obtained sequence were analyzed with ApE – A plasmid Editor.

2.2.1.9 DNA PRECIPITATION

Plasmid DNA eluates that were obtained with a plasmid midi preparation (section 2.2.1.7) and subject to transfection in *P. falciparum* parasite was analyzed with a NanoDrop to determine DNA concentration. Following a volume corresponding to 50–100 µg of DNA was mixed with 3x volume 100 % ethanol and 1/10 volume of 3 M sodium acetate. The precipitated DNA was centrifuged for a minimum of 5 minutes at maximum speed, washed with 70% ethanol and centrifugating for 10 min at max speed at 4°C. The pellet was then air dried in steril conditions and resuspended in 10 µl of sterile TE-buffer.

2.2.2 MICROBIOLOGICAL METHODS

2.2.2.1 TRANSFORMATION OF COMPETENT *E. COLI* CELLS

An aliquot of 100 µl competent *E. coli* cells was thawed on ice, 10 µl of plasmid was added, incubated on ice for 10 min and subjected to heat shock at 42°C for 40 seconds. Immediately after heat shock, the mixture was incubated on ice for 1 min, washed with LB-medium and then spread onto an LB-agar plate supplemented with 0.1 mg/ml ampicillin. This plate was then incubated at 37°C overnight.

2.2.2.2 FREEZING OF TRANSGENIC *E. COLI* CELLS

To ensure the long-term preservation of bacterial clones harboring the desired plasmid, a small sample of a bacteria clone verified through sequencing was transferred from a master plate into 2 ml of LB-Amp medium using a pipette tip. This culture was incubated shaking overnight at 37°C. Alternatively, 2ml from a plasmid DNA midi preparation (section 2.2.1.7) culture was transferred to a 2ml reaction tube. Following, the bacterial cells were pelleted by centrifugation, then resuspended in 1 ml of glycerol freezing suspension, and stored at -80°C for future use.

2.2.2.3 PREPARATION OF COMPETENT *E. COLI* CELLS

Competent *E. coli* cells of the XL10 Gold strain were prepared as described (Inoue et al., 1990) and used for transformation (section 2.2.2.1). Bacteria from glycerol stocks stored at -80°C were inoculated into 10 ml of SOB-medium supplemented with 34 µg/ml of chloramphenicol and incubated shaking overnight at 37°C. Following, 200 ml of SOB-medium was inoculated with 5 ml of the culture, and two additional 200 ml batches of SOB-medium were each inoculated with 2.5 ml of the overnight culture as backups. These cultures were then incubated shaking overnight at 18°C. After 20-24 hours, optical density at 600 nm (OD₆₀₀) was monitored until it reached 0.45-0.6, signaling the appropriate time for harvesting.

The culture was divided into four 50 ml falcon tubes and chilled on ice for 10 minutes, followed by centrifugation at 4000 rpm for 15 minutes at 4 °C. The supernatant was removed, and each cell pellet was gently resuspended in 20 ml of ice-cold transformation buffer. After another 10 minutes on ice, the cells were centrifuged again under the same conditions. The supernatant was discarded, and each pellet was resuspended in 4 ml of ice-cold transformation buffer. These resuspended pellets were combined, gently mixed with 1.2 ml of DMSO, and aliquoted into 100 µl volumes. These aliquots were immediately frozen in a mixture of dry ice and 100% ethanol before stored at -80°C.

2.2.3 CELL CULTURE METHODS

2.2.3.1 CULTURING OF MAMMLIAN CELLS

Chinese Hamster Ovary (CHO) cells engineered to express specific receptors such as CD36, ICAM-1, GFP (in CHO-745) (Metwally et al., 2017), or EPCR (in CHO-K1) (kindly provided by Thomas Lavstsen) and human brain endothelial cells (HBEC-5i) (Wassmer et al., 2006) were grown in Ham's F-12 medium (CHO cells) or Dulbecco's Modified Eagle's Limiting Medium (HBEC-5i), both supplemented with 10% fetal calf serum (PAA) and penicillin-streptomycin in a 5% CO₂ atmosphere at 37°C. Additionally, endothelium cell growth supplement was added to the HBEC-5i growth medium to a final concentration of 30 µg/ml. For selection of the receptor expressing CHO cells, 700 µg/ml G418 (CHO-745) or 100 µg/ml (CHO-K1) was added to the culture medium. If a cell confluency of 90-100% was reached and the cell were not used for seeding on coverslips (section 2.2.5.1), the culture was diluted and put back into culture.

Aliquots of cryo-preserved mammalian cells (kindly provided by Johanned Allweier and Jana Brehmer) were thawed prior to every binding assay (section 2.2.5.1). Therefore, cryo-stabilate tubes with the desired mammalian cells were thawed in a water bath at 37 °C for 1 min, the cell suspension was transferred to a 15 ml falcon tube and washed with pre-warmed culture medium. The cells were pelleted at 1200 rpm for 2 min, the supernatant was discarded, and the pellet was resuspended in prewarmed culture medium. For the CHO cells the corresponding selection drug was added and the cells were transferred to a T25 flask for further cultivation. For HBEC-5i cells the T25 flask was coated with 1 ml of 0.1 % gelatin in 1x PBS at 37 °C for 5-10 min before the thawed cells were transferred to the flask.

2.2.3.2 *P. FALCIPARUM* CELL CULTURE

P. falciparum parasites 3D7 and IT4 (Jensen and Trager, 1978; there called FCR3S1.2) were cultured using standard procedures (Trager and Jensen, 1976). In brief, the parasites cultures were maintained in petri dishes with volumes of 2 ml, 5 ml, or 10 ml, or 250 ml bottle at a temperature of 37°C in a low-oxygen atmosphere (5% CO₂, 1% O₂, and 94% N₂). Parasites were kept in RPMI complete medium supplemented with human erythrocytes of blood group O+ at a 5% hematocrit. For the selection of transgenic parasites 4 nM WR99210, 2 µg/ml Blasticidin S, 400 µg/ml G418, and/or 0.9 µM DSM1 was added to the culture corresponding to the expressed resistance genes. The parasitemia was always kept below a parasitemia of 10%,

with cultures being diluted every 1-3 days depending on parasitemia. If higher parasitemia's were needed the medium was changed twice per day. For parasites that were transfected or thawed the medium was changed every day for the first 2 (thawing) or 4-5 (transfection) days.

2.2.3.3 BLOOD SMEARS

To manage the growth of parasites, parasitemia levels were assessed using Giemsa-stained thin blood smears. Erythrocytes were scratched from the bottom of the petri dish using a pipette and a drop was placed on a glass slide and subsequently spread out with another glass slide to achieve a monolayer of the erythrocytes. The smear was then air-dried and fixed in methanol for 10-30 s. Subsequently, the cells were stained with Giemsa's solution, for 10-20 min. The slide was rinsed with water and gently dried using a tissue. The stained blood smears were then evaluated under an optical light microscope (Axio Lab A1).

2.2.3.4 FREEZING AND THAWING OF PARASITE CULTURES

To ensure the long-term preservation of parasite cell lines, cryo-stabilates were prepared and stored at -80°C. Between 5 to 10 ml of a parasite culture with predominant ring-stage parasites and a parasitemia of 1-10% was pelleted at 2,000 rpm for 5 minutes. Following centrifugation, the supernatant was discarded, and the resulting pellet was gently resuspended in 1 ml of malaria freezing solution (MFS). This suspension was then transferred into a 1.6 ml cryo-tube and immediately stored at -80°C.

For thawing of the frozen parasite cryo-stabilates, the tubes were thawed in water bath at 37 °C. The suspension was then transferred to a 15 ml falcon and centrifuged at 3000 rpm for 2 minutes. The supernatant was removed, and the pellet was gently resuspended in 1.5 ml of malaria thawing solution (MTS) by slowly pipetting the MTS on the pellet and careful mixing. The suspension was centrifuged at 2000 rpm for 5 min. The supernatant was removed, and 10 ml RPMI complete medium was slowly pipetted on the pellet and gently mixed. The parasites were spun down once more, resuspended in RPMI complete medium, added to a 5 ml petry dish and supplemented with 2-4 drops (depending on pellet size) of fresh erythrocytes. Drugs for selection of the parasites were added the following day. The reappearance of parasites was then tracked with Giemsa-stained blood smears (section 2.2.3.3) starting 2 days after thawing.

2.2.3.5 SYNCHRONIZATION OF RING STAGE PARASITES

To synchronize a parasite culture for ring stage parasites sorbitol was used as described (Lambros and Vanderberg, 1979). In short, the parasite culture was pelleted at 2000 rpm for 5

min. The supernatant was discarded, and the pellet was resuspended in 5 times the pellet volume of 5% D-sorbitol solution, pre-warmed at 37°C. The suspension was then incubated at 37°C for 10 minutes. The suspension was centrifuged at 3,000 rpm for 3 minutes, and the pellet was washed once with RPMI complete medium. The pellet was then resuspended in RPMI complete medium and was transferred to a new petri dish. To assess the successful lysis of non-ring stage parasites Giemsa-stained blood smears (section 2.2.3.3) were conducted after the synchronization.

2.2.3.6 ISOLATION OF TROPHOZOITE AND SCHIZONT STAGE PARASITES

To isolate trophozoite and schizont stage parasites Percoll was used as described (Heiber and Spielmann, 2014; Rivadeneira et al., 1983). In brief, for trophozoite stage isolation a parasite culture containing preferable high proportion of trophozoites was pelleted at 2,000 rpm for 5 minutes. Meanwhile, a 15 ml falcon tube was prepared with a layered Percoll gradient: first, 2 ml of 80% Percoll, followed by 2 ml of 60% Percoll (for 3D7 parasites) or 64% Percoll (for IT4 parasites), and topped with 2 ml of 40% Percoll. The parasite pellet was mixed with 8 ml of RPMI complete medium and carefully layered on top of the Percoll gradient. The falcon tube was then centrifuged at 2000 rpm for 10 min. Following, the falcon tube was carefully removed from the centrifuge, the top layers were discarded and the trophozoite fraction (see Heiber and Spielmann, 2014) was taken up with a stripette and transferred to a new falcon tube. The trophozoites were washed with 1x PBS at 4000 rpm for 5 min. The Pellet was then subject to a trypsin assay (section 2.2.8.1)

For the isolation of schizont stage parasites a culture of 5-10 % parasitemia with preferable schizonts was pelleted and resuspended in 10 ml of RPMI complete medium. A falcon tube with 4 ml of 60 % Percoll (3D7 parasites) or 64 % Percoll (IT4 parasites) was prepared. The parasites suspension was carefully layered on top of the Percoll and centrifuged at 2000 rpm for 8 min. The medium was removed until 1 ml above the schizont fraction and the schizont fraction was transferred to a new falcon. The schizonts were washed with 10-14 ml RPMI complete medium, the pellet was resuspended in RPMI complete medium and transferred to a new to for subsequent culturing or used for transfection (section 2.2.3.7).

2.2.3.7 TRANSFECTION OF *P. FALCIPARUM* SCHIZONT STAGE PARASITES

To transfect *P. falciparum* schizont parasites, schizonts stage parasites were isolated (section 2.2.3.6) from a culture with 5-10% parasites preferable with a high proportion of schizonts. 50-100 µg of DNA dissolved in 10 µl steril TE-buffer (section 2.2.1.9) was mixed with 90 µl

Amaxa transfection buffer and 15µl of schizont pellet. This mixture was transferred to an electroporation cuvette (Bio-Rad) and the parasites were electroporated with the “Nucleofector II AAD-1001N” (Bio-Rad). The mixture was then transferred to a previously prepared 2 ml reaction tube which contained 500 µl of RPMI complete medium and 200µl of erythrocytes, prewarmed. The suspension was then incubated shaking at 800 rpm for 30 min at 37 °C. Following, the suspension was transferred to a petri dish, 5ml of RPMI complete medium was added and the petri dish was incubated overnight at 37 °C. The following day medium was changed, and the appropriate selection drugs were added. Medium and drugs were changed the following 4-5 days and every 7 days a drop of blood was added to the culture. Reappearance of the parasites was controlled with Giemsa-stained blood smears (section 2.2.3.3) every other day.

2.2.3.8 INTRODUCING GENOMIC MODIFICATIONS VIA SLI

Selection-Linked Integration (SLI) was conducted as described (Birnbaum et al., 2017) with minor modifications. In brief, parasites harboring non-integrated SLI or SLI2 plasmids and exhibiting good proliferation rates were grown in a 10 ml dishes to a parasitemia of 10-15 %. Medium was discarded and 20 ml of fresh medium containing 400µg/ml G418 (for SLI) or 0.9 µM DSM1 (for SLI2) was added to the culture. The medium (20 ml) and drugs were changed every day for 5 days. Afterwards, medium was changed every 2-3 days and only 10 ml of selection drug containing medium was added. The reappearance of parasites was controlled every 3-5 days using Giemsa-stained blood smears (section 2.2.3.3). The parasite cultures were kept for a maximum of 3 month until the culture was discarded as a failed integration attempt.

2.2.3.9 PLAQUE ASSAY

Plaque assays to subclone parasite cell lines was conducted as described (Thomas et al., 2016). In short, parasitemia of the parasite culture was determined using Giemsa smears and a parasite suspension with 1 % parasitemia and 0.75% hematocrit in RPMI complete medium was prepared. The parasites were diluted 1:10 with 0.75 % hematocrit RPMI complete medium and added to the top row of a 96-well plate. This dilution process was continued for every row resulting in a dilution of 10⁻¹ in the top row and 10⁻⁸ in the bottom row. The 96-well plate was then incubated under culture atmosphere at 37 °C for 11 day without moving or shaking the plate. The wells were then evaluated for plaques with the EVOS xl microscope. Parasite culture from wells containing only a single plaque were transferred to a 5 ml petri dish and cultured as

described (section 2.2.3.2). The reappearance of parasites was controlled with Giemsa-stained blood smears (section 2.2.3.3) every 2-3 days.

2.2.3.10 ENRICHMENT OF KNOBBY PARASITES

To enrich for parasites that contain knobs on the surface of the infected erythrocytes, a 1% gelatin solution was employed as described (Goodyer et al., 1994). Therefore, 10 ml of parasite culture with 5-10% parasitemia and preferably containing trophozoite stage parasites was centrifuged at 2000 rpm for 5 min, resuspended in RPMI glucose-free medium and pelleted once more. The pellet was resuspended in 500 μ l RPMI glucose-free medium and 2 ml of 1% gelatin solution in a 15 ml falcon tube avoiding formation of bubbles, both solutions were prewarmed to 37 °C. The falcon tube was incubated standing up in the water bath for 20 min at 37 °C. Knobby parasites float in the upper fraction while the knob-less parasites fall into the pellet. 1-1.5 ml of the top fraction was transferred to a new 15 ml falcon tube and washed with either binding medium (if parasites were subject to binding assays) or RPMI complete medium (if further cultured).

2.2.3.11 PTEX CO-BLOCK ASSAY

The effect of co-blocking the PTEX channel with a mDHFR-fusion construct was conducted following the principles previously described (Eilers and Schatz, 1986; Grüning et al., 2012). For the late block of the PTEX channel, the pARL2-SBP1-mDHFR-GFP-2A-KAHRP-mScarlet (Mesén-Ramírez et al., 2016) plasmid containing a *crt* promotor instead of the *mal7* promotor (kindly generated by Paolo Mesén-Ramírez), was transfected into the 3D7-varUPSB6-HA^{endo} cell line. Schizonts were isolated (section 2.2.3.6) from the 3D7varUPSB6-HA^{endo} parasite culture containing preferably schizont-stage parasites, washed and grown in a 2 ml preti dish for 2 hours. The culture was then incubated for 24 hours either in the presence or absence of 4 nM WR99210, after which the export of proteins was analyzed through live cell imaging and IFAs (section 2.2.4 and 2.2.4.1).

2.2.4 FLUORESECE MICROSCOPY

Live or fixed parasites were imaged and assessed using the Zeiss AxioImager M1 or M2 microscopes, equipped with a Hamamatsu Orca C4742-95 camera. Imaging was conducted using lenses with either a 100 \times /1.4 or a 63 \times /1.4 numerical aperture. Field of views were captured with the AxioVision software (version 4.7). The imaging of live parasites that express fluorescent proteins was performed as described (Grüning and Spielmann, 2012). The parasite

DNA was stained using 1 µg/µl DAPI or 50 ng/ml Hoechst 33342 in RPMI complete medium for 10 minutes at a temperature of 37°C. Subsequently, the parasites were washed, applied between a glass slide and glass cover slip and consequently imaged. Subsequent image processing was carried out in Corel Photo-Paint (version 2021), and processed images were organized using Corel Draw (version 2021).

2.2.4.1 IMMUNOFLUORESCENCE AND STREPTAVIDIN-FLUORESCENCE ASSAY

Immunofluorescence assays (IFAs) were conducted as described (Spielmann et al., 2003). In brief, pelleted parasites were obtained by centrifugation at 2000 rpm for 5 minutes, followed by a wash in 1x PBS or RPMI glucose-free medium. The washed parasites were then adjusted to a hematocrit of 1-2.5% and applied to 10-well glass slides in a thin layer, where they were allowed to air-dry before being fixed in acetone for 30 minutes. Slides were stored at room temperature until needed (but never longer than 14 days). The fixed samples on slides were rehydrated with 1x PBS for 15-30 min and subsequently washed five times with 1x PBS.

The first antibodies were applied on the wells in 3% BSA in 1x PBS and incubated at 4°C overnight. Subsequently, the antibody solution was discarded, the wells were washed 5 times with 1x PBS, the second antibodies with 1 µg/µl DAPI or 50 ng/ml Hoechst 33342 in 3% BSA in 1xPBS were applied and slides were incubated for 1 h at room temperature. For the Streptavidin-fluorescence assay, streptavidin coupled to Alexa Fluor 594 was added to the second antibody solution to a final concentration of 1:2000. After incubation the antibody solution was removed, wells were washed 5 times with 1x PBS before the wells were air-dried and a cover slip was mounted using Dako. Following the samples were analyzed (section 2.2.4) or stored wrapped in aluminum foil at 4 °C.

2.2.5 BINDING ASSAYS

2.2.5.1 STATIC BINDING ASSAYS AGAINST MAMMALIAN CELLS OR DECORIN

Receptor-expressing CHO cell or HBEC-5i (section 2.1.7) cells were prepared by seeding them on coverslips in 24-well plates containing coverslips in the wells. Therefore, the cells were treated with 500µl trypsin for 5 min at 37 °C to remove them from the culture bottle and subsequently resuspended in corresponding culture medium. The suspension was adjusted to 2x10⁵ cells/ml two days before the assay, or 1x10⁵ cells/ml three days before the binding assay, selection drugs were added and 500µl of the suspension was added to the wells (three wells per

P. falciparum cell lines and receptor). For the HBEC-5i cells the coverslips were coated with 0.1% gelatine for 10 min at 37 °C (section 2.2.3.1) prior to seeding the cells. The medium and drugs were replenished one day before the binding assay.

For binding assays targeting the interaction of VAR2CSA to immobilized CSA, cover slips were coated with decorin (chondroitin sulfate proteoglycan from bovine articular cartilage) (Dahlbäck et al., 2011). Therefore, the coverslips were incubated with 500 µl of decorin in 1x PBS (5 µg/ml) solution or BSA in 1x PBS (5 µg/µl) (control) in a 24-well plate overnight at 4 °C. Following the solutions were removed, the wells were washed with 1x PBS and blocked with 1% BSA in 1x PBS for 2 h. Subsequently the wells were washed two times with 1x PBS (Renn et al., 2021).

Knob-enriched parasites (section 2.2.3.10) of the tested *P. falciparum* cell lines were washed with binding medium and resuspending in 3ml of binding medium. The erythrocytes per ml (Neubauer counting chamber) and percentage of infected erythrocytes in the suspension (Giemsa-stained blood smears) was determined. Following, the suspension was adjusted to 2×10^6 infected erythrocytes/ml in binding medium. The receptor expressing CHO or HBEC-5i cells adhering to the coverslips in 24-well plates were incubated with binding medium for 30 minutes before the parasite suspension was added to the wells.

In experiments involving decorin or HBEC-5i cells, the adjusted parasite suspension was split and incubated either with soluble CSA in binding medium (100 µg/ml) or soluble BSA in binding medium (100 µg/ml; control) for 30 minutes at 37 °C prior to adding the parasite suspension to the wells.

Subsequently, the binding medium was removed from the wells and 500µl of adjusted parasite suspension was added to the wells (1×10^6 infected erythrocytes per well). The binding reaction was incubated for 60 minutes at 37°C, with gentle shaking every 15 minutes. Following incubation, the coverslips were washed by gently dunking them in binding medium 6 times (excess medium was blotted onto paper after 3 dunks) before placing them face-down in a 24-well plate that was angled at 45° (face-side hanging downwards free in the binding medium) for 30 min, so that the unbound parasites can fall off from the coverslips. The coverslips were then fixed in 1% glutaraldehyde in 1x PBS for 30 min and subsequently stained with filtered 10% Giemsa (Merck) in 1x PBS for 15 min. The stained coverslips were washed with water, air-dried and glued face-down onto glass slides with CV-Mount. Five images per coverslip (per

experiment 15 images per parasite line and condition or 5 images per coverslip) were captured with a Thermo Fisher EVOS XL (75% light intensity at 40x magnification).

2.2.5.2 AUTOMATED SCORING OF BINDING ASSAYS

The evaluation of images of binding assays was automated using Ilastik v1.3.3post3 (Berg et al., 2019) and CellProfiler v4.2.1 (Stirling et al., 2021) (Figure 16). First the images of the binding assays were processed with a trained Ilastik model for the segmentation of the foreground (infected erythrocytes) and background (CHO/HBEC-5i cells and plastic). For the training, the pixel classification module was manually trained with 20 microscopy images representing different shapes of infected erythrocytes, backgrounds, and artefacts. All the color/intensity, edge and texture features were enabled for training. The resulting processed images were exported as probability images with pixel intensities from 0.0–1.0 for the probability of a foreground pixel (regression values; 1.0 = 100 % probability for foreground pixel). Ilastik pre-processed images were then fed to a CellProfiler pipeline (Figure 16B) using the “IdentifyPrimaryObjects” module to identify and count roundish objects with a diameter of 15–35 pixel units. Robust background thresholding and de-clumping by shape was selected. Number of counted infected erythrocytes scored per image was given out as a spreadsheet. To show the reliability of the automated pipeline in comparison to the manual scoring statistical tests between the two methods were conducted as shown in Figure 16C-E.

2.2.6 RNA SEQUENCING

For RNA isolation synchronous ring-stage *P. falciparum* parasites exhibiting a parasitemia of 3-5% were centrifuged at 2000 rpm for 5 min and resuspended in five volumes of prewarmed Trizol, thoroughly mixed, and subsequently stored at -80°C. Upon thawing the Trizol sample, chloroform (1/5 volume of the Trizol used) was added, mixed thoroughly, and then centrifuged at 16,000g for 30 minutes at 4°C to separate the phases. The clear supernatant was carefully transferred to a new tube and processed using the Qiagen miRNeasy Mini Kit following the instructions provided by the manufacturer.

The integrity of the isolated RNA was verified using the Agilent 2100 Bioanalyzer System with the RNA 6000 Pico Kit, selecting only samples with a RNA integrity number greater than 8 for analysis. Ribosomal RNA was depleted from the samples using the QIAseq FastSelect RNA Removal Kit, followed by library preparation with the QIAseq Stranded mRNA Library Kit.

Sequencing was performed on an Illumina NextSeq 550 system utilizing the NextSeq 500/550 Mid Output Kit v2.5 for 150 cycles.

The raw sequencing reads were aligned to the reference genomes from PlasmoDB using hisat2 (version 2.2.1). The aligned reads were then sorted and indexed using samtools (version 1.17). Gene feature counts were obtained with featureCounts (version 2.0.4) and only transcript from exon 1 of the *var* genes considered. The reads were normalized to Transcripts Per Million (TPM) and coverplots were generated, using Python3 (version 3.11.4) with the bioinfokit (version 2.1.2) and matplotlib (version 3.7.2) for data visualization.

2.2.7 BIOID AND MASS SPECTROMETRY

For proximity biotinylation, biotin (50 μ M final) was added to asynchronous parasites expressing the BirA*-PfEMP1 fusion constructs as well as to IT4 parent parasites (5% parasitemia, 150 ml per condition and experiment) and cultured for 24 h with one exchange of medium with fresh biotin after 12 h. Subsequent, the parasites were washed twice with Dulbecco's Phosphate-Buffered Saline (DPBS) and then subjected to saponin lysis (0.03% saponin solution in DPBS) on ice for 10 minutes. This was followed by five DPBS washes before lysing the samples in 2 ml of a BioID lysis buffer. The lysates were then stored at -80°C.

For the isolation of proteins, the frozen samples were thawed and subjected to a freeze-thaw cycle twice before centrifugation at 16,000 g for 10 minutes. The supernatant (Triton-extract) was saved, the pellet was frozen and thawed once more and underwent a second extraction process using a 4% SDS containing BioID lysis buffer (SDS-extract). The SDS-extract was cleared by centrifugation at 16,000g for 10 minutes. Both extracts were diluted 2:1 in 50 nM Tris-HCl and incubated with 50 μ l Streptavidin Sepharose rotating overnight at 4 °.

The Sepharose beads were washed twice in BioID lysis buffer, once in H₂O, twice in Tris-HCl pH 7.5 and three times in 100 nM Triethylammonium bicarbonate buffer. Subsequently steps were kindly conducted by the Bartfai lab. The proteins were digested on the beads as described (Hubner et al., 2015).

The samples were analysed on an Easy-nLC 1000 (Thermo Fisher Scientific) with a 30 cm C18-reverse phase column coupled on-line to an Orbitrap Fusion mass spectrometer (Thermo Fisher Scientific). Data was acquired in data-dependent top speed mode. The mass spectrometry data were processed with MaxQuant software (Cox and Mann, 2008). Default settings were used

with the following exceptions: Deamidation (NQ) was specified as a variable modification, in addition to oxidation (M) and acetyl (N-term). The 'match-between-runs' and 're-quantify' features were enabled with default configurations, and iBAQ values were subsequently calculated. Mass spectral data were matched against peptide masses derived from the annotated proteome of *P. falciparum* IT4 (PlasmoDB v64). Analysis of the “proteinGroups” file generated by MaxQuant was conducted using Perseus software (Tyanova et al., 2016) (version 1.4.0.20). Data were refined by excluding peptides identified as “only identified by site”, “reverse”, and “potential contaminant” in the datasets. IBAQ values underwent logarithmic transformation to \log_2 , and missing values were imputed based on a normal distribution. Samples from the Triton-extraction and SDS-extraction were analyzed separately. Significant outliers at each position were determined using a two-sided Benjamini-Hochberg test, applying a false discovery rate (FDR) threshold of 0.05.

2.2.8 BIOCHEMICAL METHODS

2.2.8.1 TRYPSIN CLEAVAGE ASSAY

Parasite cultures exhibiting a parasitemia level of 5-10% were synchronized for ring stage parasites (section 2.2.3.5), washed in RPMI complete medium and grown for 12 hours at 37°C to achieve a culture with parasites with maximum age of 30 hours post invasion. Following, trophozoite stage parasites were isolated (section 2.2.3.6), washed in 1x PBS, split into two 1.5 ml reaction tubes and washed once more with 1x PBS. The pellete of one sample was resuspended in 100µl of TPCK-treated Trypsin (50 µg/ml) in 1x PBS at 37°C for 30 minutes, while the other sample (control) was incubated in 1x PBS at the same conditions. Subsequently, trypsin inhibitor from soybean was added to both samples to a final concentration of 1 mg/ml and samples were incubated on ice for 15 minutes. The samples were spun down and washed with 1x PBS before adding 50-100 µl (depending on pellet size) lysis buffer supplemented with 1 mg/ml trypsin inhibitor, 1 mM PMFS, and 1x protein inhibitor cocktail to the pellets. Following the extracts were either immediately analyzed by SDS-PAGE (section 2.2.8.2) or stored at -20°C for future use.

2.2.8.2 WESTERN BLOT

Western blot analysis was performed following the protocol as described (Heiber and Spielmann, 2014). Initially, extracts from BioID experiments (section 2.2.7) or trypsin cleavage assays (section 2.2.8.1) were centrifuged at 16,000g, and the supernatant was mixed with 4x

Laemmli sample buffer. This mixture was then incubated at 90°C for 10 minutes prior to electrophoresis on 10% sodium dodecyl sulfate polyacrylamide polyacrylamide gels (SDS-PAGE). Following separation by SDS-PAGE, the proteins on the gels were transferred onto nitrocellulose membranes using transfer buffer.

For antibody-based protein detection, the membranes were first blocked with 5% skim milk in 1x TBS for 2 hours at room temperature. After blocking, membranes were washed thrice for 15 min with 1x TBS containing 1% Tween and then incubated overnight at 4°C with the primary antibody in 1x TBS with 3% skim milk. Following the membranes were washed three times with 1x TBS with 1% Tween for 15 min each wash. Secondary antibodies in 1x TBS with 3% skim milk were applied and incubated with the membrane for 2 hours at room temperature.

For the specific detection of biotinylated proteins, HRP-conjugated streptavidin (1:2000) in 5% BSA in 1x TBS was utilized and incubated with the membrane overnight at 4°C as described (Cui and Ma, 2018). Following the incubation with secondary antibodies or HRP-conjugated streptavidin, the membrane was washed three times in 1x TBS with 1% Tween. The membrane was then treated with ECL working solution or the ECL-Clarity Detection Kit prior to the detection of the ECL signal with the ChemiDoc XRS imaging system.

2.2.9 QUANTIFICATION, STATISTICAL ANALYSIS AND FIGURE CONSTRUCTION

P values are presented within the figures, with a threshold of $P < 0.05$ set as statistical significance. All error bars represent Standard deviations are represented. The unpaired t-test was utilized to test statistical significance. Comparisons between individual images from the binding assays, assessed both manually and through an automated pipeline, employed a ratio-paired t-test. GraphPad Prism (version 9) was used for statistical analyses. The Intraclass correlation coefficient (ICC) was determined using Microsoft Excel; a two-factor ANOVA without replication was conducted, and ICC values were derived from the variance components of the ANOVA using the formula: $ICC = (MS_{Row} - MS_{Error}) / (MS_{Row} + (df_{Column} \times MS_{Error}) + ((df_{Column} + 1) \times (MS_{Column} - MS_{Error}) / (df_{Row} + 1)))$. Graphs were created in GraphPad (version 9) and subsequently refined in CorelDraw (version 2021) for stylistic enhancements, ensuring no modifications to the original data. CorelDraw (version 2021) was also utilized for the final figure preparation.

3 RESULTS

3.1 EXPLOITING SLI-GENERATED *VAR* GENE CELL LINES

In this study, the SLI-system (Birnbaum et al., 2017) was employed to generate *P. falciparum* parasite cell lines expressing a single *var* gene of choice in the entire population. In this section these cell lines are used to study *var* gene expression (section 3.1.2, 3.1.3 and 3.1.7), PfEMP1 transport (section 3.1.4) and PfEMP1-mediated binding (section 3.1.6 and 3.1.7).

3.1.1 SLI STRATEGY

The rationale behind this is to link expression of a particular *var* gene with the expression of a resistance conferring gene, thereby selecting only those parasites expressing that *var* gene. Given the mutually exclusive expression pattern of *var* genes, the entire parasite population should exclusively express that specific *var* gene. To do this the following steps are needed for each targeted *var* gene: first a pSLI plasmid containing a homology region corresponding to the C-terminal stretch encoding the ATS domain of the targeted *var* gene is generated and transfected into *P. falciparum* parasites (Figure 12) (Appendix A2 for primers). Selection of transfectants harboring this plasmid is then achieved using the drug WR99210. Due to homologous recombination parasites can integrate the plasmid into the gene locus at the targeted homology site. This low probability integration event results in the expression of the desired *var* gene, now fused to a 3xHA tag, followed by a skip peptide (T2A) and a neomycin resistance gene (Neo R, conferring resistance to G418), all under the control of the same endogenous *var* gene promoter (Figure 12). Subsequent cultivation with G418 ensures that only those parasites expressing the targeted modified *var* gene and conferring neomycin resistance

survive. The resultant modified PfEMP1 variant proteins can be detected and tracked using the 3xHA tag.

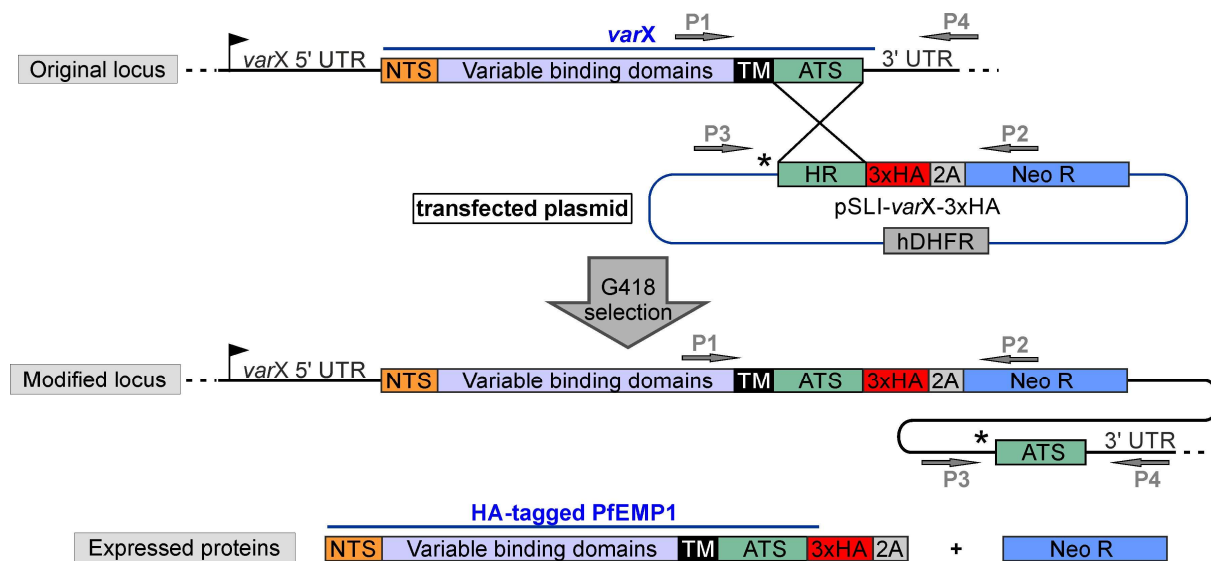


Figure 12: Integration strategy for the activation of a specific *var* gene. Illustration shows strategy and process for the modification of *var* gene loci via SLI. Selection of the parasite culture on WR99210 selects for the parasites harboring the plasmid in the entire parasite population. Selection of the parasite culture on G418 selects for parasites that integrated the pSLI-*varX*-3xHA plasmid into the targeted *var* gene locus. ATS: acidic terminal segment; NTS: NTS domain; 2A: T2A skip peptide; Neo-R: G418-resistance (conferring resistance to G418); hDHFR: human dihydrofolate reductase (conferring WR99210 resistance); asterisk: stop codon; arrows P1-4: primers for PCR to confirm correct integration; X: desired *var* gene. P1 + P4: original locus; P1 + P2: 5' integration junction; P3 + P4: 3' integration junction.

3.1.2 SLI-MODIFIED *VAR* GENES ARE PREDOMINANTLY EXPRESSED

The functionality of the approach was evaluated using two *var* genes from 3D7 parasites. The first gene, PF3D7_0809100 (3D7*var*UPSB6-HA^{endo}), is the predominant *var* gene expressed in the employed 3D7 cell line (Vaaben, 2018) and encodes a CD36-binding PfEMP1 variant (Figure 13A; cell line kindly generated by Paolo Mesén-Ramírez). The second *var* gene, *var2csa* (PF3D7_1200600, 3D7*var*2csa-HA^{endo}) (Figure 13B; cell line kindly generated by Paolo Mesén-Ramírez), encodes the PfEMP1 binding to CSA. Diagnostic PCRs (kindly performed by Paolo Mesén-Ramírez) confirmed successful integration of the plasmid into the genome in all parasites following G418 selection (Figure 13A, B). PCR products were detected for the 5' and 3' integration junctions while no products were detected for the original locus, contrasting the IT4 wildtype parasites. Immunofluorescence assays (IFAs) (kindly performed by Paolo Mesén-Ramírez) revealed a signal for the HA-tagged PfEMP1 in both cell lines, co-localizing with the Maurer's clefts marker SBP1 (Figure 13A, B), corresponding to the usual location PfEMP1 is detected in with antibodies. Typically, PfEMP1 on the erythrocyte

membrane remains undetected by standard IFA with antibodies against the C-terminus (Dixon et al., 2011; Maier et al., 2008). Notably, in the 3D7var2csa-HA^{endo} cell line, additional signals not co-localizing with SBP1 were observed (Figure 13B, arrows/enlargement), potentially representing PfEMP1 molecules at the erythrocyte membrane or in transport structures.

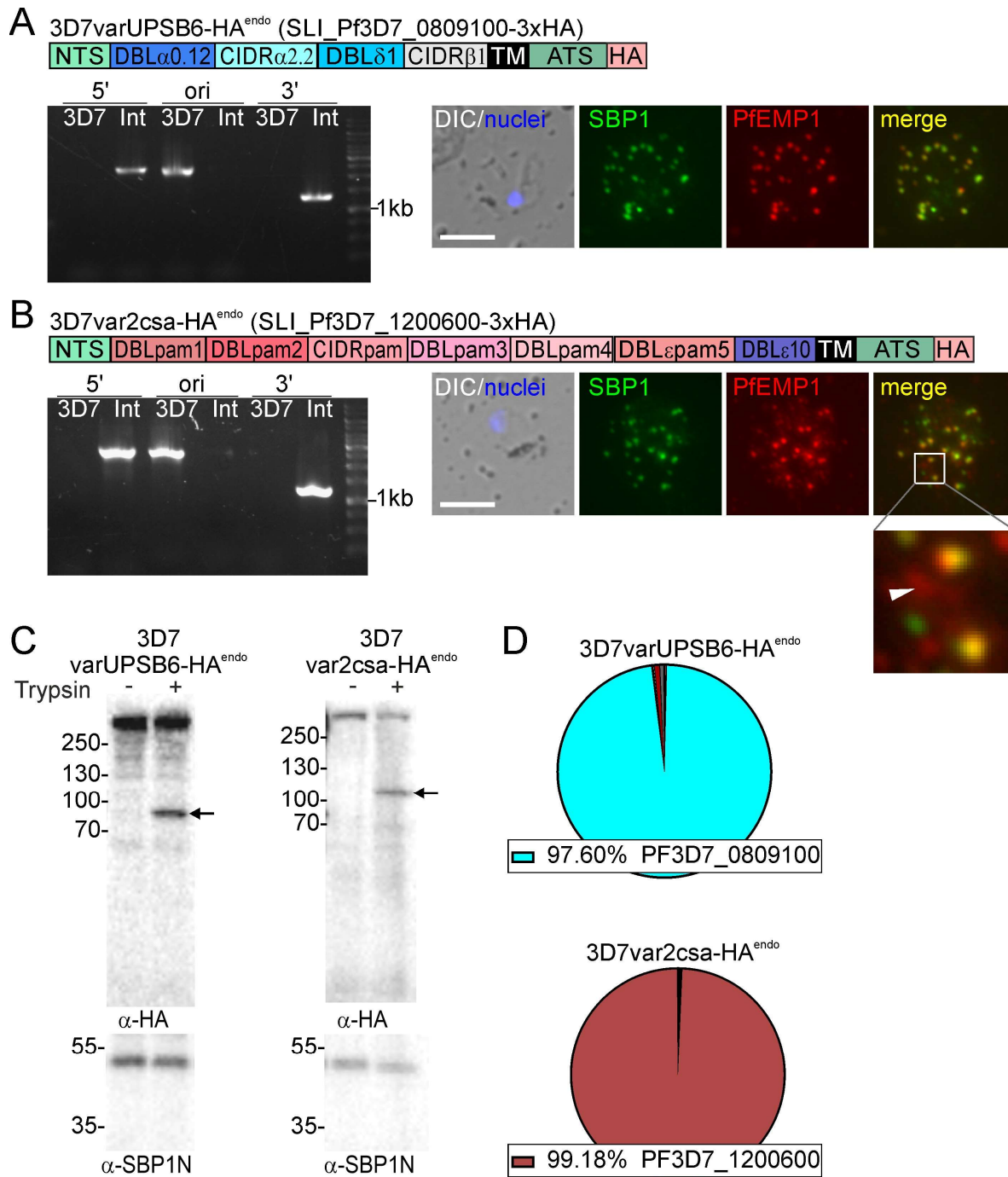


Figure 13: Confirmation of predominant expression of specific *var* genes modified with SLI in 3D7. (A, B) Confirmation of the activation of PF3D7_0809100 and PF3D7_1200600 in 3D7 parasites. Schemes show domain organization and HA-tagging of the modified *var* gene. Agarose gels show PCR products confirming correct integration of the SLI plasmid. Product over 5' integration junction (5'): P1 + P2; 3' integration junction (3'): P3 + P4; original locus (ori): P1 + P4; see Figure 12A for primer positions and Appendix A2 for sequences; 3D7: parent; Int: integrant cell line. Expected bands: 3D7var2csa-HA^{endo} (5': 2884 bp; ori 2790 bp; 3': 1269 bp);

3D7varUPSB6-HA^{endo} (5': 2640 bp; ori: 2631 bp; 3': 1354 bp). Fluorescence microscopy images show IFAs with acetone fixed parasites using anti-HA antibodies (detection of PfEMP1) and anti-SBP1 (detection of Maurer's clefts marker SBP1). Nuclei: DAPI; DIC: differential interference contrast; size bars 5 μ m. Enlargement showing PfEMP1 signal not co-localizing with SBP1-signal. Arrow shows non-co-localization of PfEMP1 and SBP1 example. (C) Western blot of trypsin cleavage assays with indicated parasites. Arrows show protected PfEMP1 fragment indicative of surface exposure. α -SBP1-N: control for integrity of host cell (breach of ERYTHROCYTE would result in a smaller SBP1 fragment). Marker in kDa. Replicates and full blots in Appendix B. (D) Pie charts show proportions of *var* gene transcripts of the indicated cell lines determined by RNAseq, normalized to TPM.

To further investigate the surface presentation of the "activated" PfEMP1, trypsin cleavage assays were performed (Figure 13C). Isolated trophozoites (18 – 30 hours post-infection) were treated with trypsin or mock treated as a control. Western blot analysis of the extracts detected a shorter PfEMP1 fragment in trypsin-treated parasites which was not present in the control, indicative of surface-exposed PfEMP1. For 3D7varUPSB6-HA^{endo} a protected fragment was detected at ~90 kDa and for 3D7var2csa-HA^{endo} the protected fragment showed a size of ~110kDa (Figure 13C). The integrity of the host erythrocyte was assessed using anti-SBP1-N antibodies against the N-terminus of SBP1. This control confirmed that trypsin did not breach the host cells membrane, as only full length SBP1 was detected (Figure 13C). If the erythrocyte membrane had been breached, intracellular SBP1 would have been digested, resulting in a detectable ~35 kDa band in the trypsin-treated samples which corresponds to the Maurer's clefts internal part and the TM of SBP1.

To validate the exclusive expression of the targeted *var* gene, RNA sequencing (RNAseq) analysis was conducted (performed by Johannes Allweier). Reads corresponding to exon 1 of the *var* genes were normalized to transcripts per million (TPM) for quantitative analysis. These results showed that a majority of the expressed *var* gene transcripts were from the targeted *var* gene: 97.60% in the 3D7varUPSB6-HA^{endo} cell line and 99.18% in the 3D7var2csa-HA^{endo} cell line (Figure 13D). These findings demonstrate that the SLI-system permits the effective generation of parasites with predominant expression of the targeted *var* gene.

3.1.3 COPENHAGEN 3D7 CELL LINE SHOWS DEFECT IN MUTUALLY EXCLUSIVE EXPRESSION

Joergensen et al. (2010) provided evidence of multiple PfEMP1 variants being expressed within a single parasite in a 3D7 cell line from the Lavstsen lab (University of Copenhagen). Building on this, the *var* gene PF3D7_0425800 was SLI-activated in both a "healthy" 3D7 cell line (3D7 strain from Hamburg (Spielmann lab), Figure 14A; 3D7varUPSA1-HA^{endo}; cell line kindly

generated by Jan Stacker) and the “sick” 3D7 cell line (3D7 strain from Copenhagen; Lavstsen lab), Figure 14B; 3D7^{MEED}varUPSA1-HA^{endo}; MEED: mutually exclusive expression defect; cell lines kindly generated by Jan Stacker) (Vaaben, 2018).

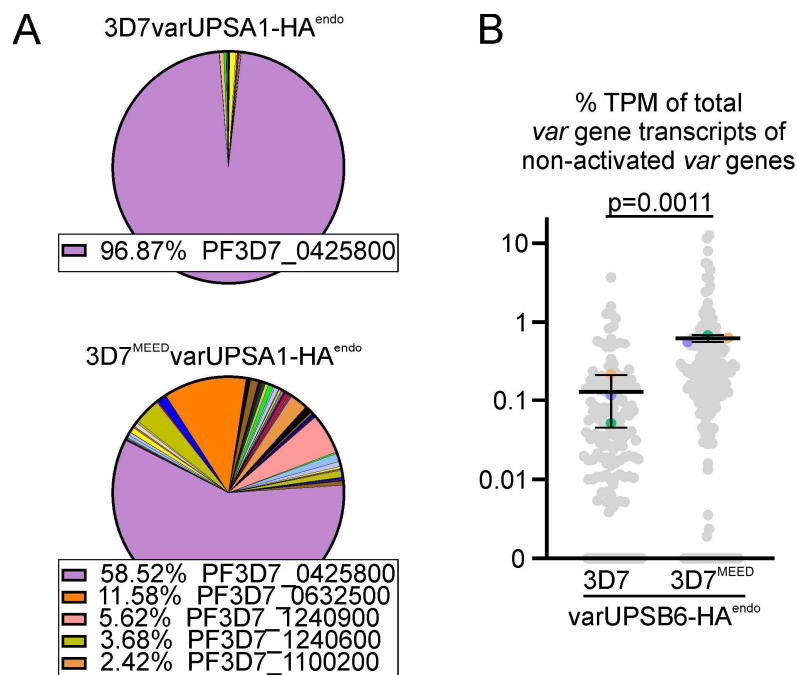


Figure 14: 3D7^{MEED} shows a defect in mutually exclusive expression. (A) Pie charts show proportions of *var* gene transcripts of the indicated cell lines determined by RNAseq and normalized to TPM. (B) SuperPlot (Lord et al., 2020) showing percentage (log scale) of total *var* gene transcripts for non-activated *var* genes of the indicated cell line determined by RNAseq (normalized to TPM; small grey dots: individual *var* genes; large colored dots: average of each replicate; bars: mean of averages of replicates with SD; n = 3 biological replicates; unpaired t-test; p-values indicated).

RNA sequencing (kindly performed by Johannes Allweier) indicated that 96.87% of total *var* gene transcripts in the 3D7varUPSA1-HA^{endo} line, and only 58.52% in the 3D7^{MEED}varUPSA1-HA^{endo} line, originated from the activated *var* gene PF3D7_0425800 (Figure 14C). These results are in agreement with previous performed qPCR results (Vaaben, 2018). To further investigate, experiments were repeated and the transcript proportions of total *var* gene transcripts for non-activated *var* genes within both cell lines were compared for three biological replicates. The results revealed a significant increase in transcripts from non-activated *var* genes in the 3D7^{MEED} parasites, further confirming a defect in the mechanism of mutually exclusive expression in that cell line (Figure 14D).

3.1.4 EVIDENCE THAT PfEMP1 IS EXPORTED THROUGH THE PTEX CHANNEL

Next, the SLI cell line 3D7varUPSA1-HA^{endo} was employed to investigate the export mechanisms of PfEMP1 to reach the host cell cytosol. It is unclear whether PfEMP1 is translocated through the PTEX channel or uses a different pathway to cross the PVM. The mDHFR domain was utilized, a domain that is known to increase its structural stability upon ligand binding, a property that was first used to study protein translocation into mitochondria (Eilers and Schatz 1986). In malaria parasites the ligand used to stabilize mDHFR is WR, a folate analogue. If an exported protein is fused to mDHFR, addition of WR prevents the passage of that protein through the PTEX translocon and in specific cases also blocks the translocon, preventing the passage of other proteins (termed “co-block”) (Grüring et al., 2012). Previous research (Naranjo Prado, 2020) suggested that PfEMP1 export is hindered when the PTEX channel is obstructed using a SBP1-mDHFR-GFP construct to block the PTEX channel after WR addition. However, in that study, the construct was either episomally expressed under an episomal *mal7* promoter or under the endogenous SBP1 promoter, both of which mediate expression very early after invasion (Grüring et al., 2011). This early induction potentially blocks exported proteins crucial for PfEMP1 transport and parasite survival, indirectly affecting PfEMP1 transport.

To address this, a co-block construct and a block-reporter (to show that PTEX was indeed blocked) was used, expressed under the same late-expressing *crt* promoter (Grüring et al., 2011) (Figure 15A, B). The construct to achieve this contained the blocking component SBP1-mDHFR-GFP linked to a skip peptide and KAHRP-mScarlet which served as the reporter for a successful PTEX channel blockage (Figure 15A, B).

Following WR treatment, live imaging confirmed the successful retention of both SBP1-mDHFR-GFP and KAHRP-mScarlet in the parasite periphery, consistent with an arrest in export in the parasitophorous vacuole (Figure 15D). IFAs using antibodies against the HA-tag indicated that PfEMP1-HA is also arrested in the PV when KAHRP-mScarlet is retained after WR treatment (+WR). In contrast, in the control (-WR), PfEMP1 and KAHRP-mScarlet were both exported to the host cell (Figure 15D).

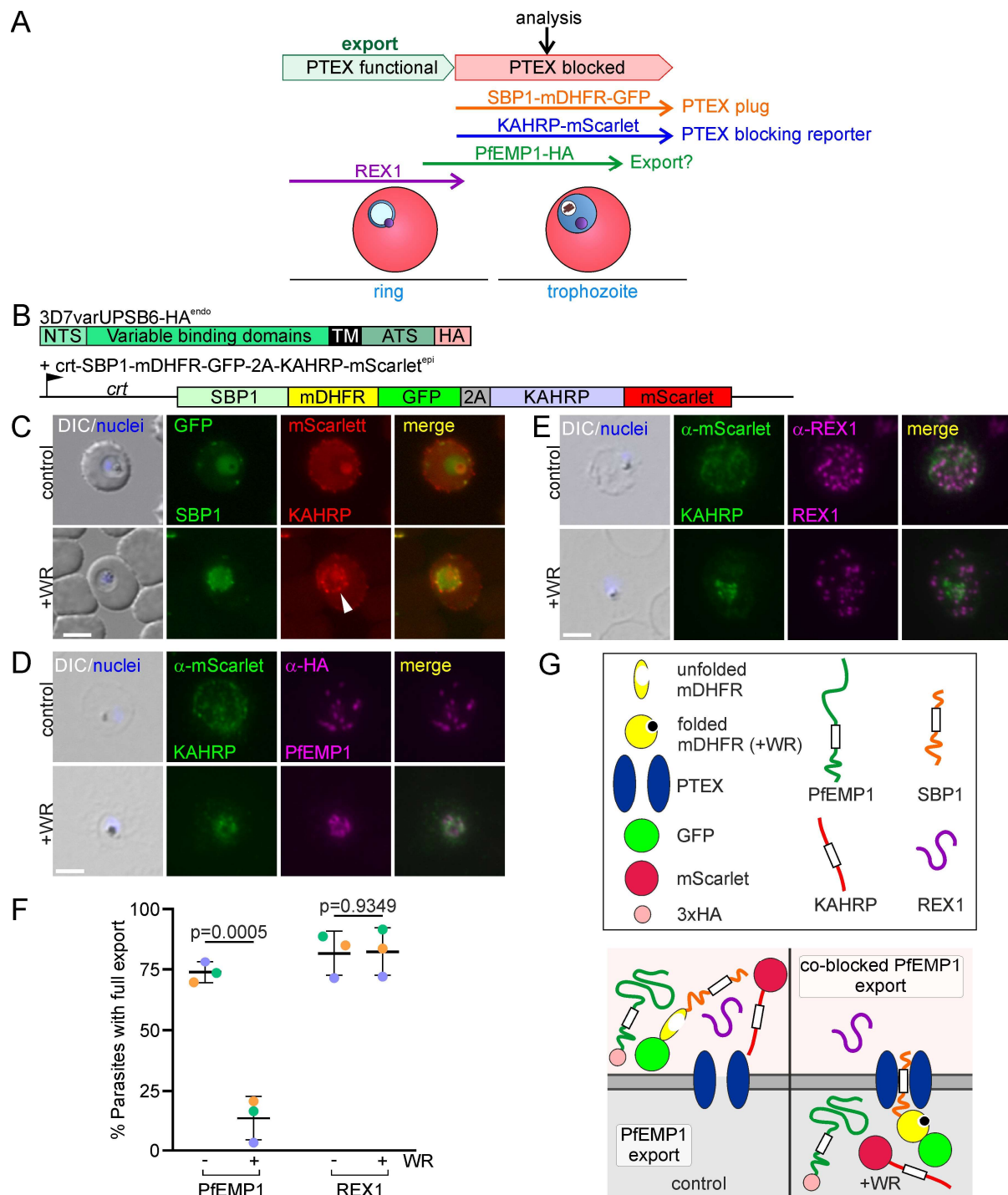


Figure 15: Export of PfEMP1 is prevented by blocking PTEX at the onset of the trophozoite stage. (A) Illustration shows the experimental strategy and timing to jam PTEX with a late expressed (*crt* promoter) episomal co-blocking construct (Mesén-Ramírez et al., 2016) in 3D7varUPSA1-HA^{endo}. (B) Scheme of domain organization of the expressed PfEMP1 and early (*crt* promoter) expressed co-block construct. (C) Live cell images of the co-blocking cell line – and +WR. White arrow: KAHRP-mScarlet arrested in the parasite's periphery; nuclei: Hoechst 33342; DIC: differential interference contrast; size bars 5 μ m. (D, E) Fluorescence microscopy images show IFAs with acetone fixed parasites with the indicated antibodies. Nuclei: Hoechst 33342; DIC: differential interference contrast; size bars 5 μ m. (F) Graph: quantification of parasites with a PfEMP1 or REX1 export phenotype + and - WR from 3 biological replicates (-WR, PfEMP1: n = 34, 76, 60; +WR, PfEMP1: n = 18, 48, 30; -WR, REX1: n = 18, 27, 35; +WR, REX1: n = 12, 31, 25; +WR only parasites with an KAHRP-mScarlet (PTEX block reporter) export phenotype were scored; bars: mean of replicates with SD; unpaired t-test; p-values indicated. (G) Legend showing meaning of the pictograms below. Scheme shows the effect of WR-dependent clogging of PTEX (right)

or control (left) on the tested proteins.

Further investigations in these parasites focused on the export of the early exported protein REX1 (McMillan et al., 2013) as these could influence the export of PfEMP1. IFAs revealed that REX1 was fully exported in WR-treated parasites, despite the retention of KAHRP-mScarlet in the PV, showing that the block of PTEX occurred only after most exported proteins already reached the host cell (Figure 15E). In the control condition, both KAHRP-mScarlet and REX1 were exported to the host cell (Figure 15E). Quantitative analysis of PfEMP1 and REX1 export in WR-treated parasites demonstrated a significant difference between the export of REX1 and PfEMP1 after WR treatment compared to the control (Figure 15F). This indicates that the ablation in the export of PfEMP1 is not attributed to the absence of earlier exported proteins in the host cell but that PfEMP1's export itself is directly reliant on the PTEX channel (Figure 15G).

3.1.5 ESTABLISHMENT OF A PIPELINE FOR AUTOMATED EVALUATION OF BINDING ASSAYS

One of the challenges in the study of PfEMP1 is the testing of the functionality of PfEMP1 molecules on the surface, i.e. its capacity to bind to receptors and mediate cytoadherence. Even though FACS analysis (Avril et al., 2006) or trypsin cleavage assays (Waterkeyn et al., 2000) can determine the surface presentation of PfEMP1 this does not let one conclude that the PfEMP1 molecules presented are in a functional state. Therefore, binding assays to supports or cells carrying receptor(s) under static and flow conditions or in tissue models have been employed as functional assays for the clarification of the binding capacity of the PfEMP1 molecules in a parasite population (Bernabeu et al., 2019; Fried and Duffy, 1996; Gray et al., 2003).

However, binding assays against receptor-expressing cells face the challenge of high variability due to the non-uniform confluency of receptor-expressing cells and by the heterogeneous expression levels of receptors between individual cells. This necessitates the evaluation of larger areas of the used cell culture to obtain accurate results. However, manual scoring of binding of large areas is time intensive. Preliminary experiments indicated that evaluating 225 images required 11.25 hours manual scoring time, averaging 180 seconds per image. This volume of data corresponds to the assessment of five parasite cell lines against three receptors,

with 15 fields of view per receptor and cell line imaged (number of images analyzed was increased compared to previous standard protocols (3 images per coverslip) to account for the observed variation). To complete three replicates, an additional 22.5 hours would be needed. It is noteworthy that the time required is directly proportional to the number of bound infected erythrocytes per image; a greater number would extend the duration of the evaluation.

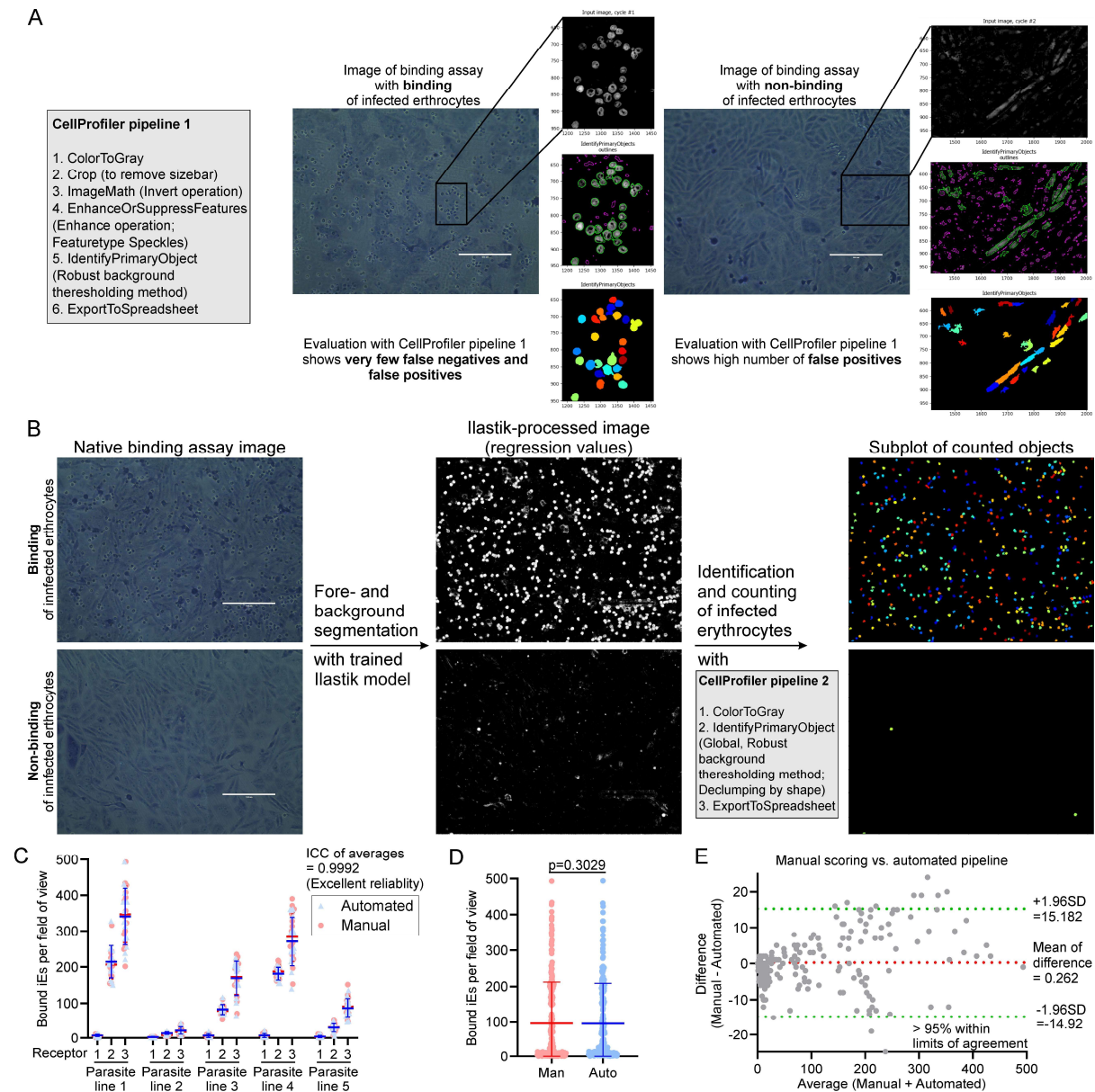


Figure 16: Establishment of an automated pipeline for the evaluation of binding assay images. (A) Images of binding assays with binding or non-binding (control) of infected erythrocytes to receptor expressing cells evaluated by a generated CellProfiler (*Stirling et al., 2021*; version 4.2.1) pipeline. Table shows CellProfiler pipeline 1. Large images show native captured input image. Smaller pictures show processing by the pipeline (from top to bottom). (Top) Images after processing by “EnhanceOrSupressFeatures” that was fed to the next module. (Middle) Images with accepted and rejected outlines of objects determined by shape and “robust background” thresholding in the “IdentifyPrimaryObjects” module. Green outlines: accepted objects; purple outlines: rejected objects. (Bottom) Objects that were counted with colors representing different accepted objects. (B) Illustration of the pipeline for automated scoring of the number of bound infected erythrocytes in images captured from binding assays. Left: representative image of a binding assay showing binding (top) or no binding

(bottom) of infected erythrocytes. Ilastik (*Berg et al., 2019*; version 1.3.3post3) model (trained on 20 images) separates fore- and background of native captured images (left, input images; middle, output images). Foreground: infected erythrocytes; background: CHO/HBEC-5i cells and plastic. Gray box: CellProfiler pipeline 2 to score pre-segmented images (middle, input images; right, output images). (C) Results of binding assays for five parasite lines tested against three different receptor expressing CHO-cells evaluated by manual scoring and the automated pipeline (15 fields of views were analysed per cell line and receptor, total: 225; bars: mean and SD). ICC: intraclass correlation coefficient. (D) Comparison of all images from (C) evaluated by manual scoring against scoring by the automated pipeline. Red dots: bound infected erythrocytes (iE) in individual images from manual scoring (blue dots) or scoring by the automated pipeline. Man: manual scoring; auto: automated pipeline (n = 225; bars: mean and SD; paired t-test; p-value is indicated). (E) Bland-Altman plot comparing evaluation of images of binding assays from (B) by manual scoring and scoring by the automated pipeline. Green lines, limits of agreement.

In an attempt to automate the evaluation of images of binding assays CellProfiler (Stirling et al., 2021), a widely recognized cell image analysis software was tested for its capacity to count the number of bound infected erythrocytes. To precisely identify infected erythrocytes in captured images, various CellProfiler (version 4.2.1) pipelines were designed for testing. It is noteworthy that CellProfiler is commonly employed for analyzing images with fluorescent signals (such as nuclei stained with DAPI), histological images stained with various dyes, or brightfield microscopy images with distinct backgrounds. The images in this analysis, however, presented a unique challenge due to the substantial amount of background signal (CHO/HBEC-5i cells) with color and shape characteristics similar to the infected erythrocytes, a scenario not typically encountered in standard applications of CellProfiler. Therefore, a crucial aspect of this automation was thresholding, which discriminates between the foreground (the signal of interest: infected erythrocytes) and the background (unwanted signals: plastic artefacts and receptor-expressing cells).

After testing several CellProfiler pipelines differing in models used and settings in the modules, one pipeline was further evaluated as it was able to reliably score infected erythrocytes comparable to the manual scoring. The central module in most CellProfiler pipelines is the “IdentifyPrimaryObjects” module for the identification and counting of objects. This module alone was not able to segment the fore- and background in the images correctly regardless of the tested settings. For that reason, the “EnhanceOrSupressFeatures” module was employed to enhance “speckles” (Feature type: speckles) with a feature size of 25 pixels (diameter; pictures were captured in 400x magnification). This enabled a successful pre-segmentation for the following processing. After evaluating several thresholding techniques such as 'robust background', 'minimum cross-entropy' and 'otsu', the 'robust background' thresholding method in the “IdentifyPrimaryObjects” module was chosen due to its effectiveness in separation of fore- and background, for identifying infected erythrocytes with minimal false positives or negatives (Figure 16A). However, challenges arose when applying this pipeline to images with

few or no bound infected erythrocytes. In these cases, the pipeline incorrectly scored receptor-expressing cells as foreground objects (high number of false positives) (Figure 16A). Adjustments to the settings intended to rectify this issue inadvertently led to a large number of false negatives in images with a high number of infected erythrocytes. Hence, adjustments in the pipeline can render the pipeline functional for both cases individually, however this would not lead to a satisfactory automation and comparable results of the evaluation.

To solve this issue a second computer software, Ilastik (Berg et al., 2019; version 1.3.3post3), was used that employs a neural network based on a pre-trained model. This “pixel classification” model uses a simple but robust random forest machine learning algorithm that must be manually trained to classify pixels of a given image. Its output are values for each pixel of the image in either regression values (0.0 to 1.0) or classification (0 or 1) of the input image. This enables a pre-segmentation of background and infected erythrocytes. The model was trained for the separation of fore- and background across 20 images, obtained from the previous experiments. It was trained with all available features selected for more precise processing with a trade-off in processing time. The selected images were chosen to represent a wide range of artifacts and morphologies of infected erythrocytes and receptor-expressing mammalian cells. After processing the native captured images of binding assays with the trained Ilastik model the output images were shown in regression values (0.0 = black = 0% certainty for foreground; 1.0 = white = 100% certainty for infected erythrocytes) for the individual pixels (Figure 16B).

A new more simplified and robust CellProfiler pipeline was constructed customized to the Ilastik-processed images (Figure 16B). The 225 images evaluated by manual scoring were used to test the reliability of the pipeline and the outcome was compared to the manual scoring. The results showed no significant difference between the evaluation of the images with the manual scoring and with the automated pipeline (Figure 16C) (Intraclass correlation coefficient of 0,9992 (excellent reliability); averages compared). A comparison of the total analyzed individual pictures evaluated by both methods did not show a significant difference (t-test: p-value = 0.3029) (Figure 16D). A Bland-Altman plot comparison showed that > 95 % of the differences in evaluation are within the limits of agreement (Figure 16E). These statistical tests indicated that the difference between the automated pipeline and manual scoring is statistically insignificant. Therefore, this pipeline for the evaluation of binding assays can be considered highly reliable and will be applied throughout this work.

3.1.6 3D7 SHOW POOR BINDING PHENOTYPES

Anecdotal evidence suggests that the most used laboratory *P. falciparum* strain, 3D7, shows poor cytoadherence levels. Contrastingly, previous studies have shown that the IT4 laboratory strain (Jensen and Trager, 1978; there called FCR3S1.2) retains high levels of cytoadherence. Initial experiments using parasites with a SLI-activated *IT4var01* gene in IT4 parasites were capable of binding to the expected receptors (CD36 and ICAM-1) expressed on CHO cells (Blancke-Soares et al., 2021; Stacker, 2021).

To further explore the usefulness of IT4 for binding studies compared to 3D7, two PfEMP1 variants were selected for activation with SLI in IT4 that have comparable binding domains to those activated in 3D7 (Figure 13). The first was the only CSA-binding PfEMP1 variant VAR2CSA (PfIT_120006100, *IT4var4*, *IT4var2csa*-HA^{endo}) which is conserved across parasite isolates (Figure 17A). The second was a CD36-binding PfEMP1 variant (PfIT_040025500, *IT4var66*, *IT4var66*-HA^{endo}), the predominant *var* gene in the IT4 parental cell line and containing similar binding domains to the PfEMP1 expressed in 3D7varUPSB6-HA^{endo} parasites (Figure 17B). Diagnostic PCR confirmed correct integration of the SLI-plasmids into the genome for both parasite populations (Figure 17A, B). PCRs showed products for the 5' and 3' integration junctions while no products were detected for the original locus, contrasting the IT4 wildtype parasites. IFAs revealed expression of the HA-tagged PfEMP1s and their colocalization with SBP1 in both cell lines (Figure 17A, B). RNA sequencing (performed by Johannes Allweier) showed predominant expression of the targeted *var* genes: 97.81% in *IT4var66*-HA^{endo} and 80.04% in *IT4var2csa*-HA^{endo} (Figure 17D) of the total *var* gene transcripts. Interestingly, in the *IT4var2csa*-HA^{endo} cell line, exhibited a notable expression of *var66* (4.92%), the predominantly expressed *var* gene in the parental cell line (Appendix D), and *var1csa* (12.93%). Previous research indicated that while *var1csa* is frequently expressed in IT4, it does not produce a functional protein due to the lack of an ATS domain (premature stop codon) and might have regulatory purposes (Kyes et al., 2003; Winter et al., 2003).

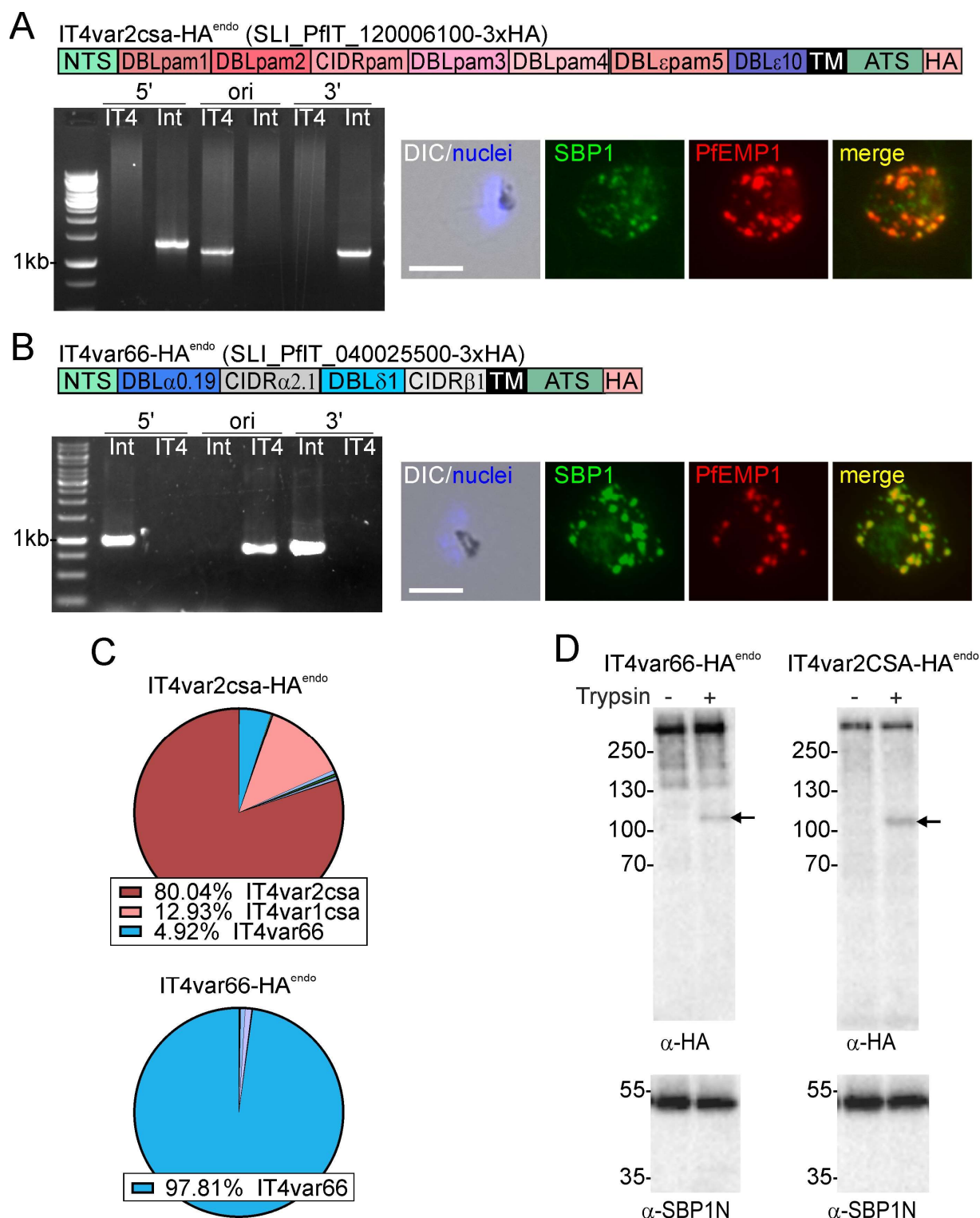


Figure 17: Confirmation of SLI-activation of two *var* genes in IT4. (A, B) Activation of PfIT_120006100 and PfIT_040025500 in IT4 parasites via SLI. Schemes show domain organization and HA-tagging of the modified *var* gene. Agarose gels show PCR products confirming correct integration of the SLI plasmid. Product over 5' integration junction (5'): P1 + P2; 3' integration junction (3'): P3 + P4; original locus (ori): P1 + P4; see Figure 12A for primer positions and Appendix A2 for sequence; IT4: parent; Int: integrant cell line. Expected bands: IT4var2csa-HA^{endo} (5': 1346 bp; ori 1158 bp; 3': 1175 bp); IT4var66-HA^{endo} (5': 1064 bp; ori: 884 bp; 3': 901 bp). Fluorescence microscopy images show IFAs with acetone fixed parasites with α -HA (detection of PfEMP1) and α -SBP1 (detection of Maurer's clefts marker SBP1). Nuclei: Hoechst 33342; DIC: differential interference contrast; size bars 5 μ m. (C) Western blot of trypsin cleavage assays with indicated parasites. Arrows show protected

PfEMP1 fragment indicative of surface exposure. α -SBP1-N: control for integrity of host cell (breach of ERYTHROCYTE would result in a smaller SBP1 fragment). Marker in kDa. Replicates and full blots in Appendix B. **(D)** Pie charts show proportions of *var* gene transcripts of the indicated cell lines determined by RNAseq and normalized to TPM.

To assess the surface presentation of the HA-tagged PfEMP1s, trypsin cleavage assays were conducted with intact infected erythrocytes. These experiments showed a band at approximately 110 kDa for both cell lines in the trypsin-treated samples, corresponding to a C-terminal protected fragment of PfEMP1 (Figure 17E). No such bands were detected in the control samples that were not treated with trypsin. Only bands corresponding to full-length SBP1 were detected with an antibody against the N-terminus of SBP1, thus there was no evidence of trypsin breaching the host cell membrane. Taken together these findings confirm the successful activation of the targeted PfEMP1 variants in IT4, along with their typical localization in the Maurer's clefts and presentation on the host cell surface, similar to the results with the activated PfEMP1s in the 3D7 cell line (Figure 13)..

In order to compare the binding properties of IT4 and 3D7 parasites, binding assays were conducted. Initially, the *var2csa*-expressing 3D7 and IT4 SLI-lines were tested against the primary brain cell line HBEC-5i, known to express CSA on its surface (Wassmer et al., 2006). The results demonstrated that erythrocytes infected with IT4*var2csa*-HA^{endo} parasites exhibited binding to HBEC-5i cells while erythrocytes infected with 3D7*var2csa*-HA^{endo} parasites showed very low, non-significant binding compared to the wildtype (Figure 18A, B). The binding of IT4*var2csa*-HA^{endo} parasites was significantly inhibited by the addition of soluble CSA (sCSA) to the binding reaction, indicating specific binding to CSA. Erythrocytes infected with parasites from either the 3D7 or IT4 wildtype cell lines (the parents without a specifically activated *var* gene) did not show binding to the HBEC-5i cells (Figure 18A, B).

To further delineate these binding phenotypes and rule out non-specific interactions with other proteins or proteoglycans expressed on the HBEC-5i cells, binding assays against decorin (leucine repeats coupled to CSA) immobilized on coverslips were performed. Here again, only the erythrocytes infected with IT4*var2csa*-HA^{endo} parasites demonstrated binding, and this interaction was also inhibited by addition of sCSA to the binding reaction (Figure 18C, D). No binding to decorin was observed for erythrocytes infected with 3D7, IT4, or 3D7*var2csa*-HA^{endo} parasites (Figure 18C, D). These findings suggest that the binding observed for IT4*var2csa*-HA^{endo} parasites is specifically attributable to the activation of *var2csa* and directed against CSA, not other components of the HBEC-5i cell line.

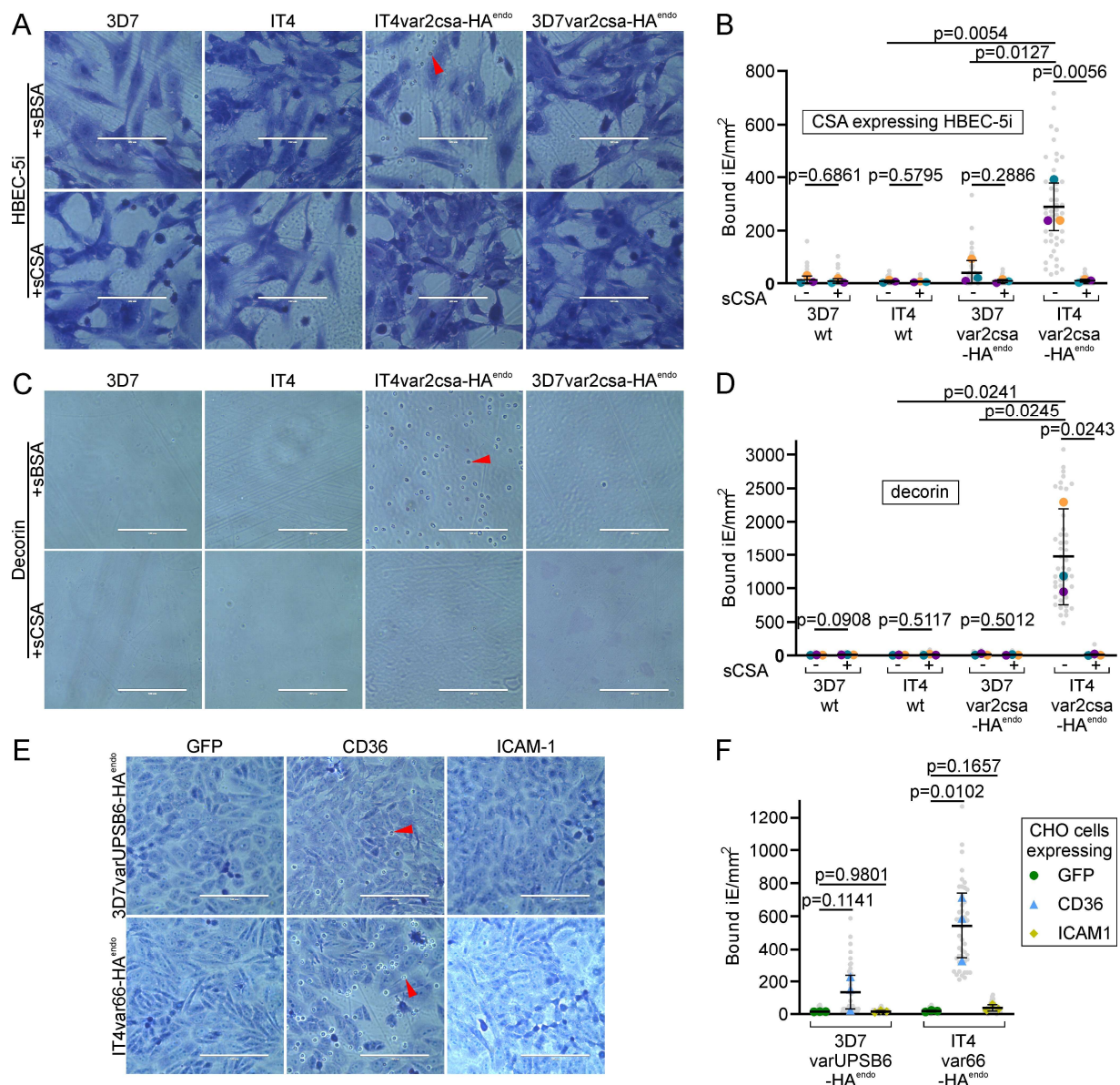


Figure 18: Comparison of the cytoadherence properties of 3D7 and IT4 parasites. Results of binding assays of the indicated cell lines. (A, C, E) Image panels show representative sections of microscopy images captured of binding assays with the indicated cell line against CSA- expressing HBEC-5i, immobilized decorin or CHO cell expressing the indicated receptor, respectively; arrows show examples of bound infected erythrocyte; brightness of images adjusted with CorelDraw 2021 with intensity command. (B, D, F) SuperPlots show results from three biological replicates of binding assays against HBEC-5i, immobilized decorin or CHO cells expressing the indicated receptor, respectively (15 field of views were counted per experiment and condition; SD; unpaired t-test; p-values are indicated). Small grey dots show number of bound iE for every field of view captured, extrapolated to mm². In (B) and (D) larger colored dots show average bound iE/mm² for each experiment. Each color represents an individual experiment. In (F) Small grey dots show bound iE for every field of view captured, extrapolated to mm². Larger colored dots show average number bound iE/mm² for each experiment. Green circle: CHO-GFP; blue triangle: CHO-CD36; yellow rhombus: CHO-ICAM-1.

Next, the binding properties of CD36-binding PfEMP1 variants activated in 3D7 and IT4 parasites were compared. For this, the binding of erythrocytes infected with IT4var66-HA^{endo} or 3D7varUPSB6-HA^{endo} parasites against CHO cells expressing GFP, CD36, and ICAM-1 was

evaluated. The results indicated that erythrocytes infected with parasites from both cell lines exhibited binding to CD36-expressing CHO cells, but not to those expressing GFP or ICAM-1 (Figure 18E, F). However, comparing the binding efficacy to CD36, IT4var66-HA^{endo} parasites showed significant binding compared to the GFP control (p-value = 0.0102) while 3D7varUPSB6-HA^{endo} binding to CD36 was not significant when compared to the GFP control (p-value = 0.1141). While this can be taken as evidence to further underscore the different ability in binding of 3D7 and IT4 parasites it is important to note that in contrast to VAR2CSA, these two PfEMP1 variants are less conserved and not truly comparable.

In conclusion, these results established a clear difference in the binding capabilities between the two parasite strains: the IT4 strain demonstrates robust binding efficiency while the 3D7 strain exhibited a diminished binding capacity. This contrast underlines the usefulness of the IT4 strain as a model for investigating PfEMP1-mediated *in vitro* cytoadherence.

3.1.7 GENERATION OF A COLLECTION OF IT4 LINES WITH DIFFERENT ACTIVATED *VAR* GENES

The previous findings established that the SLI-system can effectively activate and modify functional PfEMP1 variants in the IT4 strain. This advancement presents an opportunity to establish parasite cell lines expressing a defined PfEMP1 binding to each of the known major receptors. It also enables to investigate the binding properties of PfEMP1 variants with unidentified binding partners or comparison of the binding capacities of two different PfEMP1s to a specific receptor.

Table 17: List of *var* genes chosen for the activation in IT4 parasites.

<i>var</i> gene	Accession number	Group	Predicted binding partners	obtained on G418	integration confirmed
<i>IT4var02</i>	PfIT_090005100	A	unknown	✓	✓
<i>IT4var03</i>	PfIT_140006400	A	unknown	✓	✓
<i>IT4var07</i>	PfIT_060036700	A	EPCR, ICAM-1	-	-
<i>IT4var08</i>	PfIT_070005900	A	unknown	✓	✓
<i>IT4var09</i>	PfIT_130005300	A	unknown	✓	-
<i>IT4var18</i>	PfIT_030029700	A	EPCR	-	-
<i>IT4var22</i>	PfIT_100044000	A	EPCR	✓	X
<i>IT4var35</i>	PfIT_050037800	A	None/pseudogene	✓	-

(<i>var1csa</i>)					
<i>IT4var64</i>	PfIT_070017100	A	unknown	-	-
<i>IT4var06</i>	PfIT_020027600	B	EPCR	-	-
<i>IT4var16</i>	PfIT_120024500	B	CD36, ICAM-1	✓	✓
<i>IT4var19</i>	PfIT_010005000	B	EPCR	✓	✓
<i>IT4var20</i>	PfIT_070017000	B	EPCR	✓	✓/hybrid
<i>IT4var66</i>	PfIT_040025500	C	CD36	✓	✓
<i>IT4var4</i> (<i>var2csa</i>)	PfIT_120006100	PAM	CSA	✓	✓

Therefore, 13 further *var* genes from the IT4 strain, in addition to the two previously activated *var* genes, were targeted for activation by SLI (Table 17). This selection now comprised 9 *var* genes belonging to group A, 4 of group B, one of group C and *var2csa* from group E. The group A *var* genes were selected as this group is associated with severe malaria manifestations (Rottmann et al., 2006). Among these, two *var* genes feature domains that are predicted to bind to EPCR, one contains domains predicted for EPCR-ICAM-1 dual-binding, and the remaining four encompass domains whose binding properties are yet to be identified. The group B *var* genes were chosen for their confirmed EPCR-binding domains (Nunes-Silva et al., 2015; Turner et al., 2013) which are associated with the pathology of malaria (Mosnier and Lavstsen, 2016), along with one *var* gene possessing confirmed binding domains for CD36 and ICAM-1 (Avril et al., 2016; Janes et al., 2011). The CD36-binding group C *var* gene, *IT4ar66* and CSA-binding group E *var* gene *var2csa* were chosen for the comparison to the *var* genes activated in 3D7 (Figure 18).

For the SLI-activation, homology regions had to comprise the C-terminus of the ATS domains of each *var* gene. The chosen homology regions were approximately 1000 base pairs in length. As the region encoding the ATS is often rather conserved, the targeting regions were extended further into the N-terminal region to increase the length of sequence specific for the desired *var* gene. This strategy was employed across all the *var* genes under investigation.

For 11 of the 15 *var* genes SLI cell lines were obtained after the selection on G418 (Table 17), including the parasites expressing *IT4var2csa* and *IT4var66* (section 3.1.6). In most cases parasites were obtained after 3 integration attempts and for those this was not successful, at least 5 attempts were made before abandoning further attempts. For 8 of the 11 cell lines correct

integration of the SLI plasmid into the targeted *var* gene was confirmed (Table 17) and are described in the following sections.

3.1.7.1 *IT4VAR02*

The *IT4var02* gene encodes binding domains of unknown binding properties which renders this a *var* gene of interest. The SLI-generated cell line was termed IT4var02-HA^{endo}. Diagnostic PCRs confirmed the correct 5' integration with a detected band at ~1450 bp (Figure 19A). The PCR targeting the original locus showed a band for the IT4 wild type at ~1400 bp which was absent in the integrant cell line, suggesting successful integration. Although a band for the 3' integration was not observed, the collective PCR evidence supports the likelihood of correct integration in the parasite population. IFAs demonstrated expression of the HA-tagged PfEMP1 and co-localization with SBP1 at the Maurer's clefts (Figure 19A). RNA sequencing data further verified the correct integration of the plasmid and predominant expression of *IT4var2* with 95.95% of total *var* gene transcripts (Figure 19B) (kindly conducted by Johannes Allweier). This dataset also identified low-level expression of *var1csa* and *IT4var66*. Trypsin cleavage assays indicated the surface presentation of the corresponding PfEMP1 with a faint detectable band at ~110 kDa (Figure 19C) corresponding to a protected PfEMP1 fragment after trypsin treatment. No such band was observed in the control samples. Integrity of the erythrocyte was confirmed by an absence of a protected fragment for SBP1 when probed with α -SBP1-N antibodies (Figure 19C).

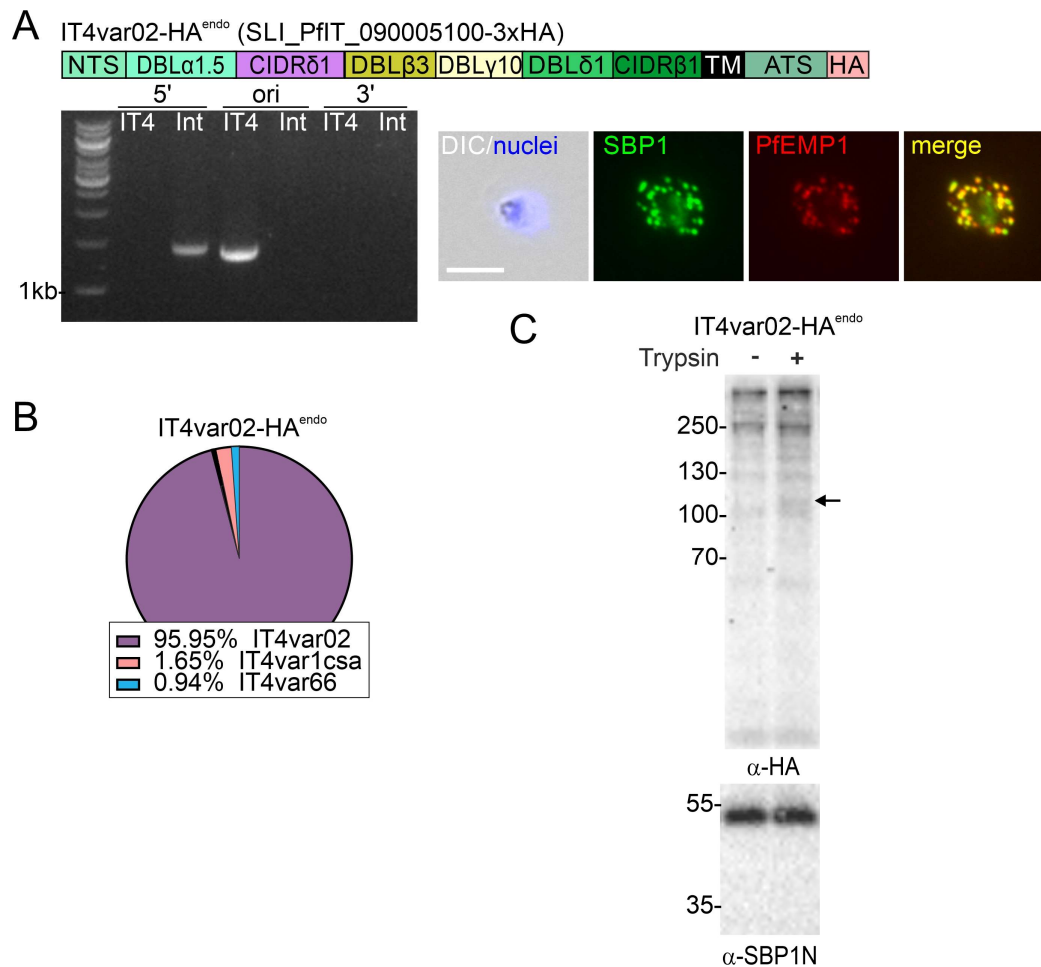


Figure 19: Characterization of the activation of *var02* in IT4 parasites. (A) Confirmation of the activation of PfIT_090005100 in IT4 parasites. Scheme shows domain organization and HA-tagging of the targeted PfEMP1. Agarose gel shows PCR products confirming correct integration of the SLI plasmid into the genome. Product over 5' integration junction (5'): P1 + P2; 3' integration junction (3'): P3 + P4; original locus (ori): P1 + P4; see Figure 12A for primer positions and Appendix A2 for sequence; IT4: parent; Int: integrant cell line. Expected bands: 5': 1470 bp; ori 1409 bp; 3': 1401 bp. Fluorescence microscopy images show IFAs with acetone fixed parasites probed with α -HA (detection of PfEMP1) and α -SBP1 (detection of Maurer's clefts marker SBP1) antibodies. Nuclei: Hoechst 33342; DIC: differential interference contrast; size bars 5 μ m. (B) Pie chart shows proportions of *var* gene transcripts determined by RNAseq and normalized to TPM. (C) Western blot of trypsin cleavage assay ($n = 2$). Arrow shows protected PfEMP1 fragment indicative of surface exposure. α -SBP1-N: control for integrity of host cell (breach of ERYTHROCYTE would result in a smaller SBP1 fragment). Marker in kDa. Full blot in Appendix B.

3.1.7.2 *IT4VAR03*

The *IT4var03* gene in IT4 encodes a PfEMP1 variant containing only two extracellular binding domains which is rather unusual for PfEMP1s. The SLI-generated cell line was termed IT4var03-HA^{endo}. Diagnostic PCR results confirmed the correct integration of the plasmid into the gene locus of *var3* (Figure 20A). PCR products were detected for the 5' and 3' integration junctions while no product was detected for the original locus, which was in contrast to the IT4 wildtype parasites. IFAs showed the co-localization of the HA-tagged PfEMP1 with SBP1 in

the Maurer's clefts, indicating the appropriate cellular location of the modified PfEMP1 (Figure 20A). RNA sequencing analysis (conducted by Johannes Allweier) showed a predominant expression of *IT4var3* with 94.84 % of all detected *var* gene transcripts in the IT4var3-HA^{endo} parasites (Figure 20B). Again, low levels of *var1csa* (2.48 %) and *IT4ar66* (1.12 %) transcripts were detected. Trypsin cleavage assays, however, did not yield a protected fragment in the trypsin-treated sample, indicating a lack or low level of surface presentation of this PfEMP1 variant (Figure 20C). It is possible that the small size of the expressed PfEMP1 resulted in a loss of critical regions needed for surface exposure or that these parasites lost a genomic region needed for cytoadherence function during the procedures to establish this cell line.

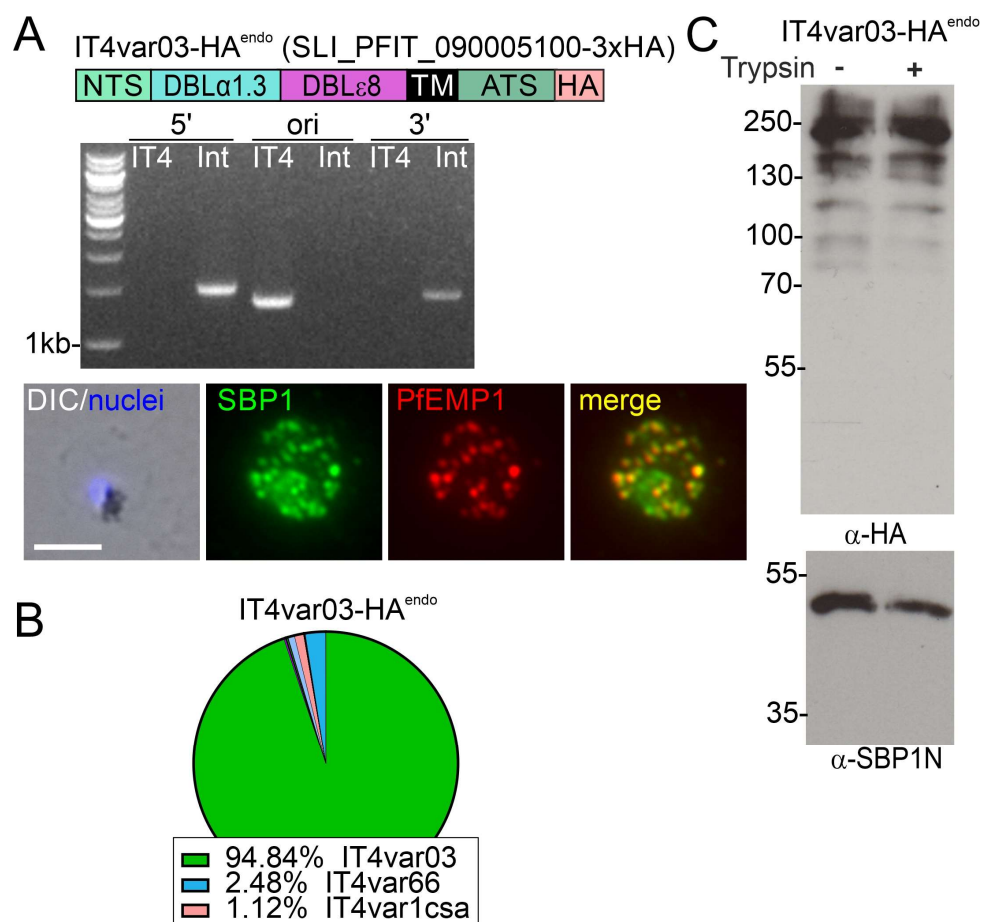


Figure 20: Characterization of the activation of *var03* in IT4 parasites. (A) Confirmation of the activation of PFIT_140006400 in IT4 parasites. Scheme shows domain organization and HA-tagging of the targeted PfEMP1. Agarose gel shows PCR products confirming correct integration of the SLI plasmid. Product over 5' integration junction (5'): P1 + P2; 3' integration junction (3'): P3 + P4; original locus (ori): P1 + P4; see Figure 12A for primer positions and Appendix A2 for sequence; IT4: parent; Int: integrant cell line. Expected bands: 5': 1542 bp; ori: 1370 bp; 3': 1412 bp. Fluorescence microscopy images show IFAs with acetone fixed parasites probed with α -HA (detection of PfEMP1) and α -SBP1 (detection of Maurer's clefts marker SBP1) antibodies. Nuclei: Hoechst 33342; DIC: differential interference contrast; size bars 5 μ m. (B) Pie charts show proportions of *var* gene transcripts determined by RNAseq and normalized to TPM. (C) Western blot of trypsin cleavage assays (n=1). Arrows show protected PfEMP1 fragment indicative of surface exposure. α -SBP1-N: control for integrity of host cell (breach of ERYTHROCYTE would result in a smaller SBP1 fragment). Marker in kDa. Full blot in Appendix B.

3.1.7.3 *IT4VAR08*

The *IT4var08* gene of IT4 transcribes binding domains of unknown binding properties, rendering it of interest. The SLI-generated cell line was termed IT4var08-HA^{endo}. Diagnostic PCR analysis confirmed successful integration of the plasmid into the *var08* gene locus (Figure 21A). PCR products were detected for the 5' and 3' integration junctions while no product was detected for the original locus which was in contrast to the IT4 wildtype parasites. IFAs showed the co-localization of the HA-tagged PfEMP1 with SBP1, affirming the correct localization at the Maurer's clefts (Figure 21A). RNA sequencing (kindly conducted by Johannes Allweier) identified *IT4var08* as the predominantly expressed *var* gene with 96.41 % of all *var* gene transcripts, confirming its specific activation in the parasite population (Figure 21B). Also in this cell line, low-level expression of *var1csa* (1.88%) and *IT4var66* (0.95 %) was detected.

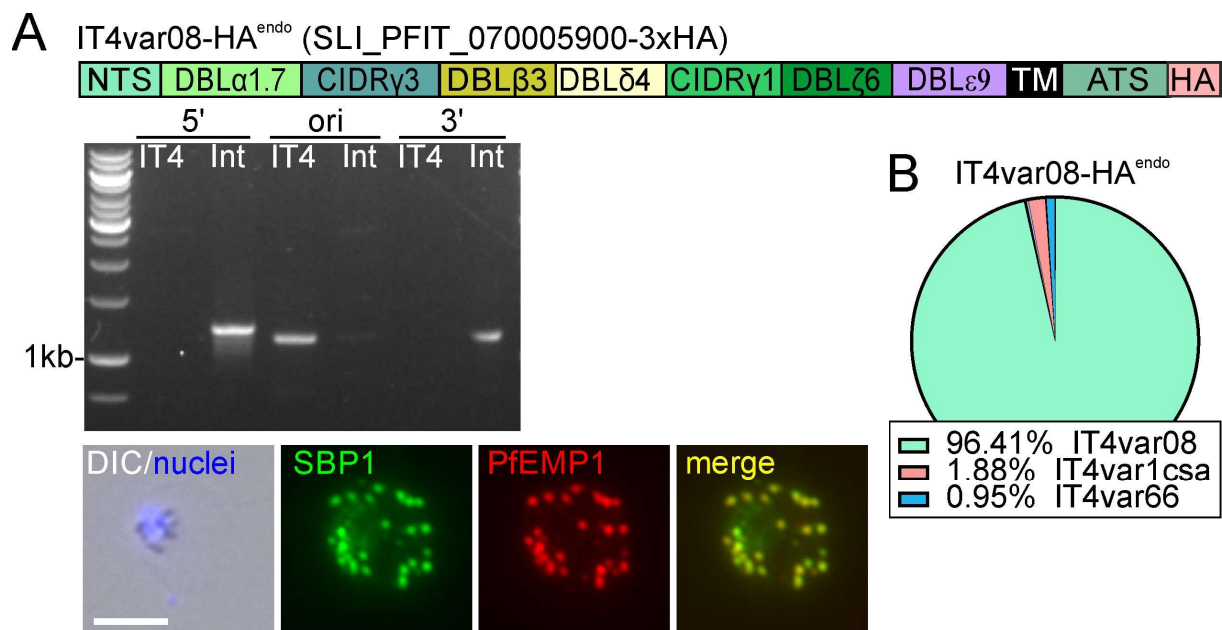


Figure 21: Characterization of the activation of *var08* in IT4 parasites. (A) Confirmation of the activation of PFIT_070005900 in IT4 parasites. Scheme shows domain organization and HA-tagging of the targeted PfEMP1. Agarose gel shows PCR products confirming correct integration of the SLI plasmid. Product over 5' integration junction (5'): P1 + P2; 3' integration junction (3'): P3 + P4; original locus (ori): P1 + P4; see Figure 12A for primer positions and Appendix A2 for sequence; IT4: parent; Int: integrant cell line. Expected bands: 5': 1251 bp; ori: 1129 bp; 3': 1156 bp. Fluorescence microscopy images show IFAs with acetone fixed parasites probed with α -HA (detection of PfEMP1) and α -SBP1 (detection of Maurer's clefts marker SBP1) antibodies. Nuclei: Hoechst 33342; DIC: differential interference contrast; size bars 5 μ m. (B) Pie charts show proportions of *var* gene transcripts determined by RNAseq and normalized to TPM.

3.1.7.4 *IT4VAR16*

The *IT4var16* gene in IT4 encodes a PfEMP1 variant with domains that are predicted to bind to CD36 and ICAM-1 (Figure 22A), with experimentally demonstrated binding to ICAM-1 in

the literature (Howell et al., 2008; Metwally et al., 2017). The SLI-engineered cell line to express this *var* gene was termed IT4var16-HA^{endo}. Diagnostic PCRs confirmed the correct integration of the plasmid into the *IT4var16* locus (Figure 22A). PCR products for the 5' and 3' integration junctions were detected in the integrant cell line that were absent in PCRs with the IT4 wildtype parasites. PCR products were detected for the original locus in IT4 wildtype parasites but were absent in the integrant cell line, indicative of an absence of unmodified locus (Figure 22A). IFAs showed co-localization of the HA-tagged PfEMP1 with the Maurer's cleft marker SBP1 (Figure 22A). RNA sequencing (performed by Johannes Allweier) indicated that *IT4var16* transcripts accounted for 95.11% of all detected *var* gene transcripts in the IT4var16-HA^{endo} parasite population (Figure 22B). Surface exposure of the PfEMP1 variant was verified by a trypsin cleavage assay, which displayed a band at ~ 100 kDa only present in the trypsin-treated sample corresponding to a protected fragment of digested HA-tagged PfEMP1 on the surface of the erythrocyte (Figure 22C). Whereas no digested fragment was observed for SBP1 using anti-SBP1-N antibodies confirming that no trypsin was able to pass the erythrocyte membrane.

Functional analysis through binding assays was conducted against CHO cells expressing GFP, CD36 and ICAM-1. These assays were compared to the binding profile of IT4var01-HA^{endo} (Blancke-Soares et al., 2021; Stäcker, 2021; SLI-activated *IT4var01* in IT4 parasites) a confirmed CD36-ICAM-1 dual binder (Blancke-Soares et al., 2021; Stäcker, 2021). The assays demonstrated that both IT4var16-HA^{endo} and IT4var01-HA^{endo} cell lines bound to CD36 and ICAM-1, but not to GFP-expressing cells (Figure 22D, E) (experiments performed by Johannes Allweier and Florian Kieferle). Quantitative comparison showed that IT4var16-HA^{endo}-infected erythrocytes exhibited reduced binding to CD36 but significantly enhanced binding to ICAM-1 compared to IT4var01-HA^{endo}-infected erythrocytes (Figure 22E), with no binding to GFP detected for either cell line. These results highlight that despite both *var* genes encoding PfEMP1 variants capable of CD36-ICAM-1 dual receptor binding, there are marked differences in their affinity towards CD36 and ICAM-1.

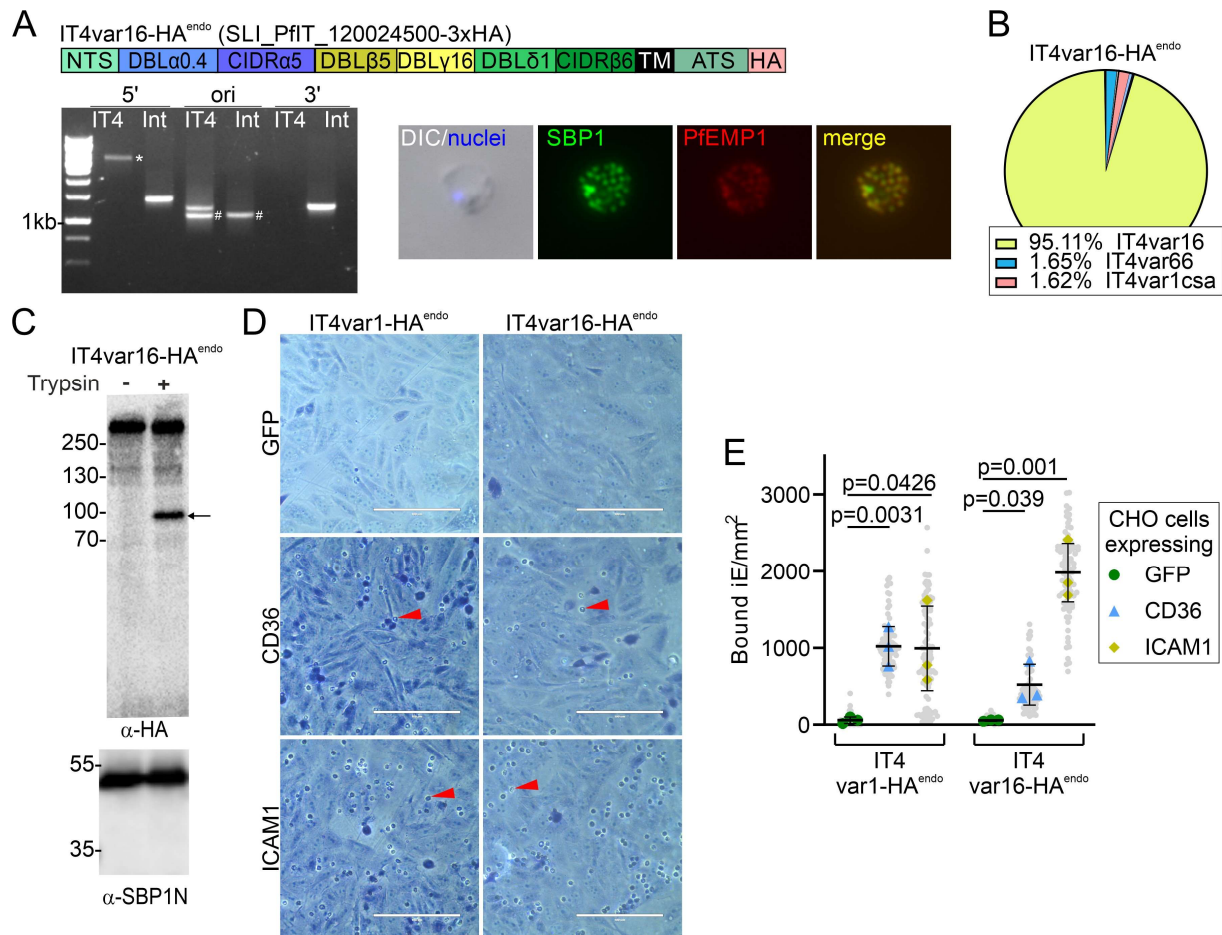


Figure 22: Characterization of the activation of *var16* in IT4 parasites. (A) Confirmation of the activation of PfIT_070005900 in IT4 parasites. Scheme shows domain organization and HA-tagging of the targeted PfEMP1. Agarose gel shows PCR products confirming correct integration of the SLI plasmid. Asterisks indicating unspecific PCR products; hash sign indicate PCR product of another *var* gene due to high sequence similarities in the ATS regions. Product over 5' integration junction (5'): P1 + P2; 3' integration junction (3'): P3 + P4; original locus (*ori*); P1 + P4; see Figure 12A for primer positions and Appendix A2 for sequence; IT4: parent; Int: integrant cell line. Expected bands: 5': 1426 bp; *ori* 1200 bp; 3': 1258 bp. Fluorescence microscopy images show IFAs with acetone fixed parasites probed with α -HA (detection of PfEMP1) and α -SBP1 (detection of Maurer's clefts marker SBP1) antibodies. Nuclei: Hoechst 33342; DIC: differential interference contrast; size bars 5 μ m. (B) Pie charts show proportions of *var* gene transcripts determined by RNAseq and normalized to TPM. (C) Western blot of trypsin cleavage assays with indicated parasites. Arrows show protected PfEMP1 fragment indicative of surface exposure. α -SBP1-N: control for integrity of host cell (breach of ERYTHROCYTE would result in a smaller SBP1 fragment). Marker in kDa. Replicates and full blots in Appendix B. (D) Images show representative sections of a captured images of binding assays for the indicated cell line against CHO cell line expressing the indicated receptors quantified in (E). Red arrows show examples of bound infected erythrocytes. (E) SuperPlot shows results from three biological replicates of binding assays (15 field of views were analyzed per experiment and condition; SD; unpaired t-test; p-values are indicated). Small grey dots show bound iE for every field of view captured, extrapolated to mm². Larger colored dots show average bound iE/mm² for each experiment. Larger colored dots show average bound iE/mm² for each experiment. Green circle: CHO-GFP; blue triangle: CHO-CD36; yellow rhombus: CHO-ICAM-1.

3.1.7.5 *IT4VAR19*

The *IT4var19* gene of IT4 encodes a PfEMP1 variant that binds to EPCR (Turner et al., 2013).

This *var* gene is of significant interest in the field, as evident from numerous studies (Avril et

al., 2012; Bernabeu et al., 2019; Gillrie et al., 2015; Nunes-Silva et al., 2015; Sampath et al., 2015). The cell line developed in this study through SLI was termed IT4var19-HA^{endo}.

Analysis by diagnostic PCRs confirmed the successful integration of the SLI-plasmid into the *IT4var19* locus (Figure 23A). No PCR products were detected that derived from the original unmodified locus while products were detected for the 5' and 3' integration junction, while the opposite was the case with the IT4 wildtype parasites. IFAs showed signals in puncta in the host cell for the HA-tagged PfEMP1, matching the typical localization pattern seen with other PfEMP1s and hence likely corresponding to the Maurer's clefts (Figure 23A). RNA sequencing (performed by Johannes Allweier) demonstrated that *IT4var19* comprised 90.97% of total *var* gene transcripts in the IT4var19-HA^{endo} parasites (Figure 23B). Again, transcripts at low proportional levels were detected for *IT4var66* (4.55 %) and *var1csa* (2.86 %). Despite the effective activation of *IT4var19*, trypsin cleavage assays revealed no band corresponding a protected fragments in the trypsin-treated samples (Figure 23C), suggesting that the HA-tagged PfEMP1 was not in detectable quantities on the erythrocyte surface.

Subsequent binding assays, using CHO cells expressing GFP, CD36, ICAM-1 or EPCR, did not show significant binding to any of the tested receptors (Murk, unpublished). In an attempt to induce PfEMP1 presentation and cytoadherence, IT4var19-HA^{endo}-infected erythrocytes underwent five rounds of selection on EPCR-expressing CHO cells (kindly performed by Johannes Allweier). Post-selection, trypsin cleavage assays revealed two bands at ~ 110 kDa and ~ 60 kDa in the trypsin-treated samples that had not been present in the non-selected IT4var19-HA^{endo} parasites (Figure 23E), and that were absent in the control. This suggested surface exposure of the HA-tagged PfEMP1. The reason for the two protected fragments is unclear but may derive from two subpopulations of this PfEMP1 that exhibits different conformations exposing divergent trypsinization sites or the smaller band may represent degraded protein. Subsequent, RNA sequencing with the panned IT4var19-HA^{endo} parasites confirmed sustained predominant *IT4var19* expression with 94.56 % of total *var* gene transcripts (Figure 23E). Remarkably, the selected IT4var19-HA^{endo} parasites displayed significant EPCR binding and unanticipated binding to ICAM-1 (Figure 23F), with no detectable binding to CD36 or GFP (binding assays kindly performed by Johannes Allweier and Florian Kieferle). This discovery implies that factors beyond *var* gene expression modulate presentation in this cell line. Additionally, the detection of ICAM-1 binding might indicate that the PfEMP1 variant encoded by *IT4var19* may be an EPCR-ICAM-1 dual binder.

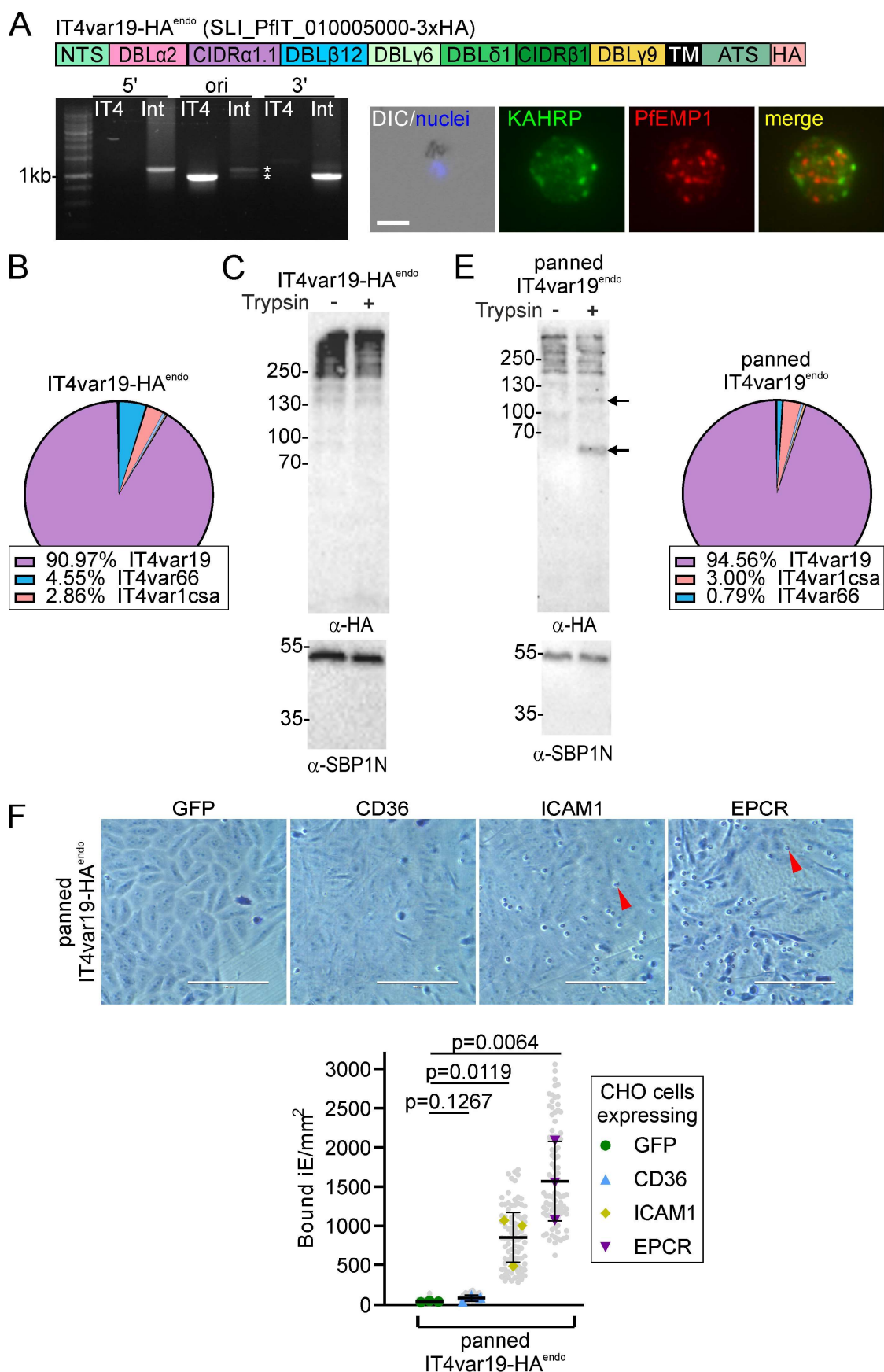


Figure 23: Characterization of the activation of *var19* in IT4 parasites. (A) Confirmation of the activation of PfIT_010005000 in IT4 parasites. The scheme shows domain organization and HA-tagging of the targeted PfEMP1.

Agarose gel shows PCR products confirming correct integration of the SLI plasmid. Asterisks indicating unspecific PCR products. Product over 5' integration junction (5'): P1 + P2; 3' integration junction (3'): P3 + P4; original locus (ori); P1 + P4; see Figure 12A for primer positions and Appendix A2 for sequence; IT4: parent; Int: integrant cell line. Expected bands: 5': 1186 bp; ori 960 bp; 3': 985 bp. Fluorescence microscopy images show IFAs with acetone fixed parasites probed with α -HA (detection of PfEMP1) and α -SBP1 (detection of Maurer's clefts marker SBP1) antibodies. Nuclei: Hoechst 33342; DIC: differential interference contrast; size bars 5 μ m. (B) Pie chart shows proportions of *var* gene transcripts determined by RNAseq and normalized to TPM. (C) Western blot of trypsin cleavage assays with indicated parasites. α -SBP1-N: control for integrity of host cell (breach of ERYTHROCYTE would result in a smaller SBP1 fragment). Marker in kDa. Replicates and full blots in Appendix B. (D, F) Pictures show representative sections of captured images of binding assays for the indicated cell line against CHO cell line expressing the indicated receptors. SuperPlot shows results from three biological replicates (15 field of views were analyzed per experiment and condition; SD; unpaired t-test; p-values are indicated). Small grey dots show bound iE for every field of view captured, extrapolated to mm². Larger colorful dots show average bound iE/mm² for each experiment. Green circle: CHO-GFP; blue triangle: CHO-CD36; yellow rhombus: CHO-ICAM-1; purple triangle: CHO-K1-EPCR. (E) Western blot of trypsin cleavage assays with indicated parasites. α -SBP1-N: control for integrity of host cell (breach of ERYTHROCYTE would result in a smaller SBP1 fragment). Marker in kDa. Replicates and full blots in Appendix B. Pie chart shows proportions of *var* gene transcripts determined by RNAseq and normalized to TPM.

3.1.7.6 *IT4VAR20* AND *IT4VAR22*

The *IT4var20* and *IT4var22* genes encode PfEMP1 variants with domains shown to bind to EPCR (Turner et al., 2013, Barber et al., 2021). The cell lines obtained after G418 selection were termed IT4var20-HA^{endo} and IT4var22-HA^{endo}. Diagnostic PCRs were conducted to assess correct integration of the SLI-plasmids into the *IT4var20* or *IT4var22* gene locus in the corresponding cell lines. The results showed populations with mixed integration phenotypes indicated by detected PCR products for both, the integration junctions and the original locus for IT4var20-HA^{endo} and IT4var22-HA^{endo} (Figure 24A). This suggested integration into both target and non-target gene loci within these parasite populations, likely due to sequence similarities in the ATS domains (which is targeted by the SLI-plasmid) of different *var* genes.

To achieve a parasite population with exclusive integration into the target *var* gene, a plaque assay (Thomas et al., 2016) was utilized for subcloning. Two clones reappeared after the subcloning for IT4var22-HA^{endo} and one for IT4var20-HA^{endo} (Figure 24A). PCRs targeting the 5' integration junction and original locus again detected products for both PCRs in all clones (Figure 24A). Given the selection of single-plaque wells, the simultaneous appearance of both bands in the results is an unexpected outcome, as all parasites in the population should derive from a single parasite with a single defined genotype. The PCR products for the original locus in these clones might derive from binding of the primers to multiple genomic locations, potentially due to sequence similarities among *var* genes.

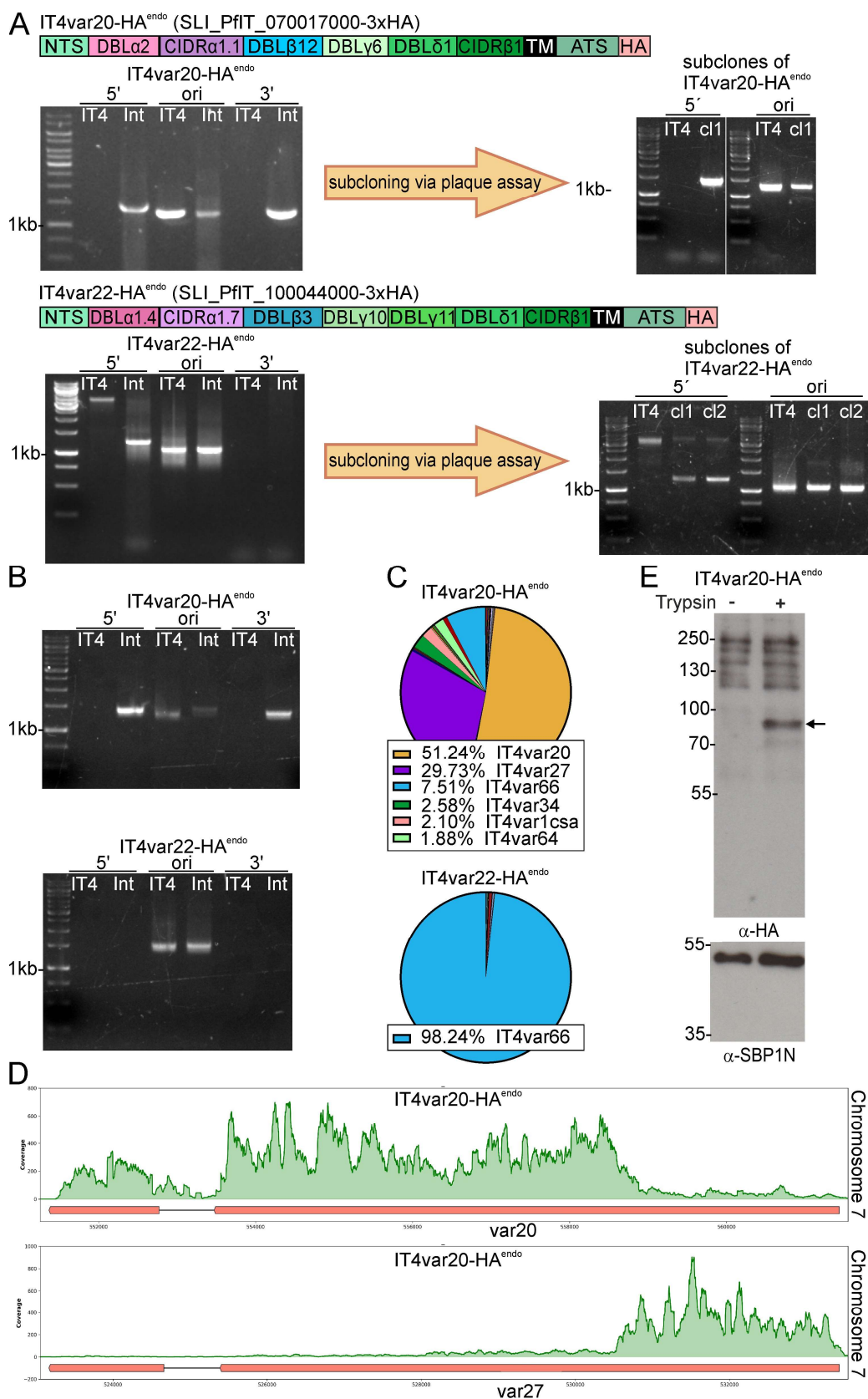


Figure 24: Attempted activation of var20 and var22. (A) Evaluation of the activation of PfIT_070017000 (var20) and PfIT_100044000 (var22) in IT4 parasites. Scheme shows domain organization and HA-tagging of the targeted PfEMP1. Agarose gels (left) show PCR products for the testing of the correct integration of the SLI plasmid with first primer pairs for the indicated cell lines. Agarose gels (right) show PCR products testing correct integration for subclones of the indicated cell lines generated by plaque assays. Product over 5' integration junction

(5'): P1 + P2; 3' integration junction (3'): P3 + P4; original locus (ori); P1 + P4; see Figure 12A for primer positions and Appendix A2 for sequence; IT4: parent; Int: integrant cell line. Expected bands IT4var20-HA^{endo}: 5': 1464 bp; ori 1298 bp; 3': 1331 bp. Expected bands IT4var22-HA^{endo}: 5': 1278 bp; ori 1092 bp; 3': 1120 bp. (C) Agarose gels show PCR products for testing of the correct integration of the SLI plasmid with second primer pairs for the indicated cell lines. Expected bands: IT4var20-HA^{endo}: 5': 1447 bp; ori 1325 bp; 3': 1377 bp; IT4var22-HA^{endo}: 5': 1435 bp; ori 1541 bp; 3': 1412 bp. (C) Pie charts show proportions of *var* gene transcripts of the indicated cell lines determined by RNAseq and normalized to TPM. (D) Coverage plots showing reads mapped to *var20* (PfIT_070017000; top) and *var27* (bottom; PfIT_070016700) determined by RNAseq with IT4var20-HA^{endo} parasites. Both genes are located on chromosome 7. Gene annotation from PlasmoDB genome browser (PlasmoDB.org) with reads mapped using Artemis (Carver et al., 2012). Red: *var* genes. (E) Western blot of trypsin cleavage assays with indicated parasites. α -SBP1-N: control for integrity of host cell (breach of ERYTHROCYTE would result in a smaller SBP1 fragment). Marker in kDa. Full blot in Appendix B.

Consequently, new primers were designed to enhance specificity. Diagnostic PCRs with the new primer pair confirmed correct integration of the SLI-plasmid only into the targeted gene locus in the IT4var20-HA^{endo} cell line (Figure 24B). However, for IT4var22-HA^{endo}, the results indicated integration into a non-targeted gene locus showing only a PCR product for the original locus corresponding to the size detected in the IT4 parasites (Figure 24B). These results were confirmed by RNA sequencing (kindly performed by Johannes Allweier) which showed predominant expression of *IT4var66* with 98.28 % of the total *var* gene transcripts in IT4var22-HA^{endo} (Figure 24C), indicating the integration of the SLI-plasmid into the *IT4var66* gene locus. Interestingly, IT4var20-HA^{endo} parasites did not show an exclusive expression of *IT4var20*, only 51.24 % of the total *var* gene transcripts derived from *IT4var20* and 29.73 % from *IT4var27*, a *var* gene previously not detected with RNA sequencing experiments with SLI *var* gene cell lines (Figure 24D). Upon closer inspection of the mapped reads (coverage plots kindly provided by Johannes Allweier) for the IT4var20-HA^{endo}, it was observed that the reads only mapped to the C-terminal part of the extracellular domains of *var20* and to the N-terminal part of the extracellular domains of *IT4var27*, indicating a chimeric *var* gene in that cell line (Figure 24E). This suggests that the parasites experienced a recombination event between *var* genes during mitosis, not during their meiosis where ectopic recombination usually takes place (Freitas-Junior et al., 2000).

Trypsin cleavage assay confirmed the presentation of the chimeric *IT4var20/var27* PfEMP1 in IT4var20-HA^{endo} parasites (Figure 24D). In the trypsin-treated samples a ~90 kDa band was detected that was absent in the control samples, indicative of surface trypsinization of the HA-tagged PfEMP1 from the surface. No band corresponding to digested SBP1 were detected when probed with anti-SBP1-N antibodies indicating the integrity of the host cell during trypsin treatment (Figure 24D).

3.1.8 DBL β 12 IN *IT4VAR19* SHOWS SIMILARITIES TO ICAM-1-BINDING DBL β 5 DOMAIN

The observed binding of IT4var19-HA^{endo} to ICAM-1 prompted an evaluation of the possibilities for such an interaction, given that the expressed PfEMP1 variant of *IT4var19* was previously published as a non-ICAM-1-binder (Adams et al., 2021; Azasi et al., 2018; Bernabeu et al., 2019; Nunes-Silva et al., 2015). In PfEMP1 variants known to bind both EPCR and ICAM-1, the EPCR-binding CIDR α domain is typically succeeded by a DBL β domain responsible for ICAM-1 interaction. Contrary to this pattern, the DBL β 12 domain following *var19*'s EPCR-binding CIDR α 1.1 domain was reported to not interact with ICAM-1 (Lennartz et al., 2017), but instead with qC1qR (Bakri et al., 2021; Magallón-Tejada et al., 2016).

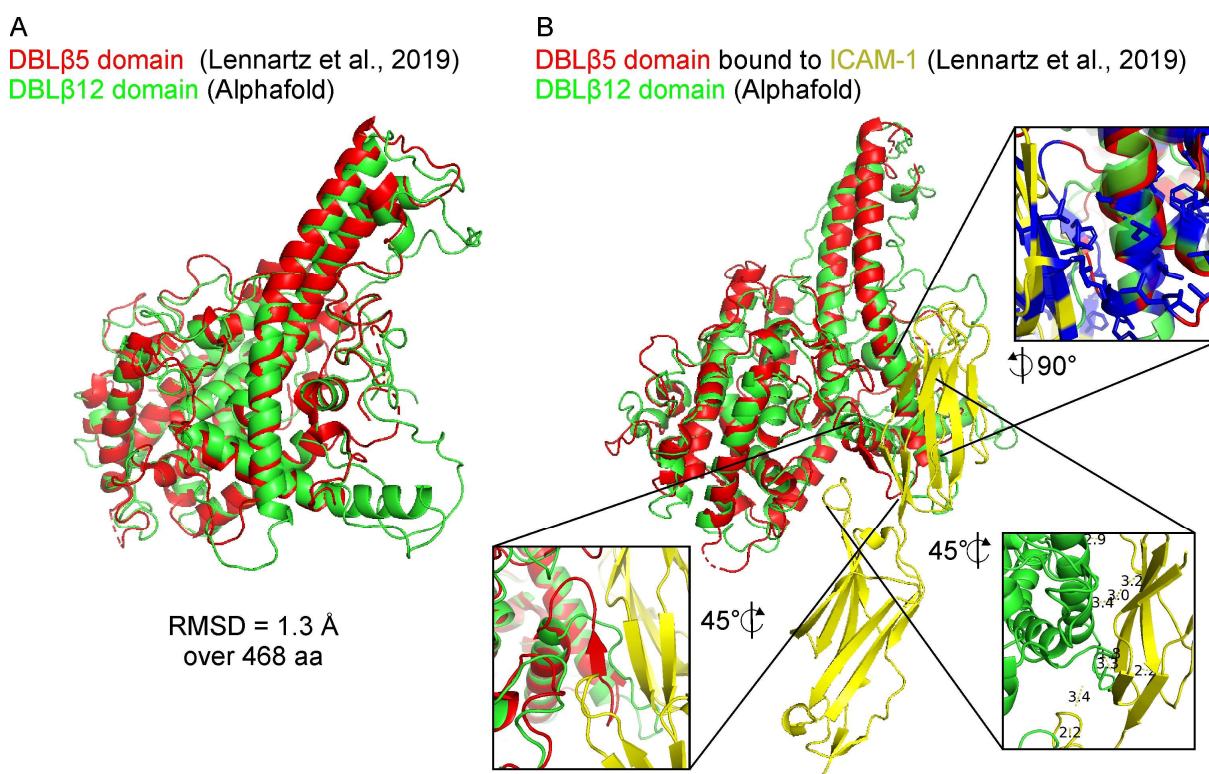


Figure 25: DBL β 12 shows structural similarities to ICAM-1-binding DBL β 5. (A) Alignment of the AlphaFold predicted structure of the DBL β 12 domain from *IT4var19* (green) and the published structure of the DBL β 5 domain from *IT4var13* (red) (Lennartz et al., 2019). RMSD: root-mean-square deviation Å: Ångström. (B) Alignment of the AlphaFold predicted structure of the DBL β 12 domain from *IT4var19* (green) and the published structure of the DBL β 5 domain from *IT4var13* (red) bound to ICAM-1 (yellow) (Lennartz et al., 2019). Magnifications: (bottom left) shows the β -sheet of DBL β supporting ICAM-1 interaction; (bottom right) shows hydrogen bonds predicted *in silico* (Pymol) between the chains of DBL β 12 and ICAM-1, if in the same spatial orientation like DBL β 5 corresponding to ICAM-1; (top right) shows hydrophobic regions and side chains (blue) of DBL β 12 (transparent green), DBL β 5 (red) and ICAM-1 (yellow).

To reconcile these discrepancies, a closer investigation of the *IT4var19*'s binding domains was undertaken. Prior studies identified an ICAM-1 binding motif in group A DBL β domains

(Lennartz et al., 2017). This motif was absent in the amino acid sequence of the *IT4var19*'s PfEMP1 variant (group B). Subsequent research by Lennartz et al. (2019) discovered that ICAM-1-binding group B DBL β domains showed a more heterogenous amino acid sequence in the binding region distinct from group A's binding motif. Comparative analyses between group A and group B ICAM-1-binding DBL β domains revealed overall structural similarities with some significant variations in regions critical for binding (Lennartz et al., 2019). However, both DBL β domains evolved independently and confer binding to ICAM-1, underscoring a potential structural adaptability or the presence of alternate binding mechanisms within these domains.

In light of this, the protein structure of group B *IT4var19*'s DBL β 12 domain was predicted using AlphaFold (Jumper et al., 2021). This predicted structure was then aligned with the protein structure of group B *ITvar13*'s DBL β 5 domain (Lennartz et al., 2019), revealing notable structural similarities in the backbone, with a RMSD of 1.3 Å across 468 amino acids (Figure 25A). Further alignment with the published ICAM-1 bound DBL β 3 domain (Lennartz et al., 2019) (Figure 25B) highlighted structural resemblances in the ICAM-1 binding region, despite some distinct differences. Notably, a hydrophobic α -barrel segment in the DBL β 5 domain, previously implicated in aiding the ICAM-1 interaction, did not exhibit hydrophobic properties in the DBL β 12 domain (Figure 25B). Moreover, a β -sheet in the DBL β 5 domain antiparallel to a corresponding β -sheet in the ICAM-1 structure, was absent in the DBL β 12 domain (Figure 25B). Nevertheless, this structural element was also missing in the unbound relaxed DBL β 5 domain (Figure 25A) and the ICAM-1-bound group A DBL β domain (Lennartz et al., 2017). Despite these discrepancies, hydrogen bonds were predicted between DBL β 12 and ICAM-1, assuming a spatial orientation of DBL β 12 in relation to ICAM similar to that of DBL β 5 (Figure 25B). These observations suggests that despite structural dissimilarities in the binding region, inherent or induced adaptability in the DBL β 12 domain may allow for effective ICAM-1 binding.

3.2 IDENTIFICATION AND CHARACTERIZATION OF PROXIOME OF A FUNCTIONAL PfEMP1

In this part, efforts were undertaken to identify the proximal proteome (proxiome) of a functional PfEMP1 in living *P. falciparum* parasites. The interactors of PfEMP1 remain largely unexplored on a systematic scale. While certain proteins have been pinpointed as vital for PfEMP1's transport and function (section 1.3.2.3.2), this does not necessarily indicate direct interaction with PfEMP1. Therefore, BioID was applied on PfEMP1 in IT4 parasites using SLI (section 3.2.1 and 3.2.2). A selection of the identified proximal candidates was localized and the effect of their disruption on PfEMP1's function and Maurer's clefts morphology was evaluated (section 3.2.4).

3.2.1 FUSION OF BIRA* TO ENDOGENOUS PfEMP1 IN THREE POSITIONS

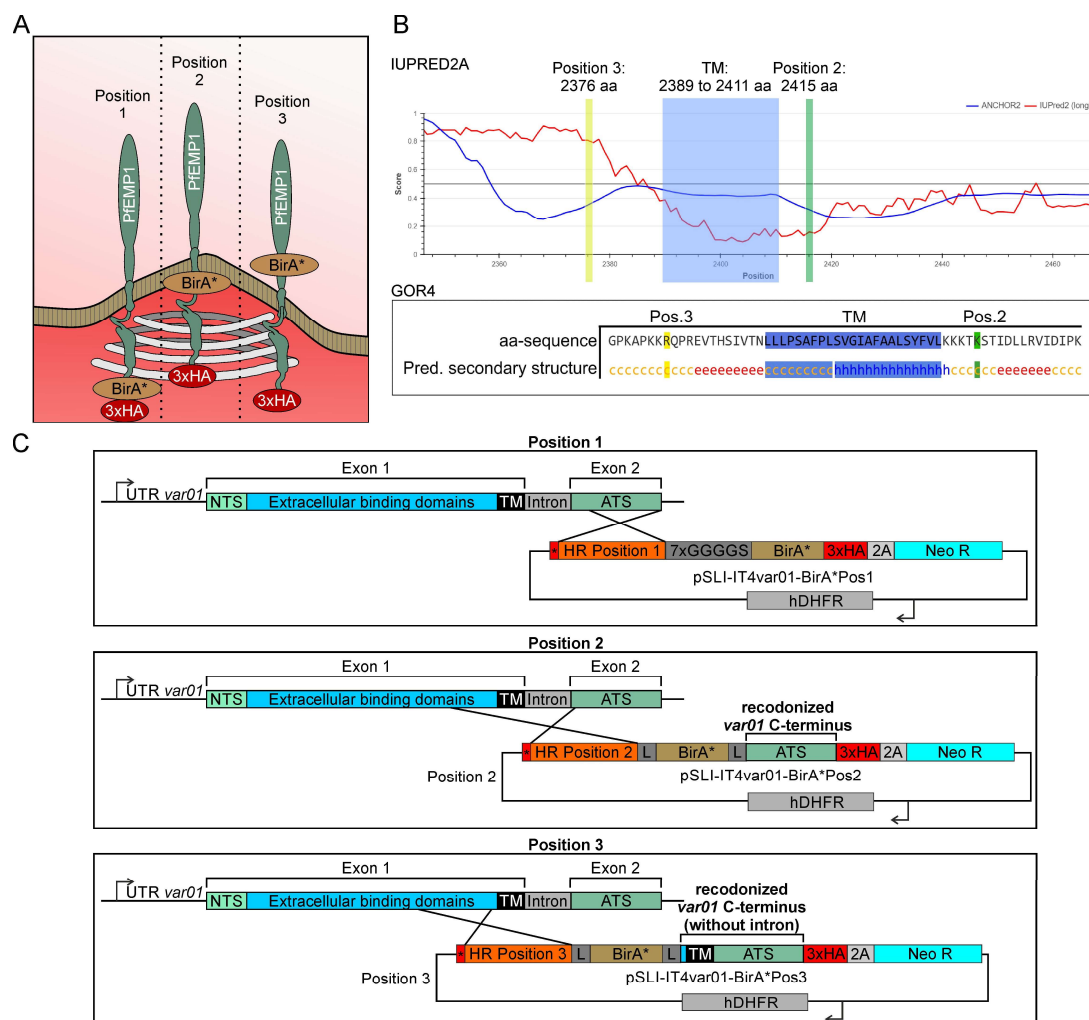


Figure 26: SLI-strategy for fusion of BirA* to *var01* in IT4. (A) Illustration showing the strategy and locations for the fusion of BirA* and HA-tag to PfEMP1 in three positions after integration of PfEMP1 into the erythrocyte membrane at the knobs. Position 1: Insertion of BirA* C-terminal of the ATS domain; Position 2: BirA* flanked by the ATS domain and the transmembrane domain; Position 3: BirA* in the extracellular space flanked by the transmembrane domain and the extracellular binding domains. (B) Graph (top) shows values for probabilities of

intrinsically disordered protein regions predicted by IUPRED2 with implementation of ANCHOR2 predicting disordered potential binding regions of globular protein partners or environmental factors for amino acid 2330 to 2465 of *IT4var01*; higher score indicates higher probability of disorder or binding. Graph (bottom) shows secondary structure for amino acid 2369 to 2428 of *IT4var01* predicted by GOR4; c, random-coiled; e: extended strand β -sheet conformation; h: α -helix. Green: position 2 insertion-site; yellow: position 3 insertion-site; blue: transmembrane domain predicted by TMHMMv2.0 (<https://services.healthtech.dtu.dk/services/TMHMM-2.0/>). (C) Schematics of plasmid constructs for SLI modification of the *IT4var01* gene locus to insert the sequence encoding BirA* in different positions. NTS: N-terminal segment; TM: transmembrane domain; ATS: acidic terminal segment, the region of PfEMP1 reaching into the host cell cytoplasm; UTR: untranslated region; HR: homology region 2A: T2A skip peptide; NEO-R: G418-resistance conferring gene; hDHFR: human dihydrofolate reductase (conferring WR resistance); asterisks: stop codon.

In order to obtain the proximiome of PfEMP1, the BioID method (Roux et al., 2012) was chosen. BioID uses enzymatic biotinylation to label proteins in close proximity to a target protein. To achieve this, a modified version of biotin holoenzyme synthetase from *Escherichia coli*, known as BirA*, is fused to a protein of choice. This BirA* - a version of BirA engineered for promiscuous biotinylation activity - biotinylates neighboring proteins in the presence of biotin, and thereby the proximiome of the target protein. These biotin-labeled proteins are then isolated using streptavidin beads, which forms a strong bond with biotin, allowing subsequent mass spectrometry analysis to identify the bound proteins.

SLI was used for the modification of a single PfEMP1 variant, now incorporating an additional fusion of the BirA* enzyme to the targeted *var* gene (Figure 26A) and ensuring that the *var* gene carrying the modification is expressed. For this purpose, the *IT4var01* gene was selected as the target, owing to its robust binding to CD36 and ICAM-1 receptors in binding assays and the previously successful integration of the SLI plasmid into this gene locus (Blancke-Soares et al., 2021; Stacker, 2021).

However, tagging PfEMP1 with a BirA* domain presents two significant challenges. Firstly, the integration of such a large domain into PfEMP1 might impede its membrane incorporation, transport, or functional presentation. Secondly, due PfEMP1's large size, and the presence of domains on both sides of the membrane, the interaction sites to other proteins are potentially physically too far apart or in a different compartment. Depending on the insertion site of BirA*, this could result in the biotinylation sites of potential interactors being too distant from BirA* or in the incorrect compartment. To address these issues, BirA* was fused to PfEMP1 in three different positions, for each of which a separate cell line was generated (Figure 26A). Two fusion sites were selected for the domain within the host cell, positioned at maximal distance from each other: Position 1 at the C-terminus of the ATS domain, and Position 2 between the ATS and the transmembrane domain. Additionally, Position 3 was chosen in the extracellular

region, between the transmembrane domain and the extracellular binding domains, reasoning that this posed the least danger of disrupting the binding domain. Linkers were added to increase the tolerability of the folded BirA* domain for PfEMP1 function (Figure 26C).

SLI plasmids were designed to enable the fusion of BirA* to the predetermined positions (Figure 26C). While for Position 1 the addition of BirA* was at the extreme C-terminus, Positions 2 and 3 gave some flexibility to the exact insertion site (Figure 26A). For this reason, the secondary structure of the protein was predicted with GOR4, and with IUPRED2 in conjunction with ANCHOR2, intrinsically disordered protein regions were predicted in an attempt to avoid insertions of BirA* into a functional folded region (Figure 26B). In the case of Position 1, a flexible linker consisting of a 7xGGGGs sequences (Birnbaum et al., 2020) was inserted between the BirA* and the C-terminus of PfEMP1. This design aims to distance the BirA* from the ATS domain of PfEMP1, minimizing potential interference in PfEMP1's correct folding and allowing BirA* greater mobility to interact with a broader range of proximal proteins (Figure 26C). For position 2 and 3 insertions into random coil regions (predicted using GOR4) just outside of the transmembrane helix boundary region was chosen, where it was unlikely that there was a folded domain (Figure 26B). Addition of linkers flanking the BirA* domain further minimized the danger of impacting neighboring folded domains. Corresponding recodonized C-terminal sequences of *IT4var01* were synthesized and cloned into the plasmids for Positions 2 and 3, following the BirA* fusion sites to render the expressed PfEMP1s complete and functional (Figure 26C). Notably, the intron of *IT4var01* was excluded for Positions 3 due to the difficulties in synthesizing long adenine- and thymine-rich stretches. It is important to acknowledge that these selections are, at best, educated guesses. Given the limited knowledge and the constraints in selection that were chosen, these are the approaches that were taken.

3.2.1.1 CHARACTERIZATION OF THE BIOD CELL LINES

The newly established cell lines, designated as IT4var01-BirA*Pos1^{endo} (Position 1), IT4var01-BirA*Pos2^{endo} (Position 2), and IT4var01-BirA*Pos3^{endo} (Position 3), were characterized for the correct integration of the plasmid following G418 selection. PCR analyses of the 5' and 3' integration junctions using corresponding primers showed products of the expected lengths for the three cell lines (Figure 27A-C). PCRs targeting the original locus in IT4var01-BirA*Pos2^{endo} and IT4var01-BirA*Pos3^{endo} cell lines did not amplify a product, in contrast to the IT4 wildtype (Figure 27B, C). In IT4var01-BirA*Pos1^{endo}, a very faint band was observed,

alongside a more intense PCR product for the IT4 wildtype (Figure 27A). This faint band in IT4var01-BirA*Pos1^{endo} is likely negligible, potentially arising from residual genomic DNA of unselected parasites in the culture.

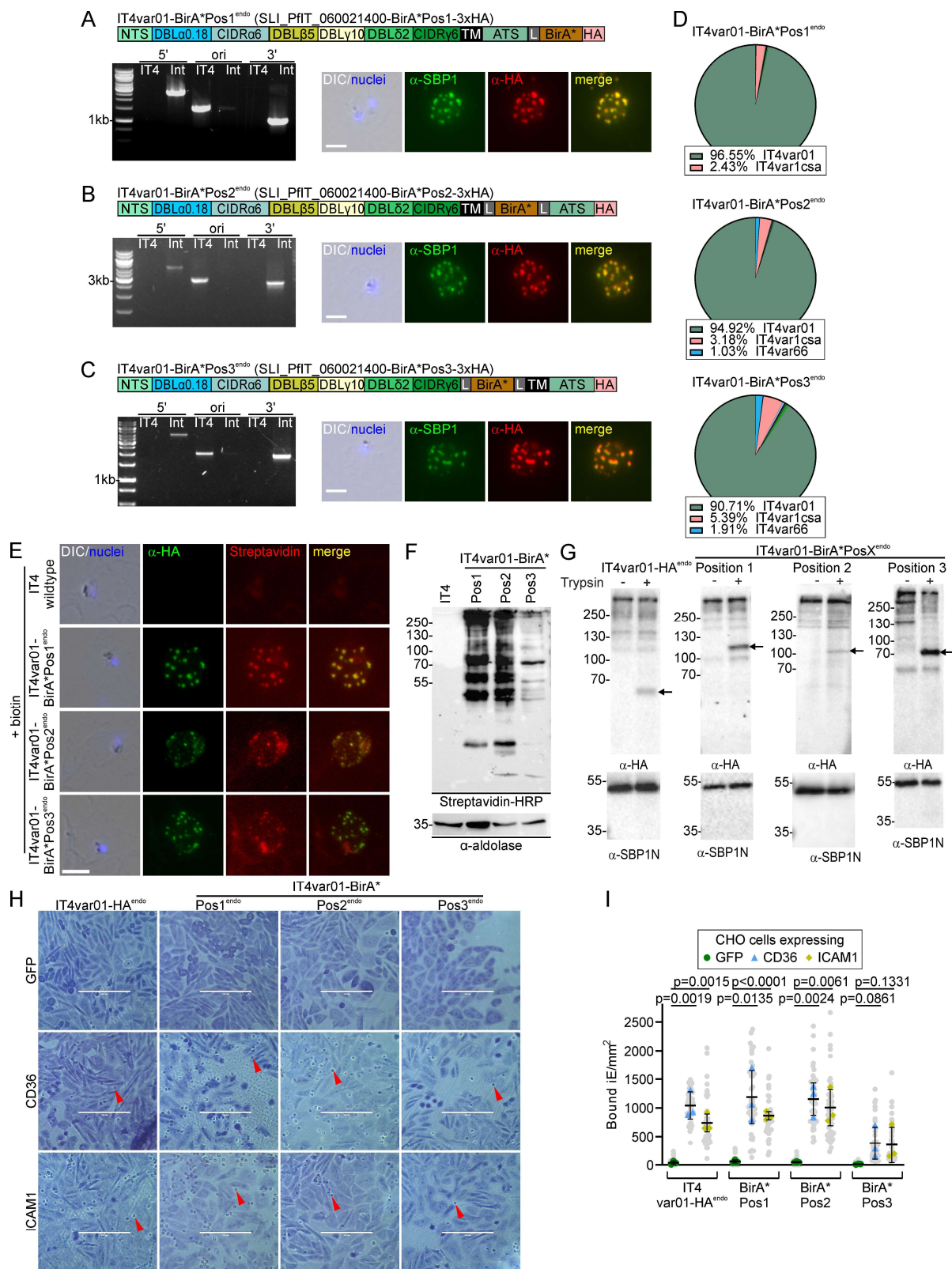


Figure 27: BirA*-fused PfEMP1s are functional and able to biotinylate. (A, B, C) Confirmation of the

activation and modification of the indicated IT4var01-BirA* fusions. Schematics show domain organization of the modified PfEMP1. Agarose gels show PCR products confirming correct integration of the SLI plasmid. Product over 5' integration junction (5'): P1 + P2; 3' integration junction (3'): P3 + P4; original locus (ori); P1 + P4; see Figure 12 for primer positions and Appendix A2 for sequence; IT4: parent; Int: integrant cell line; expected bands: IT4var01-BirA*Pos1^{endo}: 5': 2337 bp; ori: 1536 bp; 3': 971 bp; IT4var01-BirA*Pos2^{endo}: 5': 4275 bp; ori: 3059 bp; 3': 2721 bp; IT4var01-BirA*Pos3^{endo}: 5': 3760 bp; ori: 1990 bp; 3': 1886 bp. Fluorescence microscopy images show IFAs with indicated antibodies. Nuclei: Hoechst 33342; DIC: differential interference contrast; size bars 5 μm . **(D)** Pie charts show proportions of total *var* gene transcripts of the indicated cell lines determined by RNAseq (normalized to TPM). **(E)** Fluorescence microscopy images show IFAs with indicated antibodies and streptavidin after biotin treatment. Nuclei: Hoechst 33342; DIC: differential interference contrast; size bars 5 μm . **(F)** Western blot of extracts of the indicated cell lines after incubation with biotin for 24 hours. Streptavidin probes biotinylated proteins; α -aldolase is the loading control. **(G)** Western blot of trypsin cleavage assays with indicated parasites. Arrows show protected PfEMP1 fragment. α -SBP1-N: control for integrity of host cell. Marker in kDa. Replicates and full blots in Appendix B. **(H)** Images show representative sections of captured images for binding assays for the indicated parasite cell lines against CHO cell lines expressing the indicated receptors. Red arrows show examples of bound infected erythrocytes. Size bars 100 μm . **(I)** SuperPlot of binding assays of indicated cell lines against CHO cells expressing GFP, CD36 or ICAM-1 (3 biological replicates with 15 fields of view/experiment and condition; bars: mean of averages of replicates with SD; unpaired t-test; p-values are indicated). Small grey dots: bound iE/field of view, extrapolated to mm^2 . Larger colored dots: average of bound iE/ mm^2 /replicate. iE: infected erythrocytes.

IFAs revealed a signal for the HA-tagged PfEMP1, which colocalized with the Maurer's clefts marker SBP1 in all three cell lines (Figure 27A-B). This confirmed the expression, correct localization, and detectability of the modified PfEMP1. Furthermore, RNA sequencing analysis (performed by Johannes Allweier) confirmed the predominant expression of the targeted *IT4var01* gene (Figure 27D). In the three cell lines, *IT4var01* transcripts accounted for over 90% of the total *var* gene transcripts: 96.55% in IT4var01-BirA*Pos1^{endo}, 94.92% in IT4var01-BirA*Pos2^{endo}, and 90.71% in IT4var01-BirA*Pos3^{endo}. Similar to other SLI activated *var* gene cell lines, low but significant levels of *IT4var66* and *var1csa* transcripts were also detected.

Next, the functionality of BirA* in the three BioID cell lines were assessed. This was done using streptavidin fluorescence assays, where streptavidin linked to a fluorophore was used to detect biotinylated proteins in biotin-treated parasites by fluorescence microscopy. Additionally, α -HA-tag antibodies were employed to detect PfEMP1. The assays detected a streptavidin signal colocalizing with PfEMP1 in the three BioID cell lines (Figure 27E). In contrast, the IT4 wildtype showed no signal for the HA-tagged PfEMP1 and only minimal streptavidin signals within the parasites. This signal could potentially be attributed to background of the IFA, as no streptavidin signal was detected with IT4 parasites in streptavidin blots (see below).

To further evaluate the biotinylation capability of the BioID cell lines, streptavidin blots were performed. In these blots, streptavidin conjugated to horseradish peroxidase (HRP) was used to identify biotinylated proteins in extracts from biotin-treated erythrocytes infected with parasites

of the BioID cell lines or IT4 wildtype. The IT4 wildtype parasites served as a control to rule out non-specific biotinylation. The results displayed distinct bands when probed with streptavidin from protein extracts of IT4var01-BirA*Pos1^{endo}, IT4var01-BirA*Pos2^{endo}, and IT4var01-BirA*Pos3^{endo} parasites, but not for extracts of IT4 wildtype parasites (Figure 27F). To confirm the presence of parasite proteins on the blots, they were probed with α -aldolase antibodies as a loading control which showed the expected ~35 kDa bands for all samples (Figure 27F).

The aim was to identify the global proximiome of a functional PfEMP1, both at the erythrocyte periphery (from surface exposed PfEMP1) and during the transport process (from the pool of PfEMP1 found internally). Therefore, the presentation and binding capabilities of the BirA*-fused PfEMP1s in the three BioID cell lines were assessed. Initially, the surface presentation of the modified PfEMP1 was evaluated using trypsin cleavage assays. These assays revealed a distinct band in all three BioID cell lines after trypsin-treatment, which was absent in the control sample (Figure 27G). For IT4var01-BirA*Pos1^{endo} and IT4var01-BirA*Pos2^{endo}, this protected fragment of ~110 kDa, aligned with the expected size of the IT4var01-HA^{endo} fragment (Figure 27G) which included the BirA* domain (~35 kDa), linker (Position 1: ~2 kDa; Position 2: ~1kDa), 3xHA-tag (~4 kDa), and skip peptide (~2 kDa). For IT4var01-BirA*Pos3^{endo}, the detected band of ~70 kDa, corresponded to the expected size of IT4var01-HA^{endo} protected fragment which in this construct did not include BirA* (Figure 27G). These findings suggest that the BirA*-fused PfEMP1 is presented on the erythrocyte membrane surface in all three BioID cell lines with the BirA* on the intended side of the membrane.

Subsequently, the functionality of the modified PfEMP1s was evaluated through binding assays. In these assays, erythrocytes infected with parasites of the BioID cell lines were tested against CHO cells expressing either GFP, CD36, or ICAM-1, and compared to erythrocytes infected with IT4var01-HA^{endo} parasites. The results indicated that erythrocytes infected with parasites of each BioID cell line and IT4var01-HA^{endo} showed interaction with CD36 and ICAM-1, but not with the GFP control (Figure 27H). Quantitative analysis revealed that the binding capacities of IT4var01-BirA*Pos1^{endo} and IT4var01-BirA*Pos2^{endo} parasites were comparable to the IT4var01-HA^{endo} control (Figure 27I). However, IT4var01-BirA*Pos3^{endo} parasites exhibited insignificantly binding against CD36 and ICAM-1 compared to the GFP control (Figure 27H).

3.2.1.2 FUSION OF MINITURBO AND FKBP TO PfEMP1

To increase the versatility of BioID experiments with PfEMP1 cell lines with two further types of fusion constructs for BioID were generated. For the first approach, constructs were engineered to fuse the miniTurbo (Branon et al., 2018) to identical positions of PfEMP1 as the BirA* in the BioID cell lines (Figure 3). miniTurbo possesses significantly faster labeling kinetics (minutes compared to hours) (Branon et al., 2018), presenting an opportunity for stage-specific labeling of PfEMP1 interactors. In addition, this enzyme is about 20% smaller than BirA*, which may reduce the risk of a negative impact on the fusion target.

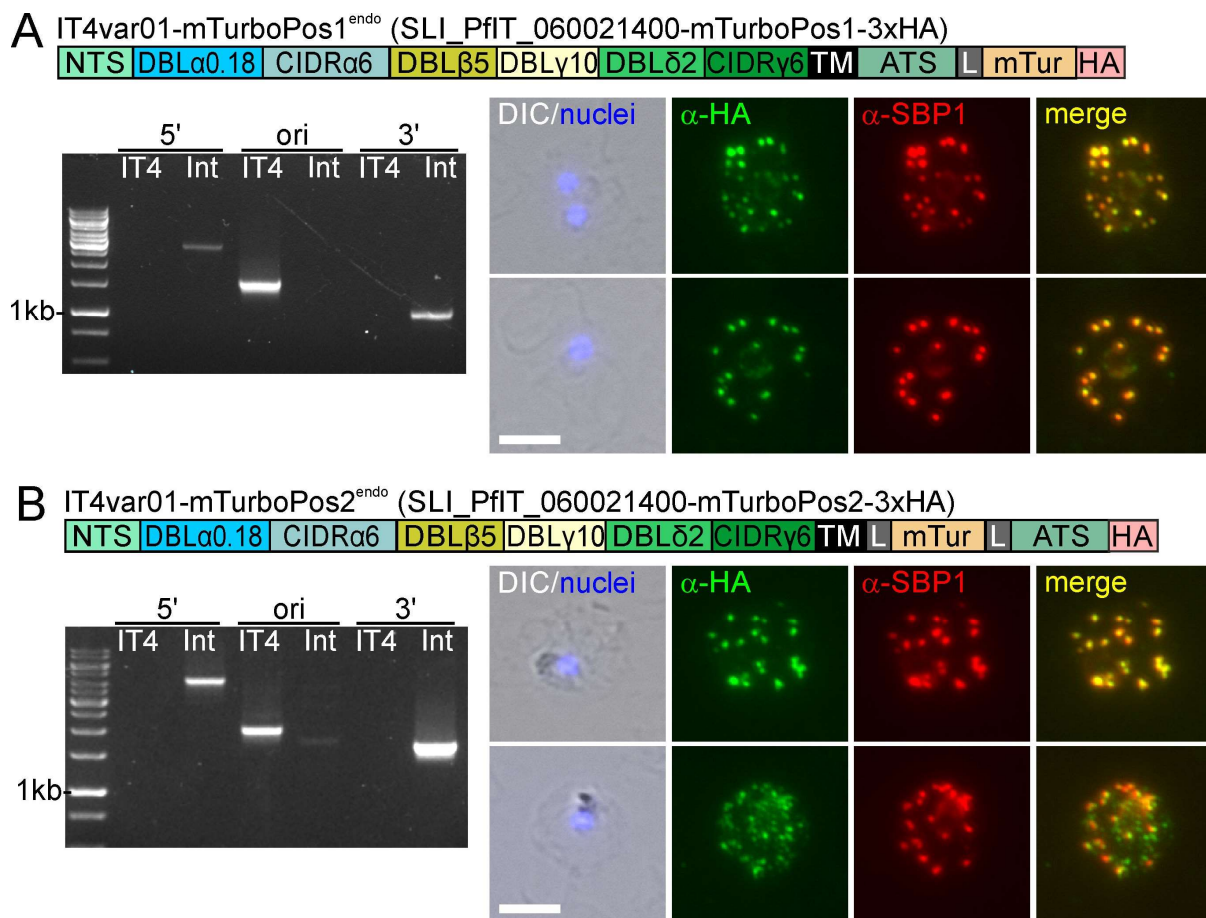


Figure 28: Generation of PfEMP1-miniTurbo cell lines. (A, B) Confirmation of the activation and modification of the indicated IT4var01-miniTurbo fusions. Schematics show domain organization of the modified PfEMP1. Agarose gel shows PCR products confirming correct integration of the SLI plasmid. Product over 5' integration junction (5'): P1 + P2; 3' integration junction (3'): P3 + P4; original locus (ori); P1 + P4; see Figure 12. for primer positions and Appendix A2 for sequence; IT4: parent; Int: integrant cell line; expected bands: IT4var01-miniTurboPos1^{endo}: 5': 2145 bp; ori: 1536 bp; 3': 971 bp; IT4var01-miniTurboPos2^{endo}: 5': 4083 bp; ori: 3059 bp; 3': 2721 bp. Fluorescence microscopy images show IFAs with indicated antibodies. Nuclei: Hoechst 33342; DIC: differential interference contrast; size bars 5 μ m.

Following the plasmid transfection and subsequent parasite selection for plasmid integration, cell lines with the miniTurbo domain at Position 1 and Position 2 were obtained, named

IT4var01-mTurboPos1^{endo} and IT4var01-mTurboPos2^{endo} respectively (Figure 28A, B). Diagnostic PCR confirmed the correct integration at the target locus (Figure 28A, B).

Subsequent IFAs detected the modified PfEMP1, showing co-localization with the Maurer's cleft marker SBP1 in both miniTurbo cell lines (Figure 28A, B). Given that the BioID cell lines demonstrated satisfactory performance in terms of PfEMP1 function and biotin labeling, and mass spectrometry data was obtained for the BioID cell lines (section 3.2.1.1 and 3.2.2) further explorations with the miniTurbo cell lines were not done.

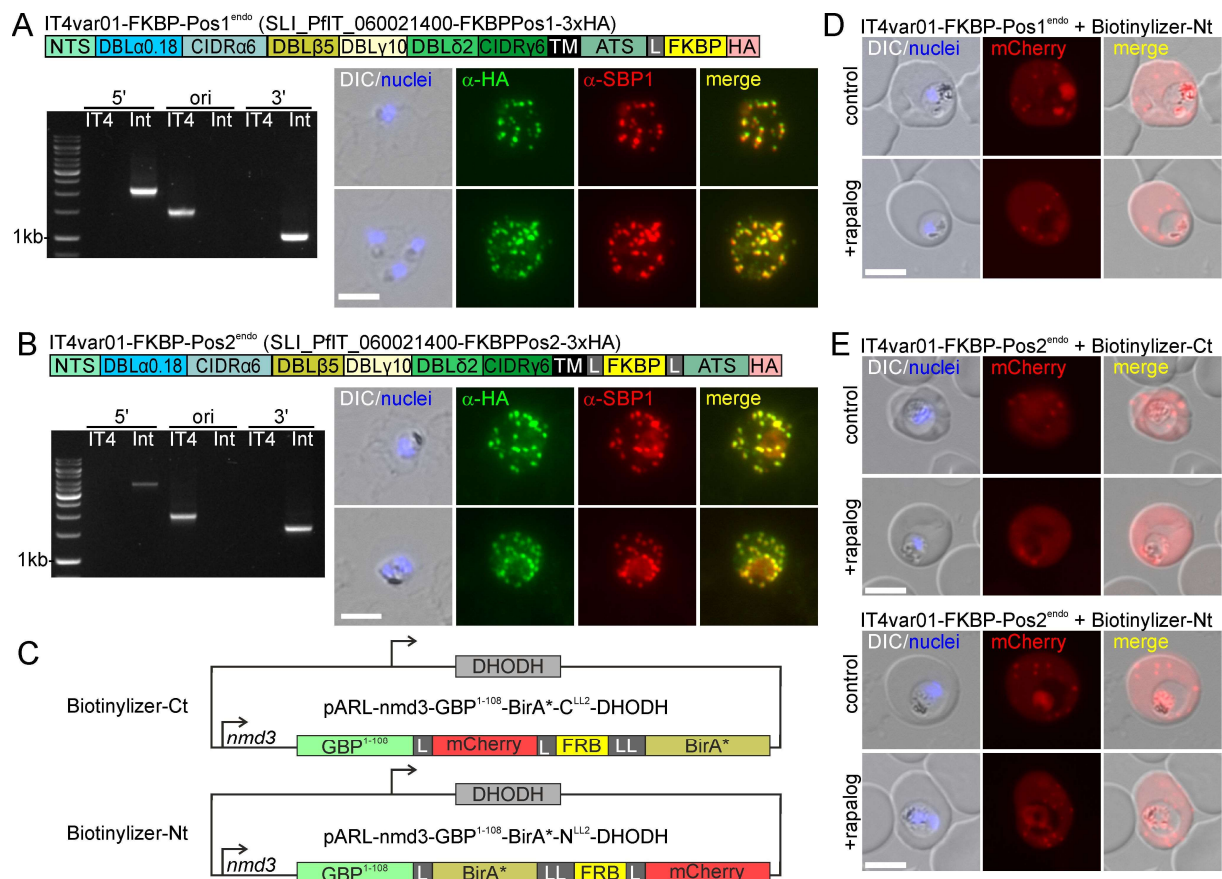


Figure 29: Attempt to establish DiQ-BioID for PfEMP1. (A, B) Confirmation of the activation and modification of the indicated IT4var01-FKBP fusions. Schematics show domain organization of the modified PfEMP1. Agarose gel shows PCR products confirming correct integration of the SLI plasmid. Product over 5' integration junction (5'): P1 + P2; 3' integration junction (3'): P3 + P4; original locus (ori): P1 + P4; see Figure 12 for primer positions and Appendix A2 for sequence; IT4: parent; Int: integrant cell line. Expected bands: IT4var01-FKBP-Pos1^{endo}: 5': 1701 bp; ori: 1536 bp; 3': 971 bp; IT4var01-FKBP-Pos2^{endo}: 5': 3639 bp; ori: 3059 bp; 3': 2721 bp. Fluorescence microscopy images show IFAs with indicated antibodies. Nuclei: Hoechst 33342; DIC: differential interference contrast; size bars 5 μ m. (C) C- and N-terminal biotinylizer constructs transfected into IT4var01-FKBP-Pos1^{endo} or IT4var01-FKBP-Pos2^{endo}. GBP¹⁻¹⁰⁸: N-terminus of GBP130 (PF3D7_1016300; exported); L: linker; LL: long linker; DHODH: conferring resistance to DSMI resistance; FRB: recruits to FKBP upon rapalog addition. (D, E) Fluorescence microscopy images show live parasites of the indicated cell line + and - rapalog treatment for 3 hours.

For the second approach, constructs were designed to fuse FKBP to Position 1 and Position 2 of the target PfEMP1 to conduct DiQ-BioID (Birnbaum et al., 2020), a strategy by which BirA* is expressed separately and conditionally recruited to the target using the FKBP-FRB heterodimerization system. The strength of this approach lies in the ability to subtract the background labelling from a highly matched parasite population (Birnbaum et al., 2020; Kimmel et al., 2022). In addition, only one FKBP domain was used which is considerably smaller than BirA* or miniTurbo (12 kDa vs 35 or 27 kDa). For both positions cell lines were obtained after selection on G418 and designated IT4var01-FKBP-Pos1^{endo} and IT4var01-FKBP-Pos2^{endo} (Figure 29A, B). Diagnostic PCRs confirmed the correct integration of the plasmids in IT4var01-FKBP-Pos1^{endo} and IT4var01-FKBP-Pos2^{endo} (Figure 29A, B). IFAs detected the modified PfEMP1 in the host cell where it co-localized with the Maurer's clefts marker SBP1 (Figure 29A, B).

Thereafter, constructs were designed for “biotinylizers” that are exported to the host cell cytosol (Figure 29C). These biotinylizers, expressed under the *nmd3* promoter, comprised a BirA* domain for biotinylation, an mCherry domain for visualization, and an FRB domain for recruiting the biotinylizer to the FKBP-fused PfEMP1. The N-terminal region of the biotinylizer included the N-terminus of GBP130 (PF3D7_1016300, amino acid 1–108), featuring a signal peptide for secretion into the PV and a PEXEL motif for translocation across the PVM into the host cell. Upon addition of rapalog to the parasites, the biotinylizer in the host cell cytosol is then expected to be recruited to the FKBP-fused PfEMP1. In the past, a Biotinylizer-Ct, with BirA* at the N-terminus and mCherry at the C-terminal to the FRB, and Biotinylizer-Nt, where the positions of BirA* and mCherry were reversed were used to maximize the area reached for biotinylation around the target (Birnbaum et al., 2020) and this was here done as well (Figure 29C).

For Position 1, only a cell line expressing Biotinylizer-Nt in IT4var01-FKBP-Pos1^{endo} was successfully obtained. Live cell imaging revealed mCherry signal dispersed throughout the cytosol with some foci (potentially indicating some aggregation) as well as a prominent signal in the food vacuole (expected due to internalization of host cell cytosol), demonstrating successful expression of the biotinylizer in the host cell cytosol (Figure 29D). However, after rapalog addition a similar localization pattern of the biotinylizer was observed without apparent recruitment to the Maurer's clefts where PfEMP1 is mostly localized, indicating that the system did not work as intended.

For the IT4var01-FKBP-Pos2^{endo} two cell lines were generated, expressing either Biotinylyzer-Ct or Biotinylyzer-Nt. Both constructs exhibited localization within the food vacuole and in the host cell with concentrated puncta and dispersed throughout the cytosol, comparable to the result with Biotinylyzer-Nt in IT4var01-FKBP-Pos1^{endo} (Figure 29E). Addition of rapalog did not alter the localization pattern, and no recruitment of the biotinylyzers to Maurer's clefts was observed, again indicating that FKBP-FRB mediated conditional recruitment, in contrast to the parasite cytosol (Birnbaum et al., 2020; Kimmel et al., 2022) or the PV (Khosh-Naucke et al., 2018), did not work.

Because the BioID cell lines IT4var01-BirA*Pos1^{endo}, IT4var01-BirA*Pos2^{endo}, and IT4var01-BirA*Pos3^{endo} showed already promising results (section 3.2.1.1 and 3.2.2), the DiQ-BioID approach was not further pursued. But it can be concluded that for unknown reasons, the system does not appear to function in the host cell and further optimization would be needed to use the DiQ-BioID approach in the host cell.

3.2.2 IDENTIFICATION OF BIOTINYLATED PROTEINS PROXIMAL TO PfEMP1

To identify specific interactors of PfEMP1, the BioID cell lines (IT4var01-BirA*Pos1^{endo}, IT4var01-BirA*Pos2^{endo} and IT4var01-BirA*Pos3^{endo}) and IT4 (control) were cultured in large-scale asynchronous cultures. Biotin was added for 24 h with one replacement with a medium change after 12 hours as done previously (Birnbaum et al., 2020; Khosh-Naucke et al., 2018). Three independent experiments were carried out, and each time the biotinylated proteins were extracted and purified. Initially, protein extraction from the pelleted parasites was performed using a mild Triton-X-100 containing lysis buffer. Subsequently, a buffer containing 4% SDS was used in a subsequent extraction from the same pellets for a secondary extraction under denaturing conditions, ensuring a comprehensive retrieval of proteins. The two extraction methods had the rationale to separate non-structurally bound membrane proteins from those strongly associated with the cytoskeleton, a property known to apply to PfEMP1 (Baruch et al., 1995; Kriek et al., 2003; Papakrivovs et al., 2005).

Following purification, the proteins were subject to label free quantitative liquid chromatography-mass spectrometry (LC-MS) analysis (performed by Pascal WTC Jansen and Richárd Bártfai, Radbaoud University, Nijmegen, Netherlands). Thereafter, a comparative analysis was conducted where the biotinylated proteins obtained from either the Triton or SDS extractions of each BioID cell line were compared with those from the IT4 cell line (performed

by Pascal WTC Jansen and Gala Ramón-Zamorano). For the comparative analysis the detected peptides were identified by comparison to the IT4 proteome (Figure 30).

The results from the Triton-extracted samples revealed only a modest number of proteins significantly enriched in the BioID cell lines relative to the IT4 control (Figure 30A). In the IT4var01-BirA*Pos1^{endo} samples, PfEMP1 was notably the most significantly enriched protein, affirming the self-biotinylation of the BirA*-fused PfEMP1 bait (Figure 30A) typical in BirA* fusions (e.g. Kimmel et al., 2023). Among the proteins enriched over the IT4 control (enrichment threshold: $\log_2(\text{Position 1, 2 or 3/IT4}) = 2$), four were exported proteins. Notably, SBP1, REX1, and PTP1 were among these proteins and are known to play a role in the cytoadherence of the parasite (Cooke et al., 2006; Maier et al., 2008, 2007; McHugh et al., 2015; Rug et al., 2014). The fourth protein, Tryptophan-threonine-rich antigen (TryThrA), a known PNEP (Heiber et al., 2013), was previously identified in the proxime of the Maurer's clefts (Blancke-Soares et al., 2021) and in an interactome of SBP1, where it was shown to be non-essential for cytoadherence (Takano et al., 2019). Additionally, under the FDR threshold two exported proteins with unknown function were detected, here termed PfEMP1-interacting candidate (EMPIC) (relevant as they reappear in the SDS-samples highly enriched; numbered based on the enrichment in SDS-samples of Position 1) as well as peripheral Maurer's clefts protein 1 (PeMP1) (Blancke-Soares et al., 2021) and PTP6.

In the IT4var01-BirA*Pos2^{endo} samples, PfEMP1 again emerged as the most enriched protein, validating the specificity and efficacy of the biotinylation (Figure 30A). Above the threshold, only two additional exported proteins, TryThrA and SBP1, were detected. Notably, proteins enriched just below the threshold included REX1, PTP5, and PTP6, all of which are essential for cytoadherence (Maier et al., 2008; McHugh et al., 2015), alongside EMPIC2, EMPIC3, and PfJ23 (Cabral et al., 2017; Kaur et al., 2018).

For the IT4var01-BirA*Pos3^{endo} samples, PfEMP1 continued to dominate as the most enriched protein (Figure 30A). Additionally, TryThrA and a PHIST protein (here termed P8; PfIT_040006400; all PHISTs were abbreviated by a P based on the SDS-samples for position 1), were identified above the threshold. Marginally below the threshold, PTP5 and the *P. falciparum* translation enhancing factor (PTEF), a PNEP at the erythrocyte membrane (Birnbaum et al., 2017) previously associated with VAR2CSA translation (Chan et al., 2017), were found to be enriched. Furthermore, PeMP1 was detected above enrichment threshold but far under the FDR threshold.

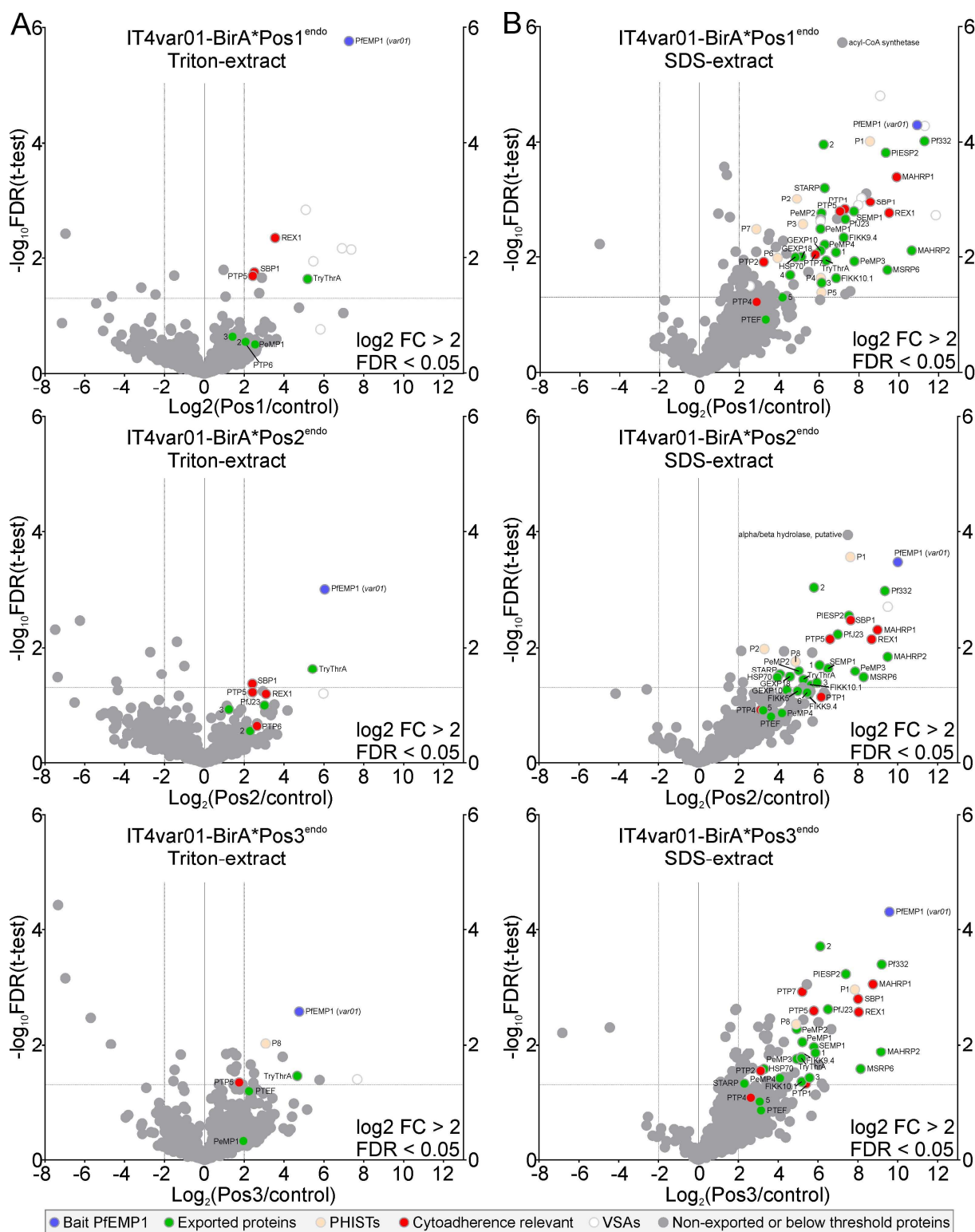


Figure 30: MS analysis of biotinylated proteins enriched in the BioID cell lines. (A, B) Volcano plots show enrichment of biotinylated proteins extracted with Triton (A) or SDS (B) from the lysates of the indicated cell lines compared to IT4 wildtype parasites (average of 3 independent replicates). Confidence above $-\log_{10}$ FDR of 0.05 and \log_2 enrichment of 2 are indicated by dotted lines. Tables with abbreviations and accession numbers for exported proteins with unknown function (green) and PHISTs (beige) in Appendix F.

Interestingly, the SDS-samples exhibited a far greater number of enriched proteins for all of the BioID cell lines compared to the Triton-samples (Figure 30B). This indicates that most of the biotinylated proteins, and therefore the proximiome of PfEMP1, is tightly associated with structural proteins in the cell.

In the IT4var01-BirA*Pos1^{endo} samples, PfEMP1 was identified as highly enriched, exhibiting a higher level of enrichment compared to the Triton-extracted sample (Figure 30B). This observation suggests that a significant proportion of PfEMP1 molecules are not extracted by the Triton buffer, in agreement with previous findings (Baruch et al., 1996; Papakrivovs et al., 2005; Waterkeyn et al., 2000). In addition to the proteins identified in the Triton samples, other proteins relevant to cytoadherence, specifically MAHRP1 (Spycher et al., 2008), PTP7 (Carmo et al., 2022), PTP2 (Maier et al., 2008), PTP1 (Maier et al., 2008; Rug et al., 2014), and just below FDR threshold PTP4 (Maier et al., 2008), were highly enriched.

Moreover, several known Maurer's clefts residents exhibited enrichment, including PfJ23, parasite-infected erythrocyte specific protein 2 (PIESP2) (Florens et al., 2004), *P. falciparum* protein 332 (Pf332) (Issar et al., 2008), small exported membrane protein 1 (SEMP1) (Dietz et al., 2014; Heiber et al., 2013), TryThrA (Heiber et al., 2013), MSP-7 related protein 6 (MSRP6) (Blancke-Soares et al., 2021) and just below the FDR threshold, PTEF (Chan et al., 2017). Additionally, recently identified MSRP6 interactors, PeMP1-4 (Blancke-Soares et al., 2021), showed enrichment. Furthermore, the analysis revealed enrichment for MAHRP2 (Pachlatko et al., 2010), EMPIC1-5, seven PHIST proteins (P1-7), gametocyte exported protein 10 (GEXP10) (localized in the erythrocyte membrane of asexual parasites) (Dantzler et al., 2019), GEXP18 proteins (localizing to J-Dots) (Zhang et al., 2017), two serine/threonine kinases (FIKK9.4 and 10.1) (Davies et al., 2020; Nunes et al., 2007; Ward et al., 2004) and the ring stage expressed sporozoite threonine and asparagine-rich protein (STARP) (Fidock et al., 1994).

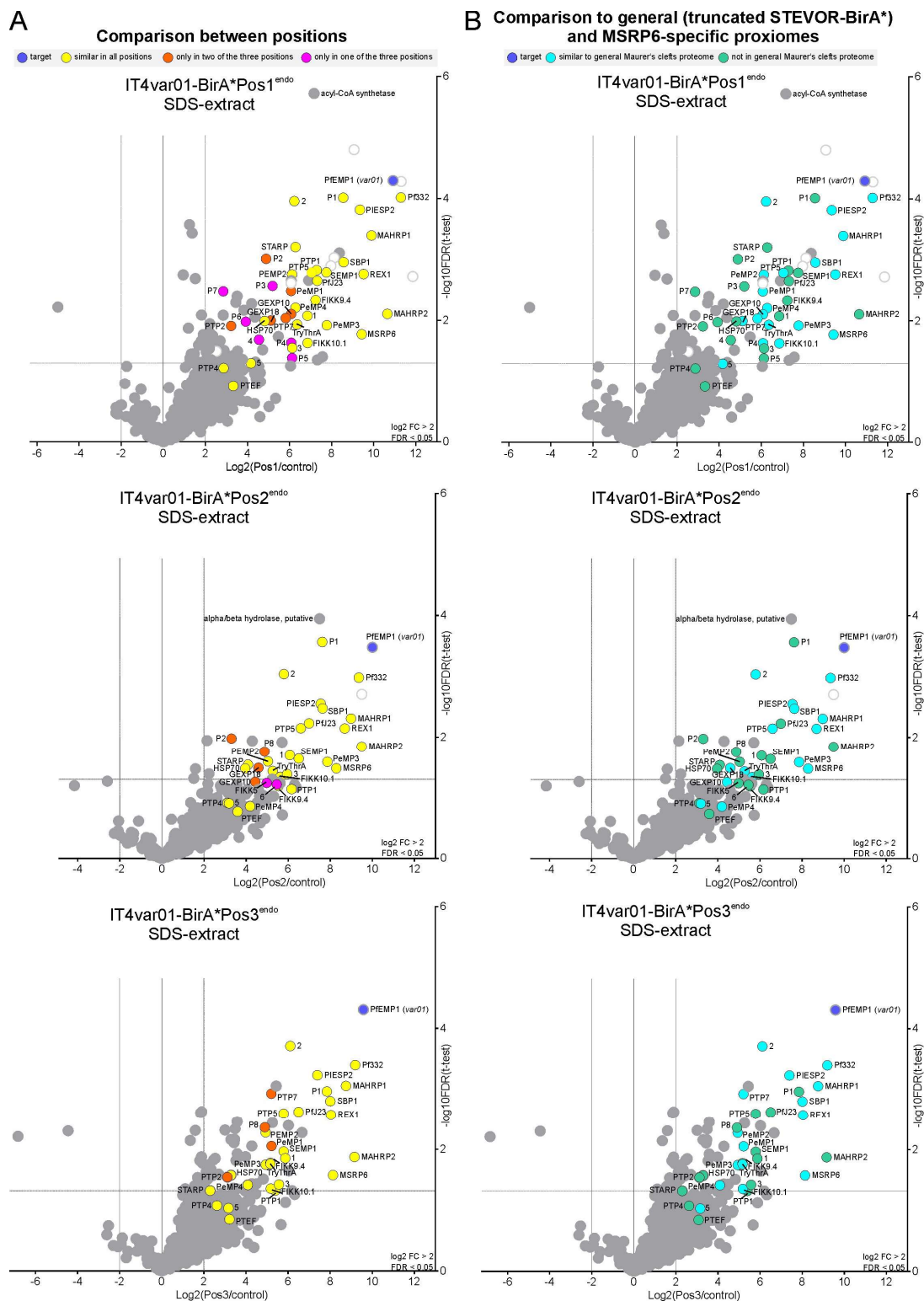


Figure 31: Comparison of the PfEMP1 proximiomes with each other and a general Maurer's clefts proximiome. (A, B) Volcano plots of SDS extracts from Figure 30 shown with color coding according to similarity between positions (A) or with a general Maurer's cleft BioID (Blancke-Soares et al., 2021) (B). Hits were considered similar in all positions (yellow) when they were in a similar relative position to other hits (A). Hits were in (B) marked as present in general Maurer's clefts proteome (light blue) if significantly enriched in BioID experiments of a general Maurer's clefts marker over a protein soluble in the host cell or in the Maurer's clefts attachment domain of MSRP6 over the control protein soluble in the host cell (Blancke-Soares et al., 2021).

For the IT4var01-BirA*Pos2^{endo} samples, the pattern of enriched proteins was similar to that observed in the IT4var01-BirA*Pos1^{endo} samples. Notably, PfEMP1 was again highly enriched. However, the overall count of proteins enriched above the threshold was lower in comparison to IT4var01-BirA*Pos1^{endo}, which could potentially be due to less efficient biotinylation in the proximal position of the BirA* relative to the membrane. Proteins that were not enriched above threshold in the Position 2 samples but were significantly enriched in the Position 1 samples were PTP2, PTP7, five PHISTs (P3-7), FIKK9.4, PeMP1 and EMPIC4. In contrast, in the IT4var01-BirA*Pos2^{endo} samples, FIKK5 and, marginally below the FDR threshold, EMPIC6 was enriched which were not significantly enriched in the IT4var01-BirA*Pos1^{endo} samples (Figure 30B).

In the SDS-extracted samples from the IT4var01-BirA*Pos3^{endo} samples, the BirA* fused PfEMP1 was significantly enriched compared to the control. The pattern of proteins enriched that are relevant for cytoadherence mirrored that of the IT4var01-BirA*Pos1^{endo} and IT4var01-BirA*Pos2^{endo} samples, exhibiting comparable fold changes in enrichment. However, certain proteins enriched in Position 1 or 2, including GEXP10, GEXP18, P2-7, EMPIC4, EMPIC6, and FIKK5, were not enriched in Position 3. Additionally, no exported proteins, not enriched in the other two BioID cell lines, were significantly enriched in the IT4var01-BirA*Pos3^{endo} samples. PTEF, PTP4 and EMPIC5 were significantly enriched but below the FDR threshold.

Interestingly, the biotinylated proximiomes of the three BioID cell lines showed only minor differences (Figure 31A), indicating that IT4var01-BirA*Pos3^{endo}, with the BirA* positioned on the extracellular side of the erythrocyte membrane, did not yield a distinct set of proteins compared to IT4var01-BirA*Pos1^{endo} and IT4var01-BirA*Pos2^{endo}. It is noteworthy that the differences were PHIST proteins that were predominantly enriched in IT4var01-BirA*Pos1^{endo} (but not in Position 2) and GEXP10 and 18 which were not enriched in IT4var01-BirA*Pos3^{endo}. Interestingly, KAHRP was not enriched in any of the three BioID cell lines.

Subsequently, the proteomes obtained were compared with the comprehensive Maurer's clefts proteomes previously delineated by Blancke-Soares et al. (2021) that also used BioID. The general Maurer's clefts proteome exhibited considerable overlap with the PfEMP1 interacting proteome, albeit with notable distinctions (Figure 31B). Proteins enriched in any of the PfEMP1 BioID cell lines compared to the control and not detected in the general Maurer's clefts BioID were identified. These included eight PHIST proteins (P1-8), four EMPICs (EMPIC1, 3, 4, 6), PfJ23, PeMP4, two FIKKs (FIKK5 and 9.4), three PTPs (PTP1, 2, 4), MAHRP2, SEMP1,

HSP70, STARP, and PTEF. These particular proteins emerge as interactors potentially engaging in interactions with PfEMP1 outside of the Maurer's clefts, during the transport process, or within the knobs. Overall, the PfEMP1 BioIDs provide a plausible proximate of PfEMP1 in living parasites although many of the hits indicate they are in proximity of PfEMP1 during transport or at the Maurer's clefts rather than at the surface of the erythrocytes.

3.2.3 SLI2 ENABLES CHARACTERIZATION OF PfEMP1 INTERACTORS

To elucidate the potential PfEMP1 connected functions of the proteins identified in the BioID experiments, a method was necessary to disrupt the interactors of PfEMP1. For this purpose, Selection Linked Integration 2 (SLI2) was employed (Blancke-Soares et al., 2021; Naranjo Prado, 2020; Stäcker, 2021). Operating on similar principles as its predecessor (SLI), SLI2 uses two distinct selection markers: BSD-R (conferring BSD resistance) for selection of parasites carrying the plasmid and yeast DHODH (conferring DSMI resistance) for genomic integration of the plasmid (Figure 32A). To validate the efficacy of this system, specifically within cell lines with a SLI-activated *var* gene, the IT4var01-HA^{endo} cell line was selected. PTP1, a protein established as crucial for cytoadherence (Maier et al., 2008; Rug et al., 2014), was targeted for gene disruption using SLI2. The plasmid, initially crafted for targeted gene disruption of PTP1 in the 3D7 strain (Naranjo Prado, 2020), was transfected, given the near-identical homology regions (only one base pair mismatch) in IT4. The generated cell line was designated as IT4var01-HA^{endo}+PTP1-TGD-GFP. Diagnostic PCR showed the correct plasmid integration into the targeted gene locus and the absence of parasites retaining an unmodified target gene locus (Figure 32B). Additionally, the sustained presence of the first SLI modification was validated through diagnostic PCR (Figure 7B, diagnostic PCR confirming SLI integration performed by Jan Stäcker).

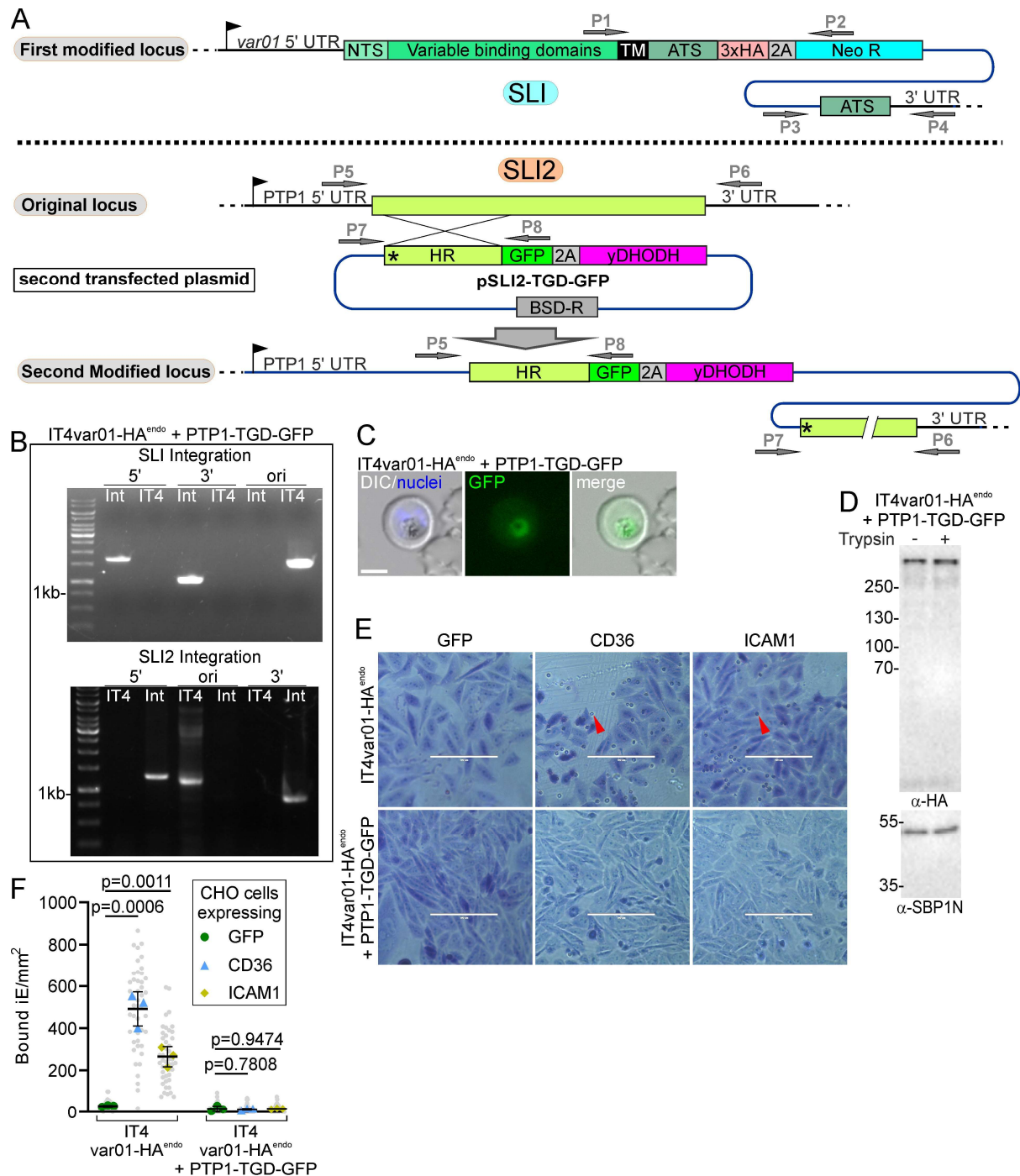


Figure 32: Second endogenous modification in cell line with a SLI-activated *var* gene. (A) Schematic for SLI2 strategy for second genome modification in SLI cell line with activated *var* gene. HR: homology region; ATS: acidic terminal segment; NTS: N-terminal sequence domain; 2A: T2A skip peptide; NEO-R: neomycin-resistance gene (conferring G418 resistance); yDHODH: yeast dihydroorotate dehydrogenase (conferring DSM1 resistance); BSD-R: BSD-resistance gene (conferring BSD resistance), arrows P1-8 primers for diagnostic PCR for SLI; X: desired *var* gene; PTP1: PfEMP1 transport protein 1. (B) Agarose gel shows PCR products confirming correct integration of the SLI2 plasmid and perpetuation of the SLI plasmid integration. SLI2 integration: product over 5' integration junction (5'): P5 + P8; over 3' integration junction (3'): P7 + P6; original locus (ori): P5 + P6; SLI integration PCRs as described in Figure 12 and (A); primers in Appendix A2; IT4: parent; Int: integrant cell line; expected bands: SLI: 5': 1698 bp; ori: 1536 bp; 3': 1040 bp; SLI2: 5': 1164 bp; ori: 1227 bp; 3': 913 bp. (C) Fluorescence microscopy images of live IT4var01-HA^{endo}+PTP1-TGD-GFP parasites. (D) Western blot of trypsin cleavage assays with IT4var01-HA^{endo}+PTP1-TGD-GFP parasites. α -SBP1-N: control for integrity of host cell. Marker in kDa. Replicates and full blots in Appendix A2. (E) Images show representative sections of captured

images of binding assays with the indicated cell line against CHO cell lines expressing the indicated receptors. Red arrows show examples of bound infected erythrocytes. Size bars 100 μm . (F) SuperPlot of binding assays of indicated cell lines against CHO cells expressing GFP, CD36 or ICAM-1 (3 biological replicates with 15 fields of view/experiment and condition; bars: mean of averages of replicates with SD; unpaired t-test; p-values are indicated). Small grey dots: bound iE/field of view, extrapolated to mm^2 . Larger colored dots: average of bound iE/ mm^2 /replicate. iE: infected erythrocytes.

Live cell imaging revealed a cytosolic GFP signal in the host cell in the PTP1-TGD-GFP parasites (Figure 32D), suggesting successful ablation of PTP1 as the truncated GFP-tagged form differed in location from intact PTP1 which is located at the Maurer's clefts (Rug et al., 2014).

Subsequently, the surface presentation of PfEMP1 and cytoadherent properties of IT4var01-HA^{endo}+PTP1-TGD-GFP were tested. Trypsin cleavage assays revealed the presence of only full-length PfEMP1 in the trypsin-treated sample and control, indicating a defect in PfEMP1 surface presentation (Figure 32E), in agreement with previous work on PTP1 (Maier et al., 2008, Rug et al., 2014). Binding assays were performed against CHO cells expressing CD36, ICAM or GFP, to assess the cytoadherence properties of the IT4var01-HA^{endo}+PTP1-TGD-GFP parasites. No binding to GFP, CD36 or ICAM-1 was observed (Figure 32F). In contrast, the parent cell line, IT4var01-HA^{endo}, exhibited significant binding to these receptors but no interaction with the GFP control.

These findings validate the SLI2 approach to obtain a second endogenous modification in parasites harboring a SLI-activated PfEMP1.

3.2.4 CHARACTERIZATION OF INTERACTING CANDIDATES OF PfEMP1

To investigate the proximity to PfEMP1 and influence of the identified interactors on the transport and function of PfEMP1, candidates were selected with a focus on PNEPs and proteins previously validated to be exported in our laboratory and covering different levels of enrichment. The selected candidates were disrupted using SLI2 and the impact on PfEMP1 function and location was assessed as in parts described for PTP1 (section 3.2.3). In addition, additional cell lines were generated wherein the candidates were tagged with Ty1 to identify their localization in relation to PfEMP1 within the cell. Both the tagging and disruption were executed in the IT4var01-BirApos1^{endo} cell line. The underlying rationale for the use of the BioID cell line was that identifying a protein which influences PfEMP1 transport will pave the way for subsequent BioID experiments of the PfEMP1 arrested in a step during transport. These

experiments might detect the proxime of transport-impeded PfEMP1 and juxtapose it with the proxime of the functional PfEMP1, thereby shedding light on the mechanics of PfEMP1 transport.

For the Ty1 tagging, SLI2 constructs with a homology region comprising the C-terminus of the target gene was cloned into pSLI2a-Ty1 (Stäcker, 2021), for the TGD constructs, homology regions were selected in the N-terminal area of the targeted gene and cloned into the pSLI2a-TGD plasmid (Naranjo Prado, 2020) (section 3.2.3), upon integration resulting in a GFP-tagged, truncated product.

3.2.4.1 TRYTHRA

TryThrA emerged as a prominently enriched protein in mass spectrometry analysis of the PfEMP1 BioID cell lines in the Triton- and SDS-samples. It features a tryptophan-threonine rich segment in its central region. It was identified in the sporozoite and liver stages of the parasite (Jaijyan et al., 2015), other research identified TryThrA as a PNEP, localizing to the Maurer's clefts during the blood stages (Heiber et al., 2013). Furthermore, TryThrA was identified as an interactor of SBP1, and it was shown that TryThrA knockout did not impede cytoadherence in 3D7 parasites (Takano et al., 2019).

After successfully tagging TryThrA with a Ty1-tag via SLI2 demonstrated by diagnostic PCRs (Figure 33A), IFAs revealed two distinct TryThrA localizations at the Maurer's clefts: a peripheral donut-shaped Ty1-signal surrounding the HA-signal of PfEMP1 (Figure 33B, top IFA panel) present in 18.4% of parasites (n=4 independent experiment with 38 cells in total) and a dot-shaped Ty1-signal overlapping with the PfEMP1's HA-signal (Figure 33B, bottom IFA panel) in 81.6% of parasites. Additionally, a signal for TryThrA was observed in smaller foci in the host cell mostly not co-localizing with the HA-signal (Figure 33B, bottom IFA panel)

The SLI2 plasmid to disrupt TryThrA in the IT4var01-BirA*Pos1^{endo} cell line was designed to disrupt the tryptophan-threonine stretch, with the expectation to thereby deactivating its function. PCRs confirmed correct integration of the SLI2 plasmid and maintenance of the initial SLI integration (cell line: TryThrA-TGD-GFP) (Figure 33C). Live imaging of truncated GFP-tagged TryThrA displayed signal concentrated in puncta in the host cell, potentially associated with Maurer's clefts but exhibiting elongated shapes and unusual foci distribution (Figure 33C).

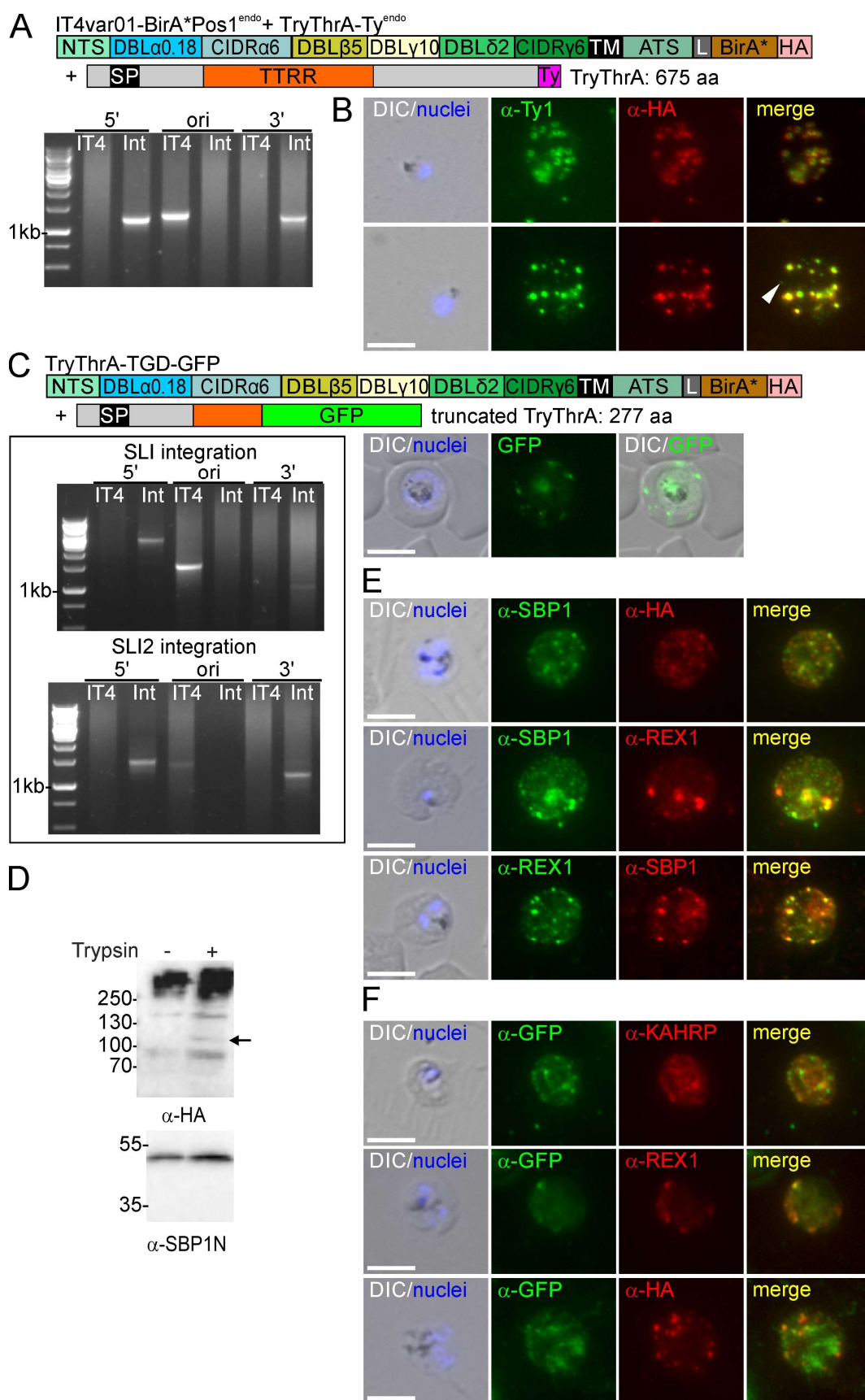


Figure 33: Characterization of TryThrA. (A) Schematic shows domain organization of the expressed products. Agarose gels show PCR products confirming correct integration of the SLI2 plasmid. PCR over 5' integration

junction (5'): P5 + P8 in Figure 12; PCR over 3' integration junction (3'): P7 + P6 in Figure 12; original locus (ori): P5 + P6 in Figure 12; IT4 parent; Int: integrant cell line; primers in Appendix A2; Expected bands: 5': 1243 bp; ori: 1317 bp; 3': 1274 bp. **(B)** Fluorescence microscopy images show IFAs with acetone fixed parasites with the indicated antibodies. Nuclei: Hoechst 33342; DIC: differential interference contrast; size bars 5 μ m. **(C)** Schematic shows domain organization of the expressed products. Agarose gels show PCR products confirming correct integration of the SLI2 plasmid and perpetuation of SLI plasmid integration. PCR over 5' integration junction (5'): P1 + P2 in Figure 12 or P5 + P8 in Figure 32A; PCR over 3' integration junction (3'): P3 + P4 in Figure 12 or P7 + P6 in Figure 32A; original locus (ori): P1 + P4 in Figure 12 or P5 + P6 in Figure 32A; primers in Appendix A2; IT4 parent; Int: integrant cell line. Expected bands: SLI: 5': 2337 bp; ori: 1536 bp; 3': 971 bp; SLI2: 5': 1441 bp; ori: 1384 bp; 3': 1149 bp. Fluorescence microscopy images show live TryThrA-TGD-GFP parasites. Nuclei: Hoechst 33342; DIC: differential interference contrast; size bars 5 μ m. **(D)** Western blot of trypsin cleavage assay with TryThrA-TGD-GFP parasites. Arrow shows protected PfEMP1 fragment. α -SBP1-N: control for integrity of host cell. Marker in kDa. Replicate and full blots in Appendix B. **(E, F)** IFAs (bottom rows) with indicated antibodies. Nuclei: Hoechst 33342; DIC: differential interference contrast; size bars 5 μ m.

Trypsin cleavage assays with erythrocytes infected with TryThrA-TGD-GFP parasites showed a faint ~110 kDa band for the trypsin-treated sample corresponding to the protected fragment of the modified PfEMP1 (Figure 33D). This suggests that TryThrA disruption does not ablate PfEMP1 surface display, although the weak signal implies possible display impairments. Only full-length SBP1 was detected probing with α -SBP1-N antibodies, showing that the integrity of the host cell was not impaired.

Next, the effect of TryThrA's truncation on Maurer's clefts structure, PfEMP1 location and KAHRP location was evaluated with IFAs (Figure 33E). First, SBP1 and HA-tagged PfEMP1 were co-localized to evaluate the Maurer's cleft morphology and PfEMP1 location in relation to SBP1 (Figure 33E). This showed that the SBP1 signal showed unusual location 66 % of the infected erythrocytes showed a phenotype (n=106 parasites across three independent IFAs evaluating SBP1 signal; phenotype: parasites with large elongated, more than 30 or unidentifiable number Maurer's clefts; diffuse SBP1 signal) suggesting an effect on Maurer's clefts morphology. Furthermore, PfEMP1 also showed a more scattered localization in the host cell overlapping with the SBP1 signal. PfEMP1 foci in proximity to SBP1 foci showed only partial overlap in most cases. Subsequently, Maurer's clefts morphology was further interrogated by co-localizing REX1 and SBP1 (Figure 33E). The REX1 signal presented an atypical localization pattern, characterized by a dispersed signal within the host cell, deviating from the distinct Maurer's clefts-associated puncta typically seen with REX1. Some REX1 foci

showed overlapped with SBP1 signal but especially smaller foci did not overlap with the SBP1 signal.

Next, the truncated TryThrA was co-localized with KAHRP, REX1 and PfEMP1 (Figure 33F). KAHRP signal exhibited normal localization in the erythrocyte membrane (Figure 33F) with some concentrated KAHRP signal overlapping the truncated TryThrA signal, implying that a subpopulation of truncated TryThrA localizes to the erythrocyte membrane. Co-localization of REX1 with GFP showed partial overlap, especially notable in foci where the signals are concentrated in larger puncta. PfEMP1 localization in relation to the truncated TryThrA showed partial overlap (Figure 33F). It is noteworthy, that the GFP signal observed in IFAs differentiated from the GFP signal in live imaging (Figure 33C, F). This could be due to incorrect folding of the GFP fused to the truncated TryThrA for a subpopulation of the protein or that IFAs are more sensitive showing signal for small amounts of proteins that might not be detected with live imaging.

Collectively, these findings suggest that TryThrA plays a crucial role in maintaining Maurer's clefts integrity, with its disruption leading to alteration in the structural integrity and typical localization of proteins within Maurer's clefts but not to the ablation of the surface display of PfEMP1.

3.2.4.2 PTEF

PTEF was previously localized to the host cell membrane and the nucleus (Birnbaum et al., 2017; Blancke-Soares et al., 2021; Chan et al., 2017). Furthermore, it was postulated that it functions as a translation enhancement factor that plays a role in the de-repression of VAR2CSA translation (Chan et al., 2017). It was consistently identified below the FDR threshold yet was significantly enriched across all mass spectrometry analyses of the BioID cell lines (Figure 30). As it was detected at the host cell membrane of infected erythrocytes in 3D7 parasites, it was chosen for analysis by disrupting it using the SLI2-TGD approach.

To confirm the location of PTEF in IT4 parasites, it was first endogenously tagged with Ty1. The correct integration of the SLI2 plasmid fusing the Ty1-tag to PTEF was corroborated through diagnostic PCRs (kindly performed by Joelle Hornebeck) (Figure 34A). No co-localization was observed between Ty1-tagged PTEF and PfEMP1 in IFAs, with the former exhibiting a distribution pattern akin to KAHRP at the erythrocyte membrane and no noticeable nuclear co-localization (Figure 34B), agreeing with the previous observations of endogenously GFP-tagged PTEF in 3D7 (Birnbaum et al., 2017).

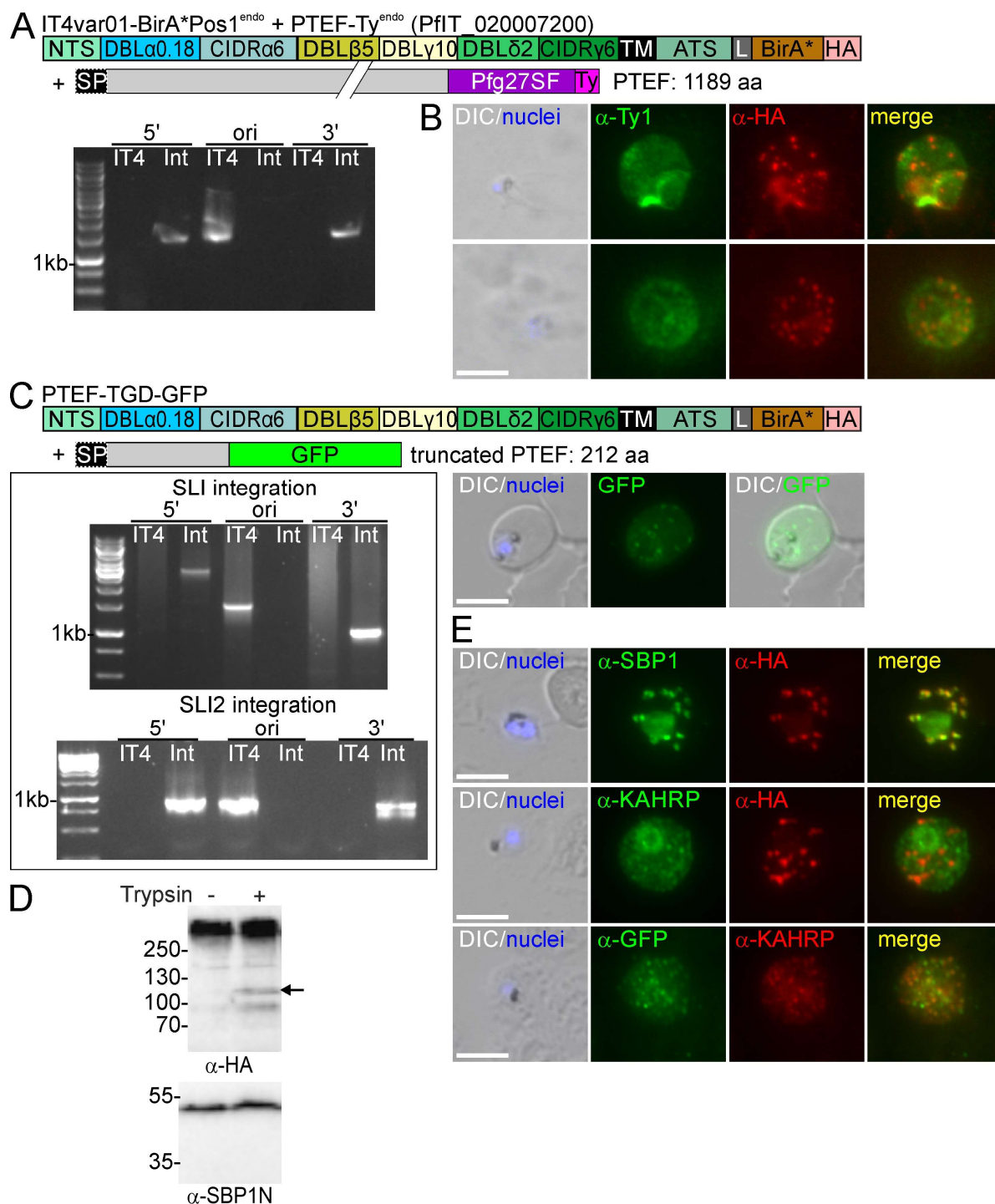


Figure 34: Characterization of PTEF. (A) Schematic shows domain organization of the expressed products. Agarose gels show PCR products confirming correct integration of the SLI2 plasmid. PCR over 5' integration junction (5'): P5 + P8 in Figure 32A; PCR over 3' integration junction (3'): P7 + P6 in Figure 32A; original locus (ori): P5 + P6 in Figure 32A; IT4 parent; Int: integrant cell line; primers in Appendix A2; expected bands: 5': 1409 bp; ori: 1462 bp; 3': 1516 bp. (B) Fluorescence microscopy images show IFAs with acetone fixed PTEF-Ty1^{endo} parasites with indicated antibodies. Nuclei: Hoechst 33342; DIC: differential interference contrast; size bars 5 μ m. (C) Schematic shows domain organization of the expressed products. Agarose gels show PCR products confirming correct integration of the SLI2 plasmid and perpetuation of SLI plasmid integration. PCR over 5' integration

junction (5'): P1 + P2 in Figure 12 or P5 + P8 in Figure 32A; PCR over 3' integration junction (3'): P3 + P4 in Figure 12 or P7 + P6 in Figure 32A; original locus (ori): P1 + P4 in Figure 12 or P5 + P6 in Figure 32A; primers in Appendix A2; IT4 parent; Int: integrant cell line; expected bands: SLI: 5': 2337 bp; ori: 1536 bp; 3': 971 bp; SLI2: 5': 874 bp; ori: 846 bp; 3': 676 bp. Fluorescence microscopy images show live parasites. Nuclei: Hoechst 33342; DIC: differential interference contrast; size bars 5 μ m. **(D)** Western blot of trypsin cleavage assays with PTEF-TGD-GFP parasites. Arrow shows protected PfEMP1 fragment. α -SBP1-N: control for integrity of host cell. Marker in kDa. Replicate and full blots in Appendix B. **(E)** Fluorescence microscopy images show IFAs with acetone fixed PTEF-TGD-GFP parasites with indicated antibodies. Nuclei: Hoechst 33342; DIC: differential interference contrast; size bars 5 μ m.

The disruption of PTEF through SLI2 integration was validated by diagnostic PCRs (SLI2 integration confirmation kindly performed by Joelle Hornebeck) (Figure 34B). Live imaging of the parasites showed signal for GFP-tagged disrupted PTEF dispersed throughout the host cell with several concentrated puncta differing from the location of the full length PTEF, indicating a successful disruption of PTEF (Figure 34C). The surface presentation of PfEMP1 was assessed using a trypsin cleavage assay, showing a ~110 kDa band, consistent with the protected fragment of the modified PfEMP1, in the trypsin-treated sample (Figure 34D). Notably, no protected fragments were detected during SBP1 probing with α -SBP1-N antibodies, ensuring erythrocyte integrity during the assay. This suggests that PTEF disruption does not impede PfEMP1's surface display.

IFAs showed that both, SBP1 and PfEMP1, still overlapped in puncta reminiscent of Maurer's clefts in the PTEF-TGD-GFP parasites, indicating no effect on Maurer's cleft localization or PfEMP1 location (Figure 34E). Typical localizations were observed for probing KAHRP and PfEMP1 (Figure 34E). However, while co-localization of the disrupted PTEF and KAHRP displayed a KAHRP-like localization for both signals, only insignificant overlapping was observed (Figure 34E).

In essence, PTEF disruption did not result in a defect in PfEMP1 surface display nor influenced the localization or distribution of SBP1, PfEMP1, or KAHRP, suggesting a non-essential role for PTEF in these processes.

3.2.4.3 EMPIC3

EMPIC3 (PfIT_070007400), consistently enriched in the mass spectrometry analyses of the BioID cell lines in the Triton- and SDS-samples, is a PNEP (Heiber et al., 2013) with unknown function. Furthermore, EMPIC3 was identified as a proximal protein of PTP4, KAHRP, and

FIKK4.1 (Davies et al., 2023), adding to its profile as a protein in proximity to proteins relevant for cytoadherence.

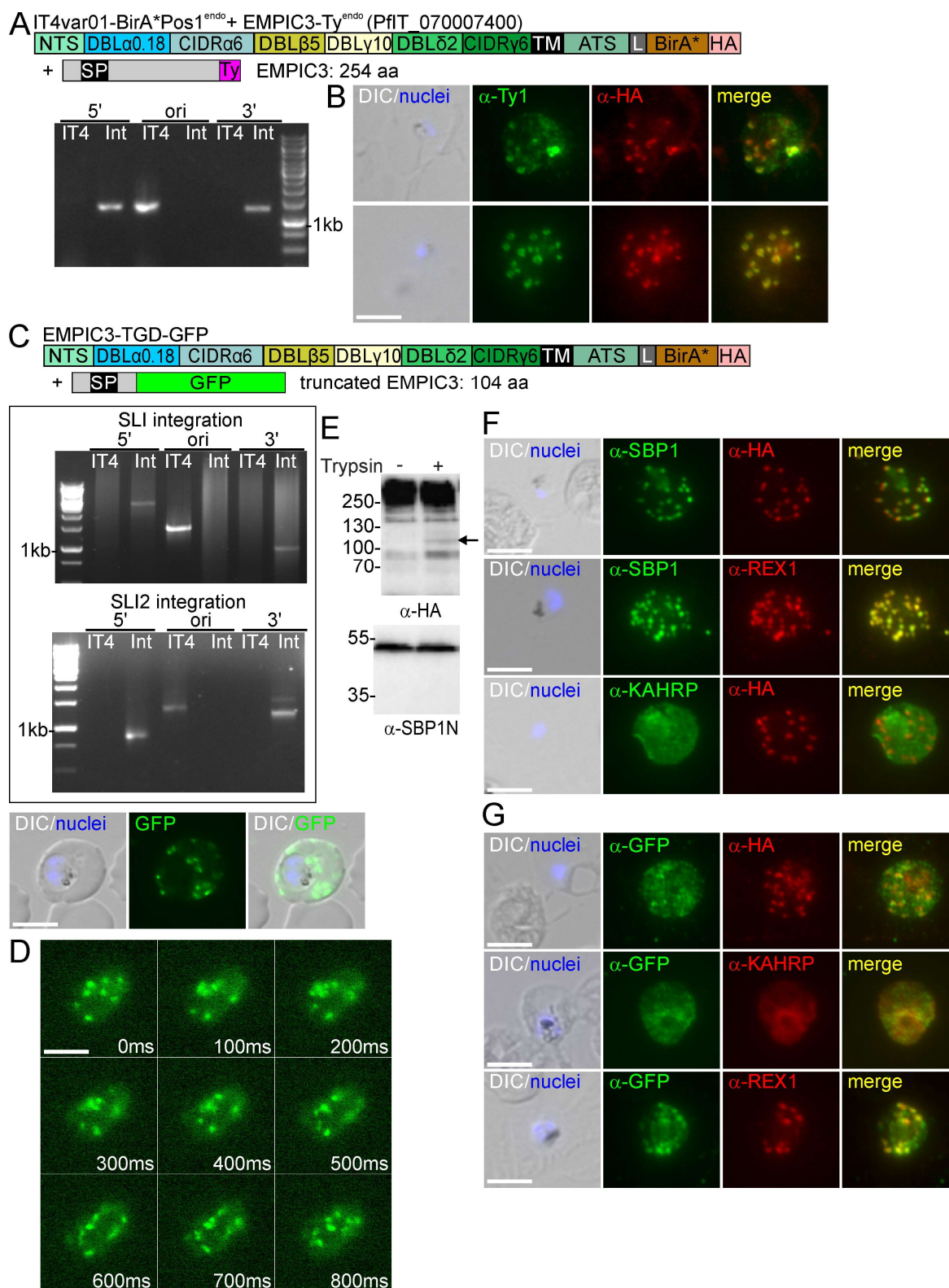


Figure 35: Characterization of EMPIC3. (A) Schematic shows domain organization of the expressed products. Agarose gels show PCR products confirming correct integration of the SLI2 plasmid. PCR over 5' integration

junction (5'): P5 + P8 in Figure 32A; PCR over 3' integration junction (3'): P7 + P6 in Figure 32A; original locus (ori): P5 + P6 in Figure 32A; IT4 parent; Int: integrant cell line; primers in Appendix A2; expected bands: 5': 1308 bp; ori: 1351 bp; 3': 1241 bp. (B) Fluorescence microscopy images show IFAs with acetone fixed EMPIC3-Ty1^{endo} parasites with indicated antibodies. Nuclei: Hoechst 33342; DIC: differential interference contrast; size bars 5 μ m. (C) Schematic shows domain organization of the expressed products. Agarose gels show PCR products confirming correct integration of the SLI2 plasmid and perpetuation of SLI plasmid integration. PCR over 5' integration junction (5'): P1 + P2 in Figure 12 or P5 + P8 in Figure 32A; PCR over 3' integration junction (3'): P3 + P4 in Figure 12 or P7 + P6 in Figure 32A; original locus (ori): P1 + P4 in Figure 12 or P5 + P6 in Figure 32A; primers in Appendix A2; IT4 parent; Int: integrant cell line; expected bands: SLI: 5': 2337 bp; ori: 1536 bp; 3': 971 bp; SLI2: 5': 899 bp; ori: 1351 bp; 3': 1241 bp. Fluorescence microscopy images show live parasites. Nuclei: Hoechst 33342; DIC: differential interference contrast; size bars 5 μ m. (D) Timelapse of fluorescence microscopy images of live EMPIC3-TGD-GFP parasites. GFP signal was captured. 0s indicated the start of capture; ms: milliseconds; size bars 5 μ m. (E) Western blot of trypsin cleavage assay with EMPIC3-TGD-GFP parasites. Arrow shows protected PfEMP1 fragment. α -SBP1-N: control for integrity of host cell. Marker in kDa. Replicate and full blots in Appendix B. (F, G) Fluorescence microscopy images show IFAs with acetone fixed EMPIC3-TGD-GFP parasites with indicated antibodies for the evaluation of Maurer's cleft morphology and localization of the truncated EMPIC3 in relation to other relevant exported proteins. Nuclei: Hoechst 33342; DIC: differential interference contrast; size bars 5 μ m.

Successful tagging of EMPIC3 with a Ty1-tag via SLI2 was confirmed with diagnostic PCRs (Figure 35A). IFAs investigating the co-localization of EMPIC3 with PfEMP1 showed two distinct patterns: EMPIC3 co-localized with PfEMP1 in punctate structures present in 40.6% of parasites (n=3 independent experiment with 32 cells in total), and 59.4% of parasites displayed EMPIC3 in a donut-shape surrounding the PfEMP1 signal, both with additional smaller puncta signals in the host cell cytosol (Figure 35B), reminiscent of the localization of TryThrA (section 3.2.4.1 and Figure 33B).

The integration of the SLI2 plasmid for a TGD of EMPIC3 was confirmed by diagnostic PCR (Figure 35C). Live cell imaging of GFP-tagged truncated EMPIC3 showed a localization within the host cell with concentrated puncta (Figure 35C). The foci changed position between time points suggesting that Maurer's clefts anchoring was impaired, or the foci are EMPIC5 aggregates that move freely in the host cell (Figure 35D).

To assess surface display of PfEMP1 of erythrocytes infected with EMPIC3-TGD-GFP, trypsin cleavage assays were conducted. A band corresponding to the protected fragment of the modified PfEMP1 was identified in the trypsin-treated sample but absent in the control (Figure 35E). No protected fragment of SBP1 was observed following probing of the same extracts

with an antibody against the N-terminus of SBP1, indicating an intact erythrocyte membrane integrity. These results suggest that EMPIC3 does not ablate PfEMP1's surface display on the surface of infected erythrocytes. Notably, a reduction of PfEMP1 surface display would not be reliably detected with this method (relevant for 3.2.4.7).

Subsequent IFAs probed various relevant exported proteins to elucidate the truncated EMPIC3's localization and its impact on these proteins (Figure 35F, G). PfEMP1, SBP1 and REX1 maintained a Maurer's clefts typical localization and indicated that Maurer's clefts morphology was not visibly altered in the parasites with a truncated EMPIC3. Furthermore, KAHRP showed usual localization in the erythrocyte membrane (Figure 35F). Next the localization in relation to PfEMP1, KAHRP and REX1 was evaluated. This showed partial colocalization with PfEMP1; larger foci overlapped with PfEMP1, while numerous smaller foci were distributed within the host cell, not colocalizing with PfEMP1. Additionally, co-localization of the truncated EMPIC3 with KAHRP revealed a uniform distribution for both proteins. The truncated EMPIC3 also partially overlapped with REX1, mirroring the observed colocalization with PfEMP1. Notably, smaller foci observed in IFAs were not detectable in live imaging, hinting at potential GFP folding issues in these locations (for example aggregates) or small amount of truncated TryThrA which are only detected with IFAs. In summary, the disruption of EMPIC3 did not visibly affect the localization of PfEMP1 and Maurer's clefts morphology nor ablate the surface display of the HA-tagged PfEMP1.

3.2.4.4 PeMP2

PeMP2, previously detected in the proteome of Maurer's clefts and part of the MSRP6 complex, was shown to subtly influence the Maurer's clefts' morphology and significantly affect their anchoring mechanisms (Blancke-Soares et al., 2021). To elucidate PeMP2's spatial relationship with PfEMP1, PeMP2 was modified with a Ty1-tag using SLI2. PCR validations confirmed the integration of the SLI2 plasmid (Figure 36A). IFAs targeting the Ty1-tag and HA-tagged PfEMP1 revealed partial co-localization of PeMP2 and PfEMP1 at the Maurer's clefts, in agreement with previously documented PeMP2 localizations (Blancke-Soares et al., 2021). Notably, PeMP2 also exhibited distinct foci in the host cell that did not co-localize with PfEMP1 (Figure 36B).

To assess PeMP2's role in cytoadherence, a SLI2 constructs was engineered to disrupt PeMP2. The successful integration of the SLI2 plasmid and perpetuation of the SLI modification for *IT4var01* were confirmed by PCR (Figure 36C). Live cell imaging detected a signal for the

truncated PeMP2 dispersed in the host cell cytosol and the food vacuole, indicating successful inactivation (Figure 36C).

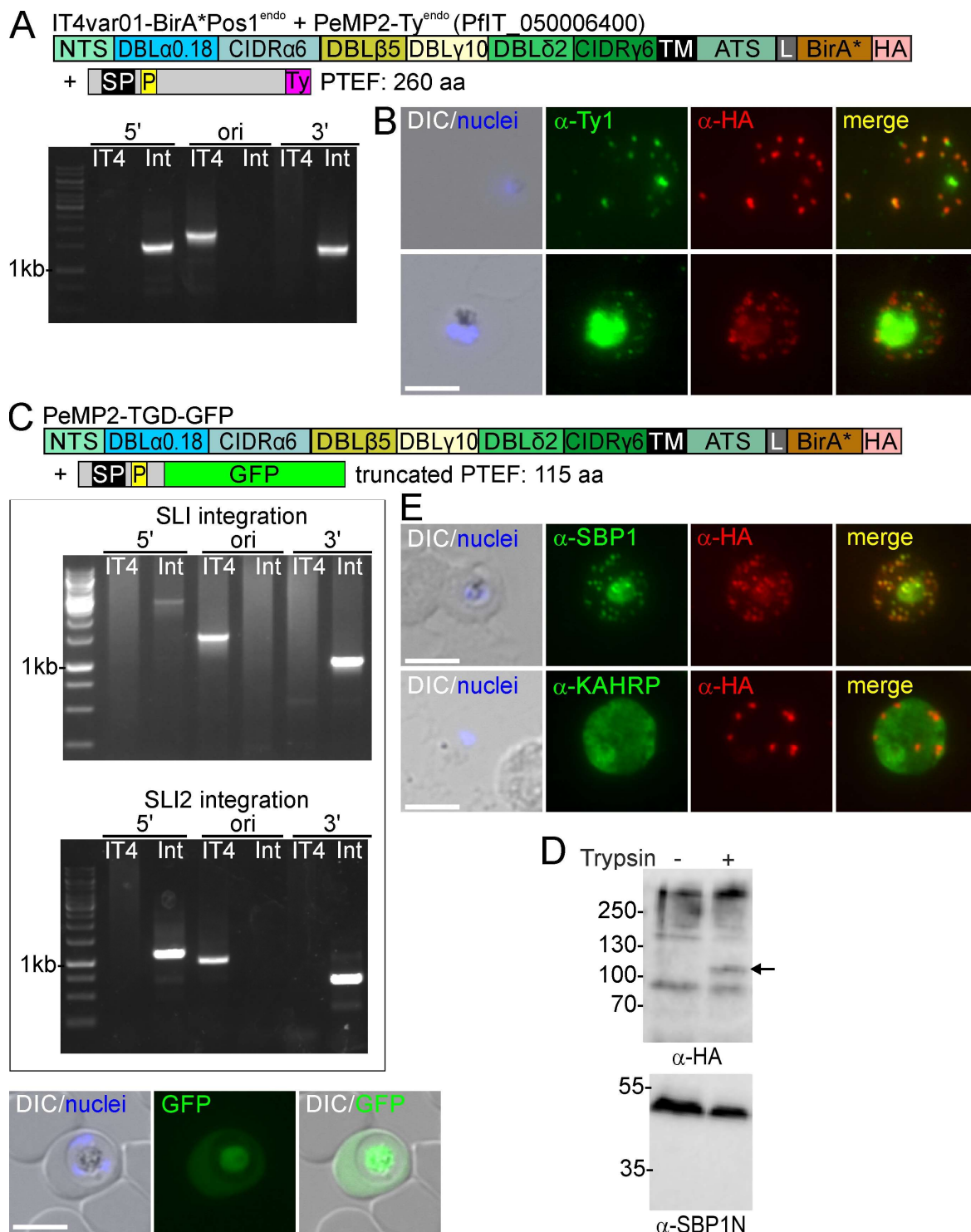


Figure 36: Characterization of PeMP2. (A) Schematic shows domain organization of the expressed products. Agarose gels show PCR products confirming correct integration of the SLI2 plasmid. PCR over 5' integration junction (5'): P5 + P8 in Figure 32A; PCR over 3' integration junction (3'): P7 + P6 in Figure 32A; original locus (ori): P5 + P6 in Figure 32A; IT4 parent; Int: integrant cell line; primers in Appendix A2; expected bands: 5': 1544 bp; ori: 1831 bp; 3': 1475 bp. (B) Fluorescence microscopy images show IFAs with acetone fixed PeMP2-Ty1^{endo}

parasites with indicated antibodies. Nuclei: Hoechst 33342; DIC: differential interference contrast; size bars 5 μ m. (C) Schematic shows domain organization of the expressed products. Agarose gels show PCR products confirming correct integration of the SLI2 plasmid and perpetuation of SLI plasmid integration. PCR over 5' integration junction (5'): P1 + P2 in Figure 12 or P5 + P8 in Figure 32A; PCR over 3' integration junction (3'): P3 + P4 in Figure 12 or P7 + P6 in Figure 32A; original locus (ori): P1 + P4 in Figure 12 or P5 + P6 in Figure 32A; primers in Appendix A2; IT4 parent; Int: integrant cell line; expected bands: SLI: 5': 2337 bp; ori: 1536 bp; 3': 971 bp; SLI2: 5': 1036 bp; ori: 994 bp; 3': 638 bp. Fluorescence microscopy images show live parasites with indicated antibodies. Nuclei: Hoechst 33342; DIC: differential interference contrast; size bars 5 μ m. (D) Western blot of trypsin cleavage assay with PeMP2-TGD-GFP parasites. Arrow shows protected PfEMP1 fragment. α -SBP1-N: control for integrity of host cell. Marker in kDa. Replicate and full blots in Appendix B. (E) Fluorescence microscopy images show IFAs with acetone fixed PeMP2-TGD-GFP parasites with indicated antibodies. Nuclei: Hoechst 33342; DIC: differential interference contrast; size bars 5 μ m.

Trypsin cleavage assays confirmed presentation of PfEMP1 on the erythrocyte's surface: a band of ~110 kDa, was detected in the trypsin-treated sample, matching the expected size for surface-trypsinized PfEMP1 whereas no such band was detected in the control sample (Figure 36D). Furthermore, only full-length SBP1 was detected using SBP1-N antibodies, indicating the integrity of the host cell was not impaired. This indicates that PeMP2 disruption does not influence the surface presentation of PfEMP1.

Further IFAs were conducted to examine PfEMP1's localization in relation to SBP1 and KAHRP in the parasites with the PeMP2 disruption. These assays indicated usual co-localization of PfEMP1 with SBP1 and typical localization for KAHRP in relation to PfEMP1.

In summary, these findings suggest that PeMP2 disruption neither affects the surface display of PfEMP1 nor induces significant abnormalities in the morphology of Maurer's clefts.

3.2.4.5 EMPIC5

EMPIC5 (PfiT_010016300) was identified as a protein of interest due to the consistent enrichment in the SDS-samples of the BioID cell lines. It was classified as a potentially exported protein (Sargeant et al., 2006), featuring a PEXEL motif, and later shown to partially co-localize with REX1 in the host cell (Jonsdottir et al., 2021). Integration of the SLI2 plasmid to endogenously tag EMPIC5 with a Ty1-tag in the IT4var01-BirA*Pos1^{endo} cell line was confirmed by PCR (Figure 37). Co-localization analysis with PfEMP1 and SBP1 demonstrated partially overlap of these with EMPIC5 while other EMPIC5 foci show localization outside of the Maurer's clefts (Figure 37). This is in agreement with the previous observations but there, more of the foci were overlapping with the Maurer's clefts marker REX1 (Jonsdottir et al.,

2021). This suggests that EMPIC5 predominantly resides in distinct foci within the host cell, that are not Maurer's clefts.

Attempts to disrupt EMPIC5 in IT4var01-BirA*Pos1^{endo} parasites had not been successful in the course of the work for this thesis.

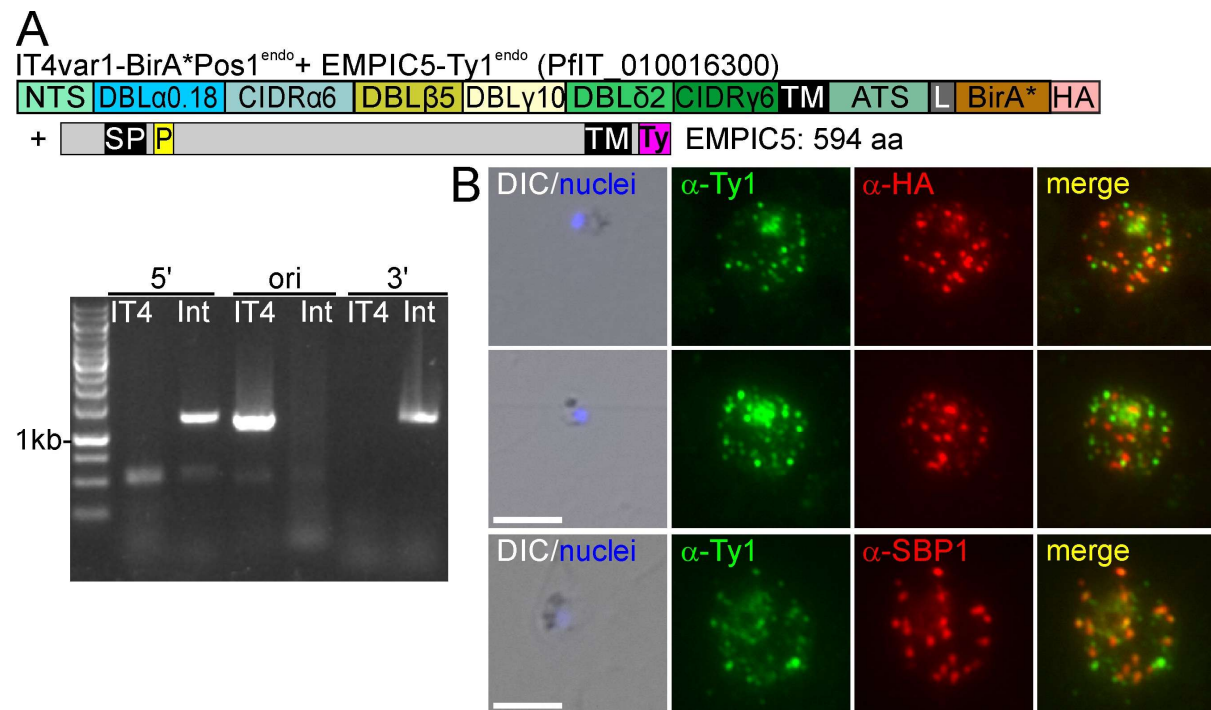


Figure 37: Characterization of EMPIC5. (A) Schematic shows domain organization of the modified expressed products. Agarose gels show PCR products confirming correct integration of the SLI2 plasmid. PCR over 5' integration junction (5'): P5 + P8 in Figure 6A; PCR over 3' integration junction (3'): P7 + P6 in Figure 6A; original locus (ori): P5 + P6 in Figure 6A; IT4 parent; Int: integrant cell line; primers in Appendix A2; expected bands: 5': 1310 bp; ori: 1285 bp; 3': 1278 bp. (B) Fluorescence microscopy images show IFAs with acetone fixed EMPIC5-Ty1^{endo} parasites with indicated antibodies. Nuclei: Hoechst 33342; DIC: differential interference contrast; size bars 5 μ m.

3.2.4.6 PTP7

PTP7 was enriched in the IT4var01-BirA*Pos1^{endo} and IT4var01-BirA*Pos3^{endo} SDS-samples (Figure 30). Its influence on PfEMP1 surface display and cytoadherence had previously been comprehensively assessed (Carmo et al., 2022). Parasites with PTP7 deletion exhibited structural anomalies in both knobs and Maurer's clefts, characterized by reduced numbers and increased size. Additionally, PfEMP1 presentation was entirely abolished, resulting in the absence of cytoadherence. Therefore, PTP7 disruption was here used as another control in verifying the reliability of the experimental systems and methodologies employed for the chosen candidates.

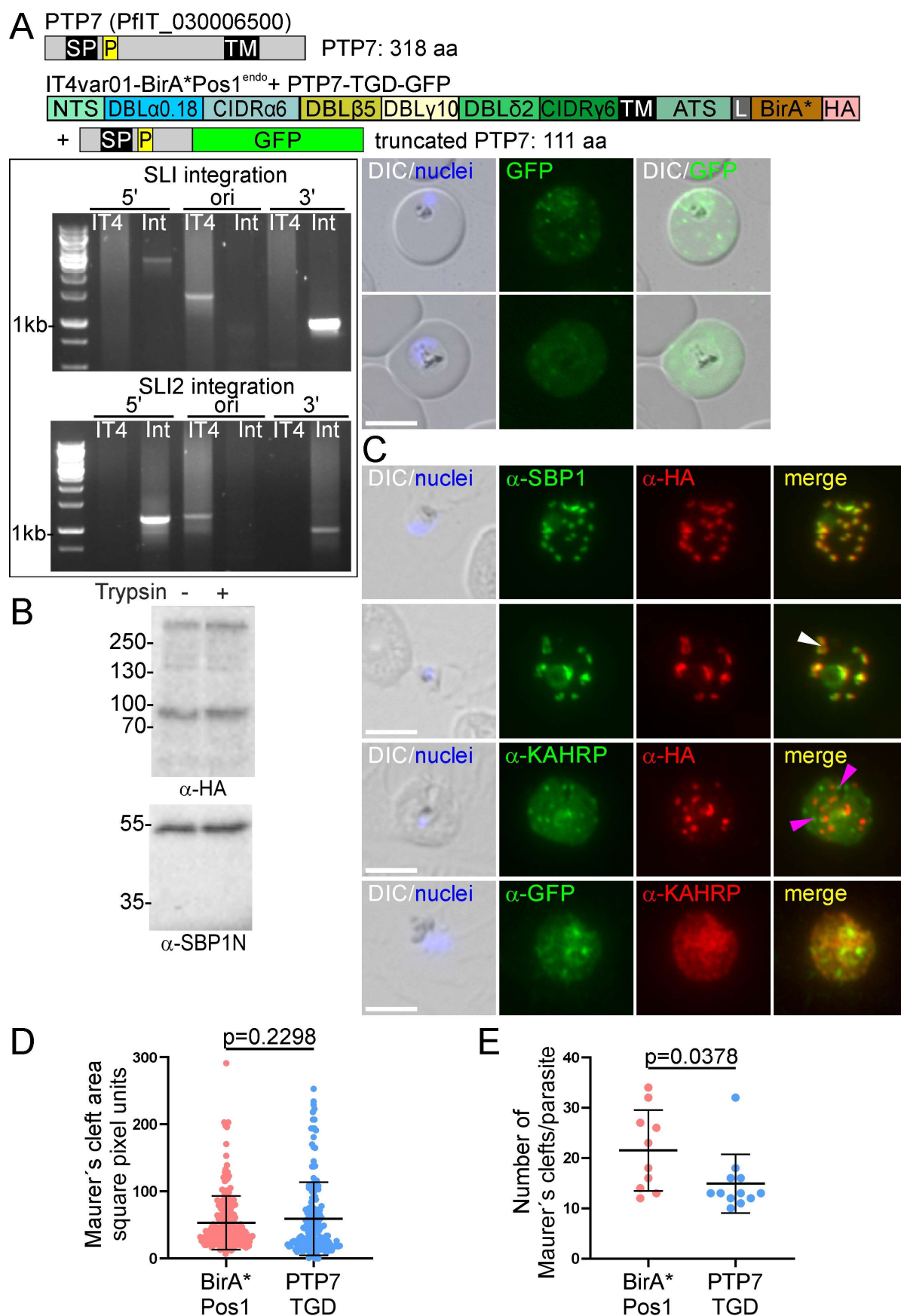


Figure 38: Characterization of PTP7. (A) Schematic shows domain organization of the modified gene loci and full-length PTP7. Agarose gels show PCR products confirming correct integration of the SLI2 plasmid and

perpetuation of SLI plasmid integration. PCR over 5' integration junction (5'): P1 + P2 in Figure 12 or P5 + P8 in Figure 32A; PCR over 3' integration junction (3'): P3 + P4 in Figure 12 or P7 + P6 in Figure 32A; original locus (ori): P1 + P4 in Figure 12 or P5 + P6 in Figure 32A; primers in Appendix A2; IT4 parent; Int: integrant cell line; expected bands: SLI: 5': 2337 bp; ori: 1536 bp; 3': 971 bp; SLI2: 5': 1184 bp; ori: 1215 bp; 3': 962 bp. Fluorescence microscopy images show live PTP7-TGD-GFP parasites with indicated antibodies. Nuclei: Hoechst 33342; DIC: differential interference contrast; size bars 5 μ m. **(B)** Western blot of trypsin cleavage assays with PTP7-TGD-GFP parasites. Arrow shows protected PfEMP1 fragment. α -SBP1-N: control for integrity of host cell. Marker in kDa. Replicate and full blots in Appendix B. **(C)** Fluorescence microscopy images show IFAs with acetone fixed PTP7-TGD-GFP parasites with indicated antibodies. White arrow; Maurer's cleft phenotype; pink arrow: concentrated puncta of KAHRP signal; nuclei: Hoechst 33342; DIC: differential interference contrast; size bars 5 μ m. **(D)** Quantification of the area of Maurer's clefts determined by images of IFAs probed with antibodies against SBP1. IT4var01-HA^{endo}: 215 cell Maurer's clefts scored across 10 parasites from two independent IFAs; PTP7-TGD-GFP: 178 Maurer's clefts scored across 12 parasites from two independent IFAs. **(E)** Quantification of the number of Maurer's clefts determined by images of IFAs probed with antibodies against SBP1. IT4var01-HA^{endo}: 10 parasites scored; two independent IFAs; PTP7-TGD-GFP: 12 parasites scored from two independent IFAs.

SLI2 plasmids were generated to disrupt PTP7. Therefore, a short homology region was selected, to ensure functional disruption of the protein (Figure 38). A cell line was obtained under G418 selection (cell lines PTP7-TGD-GFP; cell line kindly generated by Joelle Hornebeck) and PCR validations confirmed the correct integration of the SLI2 plasmid and the perpetuation of the SLI integration (Figure 38A). Live cell imaging corroborated PTP7 disruption, revealing a dispersed signal within the host cell with only partial localization of truncated PTP7 at the Maurer's clefts (Figure 38A). Trypsin cleavage assays showed no bands indicative of surface-exposed, trypsinized PfEMP1 in the trypsin-treated samples (Figure 38B). Moreover, the absence of a protected fragment upon probing with an α -SBP1-N antibody affirmed the integrity of the host cell, confirming that PTP7 disruption via SLI2 effectively prevented PfEMP1's presentation on the host cell.

IFAs were performed to detect PTP7-TGD-GFP, PfEMP1, SBP1, and KAHRP (Figure 38C). While SBP1 and PfEMP1 co-localized with signals matching typical Maurer's cleft patterns, the parasites exhibited slightly enlarged clefts (not significant) with atypical morphology in lower numbers (Figure 38C, D, E; white arrows). Co-localization of PfEMP1 and KAHRP revealed concentrated KAHRP puncta in 66% of the infected erythrocytes (n=15 cell scored from two independent experiments), potentially indicative of knob enlargement (Figure 38C). Moreover, co-localization of truncated PTP7 with KAHRP did not overlap.

In conclusion, the SLI2-mediated disruption of PTP7 aligns with previously documented effects of PTP7 disruption on PfEMP1 presentation, Maurer's cleft morphology, and knob structure (Carmo et al., 2022). Furthermore, as this is done in a cell line with a tagged and expressed PfEMP1, tracking of PfEMP1 is substantially more convenient.

3.2.4.7 TRYTHR A AND EMPIC3 ARE RELEVANT FOR EFFICIENT CYTOADHERENCE OF *P. FALCIPARUM* PARASITES

Finally, a series of binding assays was conducted to assess the cytoadherence properties of the TGD cell lines, specifically investigating the functionality of PfEMP1. As the disruption was executed in the IT4var01-BirA*Pos1^{endo}, binding assays were conducted against CHO cells expressing CD36, ICAM-1, or GFP.

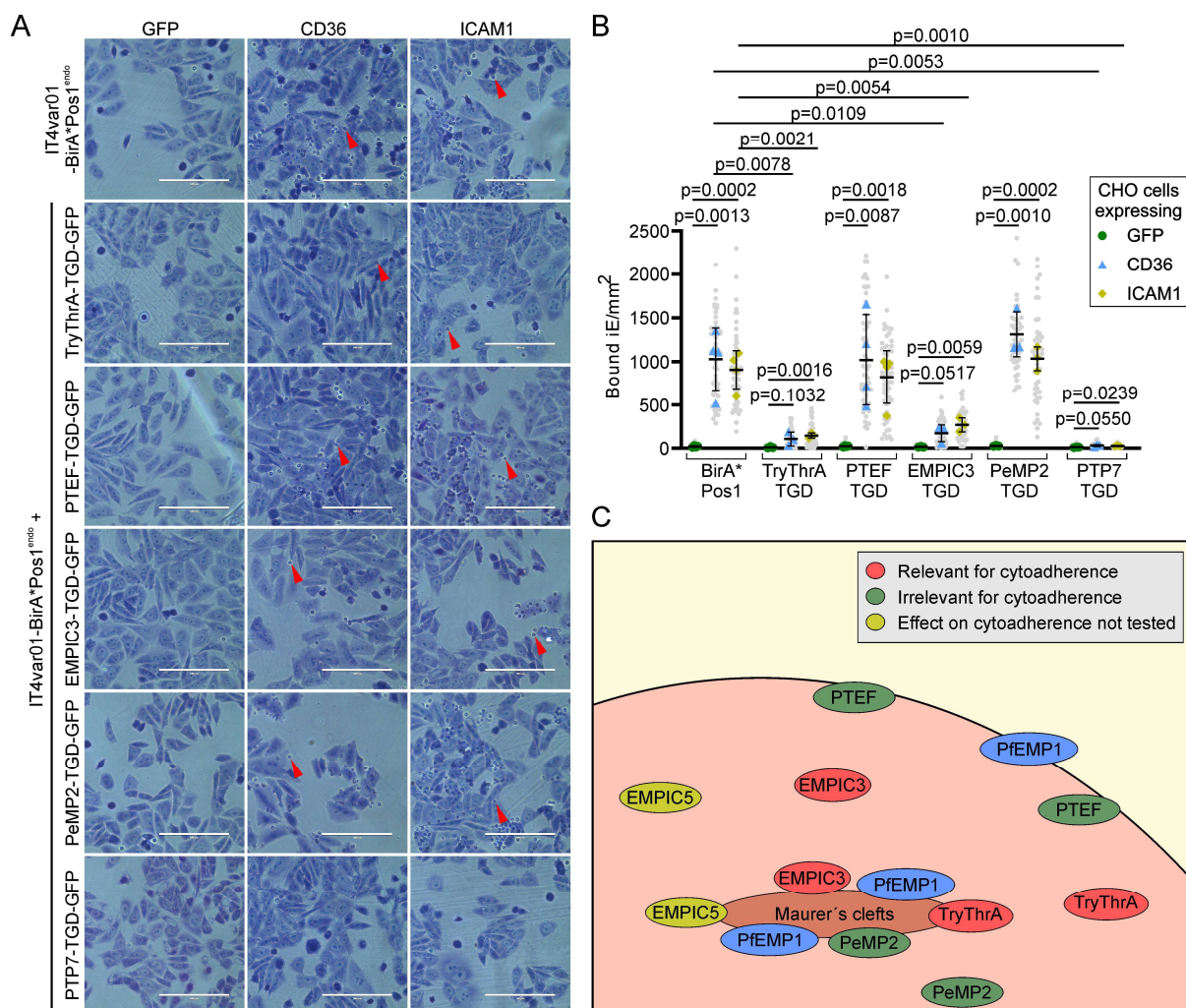


Figure 39: TryThrA and EMPIC3 are relevant for cytoadherence. (A) Images show representative sections of captured images of binding assays for the indicated cell line against CHO cell line expressing the indicated receptors. (B) SuperPlot of binding assays of the indicated cell lines against CHO cells expressing GFP, CD36 or ICAM-1 (3 or 4 (control and PTEF-TGD-GFP biological replicates with 15 fields of view/experiment and condition; bars: mean of averages of replicates with SD; unpaired t-test; p-values are indicated). Small grey dots: bound iE/field of view, extrapolated to mm². Larger coloured dots: average of bound iE/mm²/replicate. iE: infected

erythrocytes. (C) Illustration showing locations of characterized interactors and effect on cytoadherence. Red background: host cell cytosol; yellow background: extracellular space.

The binding assays showed that erythrocytes infected with PTEF-TGD-GFP and PeMP2-TGD-GFP showed binding capacities comparable to the IT4var01-BirA*Pos1^{endo} parent cell line, indicating that the disruptions did not compromise the function of PfEMP1 (Figure 39A, B). In contrast, PTP7-TGD-GFP, as expected from prior characterizations (Carmo et al., 2022), showed an absolute lack of binding (Figure 39A, B). None of the cell lines showed interaction with the GFP control, reinforcing the specificity of the binding interactions observed. Interestingly, TryThrA-TGD-GFP and EMPIC3-TGD-GFP showed a significantly reduced binding to CD36 and ICAM-1 compared to the IT4var01-BirA*Pos1^{endo} parent cell line, indicating that these proteins are needed for PfEMP1-based cytoadherence of infected erythrocytes (Figure 39A, B). Trypsin cleavage assays with erythrocytes infected with TryThrA-TGD-GFP and EMPIC3-TGD-GFP PfEMP1 previously showed that PfEMP1 is displayed on the surface. However, trypsin cleavage assays are not quantitative so that it can not be concluded whether these cell lines show reduced binding due reduced surface display of PfEMP1 or a defect in functional presentation of PfEMP1.

In summary, these findings indicate that PTP7, TryThrA and EMPIC3 are proteins needed for effective cytoadherence of infected erythrocytes whereas PTEF and PeMP2 have no such role (Figure 39C).

4 DISCUSSION

4.1 ACTIVATION OF *VAR* GENES WITH SLI

Utilizing the SLI-system, this study established cell lines that predominantly express a single targeted *var* gene in 3D7 or IT4 *P. falciparum* parasites. The targeted activation and predominant expression were confirmed for three *var* genes in 3D7 (cell line generated and experiments conducted by Paolo Mesén-Ramírez and Jan Stäcker) and eight *var* genes in IT4. These cell lines facilitate the study of *var* gene expression (section 4.1.1), PfEMP1 binding (section 4.1.4), PfEMP1 export (section 4.1.6), helped to identify a potentially new ICAM-1 binding domain (section 4.1.5) and established IT4 as the superior cell line for studying binding (section 4.1.3). This work therefore presents an important resource for studying *var* genes and PfEMP1 variants in a more controlled environment than formerly possible, expanding the options to study PfEMP1.

4.1.1 EXPRESSION OF TARGETED *VAR* GENES

Previously specific *var* genes and especially PfEMP1 variants were studied in cell lines obtained by selecting *P. falciparum* parasites on receptor expressing mammalian cells (panning), receptors immobilized on supports (panning) or with antibodies against the targeted *var* gene or extracellular *var* gene domains (Avril et al., 2012; Claessens et al., 2012; Cooke et al., 1996; Nunes-Silva et al., 2015; Turner et al., 2013). These approaches harbor certain limitations: first, these cell lines are potentially selected for attributes, changing the phenotype of the parasites and secondly separation of PfEMP1 variants that bind to the same receptor with similar affinities or contain the same binding-domains is difficult. Moreover, cell lines generated by selection must be kept under perpetual selection to express the desired *var* gene as they continuously experience switching. However, the CS2 cell lines obtained by selection on CSA express *var2csa* relatively stable (Maier et al., 2008; Salanti et al., 2004). In addition, cell lines with predominant expression of *var2csa* were achieved by treating the parasites with a histone methyltransferase inhibitor (chaetocin) or overexpressing a truncated form of its target PfSET (dominant negative effect) over an extended period of time (Ukaegbu et al., 2015). Furthermore, *var* gene switching towards *var2csa* was achieved by altering the parasites' access to choline, serine or methionine, or overexpressing the parasites' S-adenosylmethionine synthetase (PfSAMS) (Schneider et al., 2023). However, these approaches are limited to *var2csa* while SLI can target every *var* gene.

The data in this thesis showed that the SLI *var* gene cell lines express transcripts of the targeted *var* genes with over 90 % of the total *var* gene transcripts for most cell lines, sometimes going as high as 99.18 % (3D7var2csa-HA^{endo}). The *var* genes frequently transcribed besides the targeted *var* genes in the IT4 SLI-parasites were *var1csa* and *var66*. The *var1csa* pseudogene was previously shown to possess impaired silencing and an unusual expression pattern throughout the parasite asexual stages (Kyes et al., 2003; Winter et al., 2003), suggesting that this *var* gene is continuously transcribed in the parasites. As it is not assumed to be functional, its expression is not expected to be of relevance in these parasite lines. *var1csa* might influence switching and silencing of *var* genes as shown for *var2csa* (Zhang et al., 2022). Why frequently also transcripts of *var66* are expressed poses some questions. The *IT4var66* gene is the predominantly expressed *var* gene in the IT4 parental strain with over 50 % of the total *var* gene transcripts (Appendix E). It is possible that the samples taken for RNA sequencing of the SLI cell lines contained parasites that just switched from the activated *var* gene to the *var66*. These parasites would die because they are no longer G418 resistant but might be present at all times and hence are present whenever RNA samples are taken. Another possibility is that some parasites express multiple *var* genes like in the 3D7^{MEED} cell line. Nevertheless, these small proportions of untargeted *var* gene transcripts are neglectable for most experiments and panned cell lines typically show even higher proportions of undesired *var* transcripts (Avril et al., 2012; Claessens et al., 2012).

Yet limitation in the activation of *var* genes with SLI exist. The generated integrant cell lines also go through bottlenecks during selection after the transfection and selection for plasmid integration. However, the cell lines experience these bottlenecks only twice which probably has less effect on the parasites than continuous panning, especially in respect to comparability of PfEMP1 binding between individually generated parasite lines. Furthermore, cell lines were not obtained for every targeted *var* gene. One obstacle was the incorrect integration of the plasmid into a non-targeted *var* gene as observed for IT4var22-HA^{endo} (section 3.1.7.6) due to similarities of the region encoding the ATS region. This problem could be circumvented by moving the HR further towards the N-terminus as done for the BioID cell lines. Additionally, some cell lines were not obtained on G418 which could be due non-expression of the targeted *var* gene or expression by a very low number of the parasites in the population although previous work indicated that SLI can work even if expression is undetectable (Birnbaum et al., 2017; Kimmel et al., 2023). For SLI to function with *var* genes, two low probability events must occur at the same time in the parasite culture. The plasmid must integrate into the targeted

var gene via homologous recombination and at the time of drug selection these parasites also have to express the targeted *var* gene. This likely is not problematic for *var* genes such as *IT4var66* that are highly expressed in the parent cell line (Appendix E) but could be problematic for other *var* genes, especially group A *var* genes that are lowly expressed in culture (Peters et al., 2007; Zhang et al., 2011).

Using RNASeq, the 3D7^{MEED} cell lines was shown to express non-activated *var* genes to a higher proportion than the “healthy” 3D7 cell lines were the same *var* gene was activated. These results were previously confirmed by qPCR (Vaaben, 2018). This renders this cell line of potentially interest to study switching and silencing mechanisms of variant surface antigens. Previous work showed that the 3D7^{MEED} parasites present multiple PfEMP1s on a single parasite (Joergensen et al., 2010). The presentation of multiple PfEMP1 variants on a single parasite was not demonstrated in this work. But, given the stringent selection on G418 parasites and the results of the other SLI *var* gene cell lines, parasites that do not express the targeted *var* gene should not be able to survive, indicating the expression of multiple *var* genes in most of the parasites. It is however unclear whether every parasite expresses the SLI-activated PfEMP1 and one or a few further PfEMP1 variants or if there is a general relaxation and all parasites show some expression of all or most other PfEMP1. Parasite populations expressing multiple *var* genes per parasite were also observed in other work, where it was not clear whether mutually exclusive expression is defect (Schneider et al., 2023). This could be tested using single-cell RNASeq technology or by using antibodies available to select PfEMP1s such as IT4var19 (Nunes-Silva et al., 2015) and IT4VAR2CSA (Amulic et al., 2009). These findings highlight the 3D7^{MEED} parasites as a potentially useful tool for studying the genetic and epigenetic controls of *var* gene expression. A critical question arises as to what factors or defects result in the simultaneous expression of multiple *var* genes in these parasites. Genome, transcriptome, proteome and epigenomic mark comparisons between 3D7 and the 3D7^{MEED} parasites might provide leads to find the relevant factors.

In the future cell lines with disrupted mutually exclusive expression of *var* genes could maybe be generated artificially to complement findings of the 3D7^{MEED} cell line. For instance, selecting a SLI cell line against a receptor that does not bind the targeted PfEMP1 under drug selection might force the parasite to activate multiple *var* genes simultaneously. If only a small proportion of the parasites harbor the defect in mutually exclusive expression, subcloning could lead to parasite line that completely lacks silencing of non-activated *var* genes and could aid in the understanding of the underlying mechanisms. Comparing such cell lines with ones retaining the

mutually exclusive expression could shed light on the regulatory circuits controlling *var* gene silencing.

Interestingly, *IT4var20* was successfully HA-tagged in IT4 parasites but RNA sequencing showed that this gene had recombined with *IT4var27*, resulting in a chimeric *var* gene. Initially ectopic recombination events were shown during meiosis and only suggested during mitosis (Freitas-Junior et al., 2000) but later evidence demonstrated ectopic recombination, especially in subtelomeric regions where the VSAs are situated, during mitosis (Bopp et al., 2013; Claessens et al., 2014). Here another example of mitotic recombination of *var* genes is presented which in this case hinders the insights into the binding properties of the PfEMP1 variant encoded by this *var* gene. Initially the IT4var20-HA^{endo} parasites were intended as a tool to study EPCR binding. As the N-terminal EPCR-binding domains of *IT4var20* were substituted by the N-terminal CD36-binding domains of *IT4var27*, the IT4var20-HA^{endo} cell line cannot be used to study EPCR.

Future research utilizing SLI-activated *var* gene cell lines offer a promising avenue for unraveling the genetic mechanisms underlying the parasites immune evasion strategies. Intact gene switching was observed in these cell lines (Vaaben, 2018) by cultivating the cell lines under G418 selection and subsequently lifting the drug pressure. This approach facilitates the monitoring of *var* gene expression dynamics over time, aiming to discern whether *P. falciparum* parasites undergo a predetermined sequence of *var* gene activation or if the switching pattern is inherently stochastic, potentially with variable activation and silencing rates for specific *var* genes. However, the data collected are not sufficient as more replicates are needed to corroborate on this.

In summary, this study utilized the SLI-system to create *P. falciparum* cell lines with targeted expression of specific *var* genes, which is expected to provide versatile methodology with benefits over previous selection-based methods. Despite facing challenges such as potential bottlenecks during selection and the necessity for simultaneous low-probability events for activation, this approach successfully produced cell lines with relatively high specificity for targeted *var* genes. This approach not only provides more controlled type of PfEMP1-expressing parasites for studying *var* genes and PfEMP1 variants but also highlight new avenues for exploring the genetic and epigenetic mechanisms of *var* gene expression control. While the occurrence of ectopic recombination can introduce complexity into understanding *var* gene functions, shifting the targeting region into the variable domain solves this issue.

Notably, *var* genes have been activated in 3D7 and IT4 using SLI before, in part for the work leading up to this thesis, but these cell lines were not characterized to the extent presented here (Blancke-Soares et al., 2021; Omelianczyk et al., 2020; Stäcker, 2021).

4.1.2 IMPROVING BINDING ASSAYS

In this study, a semi-automated pipeline was developed and validated for scoring images of binding assays, achieving outcomes statistically similar to those obtained through human manual scoring. This innovation represents a significant improvement, facilitating a high-throughput and more time-efficient evaluation process compared to traditional manual scoring. Binding assays remain the gold standard for assessing the functionality of surface presented PfEMP1 molecules, underscoring their indispensable part to study the cytoadherence of PfEMP1 (e.g. Adams et al., 2021; Bernabeu et al., 2019; Carmo et al., 2022; Maier et al., 2008). The data for the 3D7 (section 3.1.6), SLI2 TGD cell lines (section 3.2.4) or from previous publications (Maier et al., 2008; Proellocks et al., 2014) demonstrated that the mere surface presentation of PfEMP1 does not guarantee its functional integrity, highlighting the necessity for functional validation.

Moreover, this work illuminates the complex landscape of PfEMP1 binding properties, which is currently obscured by a multitude of variables and complexities, such as cultures with mixed populations regarding PfEMP1 expression, specific PfEMP1s binding multiple receptors and the type of receptor binding assay used (section 1.3) (Andradi-Brown et al., 2024; Bachmann et al., 2022). Given this intricacy, there is an urgent need to refine binding assay methodologies, aiming for simplification and standardization to enhance reproducibility and comparability across studies.

Static binding assays, involving receptor-presenting mammalian cells, suffer from high variability due to fluctuations in receptor expression and cell confluency, leading to inconsistent parasite binding results which can be countered by increasing the replicates (images captured per experiment and experiments conducted) (Altman and Krzywinski, 2015). While binding assays under flow conditions (Gray et al., 2003) or in cell tissue models (Bernabeu et al., 2019) mimic more physiological environments, they introduce increased complexity and costs. These factors not only limit experimental throughput but also introduce additional variables that can reduce the coherence of results. Conversely, binding to immobilized receptors on plastic slips

(Janes et al., 2011) presents a more controlled experimental setup. However, this approach is hindered by the high cost and the limited availability for some recombinant proteins.

Effective management of human resources within research projects can significantly influence the overall costs incurred. Additionally, tasks characterized by repetition and monotony are particularly susceptible to human error (Liang et al., 2010) and can adversely affect the motivation of research teams (Staaby et al., 2021). In this context, the establishment of the automated pipeline revealed an average manual scoring time of 180 seconds per image (section 3.1.5). Consequently, the evaluation of the 3060 images required for this study would necessitate approximately 153 hours of human labor, amounting to close to 4 weeks work time assuming standard hours. Considering the salary for scientists in Germany under the TV-L E13 scale, which ranges from ~25 to 36€ per hour the costs for manually scoring the images alone would amount to between ~3500 and 5500€ (depending on experience or researcher and whether PhD or postdoc). This underscores the economic and operational advantages of implementing automated processes in scientific research.

The advent of machine learning and its exponential integration into research methodologies have recently unlocked unprecedented opportunities for automation, particularly within the realm of bioimaging analysis. This field, though relatively nascent, has witnessed rapid expansion, fueled by the proliferation of advanced analytical tools now at our disposal (Meijering, 2020). In malaria research, numerous evaluation methods, from assessing drug effects to exploring the effect of genetic manipulations of the parasites, rely heavily on microscopic imaging to analyze organelle or parasites size, location and abundance of fluorescence-tagged proteins, morphology, and parasite stage (Birnbaum et al., 2020; Carmo et al., 2022; Elsworth et al., 2014; Kimmel et al., 2023; Klaus et al., 2022; Looker et al., 2019; Sabitzki et al., 2023). The automation of these evaluative processes offers a multitude of benefits. Firstly, automation can significantly mitigate biases inherent in manual assessments, streamline the time required for analysis, and reduce the financial burden associated with labor costs. Secondly, the consistency and accuracy of experimental evaluations are poised to improve, enhancing both the comparability and reproducibility of research outcomes. This is particularly true when automated analysis pipelines are made publicly accessible, allowing for standardized methodologies across the scientific community. In case of binding assays, the next step would be to eliminate manual imaging and capture a greater number of field of views per coverslip. Thereby the bias in capturing would be eliminated and additional human resources could be saved. However, the use of computer assisted evaluation of images possess some

dangers. Poor image quality or parasites health can affect the outcome. Hence, quality control steps should be in place, to ensure meaningful data is inputted and the pipeline performs as expected.

This study introduces a semi-automated pipeline for scoring PfEMP1 binding assays, enhancing the efficiency and accuracy of such analyses. It emphasizes the benefit of advocating for a simplification and standardization in binding assays, contributing to more precise and reproducible studies of malaria pathogenesis.

4.1.3 3D7 IS NOT SUITABLE FOR BINDING STUDIES

Comparing the binding capacities of 3D7 and IT4 parasite strains revealed strain-specific differences in PfEMP1-mediated cytoadherence, validating the IT4 strain as a superior model for studying PfEMP1 functions. This was shown in the comparison of two PfEMP1 variants that were activated in 3D7 or IT4 which should have comparable binding properties in both cell lines as they contain, in case of *var2csa* identical and in the case of *IT4var66* and *3D7varUPSB6* very similar binding domains (Rask et al., 2010).

Yet, the only PfEMP1 variant fully suitable for comparison of the binding properties between parasite strains is VAR2CSA, as this is highly conserved across parasite isolates and is considered to specifically bind to CSA. However, there are reports about differences in the VAR2CSA of IT4 and 3D7 which can complicate the comparability (Sander et al., 2009). The binding assays against HBEC-5i and decorin showed significant binding of IT4var2csa-HA^{endo} but only very low levels of binding for 3D7var2csa-HA^{endo}. Even though the binding was specifically inhibited by the addition of sCSA in the assay, it is unclear what the HBEC-5i cell express on their surface. The interaction could, even though it is very unlikely, be due to unknown proteins or glycoproteins presented on the surface of the HBEC-5i cell. But considering the results of the binding assays against decorin, the interaction of the IT4var2csa-HA^{endo} parasites can be considered as specific for CSA. The interaction to CSA was only present after selection of VAR2CSA expression through SLI and absent in the IT4 parent strain which corroborates the specificity of the interaction between the HA-tagged PfEMP1 and CSA.

The comparison of the CD36-binding PfEMP1s in 3D7 and IT4 are not as meaningful as the VAR2CSA binding, as the difference in binding efficacy could also be due to differences in sequences of the extracellular domains. *IT4var66* possesses a DBL α 0.19-CIDR α 2.1 head structure while *varUPSB6* harbors a DBL α 0.12-CIDR α 2.2 head structure (Rask et al., 2010).

Nevertheless, the significantly stronger interaction of IT4var66-HA^{endo} with CD36 compared to 3D7varUPSB6-HA^{endo} further supports the superior binding of IT4 parasites.

The trypsin assays revealed the presentation of the HA-tagged PfEMP1 on the erythrocytes surface for 3D7var2csa-HA^{endo} and 3D7varUPSB6-HA^{endo} (Figure 13D; Appendix B). Even though no conclusion can be made about the quantities of PfEMP1 molecules expressed on the erythrocyte surface from the trypsin assay, the intense bands for the protected fragment in the 3D7 samples indicate a considerable amount of PfEMP1 molecules on the surface. These results suggest that the mere presentation of PfEMP1 on the erythrocyte surface is insufficient for binding as for instance also observed in parasites carrying a disruption of the PHIST protein LyMP (Proellocks et al., 2014). Hence, additional factors, such as loss of expression or mutation of other proteins needed for functional PfEMP1 surface display, likely contribute to the inefficient cytoadherence observed in 3D7 parasites. This is reinforced by the significantly decrease in binding of the TryThrA-TGD-GFP and EMPIC3-TGD-GFP cell lines where the disruption did not abolish the presentation of PfEMP1, although it should be noted that in these cases it is unclear how much PfEMP1 is still on the surface and it might as well be a binding phenotype due to reduced transport of PfEMP1 to the erythrocyte surface (Figure 33D, Figure 35E, Appendix B) (section 4.2.2).

While the 3D7varUPSB6-HA^{endo} parasites showed low but significant levels of binding, the binding of 3D7var2csa-HA^{endo} parasites was barely detectable. Even though the binding assays are not comparable, a reason for the stronger binding of this cell lines compared to the 3D7var2csa-HA^{endo} cell line could be that VAR2CSA (7 extracellular domains) is a relatively large PfEMP1 that might be more dependent on co-factors for correct folding or transport for efficient binding compared to the smaller *varUPSB6*-encoded PfEMP1 (4 extracellular domains) (section 4.1.4 and 4.1.5).

This evidence suggests that the 3D7 strain of *P. falciparum*, at least the version used in our lab, is unsuitable for assessing the binding properties of PfEMP1 variants and the impact of genetic knockouts on the parasite's cytoadherence capabilities. Many publications nevertheless were able to detect binding using 3D7 parasites (e.g. Batinovic et al., 2017; Takano et al., 2019). It is important to acknowledge, however, that the observed deficiencies in binding associated with the 3D7 strain in this study may not universally apply to all 3D7 strains utilized in different laboratories. Nevertheless, limitations of the 3D7 strain for studying cytoadherence have been previously speculated on, leading researchers to preferentially employ the IT4 or other strains

known for their cytoadherent properties (e.g. Bernabeu et al., 2019; Turner et al., 2013) or CS2 (e.g. Maier et al., 2008; Salanti et al., 2004) which up to now was the cell line most commonly used for PfEMP1 trafficking studies. The findings presented herein offer empirical evidence for using alternative strains to 3D7 to study PfEMP1-mediated cytoadherence.

4.1.4 SURFACE PRESENTATION AND BINDING OF HA-TAGGED PfEMP1 VARIANTS

The IT4 cell lines generated expressing PfEMP1 variants, possessing known domains for CD36, CD36-ICAM-1 or CSA binding (encoded by *IT4var01* (Blancke-Soares et al., 2021; Stäcker, 2021), *IT4var16*, *IT4var66*, *IT4var2csa* and chimeric *IT4var20/var27*) showed presentation and interaction with these receptors (chimeric *IT4var20/var27* not tested) immediately after the corresponding parasite cell lines were obtained. This shows that these cell lines can be valuable tools for the investigation of binding of PfEMP1 variants, especially of different PfEMP1 variants with identical binding partners. For the first time, these properties can be compared in un-panned cell lines, potentially revealing diverging affinities among PfEMP1 variants. However, it should also be noted that direct comparisons between different parasite cell lines may not be directly comparable as expression levels of PfEMP1 between parasite lines might differ and the distribution of parasite stages between lines might not be fully comparable. One way to reduce variation could be to use similarly synchronized parasites and label cells coming from different PfEMP1 expressors with different fluorescent dyes (either using fluorescent agents or by additional genetic modification) and assess the binding together in the same binding assay.

However, the SLI cell lines *IT4var02-HA^{endo}*, *IT4var03-HA^{endo}*, *IT4var08-HA^{endo}* and *IT4var19-HA^{endo}* showed no or insignificant presentation of the HA-tagged PfEMP1 variants on the surface of the erythrocyte membrane. Furthermore, binding to the expected receptor was not detected for *IT4var19-HA^{endo}*. Preliminary results also showed no binding of *IT4var02-HA^{endo}*, *IT4var03-HA^{endo}* and *IT4var08-HA^{endo}* to an array of receptors although the binding partners for these PfEMP1s are unclear, and it is possible that these were not included in the testing (Brehmer, 2021). However, *IT4var02* was enriched on CD9 and P-selectin (Metwally et al., 2017) and did not show interaction to these receptors even though a very faint band corresponding to a protected fragment was detected in the trypsin assay. It is at present therefore

unclear whether these PfEMP1 were not sufficiently surface exposed, the correct receptor was not available or whether these PfEMP1 do not bind host cell receptors.

Upon initial examination, a difference between PfEMP1 variants that underwent activation and immediate surface presentation and those that failed to show surface presentation post-activation was observed in the number of extracellular domains and the *var* gene groups to which they belong. *IT4var02*, *IT4var08* and *IT4var19* possess 7 extracellular domains and belong to *var* gene group A or A/B while *IT4var01*, *IT4var16*, *IT4var66* and chimeric *IT4var20/var27* possess four or six extracellular domains and belong to group B or C. Exceptions were group A *var03*, which has two extracellular domains and group E *var2csa*, which contains 7 extracellular domains (Rask et al., 2010). Due to its unique binding property and conservation, *var2csa* may not be informative for this comparison of binding and non-binding PfEMP1s. Equally, this might also apply to *var3*, which is also semi-conserved across parasite strains and might encode a non-functional PfEMP1 variant.

Future research could elucidate the differential binding properties and the characteristics of dual binders, such as CD36-ICAM-1-binding of *IT4var01*-HA^{endo} and *IT4var16*-HA^{endo}, in depth. Preliminary results indicated that the PfEMP1 protein encoded by *var16* exhibits a higher affinity for ICAM-1, whereas PfEMP1 encoded by *IT4var01* demonstrates a greater affinity for CD36 (section 3.1.7.4) (Kieferle, 2023). The novel opportunity to systematically study these differences could be used to understand the molecular basis of receptor specificity and its implications for malaria pathogenesis. Moreover, domain cassettes can now be examined in their entirety, functionally presented on the surface of the erythrocyte membrane. Point mutations can be introduced either directly using the SLI-plasmid or through CRISPR, enabling identification of binding relevant protein regions.

Moreover, exploring the binding interactions of *IT4var02*-HA^{endo}, *IT4var03*-HA^{endo}, and *IT4var08*-HA^{endo} could reveal previously unidentified ligands for PfEMP1, thereby expanding our understanding of the parasite-host interaction landscape. However, this could be problematic, as these cell lines might have to be panned to obtain surface presentation, which is impractical if the interacting receptor is unknown. This exploration could be further extended by developing new cell lines to investigate additional PfEMP1 variants with yet-to-be-determined binding partners. Such studies would not only advance our knowledge of PfEMP1's role in malaria's clinical manifestations.

4.1.5 *IT4VAR19* CONTAINS AN ICAM-1 BINDING DOMAIN

Intriguingly, after selection on G418, the *IT4var19*-HA^{endo} did not demonstrate surface presentation of the HA-tagged PfEMP1 on erythrocytes, nor did it bind to CD36, ICAM-1, or its anticipated binding partner, EPCR (Murk, unpublished) even though predominant *IT4var19* expression was confirmed. The successful presentation of *IT4var19*-encoded PfEMP1 on the surface following panning suggests that even in the unpanned parasite population, PfEMP1 was present on the surface in very small quantities. It remains to be elucidated whether this presentation was due to the majority of parasites presenting very low quantities of PfEMP1 or a minority displaying a significant number of molecules on the surface. This observation indicates that additional factors within the parasite may play a crucial role in the functional presentation of specific PfEMP1 variants, beyond the mere expression of the encoding *var* gene. Before and after panning *IT4var19*-HA^{endo} parasites predominantly expressed *IT4var19*. However, not enough replicates were conducted to conclude whether *IT4var19* is expressed in higher quantities in the panned cell line than in the unpanned one which might be a simple explanation for the surface presentation after panning although it seems unlikely that this could be the sole reason as *IT4var19* expression and in both cases full length HA-tagged PfEMP1 was detected by Western blot. Another explanation could be that the PfEMP1 variant encoded by *IT4var19* is a relatively large PfEMP1 with 7 extracellular domains, rather than 4-6 seen with most (Rask et al., 2010). Therefore, this variant could be more dependent on co-factors for its presentation than smaller PfEMP1s, which could be a reason for the insufficient presentation as discussed before (section 4.1.4). It is also possible that the need for panning is associated with particular binding property, for instance if EPCR-binding PfEMP1s require specific co-factors to reach the host cell surface.

The *IT4var19* gene has garnered significant attention in the field (e.g. Adams et al., 2021; Bernabeu et al., 2019; Gillrie et al., 2015; Sampath et al., 2015) as generation of cell lines with predominant *IT4var19* expression was achieved by selecting parasites on EPCR-expressing mammalian cells (Avril et al., 2012; Claessens et al., 2012) or antibodies targeting *IT4var19* (Nunes-Silva et al., 2015). However, it is unclear whether the *IT4var19* cell lines produced through these techniques possess additional, unidentified characteristics or atypical features potentially introduced during selection for binding or the subcloning process. Moreover, these cell lines do not solely express *IT4var19* and *var* gene expression is altered by switching over time (section 4.1.1).

Interestingly, IT4var19-HA^{endo} parasites showed binding to ICAM-1, in contrast to previous observations. However, it was shown that EPCR is likely not the only interaction of this PfEMP1 variant as inhibition of EPCR did not fully ablate IT4var19 binding (Adams et al., 2021; Avril et al., 2012; Nunes-Silva et al., 2015). AlphaFold predictions for the structure of *IT4var19*'s DBL β 12 domain revealed high similarities to the group B ICAM-1-binding DBL β 5 domains, particularly in the backbone structure, while the outward-facing exposed binding regions showed some differences. Given the polymorphism in these regions across ICAM-1-binding domains from different *var* gene groups (Lennartz et al., 2019), these differences might be an evolutionary strategy of the parasites to evade the immune system and the DBL β 12 domain displaying divergent ICAM-1 binding mechanisms. The parasites are under constant selective pressure from the human immune system, which could explain the necessity for diversity in exposed binding regions. Despite structural differences in regions critical for ICAM-1 binding, there might be compensatory mechanisms within the DBL β 12 domain that allow for effective binding, highlighting the complexity of parasite-host interactions. The question of why the recombinant DBL β 12 domain did not bind to immobilized ICAM-1 in experiments, and why previous *IT4var19* cell lines did not show ICAM-1 binding, remains unclear. A reason for the non-binding of the recombinant DBL β 12 domain could be that this domain is not correctly folded if expressed in bacteria as this is a common problem (Gasser et al., 2008). The non-binding of *IT4var19*-expressing cell lines obtained by panning could be due to non-comparability of binding assays with cell lines presenting receptors differently. In the future, the research could be narrowed down on the DBL β 12 domain by introducing mutations in potential binding-sites and testing whether these affect the binding to ICAM-1.

In conclusion, the intricate interplay between PfEMP1 presentation, specifically the *IT4var19*-encoded variant, and its binding capabilities underscores the complexity of malaria parasite biology and host interaction. The differences in PfEMP1 variant binding function, influenced by gene expression and potential other factors such as accessory proteins, highlight the critical need for further research to unravel the mechanisms governing these processes. Understanding these mechanisms will not only shed light on the malaria parasite's evasion strategies but also opens avenues for the development of targeted interventions (McLean et al., 2021; Reyes et al., 2024). Future studies focusing on the structural and functional aspects of PfEMP1, particularly through the exploration of the DBL β 12 domain, promise to provide valuable insights into the parasite's adaptability and the potential for therapeutic targeting.

4.1.6 PfEMP1 IS LIKELY TRANSLOCATED VIA PTEX

Here it was demonstrated that obstructing the PTEX channel with a co-blocking construct, expressed late in the ring stage, resulted in the retention of HA-tagged PfEMP1 within the PV, alongside a reporter for the successful blocking of PTEX (section 3.1.4; Figure 15). Notably, the full export of REX1 in these parasites indicated that the block does not affect early exported proteins (Figure 15E). These findings suggest that PfEMP1 translocation to the host cell is mediated through the PTEX channel, suggesting there is no need for alternative pathways for PfEMP1 export and that such pathways most likely do not exist. Notably, it cannot be excluded that for PfEMP1 export additional structures like the potential EPIC complex are needed as well (Batinovic et al., 2017). Additionally, the use of SLI-activated PfEMP1 emerges as an effective approach to investigate the transport mechanisms of PfEMP1.

Previous studies showed the accumulation of PfEMP1 within the PV following the knockdown of essential PTEX components such as HSP101 or PTEX150 (Beck et al., 2014; Elsworth et al., 2014). Moreover, previous work in our lab showed that the retention of a HA-tagged PfEMP1 was observed when the PTEX channel was blocked with a SBP1-mDHFR-GFP constructs under the control of the early-expressed *mal7* promoter or the early endogenous SBP1 promoter (Naranjo Prado, 2020). Although these findings collectively support the hypothesis that PfEMP1 export relies on PTEX functionality, they do not definitively exclude the possibility that the export of other proteins, potentially crucial for PfEMP1 translocation, is unaffected. Furthermore, fusing PfEMP1 directly to mDHFR, did not prevent its export when the folding of the mDHFR domain was stabilized, which would speak against transport through PTEX. The approach employed here aimed to resolve these discrepancies. In order to address the limitation of also blocking PfEMP1 trafficking proteins, the *crt* promoter was used, which drives protein expression towards the end of the ring stage, directly after the beginning of PfEMP1 transcription. This timing leads to minimal PfEMP1 export prior to the activation of the PTEX-blocking construct, excluding the inhibition of proteins that are potentially essential for PfEMP1 translocation to the host cell. The partial block of PfEMP1, observed in numerous cells where the KAHRP-mScarlet block-reporter was retained (Appendix C), indicates that PfEMP1 is indeed capable of being translocated and that only the obstruction of the PTEX channel is preventing the export of PfEMP1.

Other studies on the export of PfEMP1 opted for episomal mini-PfEMP1 constructs (Batinovic et al., 2017; McMillan et al., 2013; Melcher et al., 2010). While this approach is comparably simple to implement, the mini-PfEMP1 is not expressed under its endogenous promoter

(potentially leading to differences in the phenotype due to unusual expression timing) and the mini-PfEMP1 is reduced to the NTS-, TM- and ATS-domain, sometimes additionally containing two extracellular binding domains, which has unknown consequences for its trafficking and functionality. For example, a significant amount of signal from the mini-PfEMP1s in IFAs were detected in the PV (McMillan et al., 2013) probably due to unnatural expression timing, failure of transport or degradation or processing of the GFP mini-PfEMP1 fusion protein. Despite these challenges, pull-down experiments with mini-PfEMP1 have identified all five components of the PTEX complex (Batinovic et al., 2017), reinforcing the role of the PTEX channel in PfEMP1 export.

Future experiments could focus on capturing BirA*-tagged PfEMP1 within the PTEX channel and employing BioID to elucidate its translocation mechanism conclusively. The accumulated evidence, coupled with the findings presented here, indicate that PfEMP1 translocation occurs via the PTEX channel, without evidence of an alternative export mechanism.

This study demonstrates that the obstruction of the PTEX channel after the ring stage impedes the export of HA-tagged PfEMP1, while not affecting early-exported proteins such as REX1. The accumulated evidence, enhanced by the effective use of SLI-activated PfEMP1 and corroborated by previous studies, provides evidence for the PTEX channel as the pathway for PfEMP1 export. This conclusion might provide directions for future research to further elucidate the molecular mechanisms governing PfEMP1 transport.

4.2 PROXIOME OF PfEMP1

In this study, the proximal proteome of functional PfEMP1s within living *P. falciparum* parasites was captured (section 3.2.2). This achievement led to the identification of two proteins critical for PfEMP1's functionality on the host cell surface (section 4.2.2), rendering these cell lines valuable tools for future in-depth studies on PfEMP1 transport and surface presentation.

4.2.1 IS THE PROXIOME OF PfEMP1 ITS GLOBAL INTERACTOME?

The experiments in this thesis demonstrated that fusing the large BirA* domain at three distinct positions of a PfEMP1 did not ablate the PfEMP1-mediated binding, indicating that PfEMP1 can accommodate larger tags, at least the *IT4var01*-encoded variant. This insight is particularly beneficial for tagging PfEMP1 at internal positions with other functional domains, enhancing the toolkit for future research. Notably, linkers as used in this work should be included as they potentially enable the successful tagging of functional PfEMP1s. The fusion of BirA* at position 3 reduced the binding capacity to CD36 and ICAM-1, likely due to its placement in the extracellular domains, which can interfere with the integration or functional presentation of PfEMP1 in the erythrocyte membrane. Conversely, tags at position 1 and 2 were well tolerated, maintaining similar binding levels as *IT4var01*-HA^{endo}, suggesting minimal impact on PfEMP1 functionality.

Previous approaches carried out pull downs to identify interactors of the above-mentioned mini-PfEMP1 (Batinovic et al., 2017). This revealed exported proteins such as SBP1, REX1, MAHRP1, MAHRP2 and PTP5 as well as PTEX components. The detection of the PTEX components could indicate a retention of a significant number of mini-PfEMP1 molecules in the PV as discussed before (section 4.1.6). Furthermore, the number of detected proteins was lower than in this thesis.

The mass spectrometry results of the PfEMP1 BioID experiments in this thesis yielded a high number of enriched proteins in the SDS-samples. In contrast, the triton-samples yielded only a sparse number of significantly enriched proteins compared to the SDS-samples, indicating that the majority of PfEMP1s interactors are tightly associated with poorly soluble structures or protein complexes. Noteworthy, the bait-PfEMP1 was detected in the triton-samples which could be due to high self biotinylation but also an indicator that PfEMP1 is not at all times in a strong association with Triton X-100 insoluble structures as shown before (Baruch et al., 1995; Kriek et al., 2003; Papakrivovs et al., 2005).

An unresolved question pertains to whether the proteins biotinylated in the BioID cell lines truly represent the global interactome of PfEMP1, including the knobs and transport process. The small amounts of PfEMP1 molecules in the knobs (Sanchez et al., 2019) and the status of BirA* function within the knobs could exclude the detection of interactors in that location. Additionally, the functional status of the fused BirA* during transport remains unclear. It can not be categorically excluded that the conformation of PfEMP1 in the knobs or during transport hinders the functionality of BirA*, potentially impacting the biotinylation process and, consequently, the identification of interacting knob or transport proteins.

Multiple aspects indicate the identification of proteins physiologically relevant for PfEMP1 in the obtained proteomes. Most importantly the significant difference of the proximiome detected here to the general Maurer's clefts proximiome (Blancke-Soares et al., 2021) (Figure 31B). For example, MAHRP2 was detected with all three PfEMP1 positions but was not detected in the general Maurer's clefts proteome (Blancke-Soares et al., 2021) nor in the interactome of SBP1 (Takano et al., 2019). MAHRP2 localizes to the tethers (Pachlatko et al., 2010), indicating that PfEMP1-BirA* may have interacted with it during the transport to the erythrocyte membrane. The PfEMP1 containing vesicle-like have been reported to associate with the tethers (Carmo et al., 2022; Cyrklaff et al., 2012). Furthermore, the detection of PTEF, GEXP10 and multiple PHISTs (PfIT_120058000, PfIT_040006400; PfIT_130076100) that were shown to localize to the erythrocyte membrane suggests the biotinylation of PfEMP1s interactome, at least during transport to the knobs but maybe also at the erythrocyte surface (Figure 30B) (Birnbaum et al., 2017; Chan et al., 2017; Dantzler et al., 2019; Davies et al., 2016; Kili et al., 2019; Tarr et al., 2014). If interactors at the knob were captured, then PfEMP1 does not directly interact with KAHRP as this was not enriched in any of the PfEMP1-BirA* samples. This finding is reinforced by the stronger affinity of the ATS domain to PHIST proteins (Mayer et al., 2012) and the enrichment of more PHIST proteins in position 1 compared to position 2 or 3 (see below). However, other studies indicated that the ATS domain interacts with KAHRP (Crabb et al., 1997). Additionally, previous studies detected PfEMP1 as a proximal protein of PTP4 while it was enriched significantly less in the proximiome of KAHRP (Davies et al., 2023). Notably, the cytoadherent relevant PHIST protein LyMP (Oberli et al., 2016; Proellocks et al., 2014) and PF3D7_0424600 (Maier et al., 2008) were not significantly enriched indicating that these do not directly interact with PfEMP1 or that the PHIST interaction is variant-specific as hypothesized (Warncke et al., 2016). These findings suggest a mediator between KAHRP and PfEMP1, likely PHISTs, anchoring PfEMP1 in the knobs.

The detection of multiple PTPs and exported proteins with unknown function in the proxime presented here that were absent in the general Maurer's clefts proteomes indicate that PfEMP1-specific hits with a role in PfEMP1 transport were captured. Notably, GEXP18 and HSP70x were enriched that previously were identified as proteins of the J-Dots of which HSP70x was associated with PfEMP1 transport (Külzer et al., 2012, 2010; Petersen et al., 2016; Zhang et al., 2017). Additionally, EMPIC5-Ty1's localization in puncta in the host cell resembling J-Dot or K-Dots (Kats et al., 2014; Külzer et al., 2010) proteins only sporadically overlapping with the Maurer's clefts (Figure 37B) which was also reported in other work for this protein (Jonsdottir et al., 2021) suggest J-Dot or K-Dot localization of this interactor. Furthermore, this pattern of localization was reported for other exported proteins (Schulze et al., 2015). Therefore, the PfEMP1 BirA*-fusion constructs likely biotinylated proteins during its transport process.

Comparing the enriched proteins of the three BioID cell lines shows many similarities, with most proteins detected in all three positions with comparable enrichment values. The major difference is the enrichment of PHIST proteins in position 1 (not enriched position 2 or 3) (see above). This similarity indicates that PfEMP1 is not transported as an integral membrane protein as in that case - due to its location on the other side of the membrane - position 3 would yield a more differing proxime to position 1 and 2. This agrees with the idea of non-membrane embedded transport of PfEMP1, which was hypothesized before (Batinovic et al., 2017; Grüning et al., 2012; Külzer et al., 2012; Marti and Spielmann, 2013; Papakrivovs et al., 2005; Petersen et al., 2016).

Further investigation is required to elucidate these aspects, potentially involving targeted approaches to selectively enhance the biotinylation within the knobs or to subtract the interactome of a PfEMP1 retained in the Maurer's clefts achieved by the knockout of proteins important for the transport to the knobs, e.g. PTP7 (Carmo et al., 2022). Nevertheless, the data strongly indicate the detection of a global PfEMP1 interactome.

Additionally, cell lines for two alternative systems for profiling the PfEMP1 proxime were generated, with FKBP or miniTurbo domains fused to PfEMP1 in positions 1 and 2. However, the functionality and presentation of these tagged-PfEMP1s remain to be assessed. No recruitment of biotinylizers in the DiQ-BioID cell lines was detectable, as evidenced by microscopy (Figure 29). One possibility is that the observed foci represent a proportion of aggregated protein which perhaps could result from mis-folding of the biotinylizer within the host cell cytosol, although FKBP-FRB based dimerization has previously been demonstrated

in that compartment (Oberli et al., 2016) In contrast, the miniTurbo-tagged cell lines could be promising tools for capturing time-resolved proximates of PfEMP1 - due significantly faster labelling time compare to BirA* - such as before and after its surface presentation or export to the host cell.

The here provided PfEMP1 proximates pave the way for future research into the transport and presentation mechanisms of PfEMP1. Future studies could focus on elucidating the interactome of PfEMP1-BirA* variants with impeded transport, aiming to delineate the precise sequential steps required for the effective presentation of PfEMP1 and identifying the proteins needed for each of these steps. Moreover, it is essential to validate and refine the use of miniTurbo cell lines as a research tool, given their potential for rapid biotinylation, which could significantly enhance our understanding of the temporal dynamics involved in PfEMP1 transport and presentation processes.

4.2.2 IDENTIFICATION OF PFEMP1 INTERACTORS RELEVANT FOR CYTOADHERENCE

Here two new proteins were discovered that show an effect on PfEMP1-mediated cytoadherence. Their disruption in IT4var01-BirA*Pos1^{endo} led to significantly reduced binding to CD36 and ICAM-1. Additionally, PTP1 and PTP7 were disrupted and showed similar PfEMP1 presentation and cytoadherence phenotypes to previous reports (Carmo et al., 2022; Maier et al., 2008; Rug et al., 2014). These findings show that SLI2 is a robust method to introduce a second endogenous modification to a SLI-modified cell line, indicating its feasibility for these kinds of investigations as shown before in work from our lab that led up to this thesis (Blancke-Soares et al., 2021; Naranjo Prado, 2020; Stäcker, 2021).

SLI2 also aided in the localization of five proteins from the PfEMP1 interactome. The localization of PTEF and PeMP2 was concurrent with the previous observed localization (Birnbaum et al., 2017; Blancke-Soares et al., 2021; Chan et al., 2017) but PTEFs localization in the nucleus (Chan et al., 2017) was not observed. TryThrA and EMPIC3 showed localization in the Maurer's cleft with additional localization in foci in the host cell suggesting two different locations. In previous studies episomal GFP-tagged TryThrA and EMPIC3 was only detected at the Maurer's clefts (Heiber et al., 2013). Furthermore, both candidates showed a donut-shape localization surrounding the HA-tagged PfEMP1 in some cells (Figure 33B and Figure 35B), this might indicate attaching of these proteins to the periphery of the clefts. How this influences

transport is unclear. For one thing, it could affect the state of the clefts if they are gone, thereby indirectly affecting PfEMP1 transport. Alternatively, they could work as tethering factor or are needed to bind PfEMP1 at the periphery to traffic it further. Previous, work in 3D7 only showed localization of the episomal TryThrA-GFP at the Maurer's clefts with low intensity (Heiber et al., 2013) and a retention of it the parasite periphery in ring stages while trophozoites showed export (Blancke-Soares et al., 2021; Stäcker, 2021). This could be explained by the higher sensitivity of immunofluorescence assays and the compromised folding of the GFP-tag in the host cell, impairment of transport due to the GFP tag or due to overexpression (Heiber et al., 2013) or the different parasite strain used.

EMPIC5 showed an interesting localization in the host cell with only very limited overlap with the Maurer's clefts, potentially indicative of J-Dots or K-Dots (see above) (Kats et al., 2014; Külzer et al., 2010). Given the interaction with PfEMP1, EMPIC5 might be important for the transport of PfEMP1 and other exported proteins to the Maurer's clefts or the erythrocyte membrane. However, as a TGD cell line was not successfully generated, this at present remains speculative. One reason for the failure to obtain this parasite line could be that EMPIC5 is essential for the parasite's survival. However, this would be unlikely if EMPIC5 is needed for PfEMP1 transport only. Rather this were the case if its disruptions influenced the transport of PSAC components. Further work is needed to clarify the function of EMPIC5 and to validate it as a hit in the PfEMP1 proximiome that is of relevance for cytoadherence.

For the evaluation of the effect of interaction candidates on the surface presentation and function of PfEMP1, five candidates were disrupted using SLI2. The disruption of PeMP2 and PTEF did not affect surface presentation or cytoadherence. It was previously postulated that PTEF has an effect on VAR2CSA translation (Chan et al., 2017). Even though the data shown here does not contrast this, its disruption did not seem to noticeably influence the translation of the *IT4var01* encoded PfEMP1 variant. It is possible that the previously postulated effect on translation is specific for VAR2CSA. Interestingly, PeMP2 which is in a complex that is involved in anchoring the Maurer's clefts does not influence the PfEMP1 function, similarly to other components of that complex such as PIESP2, Pf332 or MSRP6 (Blancke-Soares et al., 2021; Stäcker, 2021). It is possible that these proteins influence PfEMP1 variants that show a more problematic surface presentation like the variant that is encoded by *IT4var19* (section 3.1.7.5).

TryThrA's knockout was previously shown to have no effect on cytoadherence or Maurer's clefts structure (Takano et al., 2019) which contradicts the findings in this thesis. The data here showed that while surface presentation of PfEMP1 was not ablated (at least not fully), the disruption led to a significant reduction in PfEMP1-mediated binding to CD36 and ICAM-1. These contradicting findings might be due to the use of the 3D7 cell line (section 3.1.6) or the method used to generate the knockout cell line in Takano et al. (2019). It can at present also not be excluded that the TryThrA-TGD-GFP line in this work did not accumulate a different defect. Hence, a complementation to restore binding is a key experiment for the future. Interestingly, recent findings showed that the knockout of IPIS3, the ortholog of TryThrA in the rodent malaria parasite *P. berghei*, reduces their cytoadherent properties (Gabelich et al., 2022). Even though *P. berghei* does not confer PfEMP1-mediated cytoadherence, the inherent mechanism for the transport of virulence factors seems to be conserved across *Plasmodium* species (De Niz et al., 2016). This suggests that TryThrA may be an important protein for Maurer's clefts structure and functional PfEMP1 presentation in different malaria species.

The disruption of EMPIC3 did not ablate HA-tagged PfEMP1 presentation but significantly reduced the parasites cytoadherent capacities. It is possible that only few PfEMP1 molecules reach the host cells surface in the TryThrA-TGD-GFP and EMPIC3-TGD-GFP that confer the low binding observed in binding assays (Figure 39A, B), as the trypsin assay is not a quantitative method. Notably, EMPIC3-TGD-GFP parasites did not show a phenotype in SBP1 and HA-tagged PfEMP1 localization like the TryThrA-TGD-GFP parasites. This is reminiscent of many MC resident PfEMP1 trafficking proteins that do not alter Maurer's clefts structure upon ablation but still affect PfEMP1 trafficking (Cooke et al., 2006; Maier et al., 2008, 2007). Furthermore, EMPIC3 was detected in PerTurboID experiments with KAHRP, PTP4 and FIKK4.1 Furthermore, while KAHRP does not influence static cytoadherence (Crabb et al., 1997; Rug et al., 2006) (section 4.2.1), PTP4 and FIKK4.1 (with FIKK4.2 the only FIKK kinase known to do so), influence cytoadherence (Davies et al., 2023, 2020; Kats et al., 2014; Maier et al., 2008). These findings underscore EMPIC3 interaction with proteins relevant for cytoadherence. However, this could also indicate that EMPIC3 is abundant in the host cell in high quantities and therefore enriched in these studies. The results indicate that EMPIC3 is relevant for PfEMP1-mediated cytoadherence. However, same possibilities as for the TryThrA-TGD-GFP line apply for the EMPIC3-TGD-GFP line, therefore a complementation is mandatory to corroborate that EMPIC3 is truly relevant for cytoadherence.

In summary, the results further corroborated the versatility of SLI to study PfEMP1 and unveiled that PTEF and PeMP2 are not needed in PfEMP1 transport and function. More intriguingly, the assays have brought the roles of TryThrA and EMPIC3 in cytoadherence into focus. While TryThrA and EMPIC3 were already identified as Maurer's clefts proteins and TryThrA as an interactor of Maurer's clefts proteins (Blancke-Soares et al., 2021; Heiber et al., 2013; Takano et al., 2019), EMPIC3 was never connected to cytoadherence before. These proteins have now emerged as further elements in the complex cytoadherence mechanism. Further work will be needed to understand their specific function in PfEMP1 transport and surface display.

4.3 CONCLUSION

Despite PfEMP1 and *var* genes being in the limelight of malaria research for over two decades, progress the illumination of PfEMP1 transport and host cell receptor interactions has been limited. The challenges posed by the fact that PfEMP1s are encoded by a diverse, rapidly switching multi-gene family, along with its large size, have significantly impeded its study. The methodologies established in this study improves our ability to investigate the cell biology of these proteins (Figure 40).

Here it was shown that cell lines can be generated with SLI that predominantly express a targeted *var* gene, enabling detailed studies on *var* gene expression, silencing mechanisms, and switching patterns (Figure 40A). For the first time, it is now possible to compare PfEMP1 variants with similar binding characteristics in cell lines not selected for binding, which will aid our understanding of their potential impact on virulence (Figure 40E). Additionally, the development of a semi-automated pipeline for binding assay evaluation offers a less biased and more efficient approach to analyzing binding properties of specific PfEMP1 variants.

These cell lines have also proven valuable for tracking the transport of PfEMP1, supporting the hypothesis that PfEMP1 translocation is mediated via the PTEX channel - a conclusion that aligns with previous research findings (Figure 40B).

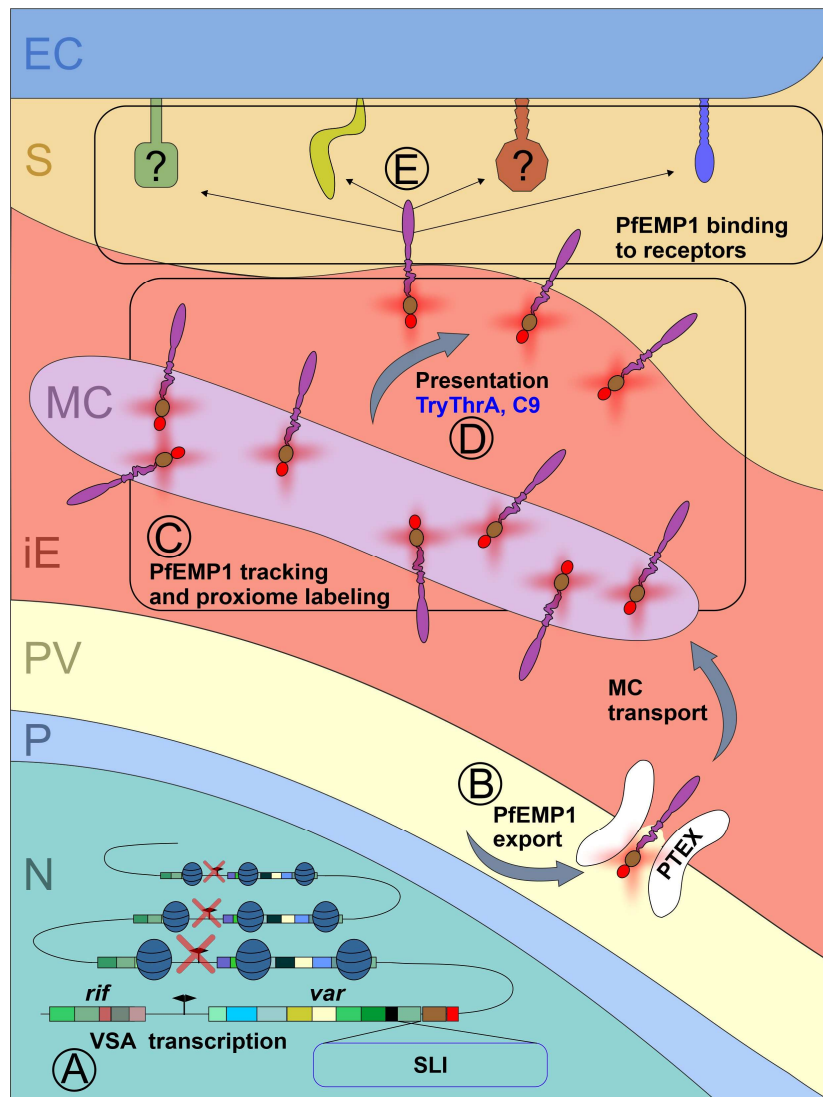


Figure 40: Exploring key processes in cytoadherence using SLI-activated *var* gene cell lines. Illustration showing the applications for cell lines with SLI-activated *var* genes. (A) Variant surface antigen expression and silencing. (B) PfEMP1 export. (C) Identification of the proxime of PfEMP1. (D) Characterization of proteins influencing PfEMP1 presentation. (E) PfEMP1 binding. VSA: variant surface antigen; N: nucleus; P: parasite; PV: paraitophorous vacuole; iE: infected erythrocyte; MC: Maurer's clefts; S: human serum; EC: endothelial cells.

The discovery of PfEMP1's interactome marks a significant breakthrough, which will aid in understanding the complex processes occurring within the host cell that facilitate PfEMP1 transport and surface presentation which so far is only poorly understood (Figure 40C). Among these findings is the identification of previously uncharacterized proteins now linked to cytoadherence, which was aided by SLI2 (Figure 40D) opening up new avenues for research. Furthermore, this validates the feasibility of SLI2 for introducing a second endogenous modification in cell lines already harboring a SLI modification.

REFERENCES

- Abkarian, M., Massiera, G., Berry, L., Roques, M., Braun-Breton, C., 2011. A novel mechanism for egress of malarial parasites from red blood cells. *Blood* 117, 4118–4124. <https://doi.org/10.1182/blood-2010-08-299883>
- Achan, J., Talisuna, A.O., Erhart, A., Yeka, A., Tibenderana, J.K., Baliraine, F.N., Rosenthal, P.J., D’Alessandro, U., 2011. Quinine, an old anti-malarial drug in a modern world: role in the treatment of malaria. *Malar. J.* 10, 144. <https://doi.org/10.1186/1475-2875-10-144>
- Acharya, P., Chaubey, S., Grover, M., Tatu, U., 2012. An Exported Heat Shock Protein 40 Associates with Pathogenesis-Related Knobs in *Plasmodium falciparum* Infected Erythrocytes. *PLoS ONE* 7, e44605. <https://doi.org/10.1371/journal.pone.0044605>
- Adams, Y., Olsen, R.W., Bengtsson, A., Dalgaard, N., Zdioruk, M., Satpathi, S., Behera, P.K., Sahu, P.K., Lawler, S.E., Qvortrup, K., Wassmer, S.C., Jensen, A.T.R., 2021. *Plasmodium falciparum* erythrocyte membrane protein 1 variants induce cell swelling and disrupt the blood-brain barrier in cerebral malaria. *J. Exp. Med.* 218, e20201266. <https://doi.org/10.1084/jem.20201266>
- Adisa, A., Rug, M., Klonis, N., Foley, M., Cowman, A.F., Tilley, L., 2003. The signal sequence of exported protein-1 directs the green fluorescent protein to the parasitophorous vacuole of transfected malaria parasites. *J. Biol. Chem.* 278, 6532–6542. <https://doi.org/10.1074/jbc.M207039200>
- Aikawa, M., Hepler, P.K., Huff, C.G., Sprinz, H., 1966. The feeding mechanism of avian malarial parasites. *J. Cell Biol.* 28, 355–373. <https://doi.org/10.1083/jcb.28.2.355>
- Aikawa, M., Miller, L.H., Rabbege, J., 1975. Caveola--vesicle complexes in the plasmalemma of erythrocytes infected by *Plasmodium vivax* and *P. cynomolgi*. Unique structures related to Schüffner’s dots. *Am. J. Pathol.* 79, 285–300.
- Aikawa, M., Miller, L.H., Rabbege, J.R., Epstein, N., 1981. Freeze-fracture study on the erythrocyte membrane during malarial parasite invasion. *J. Cell Biol.* 91, 55–62. <https://doi.org/10.1083/jcb.91.1.55>
- Alano, P., 2007. *Plasmodium falciparum* gametocytes: still many secrets of a hidden life. *Mol. Microbiol.* 66, 291–302. <https://doi.org/10.1111/j.1365-2958.2007.05904.x>
- Alkhalil, A., Cohn, J.V., Wagner, M.A., Cabrera, J.S., Rajapandi, T., Desai, S.A., 2004. *Plasmodium falciparum* likely encodes the principal anion channel on infected human erythrocytes. *Blood* 104, 4279–4286. <https://doi.org/10.1182/blood-2004-05-2047>
- Altman, N., Krzywinski, M., 2015. Points of significance: Sources of variation. *Nat. Methods* 12, 5–6. <https://doi.org/10.1038/nmeth.3224>
- Aly, A.S.I., Vaughan, A.M., Kappe, S.H.I., 2009. Malaria parasite development in the mosquito and infection of the mammalian host. *Annu. Rev. Microbiol.* 63, 195–221. <https://doi.org/10.1146/annurev.micro.091208.073403>
- Amino, R., Thiberge, S., Shorte, S., Frischknecht, F., Ménard, R., 2006. Quantitative imaging of *Plasmodium* sporozoites in the mammalian host. *C. R. Biol.* 329, 858–862. <https://doi.org/10.1016/j.crv.2006.04.003>
- Amulic, B., Salanti, A., Lavstsen, T., Nielsen, M.A., Deitsch, K.W., 2009. An Upstream Open Reading Frame Controls Translation of var2csa, a Gene Implicated in Placental Malaria. *PLoS Pathog.* 5. <https://doi.org/10.1371/journal.ppat.1000256>
- Andradi-Brown, C., Wichers-Misterek, J.S., von Thien, H., Höppner, Y.D., Scholz, J.A.M., Hansson, H., Filtenborg Hocke, E., Gilberger, T.W., Duffy, M.F., Lavstsen, T., Baum, J., Otto, T.D., Cunningham, A.J., Bachmann, A., 2024. A novel computational pipeline for var gene expression augments the discovery of changes in the *Plasmodium*

- falciparum transcriptome during transition from in vivo to short-term in vitro culture. *eLife* 12, RP87726. <https://doi.org/10.7554/eLife.87726>
- Ashley, E.A., White, N.J., 2014. The duration of *Plasmodium falciparum* infections. *Malar. J.* 13, 500. <https://doi.org/10.1186/1475-2875-13-500>
- Atkinson, C.T., Aikawa, M., Perry, G., Fujino, T., Bennett, V., Davidson, E.A., Howard, R.J., 1988. Ultrastructural localization of erythrocyte cytoskeletal and integral membrane proteins in *Plasmodium falciparum*-infected erythrocytes. *Eur. J. Cell Biol.* 45, 192–199.
- Atkinson, C.T., Aikawa, M., Rock, E.P., Marsh, K., Andrysiak, P.M., Campbell, G.H., Collins, W.E., Howard, R.J., 1987. Ultrastructure of the erythrocytic stages of *Plasmodium malariae*. *J. Protozool.* 34, 267–274. <https://doi.org/10.1111/j.1550-7408.1987.tb03173.x>
- Avril, M., Bernabeu, M., Benjamin, M., Brazier, A.J., Smith, J.D., 2016. Interaction between Endothelial Protein C Receptor and Intercellular Adhesion Molecule 1 to Mediate Binding of *Plasmodium falciparum*-Infected Erythrocytes to Endothelial Cells. *mBio* 7, e00615-16. <https://doi.org/10.1128/mBio.00615-16>
- Avril, M., Gamain, B., Lépolard, C., Viaud, N., Scherf, A., Gysin, J., 2006. Characterization of anti-var2CSA-PfEMP1 cytoadhesion inhibitory mouse monoclonal antibodies. *Microbes Infect.* 8, 2863–2871. <https://doi.org/10.1016/j.micinf.2006.09.005>
- Avril, M., Tripathi, A.K., Brazier, A.J., Andisi, C., Janes, J.H., Soma, V.L., Sullivan, D.J., Bull, P.C., Stins, M.F., Smith, J.D., 2012. A restricted subset of var genes mediates adherence of *Plasmodium falciparum*-infected erythrocytes to brain endothelial cells. *Proc. Natl. Acad. Sci. U. S. A.* 109, E1782-1790. <https://doi.org/10.1073/pnas.1120534109>
- Azasi, Y., Lindergard, G., Ghumra, A., Mu, J., Miller, L.H., Rowe, J.A., 2018. Infected erythrocytes expressing DC13 PfEMP1 differ from recombinant proteins in EPCR-binding function. *Proc. Natl. Acad. Sci.* 115, 1063–1068. <https://doi.org/10.1073/pnas.1712879115>
- Bachmann, A., Bruske, E., Krumkamp, R., Turner, L., Wichers, J.S., Petter, M., Held, J., Duffy, M.F., Sim, B.K.L., Hoffman, S.L., Kremsner, P.G., Lell, B., Lavstsen, T., Frank, M., Mordmüller, B., Tannich, E., 2019. Controlled human malaria infection with *Plasmodium falciparum* demonstrates impact of naturally acquired immunity on virulence gene expression. *PLoS Pathog.* 15, e1007906. <https://doi.org/10.1371/journal.ppat.1007906>
- Bachmann, A., Esser, C., Petter, M., Predehl, S., von Kalckreuth, V., Schmiedel, S., Bruchhaus, I., Tannich, E., 2009. Absence of erythrocyte sequestration and lack of multicopy gene family expression in *Plasmodium falciparum* from a splenectomized malaria patient. *PloS One* 4, e7459. <https://doi.org/10.1371/journal.pone.0007459>
- Bachmann, A., Metwally, N.G., Allweier, J., Cronshagen, J., Del Pilar Martinez Tauler, M., Murk, A., Roth, L.K., Torabi, H., Wu, Y., Gutsmann, T., Bruchhaus, I., 2022. CD36-A Host Receptor Necessary for Malaria Parasites to Establish and Maintain Infection. *Microorganisms* 10, 2356. <https://doi.org/10.3390/microorganisms10122356>
- Bachmann, A., Petter, M., Krumkamp, R., Esen, M., Held, J., Scholz, J.A.M., Li, T., Sim, B.K.L., Hoffman, S.L., Kremsner, P.G., Mordmüller, B., Duffy, M.F., Tannich, E., 2016. Mosquito Passage Dramatically Changes var Gene Expression in Controlled Human *Plasmodium falciparum* Infections. *PLoS Pathog.* 12, e1005538. <https://doi.org/10.1371/journal.ppat.1005538>
- Bachmann, A., Predehl, S., May, J., Harder, S., Burchard, G.D., Gilberger, T.-W., Tannich, E., Bruchhaus, I., 2011. Highly co-ordinated var gene expression and switching in clinical *Plasmodium falciparum* isolates from non-immune malaria patients. *Cell. Microbiol.* 13, 1397–1409. <https://doi.org/10.1111/j.1462-5822.2011.01629.x>

- Baer, K., Klotz, C., Kappe, S.H.I., Schnieder, T., Frevort, U., 2007. Release of hepatic *Plasmodium yoelii* merozoites into the pulmonary microvasculature. *PLoS Pathog.* 3, e171. <https://doi.org/10.1371/journal.ppat.0030171>
- Bakri, R., Rehan, M., Shamshad, H., Hafiz, A., 2021. Computational Insights into the Interaction between Cytoadherence Receptor gC1qR and the DBL β 12 Domain of a *Plasmodium falciparum* PfEMP1 Ligand. *Life Basel Switz.* 11, 993. <https://doi.org/10.3390/life11090993>
- Banerjee, R., Liu, J., Beatty, W., Pelosof, L., Klemba, M., Goldberg, D.E., 2002. Four plasmepsins are active in the *Plasmodium falciparum* food vacuole, including a protease with an active-site histidine. *Proc. Natl. Acad. Sci. U. S. A.* 99, 990–995. <https://doi.org/10.1073/pnas.022630099>
- Bannister, L.H., Dluzewski, A.R., 1990. The ultrastructure of red cell invasion in malaria infections: a review. *Blood Cells* 16, 257–292; discussion 293–297.
- Bannister, L.H., Hopkins, J.M., Dluzewski, A.R., Margos, G., Williams, I.T., Blackman, M.J., Kocken, C.H., Thomas, A.W., Mitchell, G.H., 2003. *Plasmodium falciparum* apical membrane antigen 1 (PfAMA-1) is translocated within micronemes along subpellicular microtubules during merozoite development. *J. Cell Sci.* 116, 3825–3834. <https://doi.org/10.1242/jcs.00665>
- Bannister, L.H., Hopkins, J.M., Fowler, R.E., Krishna, S., Mitchell, G.H., 2000. Ultrastructure of rhoptry development in *Plasmodium falciparum* erythrocytic schizonts. *Parasitology* 121 (Pt 3), 273–287. <https://doi.org/10.1017/s0031182099006320>
- Barry, A.E., Leliwa-Sytek, A., Tavul, L., Imrie, H., Migot-Nabias, F., Brown, S.M., McVean, G.A.V., Day, K.P., 2007. Population Genomics of the Immune Evasion (var) Genes of *Plasmodium falciparum*. *PLoS Pathog.* 3, e34. <https://doi.org/10.1371/journal.ppat.0030034>
- Bartoloni, A., Zammarchi, L., 2012. Clinical Aspects of Uncomplicated and Severe Malaria. *Mediterr. J. Hematol. Infect. Dis.* 4, e2012026. <https://doi.org/10.4084/MJHID.2012.026>
- Baruch, D.I., Gormely, J.A., Ma, C., Howard, R.J., Pasloske, B.L., 1996. *Plasmodium falciparum* erythrocyte membrane protein 1 is a parasitized erythrocyte receptor for adherence to CD36, thrombospondin, and intercellular adhesion molecule 1. *Proc. Natl. Acad. Sci. U. S. A.* 93, 3497–3502. <https://doi.org/10.1073/pnas.93.8.3497>
- Baruch, D.I., Pasloske, B.L., Singh, H.B., Bi, X., Ma, X.C., Feldman, M., Taraschi, T.F., Howard, R.J., 1995. Cloning the *P. falciparum* gene encoding PfEMP1, a malarial variant antigen and adherence receptor on the surface of parasitized human erythrocytes. *Cell* 82, 77–87. [https://doi.org/10.1016/0092-8674\(95\)90054-3](https://doi.org/10.1016/0092-8674(95)90054-3)
- Batinovic, S., McHugh, E., Chisholm, S.A., Matthews, K., Liu, B., Dumont, L., Charnaud, S.C., Schneider, M.P., Gilson, P.R., de Koning-Ward, T.F., Dixon, M.W.A., Tilley, L., 2017. An exported protein-interacting complex involved in the trafficking of virulence determinants in *Plasmodium*-infected erythrocytes. *Nat. Commun.* 8, 16044. <https://doi.org/10.1038/ncomms16044>
- Beck, J.R., Ho, C.-M., 2021. Transport mechanisms at the malaria parasite-host cell interface. *PLOS Pathog.* 17, e1009394. <https://doi.org/10.1371/journal.ppat.1009394>
- Beck, J.R., Muralidharan, V., Oksman, A., Goldberg, D.E., 2014. PTEX component HSP101 mediates export of diverse malaria effectors into host erythrocytes. *Nature* 511, 592–595. <https://doi.org/10.1038/nature13574>
- Bengtsson, A., Joergensen, L., Rask, T.S., Olsen, R.W., Andersen, M.A., Turner, L., Theander, T.G., Hviid, L., Higgins, M.K., Craig, A., Brown, A., Jensen, A.T.R., 2013. A Novel Domain Cassette Identifies *Plasmodium falciparum* PfEMP1 Proteins Binding ICAM-

- 1 and Is a Target of Cross-Reactive, Adhesion-Inhibitory Antibodies. *J. Immunol.* Author Choice 190, 240–249. <https://doi.org/10.4049/jimmunol.1202578>
- Berg, S., Kutra, D., Kroeger, T., Strachle, C.N., Kausler, B.X., Haubold, C., Schiegg, M., Ales, J., Beier, T., Rudy, M., Eren, K., Cervantes, J.I., Xu, B., Beuttenmueller, F., Wolny, A., Zhang, C., Koethe, U., Hamprecht, F.A., Kreshuk, A., 2019. ilastik: interactive machine learning for (bio)image analysis. *Nat. Methods* 16, 1226–1232. <https://doi.org/10.1038/s41592-019-0582-9>
- Bernabeu, M., Gunnarsson, C., Vishnyakova, M., Howard, C.C., Nagao, R.J., Avril, M., Taylor, T.E., Seydel, K.B., Zheng, Y., Smith, J.D., 2019. Binding Heterogeneity of Plasmodium falciparum to Engineered 3D Brain Microvessels Is Mediated by EPCR and ICAM-1. *mBio* 10, e00420-19. <https://doi.org/10.1128/mBio.00420-19>
- Besteiro, S., Dubremetz, J.-F., Lebrun, M., 2011. The moving junction of apicomplexan parasites: a key structure for invasion. *Cell. Microbiol.* 13, 797–805. <https://doi.org/10.1111/j.1462-5822.2011.01597.x>
- Beyer, K., Kracht, S., Kehrer, J., Singer, M., Klug, D., Frischknecht, F., 2021. Limited Plasmodium sporozoite gliding motility in the absence of TRAP family adhesins. *Malar. J.* 20, 430. <https://doi.org/10.1186/s12936-021-03960-3>
- Billker, O., Dechamps, S., Tewari, R., Wenig, G., Franke-Fayard, B., Brinkmann, V., 2004. Calcium and a calcium-dependent protein kinase regulate gamete formation and mosquito transmission in a malaria parasite. *Cell* 117, 503–514. [https://doi.org/10.1016/s0092-8674\(04\)00449-0](https://doi.org/10.1016/s0092-8674(04)00449-0)
- Birnbaum, J., Flemming, S., Reichard, N., Soares, A.B., Mesén-Ramírez, P., Jonscher, E., Bergmann, B., Spielmann, T., 2017. A genetic system to study Plasmodium falciparum protein function. *Nat. Methods* 14, 450–456. <https://doi.org/10.1038/nmeth.4223>
- Birnbaum, J., Scharf, S., Schmidt, S., Jonscher, E., Hoeijmakers, W.A.M., Flemming, S., Toenhake, C.G., Schmitt, M., Sabitzki, R., Bergmann, B., Fröhlke, U., Mesén-Ramírez, P., Blancke Soares, A., Herrmann, H., Bártfai, R., Spielmann, T., 2020. A Kelch13-defined endocytosis pathway mediates artemisinin resistance in malaria parasites. *Science* 367, 51–59. <https://doi.org/10.1126/science.aax4735>
- Bisio, H., Lunghi, M., Brochet, M., Soldati-Favre, D., 2019. Phosphatidic acid governs natural egress in Toxoplasma gondii via a guanylate cyclase receptor platform. *Nat. Microbiol.* 4, 420–428. <https://doi.org/10.1038/s41564-018-0339-8>
- Biswas, A.K., Hafiz, A., Banerjee, B., Kim, K.S., Datta, K., Chitnis, C.E., 2007. Plasmodium falciparum Uses gC1qR/HABP1/p32 as a Receptor to Bind to Vascular Endothelium and for Platelet-Mediated Clumping. *PLOS Pathog.* 3, e130. <https://doi.org/10.1371/journal.ppat.0030130>
- Blackman, M.J., Carruthers, V.B., 2013. Recent insights into apicomplexan parasite egress provide new views to a kill. *Curr. Opin. Microbiol.* 16, 459–464. <https://doi.org/10.1016/j.mib.2013.04.008>
- Blancke-Soares, A., Stäcker, J., Schwald, S., Hoiijmakers, W., Metwally, N.G., Schoeler, H., Flemming, S., Höhn, K., Fröhlke, U., Mesén-Ramírez, P., Bergmann, B., Khosh-Naucke, M., Bruchhaus, I., Bártfai, R., Spielmann, T., 2021. An unusual trafficking domain in MSRP6 defines a complex needed for Maurer’s clefts anchoring and maintenance in P. falciparum infected red blood cells. <https://doi.org/10.1101/2021.12.03.471078>
- Boddey, J.A., Carvalho, T.G., Hodder, A.N., Sargeant, T.J., Sleebs, B.E., Marapana, D., Lopaticki, S., Nebl, T., Cowman, A.F., 2013. Role of plasmepsin V in export of diverse protein families from the Plasmodium falciparum exportome. *Traffic Cph. Den.* 14, 532–550. <https://doi.org/10.1111/tra.12053>

- Boddey, J.A., Cowman, A.F., 2013. Plasmodium nesting: remaking the erythrocyte from the inside out. *Annu. Rev. Microbiol.* 67, 243–269. <https://doi.org/10.1146/annurev-micro-092412-155730>
- Boltryk, S.D., Passecker, A., Alder, A., Carrington, E., van de Vegte-Bolmer, M., van Gemert, G.-J., van der Starre, A., Beck, H.-P., Sauerwein, R.W., Kooij, T.W.A., Brancucci, N.M.B., Proelochs, N.I., Gilberger, T.-W., Voss, T.S., 2021. CRISPR/Cas9-engineered inducible gametocyte producer lines as a valuable tool for Plasmodium falciparum malaria transmission research. *Nat. Commun.* 12, 4806. <https://doi.org/10.1038/s41467-021-24954-4>
- Bopp, S.E.R., Manary, M.J., Bright, A.T., Johnston, G.L., Dharia, N.V., Luna, F.L., McCormack, S., Plouffe, D., McNamara, C.W., Walker, J.R., Fidock, D.A., Denchi, E.L., Winzeler, E.A., 2013. Mitotic evolution of Plasmodium falciparum shows a stable core genome but recombination in antigen families. *PLoS Genet.* 9, e1003293. <https://doi.org/10.1371/journal.pgen.1003293>
- Bradley, J., Soumaré, H.M., Mahamar, A., Diawara, H., Roh, M., Delves, M., Drakeley, C., Churcher, T.S., Dicko, A., Gosling, R., Bousema, T., 2019. Transmission-blocking Effects of Primaquine and Methylene Blue Suggest Plasmodium falciparum Gametocyte Sterilization Rather Than Effects on Sex Ratio. *Clin. Infect. Dis. Off. Publ. Infect. Dis. Soc. Am.* 69, 1436–1439. <https://doi.org/10.1093/cid/ciz134>
- Brancucci, N.M.B., Bertschi, N.L., Zhu, L., Niederwieser, I., Chin, W.H., Wampfler, R., Freymond, C., Rottmann, M., Felger, I., Bozdech, Z., Voss, T.S., 2014. Heterochromatin protein 1 secures survival and transmission of malaria parasites. *Cell Host Microbe* 16, 165–176. <https://doi.org/10.1016/j.chom.2014.07.004>
- Brancucci, N.M.B., Gerdt, J.P., Wang, C., De Niz, M., Philip, N., Adapa, S.R., Zhang, M., Hitz, E., Niederwieser, I., Boltryk, S.D., Laffitte, M.-C., Clark, M.A., Grüning, C., Ravel, D., Blancke Soares, A., Demas, A., Bopp, S., Rubio-Ruiz, B., Conejo-Garcia, A., Wirth, D.F., Gendaszewska-Darmach, E., Duraisingh, M.T., Adams, J.H., Voss, T.S., Waters, A.P., Jiang, R.H.Y., Clardy, J., Marti, M., 2017. Lysophosphatidylcholine Regulates Sexual Stage Differentiation in the Human Malaria Parasite Plasmodium falciparum. *Cell* 171, 1532-1544.e15. <https://doi.org/10.1016/j.cell.2017.10.020>
- Branon, T.C., Bosch, J.A., Sanchez, A.D., Udeshi, N.D., Svinkina, T., Carr, S.A., Feldman, J.L., Perrimon, N., Ting, A.Y., 2018. Efficient proximity labeling in living cells and organisms with TurboID. *Nat. Biotechnol.* 36, 880–887. <https://doi.org/10.1038/nbt.4201>
- Bray, R.S., 1958. Studies on malaria in chimpanzees. VI. Laverania falciparum. *Am. J. Trop. Med. Hyg.* 7, 20–24. <https://doi.org/10.4269/ajtmh.1958.7.20>
- Brehmer, J., 2021. Analyse der Bindungseigenschaften zwischen P. falciparum infizierten Erythrozyten und verschiedenen Endothelrezeptoren (Dissertation). University of Hamburg.
- Buffet, P.A., Gamain, B., Scheidig, C., Baruch, D., Smith, J.D., Hernandez-Rivas, R., Pouvelle, B., Oishi, S., Fujii, N., Fusai, T., Parzy, D., Miller, L.H., Gysin, J., Scherf, A., 1999. Plasmodium falciparum domain mediating adhesion to chondroitin sulfate A: a receptor for human placental infection. *Proc. Natl. Acad. Sci. U. S. A.* 96, 12743–12748. <https://doi.org/10.1073/pnas.96.22.12743>
- Bull, P.C., Lowe, B.S., Kortok, M., Molyneux, C.S., Newbold, C.I., Marsh, K., 1998. Parasite antigens on the infected red cell surface are targets for naturally acquired immunity to malaria. *Nat. Med.* 4, 358–360. <https://doi.org/10.1038/nm0398-358>
- Bull, P.C., Marsh, K., 2002. The role of antibodies to Plasmodium falciparum-infected-erythrocyte surface antigens in naturally acquired immunity to malaria. *Trends Microbiol.* 10, 55–58. [https://doi.org/10.1016/s0966-842x\(01\)02278-8](https://doi.org/10.1016/s0966-842x(01)02278-8)

- Bullen, H.E., Charnaud, S.C., Kalanon, M., Riglar, D.T., Dekiwadia, C., Kangwanrangsang, N., Torii, M., Tsuboi, T., Baum, J., Ralph, S.A., Cowman, A.F., de Koning-Ward, T.F., Crabb, B.S., Gilson, P.R., 2012. Biosynthesis, localization, and macromolecular arrangement of the *Plasmodium falciparum* translocon of exported proteins (PTEX). *J. Biol. Chem.* 287, 7871–7884. <https://doi.org/10.1074/jbc.M111.328591>
- Cabral, F.J., Vianna, L.G., Medeiros, M.M., Carlos, B.C., Martha, R.D., Silva, N.M., da Silva, L.H.P., Stabeli, R.G., Wunderlich, G., 2017. Immunoproteomics of *Plasmodium falciparum*-infected red blood cell membrane fractions. *Mem. Inst. Oswaldo Cruz* 112, 850–856. <https://doi.org/10.1590/0074-02760170041>
- Carmo, O.M.S., Shami, G.J., Cox, D., Liu, B., Blanch, A.J., Tiash, S., Tilley, L., Dixon, M.W.A., 2022. Deletion of the *Plasmodium falciparum* exported protein PTP7 leads to Maurer's clefts vesiculation, host cell remodeling defects, and loss of surface presentation of EMP1. *PLOS Pathog.* 18, e1009882. <https://doi.org/10.1371/journal.ppat.1009882>
- Chan, S., Frasnich, A., Mandava, C.S., Ch'ng, J.-H., Quintana, M.D.P., Vesterlund, M., Ghorbal, M., Joannin, N., Franzén, O., Lopez-Rubio, J.-J., Barbieri, S., Lanzavecchia, A., Sanyal, S., Wahlgren, M., 2017. Regulation of PfEMP1-VAR2CSA translation by a *Plasmodium* translation-enhancing factor. *Nat. Microbiol.* 2, 17068. <https://doi.org/10.1038/nmicrobiol.2017.68>
- Chang, H.H., Falick, A.M., Carlton, P.M., Sedat, J.W., DeRisi, J.L., Marletta, M.A., 2008. N-terminal processing of proteins exported by malaria parasites. *Mol. Biochem. Parasitol.* 160, 107–115. <https://doi.org/10.1016/j.molbiopara.2008.04.011>
- Charnaud, S.C., Dixon, M.W.A., Nie, C.Q., Chappell, L., Sanders, P.R., Nebl, T., Hanssen, E., Berriman, M., Chan, J.-A., Blanch, A.J., Beeson, J.G., Rayner, J.C., Przyborski, J.M., Tilley, L., Crabb, B.S., Gilson, P.R., 2017. The exported chaperone Hsp70-x supports virulence functions for *Plasmodium falciparum* blood stage parasites. *PLoS ONE* 12, e0181656. <https://doi.org/10.1371/journal.pone.0181656>
- Chisholm, S.A., McHugh, E., Lundie, R., Dixon, M.W.A., Ghosh, S., O'Keefe, M., Tilley, L., Kalanon, M., de Koning-Ward, T.F., 2016. Contrasting Inducible Knockdown of the Auxiliary PTEX Component PTEX88 in *P. falciparum* and *P. berghei* Unmasks a Role in Parasite Virulence. *PloS One* 11, e0149296. <https://doi.org/10.1371/journal.pone.0149296>
- Claessens, A., Adams, Y., Ghumra, A., Lindergard, G., Buchan, C.C., Andisi, C., Bull, P.C., Mok, S., Gupta, A.P., Wang, C.W., Turner, L., Arman, M., Raza, A., Bozdech, Z., Rowe, J.A., 2012. A subset of group A-like var genes encodes the malaria parasite ligands for binding to human brain endothelial cells. *Proc. Natl. Acad. Sci. U. S. A.* 109, E1772–E1781. <https://doi.org/10.1073/pnas.1120461109>
- Claessens, A., Hamilton, W.L., Kekre, M., Otto, T.D., Faizullahoy, A., Rayner, J.C., Kwiatkowski, D., 2014. Generation of antigenic diversity in *Plasmodium falciparum* by structured rearrangement of Var genes during mitosis. *PLoS Genet.* 10, e1004812. <https://doi.org/10.1371/journal.pgen.1004812>
- Cohn, J.V., Alkhalil, A., Wagner, M.A., Rajapandi, T., Desai, S.A., 2003. Extracellular lysines on the plasmodial surface anion channel involved in Na⁺ exclusion. *Mol. Biochem. Parasitol.* 132, 27–34. <https://doi.org/10.1016/j.molbiopara.2003.08.001>
- Collins, C.R., Hackett, F., Atid, J., Tan, M.S.Y., Blackman, M.J., 2017. The *Plasmodium falciparum* pseudoprotease SERA5 regulates the kinetics and efficiency of malaria parasite egress from host erythrocytes. *PLOS Pathog.* 13, e1006453. <https://doi.org/10.1371/journal.ppat.1006453>
- Cooke, B.M., Buckingham, D.W., Glenister, F.K., Fernandez, K.M., Bannister, L.H., Marti, M., Mohandas, N., Coppel, R.L., 2006. A Maurer's cleft-associated protein is essential

- for expression of the major malaria virulence antigen on the surface of infected red blood cells. *J. Cell Biol.* 172, 899–908. <https://doi.org/10.1083/jcb.200509122>
- Cooke, B.M., Rogerson, S.J., Brown, G.V., Coppel, R.L., 1996. Adhesion of Malaria-Infected Red Blood Cells to Chondroitin Sulfate A Under Flow Conditions. *Blood* 88, 4040–4044. <https://doi.org/10.1182/blood.V88.10.4040.bloodjournal88104040>
- Counihan, N.A., Chisholm, S.A., Bullen, H.E., Srivastava, A., Sanders, P.R., Jonsdottir, T.K., Weiss, G.E., Ghosh, S., Crabb, B.S., Creek, D.J., Gilson, P.R., de Koning-Ward, T.F., 2017. Plasmodium falciparum parasites deploy RhopH2 into the host erythrocyte to obtain nutrients, grow and replicate. *eLife* 6, e23217. <https://doi.org/10.7554/eLife.23217>
- Cowman, A.F., Tonkin, C.J., Tham, W.-H., Duraisingh, M.T., 2017. The Molecular Basis of Erythrocyte Invasion by Malaria Parasites. *Cell Host Microbe* 22, 232–245. <https://doi.org/10.1016/j.chom.2017.07.003>
- Cox, F.E., 2010. History of the discovery of the malaria parasites and their vectors. *Parasit. Vectors* 3, 5. <https://doi.org/10.1186/1756-3305-3-5>
- Cox, J., Mann, M., 2008. MaxQuant enables high peptide identification rates, individualized p.p.b.-range mass accuracies and proteome-wide protein quantification. *Nat. Biotechnol.* 26, 1367–1372. <https://doi.org/10.1038/nbt.1511>
- Crabb, B.S., Cooke, B.M., Reeder, J.C., Waller, R.F., Caruana, S.R., Davern, K.M., Wickham, M.E., Brown, G.V., Coppel, R.L., Cowman, A.F., 1997. Targeted gene disruption shows that knobs enable malaria-infected red cells to cytoadhere under physiological shear stress. *Cell* 89, 287–296. [https://doi.org/10.1016/s0092-8674\(00\)80207-x](https://doi.org/10.1016/s0092-8674(00)80207-x)
- Craig, A.G., Grau, G.E., Janse, C., Kazura, J.W., Milner, D., Barnwell, J.W., Turner, G., Langhorne, J., Malaria”, on behalf of the participants of the H.R. meeting on “Animal M. for R. on S., 2012. The Role of Animal Models for Research on Severe Malaria. *PLOS Pathog.* 8, e1002401. <https://doi.org/10.1371/journal.ppat.1002401>
- Cranston, H.A., Boylan, C.W., Carroll, G.L., Sutera, S.P., Williamson, J.R., Gluzman, I.Y., Krogstad, D.J., 1984. Plasmodium falciparum maturation abolishes physiologic red cell deformability. *Science* 223, 400–403. <https://doi.org/10.1126/science.6362007>
- Cronshagen, J., 2020. Screening and characterization of the main integral membrane proteins in the parasitophorous vacuole membrane of Plasmodium falciparum (Master thesis). University of Hamburg.
- Cui, Y., Ma, L., 2018. Sequential use of milk and bovine serum albumin for streptavidin-probed western blot. *BioTechniques* 65, 125–126. <https://doi.org/10.2144/btn-2018-0006>
- Cyrklaff, M., Sanchez, C.P., Frischknecht, F., Lanzer, M., 2012. Host actin remodeling and protection from malaria by hemoglobinopathies. *Trends Parasitol.* 28, 479–485. <https://doi.org/10.1016/j.pt.2012.08.003>
- Cyrklaff, M., Sanchez, C.P., Kilian, N., Bisseye, C., Simpo, J., Frischknecht, F., Lanzer, M., 2011. Hemoglobins S and C interfere with actin remodeling in Plasmodium falciparum-infected erythrocytes. *Science* 334, 1283–1286. <https://doi.org/10.1126/science.1213775>
- Dahl, E.L., Shock, J.L., Shenai, B.R., Gut, J., DeRisi, J.L., Rosenthal, P.J., 2006. Tetracyclines Specifically Target the Apicoplast of the Malaria Parasite Plasmodium falciparum. *Antimicrob. Agents Chemother.* 50, 3124–3131. <https://doi.org/10.1128/AAC.00394-06>
- Dahlbäck, M., Jørgensen, L.M., Nielsen, M.A., Clausen, T.M., Ditlev, S.B., Resende, M., Pinto, V.V., Anot, D.E., Theander, T.G., Salanti, A., 2011. The Chondroitin Sulfate A-binding Site of the VAR2CSA Protein Involves Multiple N-terminal Domains. *J. Biol. Chem.* 286, 15908–15917. <https://doi.org/10.1074/jbc.M110.191510>

- Dantzler, K.W., Ma, S., Ngotho, P., Stone, W.J.R., Tao, D., Rijpma, S., De Niz, M., Nilsson Bark, S.K., Jore, M.M., Raaijmakers, T.K., Early, A.M., Ubaida-Mohien, C., Lemgruber, L., Campo, J.J., Teng, A.A., Le, T.Q., Walker, C.L., Hermand, P., Deterre, P., Davies, D.H., Felgner, P., Morlais, I., Wirth, D.F., Neafsey, D.E., Dinglasan, R.R., Laufer, M., Huttenhower, C., Seydel, K., Taylor, T., Bousema, T., Marti, M., 2019. Naturally acquired immunity against immature *Plasmodium falciparum* gametocytes. *Sci. Transl. Med.* 11, eaav3963. <https://doi.org/10.1126/scitranslmed.aav3963>
- Davies, H., Belda, H., Broncel, M., Dalimot, J., Treeck, M., 2023. PerTurboID, a targeted in situ method reveals the impact of kinase deletion on its local protein environment in the cytoadhesion complex of malaria-causing parasites. *eLife* 12, e86367. <https://doi.org/10.7554/eLife.86367>
- Davies, H., Belda, H., Broncel, M., Ye, X., Bisson, C., Introini, V., Dorin-Semlat, D., Semlat, J.-P., Tibúrcio, M., Gamain, B., Kaforou, M., Treeck, M., 2020. An Exported Kinase Family Mediates Species-Specific Erythrocyte Remodelling and Virulence in Human Malaria. *Nat. Microbiol.* 5, 848–863. <https://doi.org/10.1038/s41564-020-0702-4>
- Davies, H.M., Thalassinou, K., Osborne, A.R., 2016. Expansion of Lysine-rich Repeats in *Plasmodium* Proteins Generates Novel Localization Sequences That Target the Periphery of the Host Erythrocyte. *J. Biol. Chem.* 291, 26188–26207. <https://doi.org/10.1074/jbc.M116.761213>
- de Koning-Ward, T.F., Gilson, P.R., Boddey, J.A., Rug, M., Smith, B.J., Papenfuss, A.T., Sanders, P.R., Lundie, R.J., Maier, A.G., Cowman, A.F., Crabb, B.S., 2009. A newly discovered protein export machine in malaria parasites. *Nature* 459, 945–949. <https://doi.org/10.1038/nature08104>
- De Niz, M., Burda, P.-C., Kaiser, G., Del Portillo, H.A., Spielmann, T., Frischknecht, F., Heussler, V.T., 2017. Progress in imaging methods: insights gained into *Plasmodium* biology. *Nat. Rev. Microbiol.* 15, 37–54. <https://doi.org/10.1038/nrmicro.2016.158>
- De Niz, M., Ullrich, A.-K., Heiber, A., Blancke Soares, A., Pick, C., Lyck, R., Keller, D., Kaiser, G., Prado, M., Flemming, S., Del Portillo, H., Janse, C.J., Heussler, V., Spielmann, T., 2016. The machinery underlying malaria parasite virulence is conserved between rodent and human malaria parasites. *Nat. Commun.* 7, 11659. <https://doi.org/10.1038/ncomms11659>
- Dearnley, M.K., Yeoman, J.A., Hanssen, E., Kenny, S., Turnbull, L., Whitchurch, C.B., Tilley, L., Dixon, M.W.A., 2012. Origin, composition, organization and function of the inner membrane complex of *Plasmodium falciparum* gametocytes. *J. Cell Sci.* 125, 2053–2063. <https://doi.org/10.1242/jcs.099002>
- Deitsch, K.W., Dzikowski, R., 2017. Variant Gene Expression and Antigenic Variation by Malaria Parasites. *Annu. Rev. Microbiol.* 71, 625–641. <https://doi.org/10.1146/annurev-micro-090816-093841>
- Delves, M.J., Straschil, U., Ruecker, A., Miguel-Blanco, C., Marques, S., Dufour, A.C., Baum, J., Sinden, R.E., 2016. Routine in vitro culture of *P. falciparum* gametocytes to evaluate novel transmission-blocking interventions. *Nat. Protoc.* 11, 1668–1680. <https://doi.org/10.1038/nprot.2016.096>
- Desai, S.A., 2014. Why do malaria parasites increase host erythrocyte permeability? *Trends Parasitol.* 30, 151–159. <https://doi.org/10.1016/j.pt.2014.01.003>
- Desai, S.A., Bezrukov, S.M., Zimmerberg, J., 2000. A voltage-dependent channel involved in nutrient uptake by red blood cells infected with the malaria parasite. *Nature* 406, 1001–1005. <https://doi.org/10.1038/35023000>
- Desai, S.A., Krogstad, D.J., McCleskey, E.W., 1993. A nutrient-permeable channel on the intraerythrocytic malaria parasite. *Nature* 362, 643–646. <https://doi.org/10.1038/362643a0>

- Desai, S.A., Rosenberg, R.L., 1997. Pore size of the malaria parasite's nutrient channel. *Proc. Natl. Acad. Sci. U. S. A.* 94, 2045–2049.
- Dhangadamajhi, G., Kar, S.K., Ranjit, M., 2010. The Survival Strategies of Malaria Parasite in the Red Blood Cell and Host Cell Polymorphisms. *Malar. Res. Treat.* 2010, 973094. <https://doi.org/10.4061/2010/973094>
- Diehl, M., Roling, L., Rohland, L., Weber, S., Cyrklaff, M., Sanchez, C.P., Beretta, C.A., Simon, C.S., Guizetti, J., Hahn, J., Schulz, N., Mayer, M.P., Przyborski, J.M., 2021. Co-chaperone involvement in knob biogenesis implicates host-derived chaperones in malaria virulence. *PLoS Pathog.* 17, e1009969. <https://doi.org/10.1371/journal.ppat.1009969>
- Dietz, O., Rusch, S., Brand, F., Mundwiler-Pachlatko, E., Gaida, A., Voss, T., Beck, H.-P., 2014. Characterization of the Small Exported Plasmodium falciparum Membrane Protein SEMP1. *PLoS ONE* 9, e103272. <https://doi.org/10.1371/journal.pone.0103272>
- Dimonte, S., Bruske, E.I., Enderes, C., Otto, T.D., Turner, L., Kremsner, P., Frank, M., 2020. Identification of a conserved var gene in different Plasmodium falciparum strains. *Malar. J.* 19, 194. <https://doi.org/10.1186/s12936-020-03257-x>
- Dixon, M.W.A., Hawthorne, P.L., Spielmann, T., Anderson, K.L., Trenholme, K.R., Gardiner, D.L., 2008. Targeting of the ring exported protein 1 to the Maurer's clefts is mediated by a two-phase process. *Traffic Cph. Den.* 9, 1316–1326. <https://doi.org/10.1111/j.1600-0854.2008.00768.x>
- Dixon, M.W.A., Kenny, S., McMillan, P.J., Hanssen, E., Trenholme, K.R., Gardiner, D.L., Tilley, L., 2011. Genetic ablation of a Maurer's cleft protein prevents assembly of the Plasmodium falciparum virulence complex. *Mol. Microbiol.* 81, 982–993. <https://doi.org/10.1111/j.1365-2958.2011.07740.x>
- Dluzewski, A.R., Fryer, P.R., Griffiths, S., Wilson, R.J., Gratzer, W.B., 1989. Red cell membrane protein distribution during malarial invasion. *J. Cell Sci.* 92 (Pt 4), 691–699. <https://doi.org/10.1242/jcs.92.4.691>
- Dluzewski, A.R., Mitchell, G.H., Fryer, P.R., Griffiths, S., Wilson, R.J., Gratzer, W.B., 1992. Origins of the parasitophorous vacuole membrane of the malaria parasite, Plasmodium falciparum, in human red blood cells. *J. Cell Sci.* 102 (Pt 3), 527–532. <https://doi.org/10.1242/jcs.102.3.527>
- Dobrowolski, J.M., Sibley, L.D., 1996. Toxoplasma Invasion of Mammalian Cells Is Powered by the Actin Cytoskeleton of the Parasite. *Cell* 84, 933–939. [https://doi.org/10.1016/S0092-8674\(00\)81071-5](https://doi.org/10.1016/S0092-8674(00)81071-5)
- Dondorp, A.M., Nosten, F., Yi, P., Das, D., Phyo, A.P., Tarning, J., Lwin, K.M., Ariey, F., Hanpithakpong, W., Lee, S.J., Ringwald, P., Silamut, K., Imwong, M., Chotivanich, K., Lim, P., Herdman, T., An, S.S., Yeung, S., Singhasivanon, P., Day, N.P.J., Lindegardh, N., Socheat, D., White, N.J., 2009. Artemisinin resistance in Plasmodium falciparum malaria. *N. Engl. J. Med.* 361, 455–467. <https://doi.org/10.1056/NEJMoa0808859>
- Duffy, M.F., Byrne, T.J., Elliott, S.R., Wilson, D.W., Rogerson, S.J., Beeson, J.G., Noviyanti, R., Brown, G.V., 2005. Broad analysis reveals a consistent pattern of var gene transcription in Plasmodium falciparum repeatedly selected for a defined adhesion phenotype. *Mol. Microbiol.* 56, 774–788. <https://doi.org/10.1111/j.1365-2958.2005.04577.x>
- Dvorak, J.A., Miller, L.H., Whitehouse, W.C., Shiroishi, T., 1975. Invasion of erythrocytes by malaria merozoites. *Science* 187, 748–750. <https://doi.org/10.1126/science.803712>
- Ehlgen, F., Pham, J.S., Koning-Ward, T. de, Cowman, A.F., Ralph, S.A., 2012. Investigation of the Plasmodium falciparum Food Vacuole through Inducible Expression of the Chloroquine Resistance Transporter (PfCRT). *PLOS ONE* 7, e38781. <https://doi.org/10.1371/journal.pone.0038781>

- Eilers, M., Schatz, G., 1986. Binding of a specific ligand inhibits import of a purified precursor protein into mitochondria. *Nature* 322, 228–232. <https://doi.org/10.1038/322228a0>
- Eksi, S., Morahan, B.J., Haile, Y., Furuya, T., Jiang, H., Ali, O., Xu, H., Kiattibutr, K., Suri, A., Czesny, B., Adeyemo, A., Myers, T.G., Sattabongkot, J., Su, X., Williamson, K.C., 2012. Plasmodium falciparum gametocyte development 1 (Pfgdv1) and gametocytogenesis early gene identification and commitment to sexual development. *PLoS Pathog.* 8, e1002964. <https://doi.org/10.1371/journal.ppat.1002964>
- Elford, B.C., Haynes, J.D., Chulay, J.D., Wilson, R.J., 1985. Selective stage-specific changes in the permeability to small hydrophilic solutes of human erythrocytes infected with Plasmodium falciparum. *Mol. Biochem. Parasitol.* 16, 43–60. [https://doi.org/10.1016/0166-6851\(85\)90048-9](https://doi.org/10.1016/0166-6851(85)90048-9)
- Elliott, S.R., Duffy, M.F., Byrne, T.J., Beeson, J.G., Mann, E.J., Wilson, D.W., Rogerson, S.J., Brown, G.V., 2005. Cross-reactive surface epitopes on chondroitin sulfate A-adherent Plasmodium falciparum-infected erythrocytes are associated with transcription of var2csa. *Infect. Immun.* 73, 2848–2856. <https://doi.org/10.1128/IAI.73.5.2848-2856.2005>
- Elsworth, B., Matthews, K., Nie, C.Q., Kalanon, M., Charnaud, S.C., Sanders, P.R., Chisholm, S.A., Counihan, N.A., Shaw, P.J., Pino, P., Chan, J.-A., Azevedo, M.F., Rogerson, S.J., Beeson, J.G., Crabb, B.S., Gilson, P.R., de Koning-Ward, T.F., 2014. PTEX is an essential nexus for protein export in malaria parasites. *Nature* 511, 587–591. <https://doi.org/10.1038/nature13555>
- Elsworth, B., Sanders, P.R., Nebl, T., Batinovic, S., Kalanon, M., Nie, C.Q., Charnaud, S.C., Bullen, H.E., de Koning Ward, T.F., Tilley, L., Crabb, B.S., Gilson, P.R., 2016. Proteomic analysis reveals novel proteins associated with the Plasmodium protein exporter PTEX and a loss of complex stability upon truncation of the core PTEX component, PTEX150. *Cell. Microbiol.* 18, 1551–1569. <https://doi.org/10.1111/cmi.12596>
- Escalante, A.A., Cepeda, A.S., Pacheco, M.A., 2022. Why Plasmodium vivax and Plasmodium falciparum are so different? A tale of two clades and their species diversities. *Malar. J.* 21, 139. <https://doi.org/10.1186/s12936-022-04130-9>
- Farrell, A., Thirugnanam, S., Lorestani, A., Dvorin, J.D., Eidell, K.P., Ferguson, D.J.P., Anderson-White, B.R., Duraisingh, M.T., Marth, G.T., Gubbels, M.-J., 2012. A DOC2 protein identified by mutational profiling is essential for apicomplexan parasite exocytosis. *Science* 335, 218–221. <https://doi.org/10.1126/science.1210829>
- Fast, N.M., Kissinger, J.C., Roos, D.S., Keeling, P.J., 2001. Nuclear-encoded, plastid-targeted genes suggest a single common origin for apicomplexan and dinoflagellate plastids. *Mol. Biol. Evol.* 18, 418–426. <https://doi.org/10.1093/oxfordjournals.molbev.a003818>
- Fastman, Y., Noble, R., Recker, M., Dzikowski, R., 2012. Erasing the epigenetic memory and beginning to switch--the onset of antigenic switching of var genes in Plasmodium falciparum. *PloS One* 7, e34168. <https://doi.org/10.1371/journal.pone.0034168>
- Ferreira, J.L., Heincke, D., Wichers, J.S., Liffner, B., Wilson, D.W., Gilberger, T.-W., 2021. The Dynamic Roles of the Inner Membrane Complex in the Multiple Stages of the Malaria Parasite. *Front. Cell. Infect. Microbiol.* 10, 611801. <https://doi.org/10.3389/fcimb.2020.611801>
- Fidock, D.A., Bottius, E., Brahimi, K., Moelans, I.I., Aikawa, M., Konings, R.N., Certa, U., Olafsson, P., Kaidoh, T., Asavanich, A., 1994. Cloning and characterization of a novel Plasmodium falciparum sporozoite surface antigen, STARP. *Mol. Biochem. Parasitol.* 64, 219–232. [https://doi.org/10.1016/0166-6851\(94\)00012-3](https://doi.org/10.1016/0166-6851(94)00012-3)
- Fierro, M.A., Muheljic, A., Sha, J., Wohlschlegel, J.A., Beck, J.R., 2023. PEXEL is a proteolytic maturation site for both exported and non-exported Plasmodium proteins.

- BioRxiv Prepr. Serv. Biol. 2023.07.12.548774.
<https://doi.org/10.1101/2023.07.12.548774>
- Filarsky, M., Fraschka, S.A., Niederwieser, I., Brancucci, N.M.B., Carrington, E., Carrió, E., Moes, S., Jenoe, P., Bártfai, R., Voss, T.S., 2018. GDV1 induces sexual commitment of malaria parasites by antagonizing HP1-dependent gene silencing. *Science* 359, 1259–1263. <https://doi.org/10.1126/science.aan6042>
- Flammersfeld, A., Lang, C., Flieger, A., Pradel, G., 2018. Phospholipases during membrane dynamics in malaria parasites. *Int. J. Med. Microbiol. IJMM* 308, 129–141. <https://doi.org/10.1016/j.ijmm.2017.09.015>
- Florens, L., Liu, X., Wang, Y., Yang, S., Schwartz, O., Peglar, M., Carucci, D.J., Yates, J.R., Wu, Y., 2004. Proteomics approach reveals novel proteins on the surface of malaria-infected erythrocytes. *Mol. Biochem. Parasitol.* 135, 1–11. <https://doi.org/10.1016/j.molbiopara.2003.12.007>
- Foth, B.J., Zhang, N., Chaal, B.K., Sze, S.K., Preiser, P.R., Bozdech, Z., 2011. Quantitative time-course profiling of parasite and host cell proteins in the human malaria parasite *Plasmodium falciparum*. *Mol. Cell. Proteomics MCP* 10, M110.006411. <https://doi.org/10.1074/mcp.M110.006411>
- Francis, S.E., Banerjee, R., Goldberg, D.E., 1997. Biosynthesis and maturation of the malaria aspartic hemoglobinases plasmepsins I and II. *J. Biol. Chem.* 272, 14961–14968. <https://doi.org/10.1074/jbc.272.23.14961>
- Freitas-Junior, L.H., Bottius, E., Pirrit, L.A., Deitsch, K.W., Scheidig, C., Guinet, F., Nehrass, U., Wellems, T.E., Scherf, A., 2000. Frequent ectopic recombination of virulence factor genes in telomeric chromosome clusters of *P. falciparum*. *Nature* 407, 1018–1022. <https://doi.org/10.1038/35039531>
- Frénal, K., Dubremetz, J.-F., Lebrun, M., Soldati-Favre, D., 2017. Gliding motility powers invasion and egress in Apicomplexa. *Nat. Rev. Microbiol.* 15, 645–660. <https://doi.org/10.1038/nrmicro.2017.86>
- Fréville, A., Ressurreição, M., van Ooij, C., 2024. Identification of a non-exported Plasmepsin V substrate that functions in the parasitophorous vacuole of malaria parasites. *mBio* 15, e0122323. <https://doi.org/10.1128/mbio.01223-23>
- Fried, M., Duffy, P.E., 1996. Adherence of *Plasmodium falciparum* to chondroitin sulfate A in the human placenta. *Science* 272, 1502–1504. <https://doi.org/10.1126/science.272.5267.1502>
- Gabelich, J.-A., Grütze, J., Kirscht, F., Popp, O., Matz, J.M., Dittmar, G., Rug, M., Ingmundson, A., 2022. A member of the tryptophan-rich protein family is required for efficient sequestration of *Plasmodium berghei* schizonts. *PLoS Pathog.* 18, e1010846. <https://doi.org/10.1371/journal.ppat.1010846>
- Gabriela, M., Matthews, K.M., Boshoven, C., Kouskousis, B., Jonsdottir, T.K., Bullen, H.E., Modak, J., Steer, D.L., Sleeb, B.E., Crabb, B.S., Koning-Ward, T.F. de, Gilson, P.R., 2022. A revised mechanism for how *Plasmodium falciparum* recruits and exports proteins into its erythrocytic host cell. *PLOS Pathog.* 18, e1009977. <https://doi.org/10.1371/journal.ppat.1009977>
- Gamain, B., Trimmell, A.R., Scheidig, C., Scherf, A., Miller, L.H., Smith, J.D., 2005. Identification of multiple chondroitin sulfate A (CSA)-binding domains in the var2CSA gene transcribed in CSA-binding parasites. *J. Infect. Dis.* 191, 1010–1013. <https://doi.org/10.1086/428137>
- Gardner, J.P., Pinches, R.A., Roberts, D.J., Newbold, C.I., 1996. Variant antigens and endothelial receptor adhesion in *Plasmodium falciparum*. *Proc. Natl. Acad. Sci. U. S. A.* 93, 3503–3508. <https://doi.org/10.1073/pnas.93.8.3503>

- Gardner, M.J., Hall, N., Fung, E., White, O., Berriman, M., Hyman, R.W., Carlton, J.M., Pain, A., Nelson, K.E., Bowman, S., Paulsen, I.T., James, K., Eisen, J.A., Rutherford, K., Salzberg, S.L., Craig, A., Kyes, S., Chan, M.-S., Nene, V., Shallom, S.J., Suh, B., Peterson, J., Angiuoli, S., Pertea, M., Allen, J., Selengut, J., Haft, D., Mather, M.W., Vaidya, A.B., Martin, D.M.A., Fairlamb, A.H., Fraunholz, M.J., Roos, D.S., Ralph, S.A., McFadden, G.I., Cummings, L.M., Subramanian, G.M., Mungall, C., Venter, J.C., Carucci, D.J., Hoffman, S.L., Newbold, C., Davis, R.W., Fraser, C.M., Barrell, B., 2002. Genome sequence of the human malaria parasite *Plasmodium falciparum*. *Nature* 419, 498–511. <https://doi.org/10.1038/nature01097>
- Garoff, H., Ansorge, W., 1981. Improvements of DNA sequencing gels. *Anal. Biochem.* 115, 450–457. [https://doi.org/10.1016/0003-2697\(81\)90031-2](https://doi.org/10.1016/0003-2697(81)90031-2)
- Garten, M., Nasamu, A.S., Niles, J.C., Zimmerberg, J., Goldberg, D.E., Beck, J.R., 2018. EXP2 is a nutrient-permeable channel in the vacuolar membrane of *Plasmodium* and is essential for protein export via PTEX. *Nat. Microbiol.* 3, 1090–1098. <https://doi.org/10.1038/s41564-018-0222-7>
- Gaskins, E., Gilk, S., DeVore, N., Mann, T., Ward, G., Beckers, C., 2004. Identification of the membrane receptor of a class XIV myosin in *Toxoplasma gondii*. *J. Cell Biol.* 165, 383–393. <https://doi.org/10.1083/jcb.200311137>
- Gasser, B., Saloheimo, M., Rinas, U., Dragosits, M., Rodríguez-Carmona, E., Baumann, K., Giuliani, M., Parrilli, E., Branduardi, P., Lang, C., Porro, D., Ferrer, P., Tutino, M.L., Mattanovich, D., Villaverde, A., 2008. Protein folding and conformational stress in microbial cells producing recombinant proteins: a host comparative overview. *Microb. Cell Factories* 7, 11. <https://doi.org/10.1186/1475-2859-7-11>
- Gehde, N., Hinrichs, C., Montilla, I., Charpian, S., Lingelbach, K., Przyborski, J.M., 2009. Protein unfolding is an essential requirement for transport across the parasitophorous vacuolar membrane of *Plasmodium falciparum*. *Mol. Microbiol.* 71, 613–628. <https://doi.org/10.1111/j.1365-2958.2008.06552.x>
- Gibson, D.G., Young, L., Chuang, R.-Y., Venter, J.C., Hutchison, C.A., Smith, H.O., 2009. Enzymatic assembly of DNA molecules up to several hundred kilobases. *Nat. Methods* 6, 343–345. <https://doi.org/10.1038/nmeth.1318>
- Gillrie, M.R., Avril, M., Brazier, A.J., Davis, S.P., Stins, M.F., Smith, J.D., Ho, M., 2015. Diverse functional outcomes of *Plasmodium falciparum* ligation of EPCR: potential implications for malarial pathogenesis. *Cell. Microbiol.* 17, 1883–1899. <https://doi.org/10.1111/cmi.12479>
- Gilson, P.R., Crabb, B.S., 2009. Morphology and kinetics of the three distinct phases of red blood cell invasion by *Plasmodium falciparum* merozoites. *Int. J. Parasitol.* 39, 91–96. <https://doi.org/10.1016/j.ijpara.2008.09.007>
- Ginsburg, H., Kutner, S., Krugliak, M., Cabantchik, Z.I., 1985. Characterization of permeation pathways appearing in the host membrane of *Plasmodium falciparum* infected red blood cells. *Mol. Biochem. Parasitol.* 14, 313–322. [https://doi.org/10.1016/0166-6851\(85\)90059-3](https://doi.org/10.1016/0166-6851(85)90059-3)
- Glenister, F.K., Coppel, R.L., Cowman, A.F., Mohandas, N., Cooke, B.M., 2002. Contribution of parasite proteins to altered mechanical properties of malaria-infected red blood cells. *Blood* 99, 1060–1063. <https://doi.org/10.1182/blood.v99.3.1060>
- Goel, S., Palmkvist, M., Moll, K., Joannin, N., Lara, P., Akhouri, R.R., Moradi, N., Öjemalm, K., Westman, M., Angeletti, D., Kjellin, H., Lehtiö, J., Blixt, O., Ideström, L., Gahmberg, C.G., Storry, J.R., Hult, A.K., Olsson, M.L., von Heijne, G., Nilsson, I., Wahlgren, M., 2015. RIFINs are adhesins implicated in severe *Plasmodium falciparum* malaria. *Nat. Med.* 21, 314–317. <https://doi.org/10.1038/nm.3812>

- Goldberg, D.E., Slater, A.F., Beavis, R., Chait, B., Cerami, A., Henderson, G.B., 1991. Hemoglobin degradation in the human malaria pathogen *Plasmodium falciparum*: a catabolic pathway initiated by a specific aspartic protease. *J. Exp. Med.* 173, 961–969. <https://doi.org/10.1084/jem.173.4.961>
- Goldberg, D.E., Slater, A.F., Cerami, A., Henderson, G.B., 1990. Hemoglobin degradation in the malaria parasite *Plasmodium falciparum*: an ordered process in a unique organelle. *Proc. Natl. Acad. Sci. U. S. A.* 87, 2931–2935. <https://doi.org/10.1073/pnas.87.8.2931>
- Goldberg, D.E., Zimmerberg, J., 2020. Hardly Vacuous: The Parasitophorous Vacuolar Membrane of Malaria Parasites. *Trends Parasitol.* 36, 138–146. <https://doi.org/10.1016/j.pt.2019.11.006>
- Goodyer, I.D., Johnson, J., Eisenthal, R., Hayes, D.J., 1994. Purification of mature-stage *Plasmodium falciparum* by gelatine flotation. *Ann. Trop. Med. Parasitol.* 88, 209–211. <https://doi.org/10.1080/00034983.1994.11812859>
- Gray, C., McCormick, C., Turner, G., Craig, A., 2003. ICAM-1 can play a major role in mediating *P. falciparum* adhesion to endothelium under flow. *Mol. Biochem. Parasitol.* 128, 187–193. [https://doi.org/10.1016/s0166-6851\(03\)00075-6](https://doi.org/10.1016/s0166-6851(03)00075-6)
- Gruenberg, J., Allred, D.R., Sherman, I.W., 1983. Scanning electron microscope-analysis of the protrusions (knobs) present on the surface of *Plasmodium falciparum*-infected erythrocytes. *J. Cell Biol.* 97, 795–802. <https://doi.org/10.1083/jcb.97.3.795>
- Grüning, C., Heiber, A., Kruse, F., Flemming, S., Franci, G., Colombo, S.F., Fasana, E., Schoeler, H., Borgese, N., Stunnenberg, H.G., Przyborski, J.M., Gilberger, T.-W., Spielmann, T., 2012. Uncovering Common Principles in Protein Export of Malaria Parasites. *Cell Host Microbe* 12, 717–729. <https://doi.org/10.1016/j.chom.2012.09.010>
- Grüning, C., Heiber, A., Kruse, F., Ungefehr, J., Gilberger, T.-W., Spielmann, T., 2011. Development and host cell modifications of *Plasmodium falciparum* blood stages in four dimensions. *Nat. Commun.* 2, 165. <https://doi.org/10.1038/ncomms1169>
- Grüning, C., Spielmann, T., 2012. Imaging of live malaria blood stage parasites. *Methods Enzymol.* 506, 81–92. <https://doi.org/10.1016/B978-0-12-391856-7.00029-9>
- Guérin, A., Corrales, R.M., Parker, M.L., Lamarque, M.H., Jacot, D., El Hajj, H., Soldati-Favre, D., Boulanger, M.J., Lebrun, M., 2017. Efficient invasion by *Toxoplasma* depends on the subversion of host protein networks. *Nat. Microbiol.* 2, 1358–1366. <https://doi.org/10.1038/s41564-017-0018-1>
- Gupta, A., Bokhari, A.A.B., Pillai, A.D., Crater, A.K., Gezelle, J., Saggi, G., Nasamu, A.S., Ganesan, S.M., Niles, J.C., Desai, S.A., 2020. Complex nutrient channel phenotypes despite Mendelian inheritance in a *Plasmodium falciparum* genetic cross. *PLOS Pathog.* 16, e1008363. <https://doi.org/10.1371/journal.ppat.1008363>
- Guttery, D.S., Poulin, B., Ferguson, D.J.P., Szöör, B., Wickstead, B., Carroll, P.L., Ramakrishnan, C., Brady, D., Patzewitz, E.-M., Straschil, U., Solyakov, L., Green, J.L., Sinden, R.E., Tobin, A.B., Holder, A.A., Tewari, R., 2012. A Unique Protein Phosphatase with Kelch-Like Domains (PPKL) in *Plasmodium* Modulates Ookinete Differentiation, Motility and Invasion. *PLOS Pathog.* 8, e1002948. <https://doi.org/10.1371/journal.ppat.1002948>
- Håkansson, S., Charron, A.J., Sibley, L.D., 2001. *Toxoplasma* vacuoles: a two-step process of secretion and fusion forms the parasitophorous vacuole. *EMBO J.* 20, 3132–3144. <https://doi.org/10.1093/emboj/20.12.3132>
- Hanssen, E., Dekiwadia, C., Riglar, D.T., Rug, M., Lemgruber, L., Cowman, A.F., Cyrklaff, M., Kudryashev, M., Frischknecht, F., Baum, J., Ralph, S.A., 2013. Electron tomography of *Plasmodium falciparum* merozoites reveals core cellular events that underpin erythrocyte invasion. *Cell. Microbiol.* 15, 1457–1472. <https://doi.org/10.1111/cmi.12132>

- Hanssen, E., Sougrat, R., Frankland, S., Deed, S., Klonis, N., Lippincott-Schwartz, J., Tilley, L., 2008. Electron tomography of the Maurer's cleft organelles of *Plasmodium falciparum*-infected erythrocytes reveals novel structural features. *Mol. Microbiol.* 67, 703–718. <https://doi.org/10.1111/j.1365-2958.2007.06063.x>
- Hawass, Z., Gad, Y.Z., Ismail, S., Khairat, R., Fathalla, D., Hasan, N., Ahmed, A., Elleithy, H., Ball, M., Gaballah, F., Wasef, S., Fateen, M., Amer, H., Gostner, P., Selim, A., Zink, A., Pusch, C.M., 2010. Ancestry and pathology in King Tutankhamun's family. *JAMA* 303, 638–647. <https://doi.org/10.1001/jama.2010.121>
- Hawthorne, P.L., Trenholme, K.R., Skinner-Adams, T.S., Spielmann, T., Fischer, K., Dixon, M.W.A., Ortega, M.R., Anderson, K.L., Kemp, D.J., Gardiner, D.L., 2004. A novel *Plasmodium falciparum* ring stage protein, REX, is located in Maurer's clefts. *Mol. Biochem. Parasitol.* 136, 181–189. <https://doi.org/10.1016/j.molbiopara.2004.03.013>
- Hay, S.I., Omumbo, J.A., Craig, M.H., Snow, R.W., 2000. Earth Observation, Geographic Information Systems and *Plasmodium falciparum* Malaria in Sub-Saharan Africa. *Adv. Parasitol.* 47, 173–215.
- Heiber, A., Kruse, F., Pick, C., Grüning, C., Flemming, S., Oberli, A., Schoeler, H., Retzlaff, S., Mesén-Ramírez, P., Hiss, J.A., Kadekoppala, M., Hecht, L., Holder, A.A., Gilberger, T.-W., Spielmann, T., 2013. Identification of New PNEPs Indicates a Substantial Non-PEXEL Exportome and Underpins Common Features in *Plasmodium falciparum* Protein Export. *PLOS Pathog.* 9, e1003546. <https://doi.org/10.1371/journal.ppat.1003546>
- Heiber, A., Spielmann, T., 2014. Preparation of Parasite Protein Extracts and Western Blot Analysis. *BIO-Protoc.* 4. <https://doi.org/10.21769/BioProtoc.1136>
- Henrich, P., Kilian, N., Lanzer, M., Cyrklaff, M., 2009. 3-D analysis of the *Plasmodium falciparum* Maurer's clefts using different electron tomographic approaches. *Biotechnol. J.* 4, 888–894. <https://doi.org/10.1002/biot.200900058>
- Henshall, I.G., Spielmann, T., 2023. Critical interdependencies between *Plasmodium* nutrient flux and drugs. *Trends Parasitol.* 39, 936–944. <https://doi.org/10.1016/j.pt.2023.08.008>
- Hill, D.L., Eriksson, E.M., Li Wai Suen, C.S.N., Chiu, C.Y., Ryg-Cornejo, V., Robinson, L.J., Siba, P.M., Mueller, I., Hansen, D.S., Schofield, L., 2013. Opsonising Antibodies to *P. falciparum* Merozoites Associated with Immunity to Clinical Malaria. *PLoS ONE* 8, e74627. <https://doi.org/10.1371/journal.pone.0074627>
- Hiller, N.L., Bhattacharjee, S., van Ooij, C., Liolios, K., Harrison, T., Lopez-Estraño, C., Haldar, K., 2004. A host-targeting signal in virulence proteins reveals a secretome in malarial infection. *Science* 306, 1934–1937. <https://doi.org/10.1126/science.1102737>
- Hinterberg, K., Scherf, A., Gysin, J., Toyoshima, T., Aikawa, M., Mazie, J.C., da Silva, L.P., Mattei, D., 1994. *Plasmodium falciparum*: the Pf332 antigen is secreted from the parasite by a brefeldin A-dependent pathway and is translocated to the erythrocyte membrane via the Maurer's clefts. *Exp. Parasitol.* 79, 279–291. <https://doi.org/10.1006/expr.1994.1091>
- Ho, C.-M., Beck, J.R., Lai, M., Cui, Y., Goldberg, D.E., Egea, P.F., Zhou, Z.H., 2018. Malaria parasite translocon structure and mechanism of effector export. *Nature* 561, 70–75. <https://doi.org/10.1038/s41586-018-0469-4>
- Ho, C.-M., Jih, J., Lai, M., Li, X., Goldberg, D.E., Beck, J.R., Zhou, Z.H., 2021. Native structure of the RhopH complex, a key determinant of malaria parasite nutrient acquisition. *Proc. Natl. Acad. Sci.* 118, e2100514118. <https://doi.org/10.1073/pnas.2100514118>
- Homewood, C.A., Neame, K.D., 1974. Malaria and the permeability of the host erythrocyte. *Nature* 252, 718–719. <https://doi.org/10.1038/252718a0>

- Hommel, M., David, P.H., Oligino, L.D., 1983. Surface alterations of erythrocytes in *Plasmodium falciparum* malaria. Antigenic variation, antigenic diversity, and the role of the spleen. *J. Exp. Med.* 157, 1137–1148. <https://doi.org/10.1084/jem.157.4.1137>
- Horrocks, P., Pinches, R., Christodoulou, Z., Kyes, S.A., Newbold, C.I., 2004. Variable var transition rates underlie antigenic variation in malaria. *Proc. Natl. Acad. Sci. U. S. A.* 101, 11129–11134. <https://doi.org/10.1073/pnas.0402347101>
- Howell, D.P.-G., Levin, E.A., Springer, A.L., Kraemer, S.M., Phippard, D.J., Schief, W.R., Smith, J.D., 2008. Mapping a common interaction site used by *Plasmodium falciparum* Duffy binding-like domains to bind diverse host receptors. *Mol. Microbiol.* 67, 78–87. <https://doi.org/10.1111/j.1365-2958.2007.06019.x>
- Hubner, N.C., Nguyen, L.N., Hornig, N.C., Stunnenberg, H.G., 2015. A quantitative proteomics tool to identify DNA-protein interactions in primary cells or blood. *J. Proteome Res.* 14, 1315–1329. <https://doi.org/10.1021/pr5009515>
- Inoue, H., Nojima, H., Okayama, H., 1990. High efficiency transformation of *Escherichia coli* with plasmids. *Gene* 96, 23–28. [https://doi.org/10.1016/0378-1119\(90\)90336-p](https://doi.org/10.1016/0378-1119(90)90336-p)
- Ishino, T., Yano, K., Chinzei, Y., Yuda, M., 2004. Cell-passage activity is required for the malarial parasite to cross the liver sinusoidal cell layer. *PLoS Biol.* 2, E4. <https://doi.org/10.1371/journal.pbio.0020004>
- Issar, N., Roux, E., Mattei, D., Scherf, A., 2008. Identification of a novel post-translational modification in *Plasmodium falciparum*: protein sumoylation in different cellular compartments. *Cell. Microbiol.* 10, 1999–2011. <https://doi.org/10.1111/j.1462-5822.2008.01183.x>
- Ito, D., Schureck, M.A., Desai, S.A., 2017. An essential dual-function complex mediates erythrocyte invasion and channel-mediated nutrient uptake in malaria parasites. *eLife* 6, e23485. <https://doi.org/10.7554/eLife.23485>
- Jaijyan, D.K., Singh, H., Singh, A.P., 2015. A Sporozoite- and Liver Stage-expressed Tryptophan-rich Protein Plays an Auxiliary Role in *Plasmodium* Liver Stage Development and Is a Potential Vaccine Candidate *. *J. Biol. Chem.* 290, 19496–19511. <https://doi.org/10.1074/jbc.M114.588129>
- Janes, J.H., Wang, C.P., Levin-Edens, E., Vigan-Womas, I., Guillotte, M., Melcher, M., Mercereau-Puijalon, O., Smith, J.D., 2011. Investigating the Host Binding Signature on the *Plasmodium falciparum* PfEMP1 Protein Family. *PLoS Pathog.* 7, e1002032. <https://doi.org/10.1371/journal.ppat.1002032>
- Janse, C.J., Van der Klooster, P.F., Van der Kaay, H.J., Van der Ploeg, M., Overdulve, J.P., 1986. Rapid repeated DNA replication during microgametogenesis and DNA synthesis in young zygotes of *Plasmodium berghei*. *Trans. R. Soc. Trop. Med. Hyg.* 80, 154–157. [https://doi.org/10.1016/0035-9203\(86\)90219-1](https://doi.org/10.1016/0035-9203(86)90219-1)
- Jensen, A.T.R., Magistrado, P., Sharp, S., Joergensen, L., Lavstsen, T., Chiucchiuini, A., Salanti, A., Vestergaard, L.S., Lusingu, J.P., Hermsen, R., Sauerwein, R., Christensen, J., Nielsen, M.A., Hviid, L., Sutherland, C., Staalsoe, T., Theander, T.G., 2004. *Plasmodium falciparum* associated with severe childhood malaria preferentially expresses PfEMP1 encoded by group A var genes. *J. Exp. Med.* 199, 1179–1190. <https://doi.org/10.1084/jem.20040274>
- Jensen, J.B., Trager, W., 1978. *Plasmodium falciparum* in culture: establishment of additional strains. *Am. J. Trop. Med. Hyg.* 27, 743–746. <https://doi.org/10.4269/ajtmh.1978.27.743>
- Joergensen, L., Bengtsson, D.C., Bengtsson, A., Ronander, E., Berger, S.S., Turner, L., Dalgaard, M.B., Cham, G.K.K., Victor, M.E., Lavstsen, T., Theander, T.G., Arnot, D.E., Jensen, A.T.R., 2010. Surface Co-Expression of Two Different PfEMP1 Antigens on Single *Plasmodium falciparum*-Infected Erythrocytes Facilitates Binding to ICAM1

- and PECAM1. *PLoS Pathog.* 6, e1001083. <https://doi.org/10.1371/journal.ppat.1001083>
- Joice, R., Nilsson, S.K., Montgomery, J., Dankwa, S., Egan, E., Morahan, B., Seydel, K.B., Bertuccini, L., Alano, P., Williamson, K.C., Duraisingh, M.T., Taylor, T.E., Milner, D.A., Marti, M., 2014. Plasmodium falciparum transmission stages accumulate in the human bone marrow. *Sci. Transl. Med.* 6, 244re5. <https://doi.org/10.1126/scitranslmed.3008882>
- Joiner, K.A., 1991. Rhoptry lipids and parasitophorous vacuole formation: a slippery issue. *Parasitol. Today Pers. Ed* 7, 226–227. [https://doi.org/10.1016/0169-4758\(91\)90232-d](https://doi.org/10.1016/0169-4758(91)90232-d)
- Jones, M.L., Kitson, E.L., Rayner, J.C., 2006. Plasmodium falciparum erythrocyte invasion: a conserved myosin associated complex. *Mol. Biochem. Parasitol.* 147, 74–84. <https://doi.org/10.1016/j.molbiopara.2006.01.009>
- Jonsdottir, T.K., Counihan, N.A., Modak, J.K., Kouskousis, B., Sanders, P.R., Gabriela, M., Bullen, H.E., Crabb, B.S., de Koning-Ward, T.F., Gilson, P.R., 2021. Characterisation of complexes formed by parasite proteins exported into the host cell compartment of Plasmodium falciparum infected red blood cells. *Cell. Microbiol.* 23, e13332. <https://doi.org/10.1111/cmi.13332>
- Josling, G.A., Llinás, M., 2015. Sexual development in Plasmodium parasites: knowing when it's time to commit. *Nat. Rev. Microbiol.* 13, 573–587. <https://doi.org/10.1038/nrmicro3519>
- Juillerat, A., Lewit-Bentley, A., Guillotte, M., Gangnard, S., Hessel, A., Baron, B., Vigan-Womas, I., England, P., Mercereau-Puijalon, O., Bentley, G.A., 2011. Structure of a Plasmodium falciparum PfEMP1 rosetting domain reveals a role for the N-terminal segment in heparin-mediated rosette inhibition. *Proc. Natl. Acad. Sci. U. S. A.* 108, 5243–5248. <https://doi.org/10.1073/pnas.1018692108>
- Jumper, J., Evans, R., Pritzel, A., Green, T., Figurnov, M., Ronneberger, O., Tunyasuvunakool, K., Bates, R., Židek, A., Potapenko, A., Bridgland, A., Meyer, C., Kohl, S.A.A., Ballard, A.J., Cowie, A., Romera-Paredes, B., Nikolov, S., Jain, R., Adler, J., Back, T., Petersen, S., Reiman, D., Clancy, E., Zielinski, M., Steinegger, M., Pacholska, M., Berghammer, T., Bodenstein, S., Silver, D., Vinyals, O., Senior, A.W., Kavukcuoglu, K., Kohli, P., Hassabis, D., 2021. Highly accurate protein structure prediction with AlphaFold. *Nature* 596, 583–589. <https://doi.org/10.1038/s41586-021-03819-2>
- Kafsack, B.F.C., Rovira-Graells, N., Clark, T.G., Bancells, C., Crowley, V.M., Campino, S.G., Williams, A.E., Drought, L.G., Kwiatkowski, D.P., Baker, D.A., Cortés, A., Llinás, M., 2014. A transcriptional switch underlies commitment to sexual development in malaria parasites. *Nature* 507, 248–252. <https://doi.org/10.1038/nature12920>
- Kara, U.A., Stenzel, D.J., Ingram, L.T., Kidson, C., 1988. The parasitophorous vacuole membrane of Plasmodium falciparum: demonstration of vesicle formation using an immunoprobe. *Eur. J. Cell Biol.* 46, 9–17.
- Karunaweera, N.D., Galappaththy, G.N., Wirth, D.F., 2014. On the road to eliminate malaria in Sri Lanka: lessons from history, challenges, gaps in knowledge and research needs. *Malar. J.* 13, 59. <https://doi.org/10.1186/1475-2875-13-59>
- Kats, L.M., Fernandez, K.M., Glenister, F.K., Herrmann, S., Buckingham, D.W., Siddiqui, G., Sharma, L., Bamert, R., Lucet, I., Guillotte, M., Mercereau-Puijalon, O., Cooke, B.M., 2014. An exported kinase (FIKK4.2) that mediates virulence-associated changes in Plasmodium falciparum-infected red blood cells. *Int. J. Parasitol.* 44, 319–328. <https://doi.org/10.1016/j.ijpara.2014.01.003>
- Kaur, J., Kumar, V., Singh, A.P., Singh, V., Bisht, A., Dube, T., Panda, J.J., Behl, A., Mishra, P.C., Hora, R., 2018. Plasmodium falciparum protein “PfJ23” hosts distinct binding

- sites for major virulence factor “PfEMP1” and Maurer’s cleft marker “PfSBP1.” *Pathog. Dis.* 76. <https://doi.org/10.1093/femspd/fty090>
- Kawamoto, F., Alejo-Blanco, R., Fleck, S.L., Sinden, R.E., 1991. Plasmodium berghei: ionic regulation and the induction of gametogenesis. *Exp. Parasitol.* 72, 33–42. [https://doi.org/10.1016/0014-4894\(91\)90118-g](https://doi.org/10.1016/0014-4894(91)90118-g)
- Keeley, A., Soldati, D., 2004. The glideosome: a molecular machine powering motility and host-cell invasion by Apicomplexa. *Trends Cell Biol.* 14, 528–532. <https://doi.org/10.1016/j.tcb.2004.08.002>
- Kent, R.S., Modrzynska, K.K., Cameron, R., Philip, N., Billker, O., Waters, A.P., 2018. Inducible developmental reprogramming redefines commitment to sexual development in the malaria parasite Plasmodium berghei. *Nat. Microbiol.* 3, 1206–1213. <https://doi.org/10.1038/s41564-018-0223-6>
- Khosh-Naucke, M., Becker, J., Mesén-Ramírez, P., Kiani, P., Birnbaum, J., Fröhlke, U., Jonscher, E., Schlüter, H., Spielmann, T., 2018. Identification of novel parasitophorous vacuole proteins in P. falciparum parasites using BioID. *Int. J. Med. Microbiol. IJMM* 308, 13–24. <https://doi.org/10.1016/j.ijmm.2017.07.007>
- Kieferle, F., 2023. Charakterisierung eines Oberflächenproteins Plasmodium falciparum infizierter Erythrozyten (PfEMP1_IT4_var16), welches die Bindung an verschiedene Endothelrezeptoren vermittelt (Bachelor Thesis). Hochschule für Angewandte Wissenschaften Hamburg.
- Kilejian, A., 1979. Characterization of a protein correlated with the production of knob-like protrusions on membranes of erythrocytes infected with Plasmodium falciparum. *Proc. Natl. Acad. Sci. U. S. A.* 76, 4650–4653. <https://doi.org/10.1073/pnas.76.9.4650>
- Kilejian, A., Rashid, M.A., Aikawa, M., Aji, T., Yang, Y.-F., 1991. Selective association of a fragment of the knob protein with spectrin, actin and the red cell membrane. *Mol. Biochem. Parasitol.* 44, 175–181. [https://doi.org/10.1016/0166-6851\(91\)90003-O](https://doi.org/10.1016/0166-6851(91)90003-O)
- Kilili, G.K., Shakya, B., Dolan, P.T., Wang, L., Husby, M.L., Stahelin, R.V., Nakayasu, E.S., LaCount, D.J., 2019. The Plasmodium falciparum MESA erythrocyte cytoskeleton-binding (MEC) motif binds to erythrocyte ankyrin. *Mol. Biochem. Parasitol.* 231, 111189. <https://doi.org/10.1016/j.molbiopara.2019.111189>
- Kimmel, J., Kehrer, J., Frischknecht, F., Spielmann, T., 2022. Proximity-dependent biotinylation approaches to study apicomplexan biology. *Mol. Microbiol.* 117, 553–568. <https://doi.org/10.1111/mmi.14815>
- Kimmel, J., Schmitt, M., Sinner, A., Jansen, P.W.T.C., Mainye, S., Ramón-Zamorano, G., Toenhake, C.G., Wichers-Misterek, J.S., Cronshagen, J., Sabitzki, R., Mesén-Ramírez, P., Behrens, H.M., Bártfai, R., Spielmann, T., 2023. Gene-by-gene screen of the unknown proteins encoded on Plasmodium falciparum chromosome 3. *Cell Syst.* 14, 9–23.e7. <https://doi.org/10.1016/j.cels.2022.12.001>
- Kirk, K., Horner, H.A., Kirk, J., 1996. Glucose uptake in Plasmodium falciparum-infected erythrocytes is an equilibrative not an active process. *Mol. Biochem. Parasitol.* 82, 195–205. [https://doi.org/10.1016/0166-6851\(96\)02734-x](https://doi.org/10.1016/0166-6851(96)02734-x)
- Kirk, K., Saliba, K.J., 2007. Targeting nutrient uptake mechanisms in Plasmodium. *Curr. Drug Targets* 8, 75–88. <https://doi.org/10.2174/138945007779315560>
- Klaus, S., Binder, P., Kim, J., Machado, M., Funaya, C., Schaaf, V., Klaschka, D., Kudulyte, A., Cyrklaff, M., Laketa, V., Höfer, T., Guizetti, J., Becker, N.B., Frischknecht, F., Schwarz, U.S., Ganter, M., 2022. Asynchronous nuclear cycles in multinucleated Plasmodium falciparum facilitate rapid proliferation. *Sci. Adv.* 8, eabj5362. <https://doi.org/10.1126/sciadv.abj5362>

- Koch, M., Baum, J., 2016. The mechanics of malaria parasite invasion of the human erythrocyte – towards a reassessment of the host cell contribution. *Cell. Microbiol.* 18, 319–329. <https://doi.org/10.1111/cmi.12557>
- Köhler, S., Delwiche, C.F., Denny, P.W., Tilney, L.G., Webster, P., Wilson, R.J., Palmer, J.D., Roos, D.S., 1997. A plastid of probable green algal origin in Apicomplexan parasites. *Science* 275, 1485–1489. <https://doi.org/10.1126/science.275.5305.1485>
- Kono, M., Herrmann, S., Loughran, N.B., Cabrera, A., Engelberg, K., Lehmann, C., Sinha, D., Prinz, B., Ruch, U., Heussler, V., Spielmann, T., Parkinson, J., Gilberger, T.W., 2012. Evolution and architecture of the inner membrane complex in asexual and sexual stages of the malaria parasite. *Mol. Biol. Evol.* 29, 2113–2132. <https://doi.org/10.1093/molbev/mss081>
- Kori, L.D., Valecha, N., Anvikar, A.R., 2018. Insights into the early liver stage biology of *Plasmodium*. *J. Vector Borne Dis.* 55, 9–13. <https://doi.org/10.4103/0972-9062.234631>
- Koussis, K., Withers-Martinez, C., Yeoh, S., Child, M., Hackett, F., Knuepfer, E., Juliano, L., Woehlbier, U., Bujard, H., Blackman, M.J., 2009. A multifunctional serine protease primes the malaria parasite for red blood cell invasion. *EMBO J.* 28, 725–735. <https://doi.org/10.1038/emboj.2009.22>
- Kraemer, S.M., Smith, J.D., 2006. A family affair: var genes, PfEMP1 binding, and malaria disease. *Curr. Opin. Microbiol.* 9, 374–380. <https://doi.org/10.1016/j.mib.2006.06.006>
- Kriek, N., Tilley, L., Horrocks, P., Pinches, R., Elford, B.C., Ferguson, D.J.P., Lingelbach, K., Newbold, C.I., 2003. Characterization of the pathway for transport of the cytoadherence-mediating protein, PfEMP1, to the host cell surface in malaria parasite-infected erythrocytes. *Mol. Microbiol.* 50, 1215–1227. <https://doi.org/10.1046/j.1365-2958.2003.03784.x>
- Külzer, S., Charnaud, S., Dagan, T., Riedel, J., Mandal, P., Pesce, E.R., Blatch, G.L., Crabb, B.S., Gilson, P.R., Przyborski, J.M., 2012. *Plasmodium falciparum*-encoded exported hsp70/hsp40 chaperone/co-chaperone complexes within the host erythrocyte. *Cell. Microbiol.* 14, 1784–1795. <https://doi.org/10.1111/j.1462-5822.2012.01840.x>
- Külzer, S., Rug, M., Brinkmann, K., Cannon, P., Cowman, A., Lingelbach, K., Blatch, G.L., Maier, A.G., Przyborski, J.M., 2010. Parasite-encoded Hsp40 proteins define novel mobile structures in the cytosol of the *P. falciparum*-infected erythrocyte. *Cell. Microbiol.* 12, 1398–1420. <https://doi.org/10.1111/j.1462-5822.2010.01477.x>
- Kyes, S., Pinches, R., Newbold, C., 2000. A simple RNA analysis method shows var and rif multigene family expression patterns in *Plasmodium falciparum*. *Mol. Biochem. Parasitol.* 105, 311–315. [https://doi.org/10.1016/s0166-6851\(99\)00193-0](https://doi.org/10.1016/s0166-6851(99)00193-0)
- Kyes, S.A., Christodoulou, Z., Raza, A., Horrocks, P., Pinches, R., Rowe, J.A., Newbold, C.I., 2003. A well-conserved *Plasmodium falciparum* var gene shows an unusual stage-specific transcript pattern. *Mol. Microbiol.* 48, 1339–1348.
- Kyes, S.A., Kraemer, S.M., Smith, J.D., 2007. Antigenic Variation in *Plasmodium falciparum*: Gene Organization and Regulation of the var Multigene Family. *Eukaryot. Cell* 6, 1511–1520. <https://doi.org/10.1128/EC.00173-07>
- Lalremruata, A., Jeyaraj, S., Engleitner, T., Joanny, F., Lang, A., Bèlard, S., Mombo-Ngoma, G., Ramharter, M., Kremsner, P.G., Mordmüller, B., Held, J., 2017. Species and genotype diversity of *Plasmodium* in malaria patients from Gabon analysed by next generation sequencing. *Malar. J.* 16, 398. <https://doi.org/10.1186/s12936-017-2044-0>
- Lambros, C., Vanderberg, J.P., 1979. Synchronization of *Plasmodium falciparum* erythrocytic stages in culture. *J. Parasitol.* 65, 418–420.
- Langreth, S.G., Jensen, J.B., Reese, R.T., Trager, W., 1978. Fine structure of human malaria in vitro. *J. Protozool.* 25, 443–452. <https://doi.org/10.1111/j.1550-7408.1978.tb04167.x>

- Langreth, S.G., Peterson, E., 1985. Pathogenicity, stability, and immunogenicity of a knobless clone of *Plasmodium falciparum* in Colombian owl monkeys. *Infect. Immun.* 47, 760–766. <https://doi.org/10.1128/iai.47.3.760-766.1985>
- Lauer, S., VanWye, J., Harrison, T., McManus, H., Samuel, B.U., Hiller, N.L., Mohandas, N., Haldar, K., 2000. Vacuolar uptake of host components, and a role for cholesterol and sphingomyelin in malarial infection. *EMBO J.* 19, 3556–3564. <https://doi.org/10.1093/emboj/19.14.3556>
- Laveran, A., 1880. Note sur un nouveau parasite trouvé dans le sang de plusieurs malades atteints de fièvre palustre. *Bull Acad Med* 9, 1235–6.
- Lavtsen, T., Salanti, A., Jensen, A.T., Arnot, D.E., Theander, T.G., 2003. Sub-grouping of *Plasmodium falciparum* 3D7 var genes based on sequence analysis of coding and non-coding regions. *Malar. J.* 2, 27. <https://doi.org/10.1186/1475-2875-2-27>
- Lazarus, M.D., Schneider, T.G., Taraschi, T.F., 2008. A new model for hemoglobin ingestion and transport by the human malaria parasite *Plasmodium falciparum*. *J. Cell Sci.* 121, 1937–1949. <https://doi.org/10.1242/jcs.023150>
- Lee, R.S., Waters, A.P., Brewer, J.M., 2018. A cryptic cycle in haematopoietic niches promotes initiation of malaria transmission and evasion of chemotherapy. *Nat. Commun.* 9, 1689. <https://doi.org/10.1038/s41467-018-04108-9>
- Leech, J.H., Barnwell, J.W., Miller, L.H., Howard, R.J., 1984. Identification of a strain-specific malarial antigen exposed on the surface of *Plasmodium falciparum*-infected erythrocytes. *J. Exp. Med.* 159, 1567–1575. <https://doi.org/10.1084/jem.159.6.1567>
- Lennartz, F., Adams, Y., Bengtsson, A., Olsen, R.W., Turner, L., Ndam, N.T., Ecklu-Mensah, G., Moussiliou, A., Ofori, M.F., Gamain, B., Lusingu, J.P., Petersen, J.E.V., Wang, C.W., Nunes-Silva, S., Jespersen, J.S., Lau, C.K.Y., Theander, T.G., Lavtsen, T., Hviid, L., Higgins, M.K., Jensen, A.T.R., 2017. Structure-Guided Identification of a Family of Dual Receptor-Binding PfEMP1 that Is Associated with Cerebral Malaria. *Cell Host Microbe* 21, 403–414. <https://doi.org/10.1016/j.chom.2017.02.009>
- Lennartz, F., Smith, C., Craig, A.G., Higgins, M.K., 2019. Structural insights into diverse modes of ICAM-1 binding by *Plasmodium falciparum*-infected erythrocytes. *Proc. Natl. Acad. Sci.* 116, 20124–20134. <https://doi.org/10.1073/pnas.1911900116>
- Lingelbach, K., Joiner, K.A., 1998. The parasitophorous vacuole membrane surrounding *Plasmodium* and *Toxoplasma*: An unusual compartment in infected cells. *J. Cell Sci.* 111, 1467–1475. <https://doi.org/10.1242/jcs.111.11.1467>
- Llorà-Batlle, O., Michel-Todó, L., Witmer, K., Toda, H., Fernández-Becerra, C., Baum, J., Cortés, A., 2020. Conditional expression of PfAP2-G for controlled massive sexual conversion in *Plasmodium falciparum*. *Sci. Adv.* 6, eaaz5057. <https://doi.org/10.1126/sciadv.aaz5057>
- Looker, O., Blanch, A.J., Liu, B., Nunez-Iglesias, J., McMillan, P.J., Tilley, L., Dixon, M.W.A., 2019. The knob protein KAHRP assembles into a ring-shaped structure that underpins virulence complex assembly. *PLoS Pathog.* 15, e1007761. <https://doi.org/10.1371/journal.ppat.1007761>
- Lopaticki, S., Maier, A.G., Thompson, J., Wilson, D.W., Tham, W.-H., Triglia, T., Gout, A., Speed, T.P., Beeson, J.G., Healer, J., Cowman, A.F., 2011. Reticulocyte and Erythrocyte Binding-Like Proteins Function Cooperatively in Invasion of Human Erythrocytes by Malaria Parasites. *Infect. Immun.* 79, 1107–1117. <https://doi.org/10.1128/IAI.01021-10>
- Lord, S.J., Velle, K.B., Mullins, R.D., Fritz-Laylin, L.K., 2020. SuperPlots: Communicating reproducibility and variability in cell biology. *J. Cell Biol.* 219, e202001064. <https://doi.org/10.1083/jcb.202001064>

- Low, L.M., Azasi, Y., Sherling, E.S., Garten, M., Zimmerberg, J., Tsuboi, T., Brzostowski, J., Mu, J., Blackman, M.J., Miller, L.H., 2019. Deletion of *Plasmodium falciparum* Protein RON3 Affects the Functional Translocation of Exported Proteins and Glucose Uptake. *mBio* 10, e01460-19. <https://doi.org/10.1128/mBio.01460-19>
- Magallón-Tejada, A., Machevo, S., Cisteró, P., Lavstsen, T., Aide, P., Rubio, M., Jiménez, A., Turner, L., Valmaseda, A., Gupta, H., De Las Salas, B., Mandomando, I., Wang, C.W., Petersen, J.E.V., Muñoz, J., Gascón, J., Macete, E., Alonso, P.L., Chitnis, C.E., Bassat, Q., Mayor, A., 2016. Cytoadhesion to gC1qR through *Plasmodium falciparum* Erythrocyte Membrane Protein 1 in Severe Malaria. *PLoS Pathog.* 12, e1006011. <https://doi.org/10.1371/journal.ppat.1006011>
- Magowan, C., Nunomura, W., Waller, K.L., Yeung, J., Liang, J., Van Dort, H., Low, P.S., Coppel, R.L., Mohandas, N., 2000. *Plasmodium falciparum* histidine-rich protein 1 associates with the band 3 binding domain of ankyrin in the infected red cell membrane. *Biochim. Biophys. Acta* 1502, 461–470. [https://doi.org/10.1016/s0925-4439\(00\)00069-7](https://doi.org/10.1016/s0925-4439(00)00069-7)
- Maier, A.G., Rug, M., O'Neill, M.T., Beeson, J.G., Marti, M., Reeder, J., Cowman, A.F., 2007. Skeleton-binding protein 1 functions at the parasitophorous vacuole membrane to traffic PfEMP1 to the *Plasmodium falciparum*-infected erythrocyte surface. *Blood* 109, 1289–1297. <https://doi.org/10.1182/blood-2006-08-043364>
- Maier, A.G., Rug, M., O'Neill, M.T., Brown, M., Chakravorty, S., Szestak, T., Chesson, J., Wu, Y., Hughes, K., Coppel, R.L., Newbold, C., Beeson, J.G., Craig, A., Crabb, B.S., Cowman, A.F., 2008. Exported proteins required for virulence and rigidity of *Plasmodium falciparum*-infected human erythrocytes. *Cell* 134, 48–61. <https://doi.org/10.1016/j.cell.2008.04.051>
- Maixner, F., Drescher, D., Boccalini, G., Piombino-Mascali, D., Janko, M., Berens-Riha, N., Kim, B.J., Gamble, M., Schatterny, J., Morty, R.E., Ludwig, M., Krause-Kyora, B., Stark, R., An, H.J., Neumann, J., Cipollini, G., Grimm, R., Kilian, N., Zink, A., 2023. Microscopic Evidence of Malaria Infection in Visceral Tissue from Medici Family, Italy. *Emerg. Infect. Dis.* 29, 1280–1283. <https://doi.org/10.3201/eid2906.230134>
- Marapana, D.S., Dagley, L.F., Sandow, J.J., Nebl, T., Triglia, T., Pasternak, M., Dickerman, B.K., Crabb, B.S., Gilson, P.R., Webb, A.I., Boddey, J.A., Cowman, A.F., 2018. Plasmepsin V cleaves malaria effector proteins in a distinct endoplasmic reticulum translocation interactome for export to the erythrocyte. *Nat. Microbiol.* 3, 1010–1022. <https://doi.org/10.1038/s41564-018-0219-2>
- Marsh, K., Forster, D., Waruiru, C., Mwangi, I., Winstanley, M., Marsh, V., Newton, C., Winstanley, P., Warn, P., Peshu, N., 1995. Indicators of life-threatening malaria in African children. *N. Engl. J. Med.* 332, 1399–1404. <https://doi.org/10.1056/NEJM199505253322102>
- Marti, M., Good, R.T., Rug, M., Knuepfer, E., Cowman, A.F., 2004. Targeting malaria virulence and remodeling proteins to the host erythrocyte. *Science* 306, 1930–1933. <https://doi.org/10.1126/science.1102452>
- Marti, M., Spielmann, T., 2013. Protein export in malaria parasites: many membranes to cross. *Curr. Opin. Microbiol.* 16, 445–451. <https://doi.org/10.1016/j.mib.2013.04.010>
- Martinez, M., Chen, W.D., Cova, M.M., Molnár, P., Mageswaran, S.K., Guérin, A., John, A.R.O., Lebrun, M., Chang, Y.-W., 2022. Rhoptry secretion system structure and priming in *Plasmodium falciparum* revealed using in situ cryo-electron tomography. *Nat. Microbiol.* 7, 1230–1238. <https://doi.org/10.1038/s41564-022-01171-3>
- Martinsen, E., Perkins, S., 2013. The diversity of *Plasmodium* and other haemosporidians: The intersection of taxonomy, phylogenetics and genomics. pp. 1–15.

- Mathieu, L.C., Cox, H., Early, A.M., Mok, S., Lazrek, Y., Paquet, J.-C., Ade, M.-P., Lucchi, N.W., Grant, Q., Udhayakumar, V., Alexandre, J.S., Demar, M., Ringwald, P., Neafsey, D.E., Fidock, D.A., Musset, L., 2020. Local emergence in Amazonia of *Plasmodium falciparum* k13 C580Y mutants associated with in vitro artemisinin resistance. *eLife* 9, e51015. <https://doi.org/10.7554/eLife.51015>
- Matthews, H., Duffy, C.W., Merrick, C.J., 2018. Checks and balances? DNA replication and the cell cycle in *Plasmodium*. *Parasit. Vectors* 11, 216. <https://doi.org/10.1186/s13071-018-2800-1>
- Matz, J.M., Goosmann, C., Brinkmann, V., Grützke, J., Ingmundson, A., Matuschewski, K., Kooij, T.W.A., 2015. The *Plasmodium berghei* translocon of exported proteins reveals spatiotemporal dynamics of tubular extensions. *Sci. Rep.* 5, 12532. <https://doi.org/10.1038/srep12532>
- Maurer, G., 1902. Die malaria perniciosa. *Zentralbl Bakteriol Parasitenkd.* 23, 695–719.
- Mayer, C., Slater, L., Erat, M.C., Konrat, R., Vakonakis, I., 2012. Structural Analysis of the *Plasmodium falciparum* Erythrocyte Membrane Protein 1 (PfEMP1) Intracellular Domain Reveals a Conserved Interaction Epitope. *J. Biol. Chem.* 287, 7182–7189. <https://doi.org/10.1074/jbc.M111.330779>
- McCulloch, R., Cobbold, C.A., Figueiredo, L., Jackson, A., Morrison, L.J., Mugnier, M.R., Papavasiliou, N., Schnauffer, A., Matthews, K., 2017. Emerging challenges in understanding trypanosome antigenic variation. *Emerg. Top. Life Sci.* 1, 585–592. <https://doi.org/10.1042/ETLS20170104>
- McFadden, G.I., Yeh, E., 2017. The apicoplast: now you see it, now you don't. *Int. J. Parasitol.* 47, 137–144. <https://doi.org/10.1016/j.ijpara.2016.08.005>
- McHugh, E., Batinovic, S., Hanssen, E., McMillan, P.J., Kenny, S., Griffin, M.D.W., Crawford, S., Trenholme, K.R., Gardiner, D.L., Dixon, M.W.A., Tilley, L., 2015. A repeat sequence domain of the ring-exported protein-1 of *Plasmodium falciparum* controls export machinery architecture and virulence protein trafficking. *Mol. Microbiol.* 98, 1101–1114. <https://doi.org/10.1111/mmi.13201>
- McLaren, D.J., Bannister, L.H., Trigg, P.I., Butcher, G.A., 1977. A freeze—fracture study on the parasite—erythrocyte interrelationship in *Plasmodium knowlesi* infections. *Bull. World Health Organ.* 55, 199–203.
- McLean, A.R.D., Opi, D.H., Stanisic, D.I., Cutts, J.C., Feng, G., Ura, A., Mueller, I., Rogerson, S.J., Beeson, J.G., Fowkes, F.J.I., 2021. High Antibodies to VAR2CSA in Response to Malaria Infection Are Associated With Improved Birthweight in a Longitudinal Study of Pregnant Women. *Front. Immunol.* 12, 644563. <https://doi.org/10.3389/fimmu.2021.644563>
- McMillan, P.J., Millet, C., Batinovic, S., Maiorca, M., Hanssen, E., Kenny, S., Muhle, R.A., Melcher, M., Fidock, D.A., Smith, J.D., Dixon, M.W.A., Tilley, L., 2013. Spatial and temporal mapping of the PfEMP1 export pathway in *Plasmodium falciparum*. *Cell. Microbiol.* 15, 1401–1418. <https://doi.org/10.1111/cmi.12125>
- Meijering, E., 2020. A bird's-eye view of deep learning in bioimage analysis. *Comput. Struct. Biotechnol. J.* 18, 2312–2325. <https://doi.org/10.1016/j.csbj.2020.08.003>
- Melcher, M., Muhle, R.A., Henrich, P.P., Kraemer, S.M., Avril, M., Vigan-Womas, I., Mercereau-Puijalon, O., Smith, J.D., Fidock, D.A., 2010. Identification of a Role for the PfEMP1 Semi-Conserved Head Structure in Protein Trafficking to the Surface of *Plasmodium falciparum* Infected Red Blood Cells. *Cell. Microbiol.* 12, 1446–1462. <https://doi.org/10.1111/j.1462-5822.2010.01481.x>
- Mercereau-Puijalon, O., Barale, J.-C., Bischoff, E., 2002. Three multigene families in *Plasmodium* parasites: facts and questions. *Int. J. Parasitol.* 32, 1323–1344. [https://doi.org/10.1016/s0020-7519\(02\)00111-x](https://doi.org/10.1016/s0020-7519(02)00111-x)

- Mercier, C., Adjogble, K.D.Z., Däubener, W., Delauw, M.-F.-C., 2005. Dense granules: are they key organelles to help understand the parasitophorous vacuole of all apicomplexa parasites? *Int. J. Parasitol.* 35, 829–849. <https://doi.org/10.1016/j.ijpara.2005.03.011>
- Mesén-Ramírez, P., Reinsch, F., Soares, A.B., Bergmann, B., Ullrich, A.-K., Tenzer, S., Spielmann, T., 2016. Stable Translocation Intermediates Jam Global Protein Export in *Plasmodium falciparum* Parasites and Link the PTEX Component EXP2 with Translocation Activity. *PLOS Pathog.* 12, e1005618. <https://doi.org/10.1371/journal.ppat.1005618>
- Metwally, N.G., Tilly, A.-K., Lubiana, P., Roth, L.K., Dörpinghaus, M., Lorenzen, S., Schuldt, K., Witt, S., Bachmann, A., Tidow, H., Gutschmann, T., Burmester, T., Roeder, T., Tannich, E., Bruchhaus, I., 2017. Characterisation of *Plasmodium falciparum* populations selected on the human endothelial receptors P-selectin, E-selectin, CD9 and CD151. *Sci. Rep.* 7, 4069. <https://doi.org/10.1038/s41598-017-04241-3>
- Mikkelsen, R.B., Kamber, M., Wadwa, K.S., Lin, P.S., Schmidt-Ullrich, R., 1988. The role of lipids in *Plasmodium falciparum* invasion of erythrocytes: a coordinated biochemical and microscopic analysis. *Proc. Natl. Acad. Sci. U. S. A.* 85, 5956–5960.
- Miller, L.H., Good, M.F., Milon, G., 1994. Malaria pathogenesis. *Science* 264, 1878–1883. <https://doi.org/10.1126/science.8009217>
- Miotto, O., Sekihara, M., Tachibana, S.-I., Yamauchi, M., Pearson, R.D., Amato, R., Gonçalves, S., Mehra, S., Noviyanti, R., Marfurt, J., Auburn, S., Price, R.N., Mueller, I., Ikeda, M., Mori, T., Hirai, M., Tavul, L., Hetzel, M.W., Laman, M., Barry, A.E., Ringwald, P., Ohashi, J., Hombhanje, F., Kwiatkowski, D.P., Mita, T., 2020. Emergence of artemisinin-resistant *Plasmodium falciparum* with kelch13 C580Y mutations on the island of New Guinea. *PLOS Pathog.* 16, e1009133. <https://doi.org/10.1371/journal.ppat.1009133>
- Moras, M., Lefevre, S.D., Ostuni, M.A., 2017. From Erythroblasts to Mature Red Blood Cells: Organelle Clearance in Mammals. *Front. Physiol.* 8, 1076. <https://doi.org/10.3389/fphys.2017.01076>
- Mosnier, L.O., Lavtsen, T., 2016. The role of EPCR in the pathogenesis of severe malaria. *Thromb. Res.* 141, S46–S49. [https://doi.org/10.1016/S0049-3848\(16\)30364-4](https://doi.org/10.1016/S0049-3848(16)30364-4)
- Mundwiler-Pachlatko, E., Beck, H.-P., 2013. Maurer’s clefts, the enigma of *Plasmodium falciparum*. *Proc. Natl. Acad. Sci. U. S. A.* 110, 19987–19994. <https://doi.org/10.1073/pnas.1309247110>
- Murk, A., unpublished. Characterisation of the interaction of *P. falciparum* infected erythrocytes and Human Brain Endothelial Cells (Dissertation). Christian-Albrechts-University.
- Murphy, S.C., Hiller, N.L., Harrison, T., Lomasney, J.W., Mohandas, N., Haldar, K., 2006. Lipid rafts and malaria parasite infection of erythrocytes. *Mol. Membr. Biol.* 23, 81–88. <https://doi.org/10.1080/09687860500473440>
- Naranjo Prado, I.C., 2020. Quest for factors involved in the extraction of transmembrane proteins from the PPM to the PVM and the effect of jamming PTEX on PfEMP1 export in *Plasmodium falciparum* (Dissertation). University of Hamburg.
- Newton, C., Hien, T.T., White, N., 2000. Cerebral malaria. *J. Neurol. Neurosurg. Psychiatry* 69, 433–441. <https://doi.org/10.1136/jnnp.69.4.433>
- Nguitragoon, W., Bokhari, A.A.B., Pillai, A.D., Rayavara, K., Sharma, P., Turpin, B., Aravind, L., Desai, S.A., 2011. Malaria parasite clag3 genes determine channel-mediated nutrient uptake by infected red blood cells. *Cell* 145, 665–677. <https://doi.org/10.1016/j.cell.2011.05.002>
- Noedl, H., Se, Y., Schaefer, K., Smith, B.L., Socheat, D., Fukuda, M.M., Artemisinin Resistance in Cambodia 1 (ARC1) Study Consortium, 2008. Evidence of artemisinin-

- resistant malaria in western Cambodia. *N. Engl. J. Med.* 359, 2619–2620. <https://doi.org/10.1056/NEJMc0805011>
- Nunes, M.C., Goldring, J.P.D., Doerig, C., Scherf, A., 2007. A novel protein kinase family in *Plasmodium falciparum* is differentially transcribed and secreted to various cellular compartments of the host cell. *Mol. Microbiol.* 63, 391–403. <https://doi.org/10.1111/j.1365-2958.2006.05521.x>
- Nunes-Silva, S., Dechavanne, S., Moussiliou, A., Pstrąg, N., Semblat, J.-P., Gangnard, S., Tuikue-Ndam, N., Deloron, P., Chêne, A., Gamain, B., 2015. Beninese children with cerebral malaria do not develop humoral immunity against the IT4-VAR19-DC8 PfEMP1 variant linked to EPCR and brain endothelial binding. *Malar. J.* 14, 493. <https://doi.org/10.1186/s12936-015-1008-5>
- Obaldia, N., Meibalan, E., Sa, J.M., Ma, S., Clark, M.A., Mejia, P., Moraes Barros, R.R., Otero, W., Ferreira, M.U., Mitchell, J.R., Milner, D.A., Huttenhower, C., Wirth, D.F., Duraisingh, M.T., Wellems, T.E., Marti, M., 2018. Bone Marrow Is a Major Parasite Reservoir in *Plasmodium vivax* Infection. *mBio* 9, e00625-18. <https://doi.org/10.1128/mBio.00625-18>
- Oberli, A., Zurbrügg, L., Rusch, S., Brand, F., Butler, M.E., Day, J.L., Cutts, E.E., Lavstsen, T., Vakonakis, I., Beck, H.-P., 2016. *Plasmodium falciparum* Plasmodium helical interspersed subtelomeric proteins contribute to cytoadherence and anchor *P. falciparum* erythrocyte membrane protein 1 to the host cell cytoskeleton. *Cell. Microbiol.* 18, 1415–1428. <https://doi.org/10.1111/cmi.12583>
- Oleinikov, A.V., Amos, E., Frye, I.T., Rossnagle, E., Mutabingwa, T.K., Fried, M., Duffy, P.E., 2009. High Throughput Functional Assays of the Variant Antigen PfEMP1 Reveal a Single Domain in the 3D7 *Plasmodium falciparum* Genome that Binds ICAM1 with High Affinity and Is Targeted by Naturally Acquired Neutralizing Antibodies. *PLOS Pathog.* 5, e1000386. <https://doi.org/10.1371/journal.ppat.1000386>
- Omelianczyk, R.I., Loh, H.P., Chew, M., Hoo, R., Baumgarten, S., Renia, L., Chen, J., Preiser, P.R., 2020. Rapid activation of distinct members of multigene families in *Plasmodium* spp. *Commun. Biol.* 3, 1–11. <https://doi.org/10.1038/s42003-020-1081-3>
- Otto, T.D., Assefa, S.A., Böhme, U., Sanders, M.J., Kwiatkowski, D., Berriman, M., Newbold, C., 2019. Evolutionary analysis of the most polymorphic gene family in *falciparum* malaria. *Wellcome Open Res.* 4, 193. <https://doi.org/10.12688/wellcomeopenres.15590.1>
- Pachlatko, E., Rusch, S., Müller, A., Hemphill, A., Tilley, L., Hanssen, E., Beck, H.-P., 2010. MAHRP2, an exported protein of *Plasmodium falciparum*, is an essential component of Maurer's cleft tethers. *Mol. Microbiol.* 77, 1136–1152. <https://doi.org/10.1111/j.1365-2958.2010.07278.x>
- Papakrivos, J., Newbold, C.I., Lingelbach, K., 2005. A potential novel mechanism for the insertion of a membrane protein revealed by a biochemical analysis of the *Plasmodium falciparum* cytoadherence molecule PfEMP-1. *Mol. Microbiol.* 55, 1272–1284. <https://doi.org/10.1111/j.1365-2958.2004.04468.x>
- Parkyn Schneider, M.P., Liu, B., Glock, P., Suttie, A., McHugh, E., Andrew, D., Batinovic, S., Williamson, N., Hanssen, E., McMillan, P., Hliscs, M., Tilley, L., Dixon, M.W.A., 2017. Disrupting assembly of the inner membrane complex blocks *Plasmodium falciparum* sexual stage development. *PLOS Pathog.* 13, e1006659. <https://doi.org/10.1371/journal.ppat.1006659>
- Pei, X., An, X., Guo, X., Tarnawski, M., Coppel, R., Mohandas, N., 2005. Structural and Functional Studies of Interaction between *Plasmodium falciparum* Knob-associated Histidine-rich Protein (KAHRP) and Erythrocyte Spectrin *. *J. Biol. Chem.* 280, 31166–31171. <https://doi.org/10.1074/jbc.M505298200>

- Peters, J.M., Fowler, E.V., Krause, D.R., Cheng, Q., Gatton, M.L., 2007. Differential changes in *Plasmodium falciparum* var transcription during adaptation to culture. *J. Infect. Dis.* 195, 748–755. <https://doi.org/10.1086/511436>
- Petersen, W., Külzer, S., Engels, S., Zhang, Q., Ingmundson, A., Rug, M., Maier, A.G., Przyborski, J.M., 2016. J-dot targeting of an exported HSP40 in *Plasmodium falciparum*-infected erythrocytes. *Int. J. Parasitol.* 46, 519–525. <https://doi.org/10.1016/j.ijpara.2016.03.005>
- Pradel, G., Frevert, U., 2001. Malaria sporozoites actively enter and pass through rat Kupffer cells prior to hepatocyte invasion. *Hepatology* 33, 1154–1165. <https://doi.org/10.1053/jhep.2001.24237>
- Proellocks, N.I., Herrmann, S., Buckingham, D.W., Hanssen, E., Hodges, E.K., Elsworth, B., Morahan, B.J., Coppel, R.L., Cooke, B.M., 2014. A lysine-rich membrane-associated PHISTb protein involved in alteration of the cytoadhesive properties of *Plasmodium falciparum*-infected red blood cells. *FASEB J. Off. Publ. Fed. Am. Soc. Exp. Biol.* 28, 3103–3113. <https://doi.org/10.1096/fj.14-250399>
- Qian, P., Wang, X., Zhong, C.-Q., Wang, J., Cai, M., Nguitragool, W., Li, J., Cui, H., Yuan, J., 2022. Inner membrane complex proteomics reveals a palmitoylation regulation critical for intraerythrocytic development of malaria parasite. *eLife* 11, e77447. <https://doi.org/10.7554/eLife.77447>
- Quadt, K.A., Barfod, L., Andersen, D., Bruun, J., Gyan, B., Hassenkam, T., Ofori, M.F., Hviid, L., 2012. The Density of Knobs on *Plasmodium falciparum*-Infected Erythrocytes Depends on Developmental Age and Varies among Isolates. *PLoS ONE* 7, e45658. <https://doi.org/10.1371/journal.pone.0045658>
- Rankin, K.E., Graewe, S., Heussler, V.T., Stanway, R.R., 2010. Imaging liver-stage malaria parasites. *Cell. Microbiol.* 12, 569–579. <https://doi.org/10.1111/j.1462-5822.2010.01454.x>
- Rask, T.S., Hansen, D.A., Theander, T.G., Gorm Pedersen, A., Lavstsen, T., 2010. *Plasmodium falciparum* Erythrocyte Membrane Protein 1 Diversity in Seven Genomes – Divide and Conquer. *PLoS Comput. Biol.* 6, e1000933. <https://doi.org/10.1371/journal.pcbi.1000933>
- Read, M., Sherwin, T., Holloway, S.P., Gull, K., Hyde, J.E., 1993. Microtubular organization visualized by immunofluorescence microscopy during erythrocytic schizogony in *Plasmodium falciparum* and investigation of post-translational modifications of parasite tubulin. *Parasitology* 106 (Pt 3), 223–232. <https://doi.org/10.1017/s0031182000075041>
- Recker, M., Buckee, C.O., Serazin, A., Kyes, S., Pinches, R., Christodoulou, Z., Springer, A.L., Gupta, S., Newbold, C.I., 2011. Antigenic variation in *Plasmodium falciparum* malaria involves a highly structured switching pattern. *PLoS Pathog.* 7, e1001306. <https://doi.org/10.1371/journal.ppat.1001306>
- Renn, J.P., Doritchamou, J.Y.A., Tentokam, B.C.N., Morrison, R.D., Cowles, M.V., Burkhardt, M., Ma, R., Mahamar, A., Attaher, O., Diarra, B.S., Traore, M., Dicko, A., Tolia, N.H., Fried, M., Duffy, P.E., 2021. Allelic variants of full-length VAR2CSA, the placental malaria vaccine candidate, differ in antigenicity and receptor binding affinity. *Commun. Biol.* 4, 1–12. <https://doi.org/10.1038/s42003-021-02787-7>
- Reyes, R.A., Raghavan, S.S.R., Hurlburt, N.K., Introini, V., Kana, I.H., Jensen, R.W., Martinez-Scholze, E., Gestal-Mato, M., Bau, C.B., Fernández-Quintero, M.L., Loeffler, J.R., Ferguson, J.A., Lee, W.-H., Martin, G.M., Theander, T.G., Ssewanyana, I., Feeney, M.E., Greenhouse, B., Bol, S., Ward, A.B., Bernabeu, M., Pancera, M., Turner, L., Bunnik, E.M., Lavstsen, T., 2024. Broadly inhibitory antibodies against severe malaria virulence proteins. *BioRxiv Prepr. Serv. Biol.* 2024.01.25.577124. <https://doi.org/10.1101/2024.01.25.577124>

- Ridley, R.T., 2000. The Dictator's Mistake: Caesar's Escape from Sulla. *Hist. Z. Für Alte Gesch.* 49, 211–229.
- Riglar, D.T., Rogers, K.L., Hanssen, E., Turnbull, L., Bullen, H.E., Charnaud, S.C., Przyborski, J., Gilson, P.R., Whitchurch, C.B., Crabb, B.S., Baum, J., Cowman, A.F., 2013. Spatial association with PTEX complexes defines regions for effector export into *Plasmodium falciparum*-infected erythrocytes. *Nat. Commun.* 4, 1415. <https://doi.org/10.1038/ncomms2449>
- Rivadeneira, E.M., Wasserman, M., Espinal, C.T., 1983. Separation and concentration of schizonts of *Plasmodium falciparum* by Percoll gradients. *J. Protozool.* 30, 367–370. <https://doi.org/10.1111/j.1550-7408.1983.tb02932.x>
- Roberts, D.J., Craig, A.G., Berendt, A.R., Pinches, R., Nash, G., Marsh, K., Newbold, C.I., 1992. Rapid switching to multiple antigenic and adhesive phenotypes in malaria. *Nature* 357, 689–692. <https://doi.org/10.1038/357689a0>
- Robinson, B.A., Welch, T.L., Smith, J.D., 2003. Widespread functional specialization of *Plasmodium falciparum* erythrocyte membrane protein 1 family members to bind CD36 analysed across a parasite genome. *Mol. Microbiol.* 47, 1265–1278. <https://doi.org/10.1046/j.1365-2958.2003.03378.x>
- Roth, E.F., 1987. Malarial parasite hexokinase and hexokinase-dependent glutathione reduction in the *Plasmodium falciparum*-infected human erythrocyte. *J. Biol. Chem.* 262, 15678–15682.
- Rottmann, M., Lavstsen, T., Mugasa, J.P., Kaestli, M., Jensen, A.T.R., Müller, D., Theander, T., Beck, H.-P., 2006. Differential Expression of var Gene Groups Is Associated with Morbidity Caused by *Plasmodium falciparum* Infection in Tanzanian Children. *Infect. Immun.* 74, 3904–3911. <https://doi.org/10.1128/IAI.02073-05>
- Roux, K.J., Kim, D.I., Raida, M., Burke, B., 2012. A promiscuous biotin ligase fusion protein identifies proximal and interacting proteins in mammalian cells. *J. Cell Biol.* 196, 801–810. <https://doi.org/10.1083/jcb.201112098>
- Rowe, J.A., Kyes, S.A., Rogerson, S.J., Babiker, H.A., Raza, A., 2002. Identification of a conserved *Plasmodium falciparum* var gene implicated in malaria in pregnancy. *J. Infect. Dis.* 185, 1207–1211. <https://doi.org/10.1086/339684>
- Rowe, J.A., Moulds, J.M., Newbold, C.I., Miller, L.H., 1997. *P. falciparum* rosetting mediated by a parasite-variant erythrocyte membrane protein and complement-receptor 1. *Nature* 388, 292–295. <https://doi.org/10.1038/40888>
- Ruecker, A., Shea, M., Hackett, F., Suarez, C., Hirst, E.M.A., Milutinovic, K., Withers-Martinez, C., Blackman, M.J., 2012. Proteolytic Activation of the Essential Parasitophorous Vacuole Cysteine Protease SERA6 Accompanies Malaria Parasite Egress from Its Host Erythrocyte. *J. Biol. Chem.* 287, 37949–37963. <https://doi.org/10.1074/jbc.M112.400820>
- Rug, M., Cyrklaff, M., Mikkonen, A., Lemgruber, L., Kuelzer, S., Sanchez, C.P., Thompson, J., Hanssen, E., O'Neill, M., Langer, C., Lanzer, M., Frischknecht, F., Maier, A.G., Cowman, A.F., 2014. Export of virulence proteins by malaria-infected erythrocytes involves remodeling of host actin cytoskeleton. *Blood* 124, 3459–3468. <https://doi.org/10.1182/blood-2014-06-583054>
- Rug, M., Prescott, S.W., Fernandez, K.M., Cooke, B.M., Cowman, A.F., 2006. The role of KAHRP domains in knob formation and cytoadherence of *P. falciparum*-infected human erythrocytes. *Blood* 108, 370–378. <https://doi.org/10.1182/blood-2005-11-4624>
- Russell, A.J.C., Sanderson, T., Bushell, E., Talman, A.M., Anar, B., Girling, G., Hunziker, M., Kent, R.S., Martin, J.S., Metcalf, T., Montandon, R., Pandey, V., Pardo, M., Roberts, A.B., Sayers, C., Schwach, F., Choudhary, J.S., Rayner, J.C., Voet, T., Modrzynska, K.K., Waters, A.P., Lawniczak, M.K.N., Billker, O., 2023. Regulators of male and

- female sexual development are critical for the transmission of a malaria parasite. *Cell Host Microbe* 31, 305–319. <https://doi.org/10.1016/j.chom.2022.12.011>
- Russo, I., Babbitt, S., Muralidharan, V., Butler, T., Oksman, A., Goldberg, D.E., 2010. Plasmeprin V licenses Plasmodium proteins for export into the host erythrocyte. *Nature* 463, 632–636. <https://doi.org/10.1038/nature08726>
- Sabitzki, R., Schmitt, M., Flemming, S., Jonscher, E., Höhn, K., Fröhlke, U., Spielmann, T., 2023. Identification of a Rabenosyn-5 like protein and Rab5b in host cell cytosol uptake reveals conservation of endosomal transport in malaria parasites. <https://doi.org/10.1101/2023.04.05.535711>
- Sachanonta, N., Chotivanich, K., Chaisri, U., Turner, G.D.H., Ferguson, D.J.P., Day, N.P.J., Pongponratn, E., 2011. Ultrastructural and Real-time Microscopic Changes in *P. falciparum*-infected Red Blood Cells Following Treatment with Antimalarial Drugs. *Ultrastruct. Pathol.* 35, 214–225. <https://doi.org/10.3109/01913123.2011.601405>
- Sadasivaiah, S., Tozan, Y., Breman, J.G., 2007. Dichlorodiphenyltrichloroethane (DDT) for indoor residual spraying in Africa: how can it be used for malaria control? *Am. J. Trop. Med. Hyg.* 77, 249–263.
- Salanti, A., Dahlbäck, M., Turner, L., Nielsen, M.A., Barfod, L., Magistrado, P., Jensen, A.T.R., Lavstsen, T., Ofori, M.F., Marsh, K., Hviid, L., Theander, T.G., 2004. Evidence for the Involvement of VAR2CSA in Pregnancy-associated Malaria. *J. Exp. Med.* 200, 1197–1203. <https://doi.org/10.1084/jem.20041579>
- Salanti, A., Jensen, A.T.R., Zornig, H.D., Staalsoe, T., Joergensen, L., Nielsen, M.A., Khattab, A., Arnot, D.E., Klinkert, M.Q., Hviid, L., Theander, T.G., 2002. A sub-family of common and highly conserved Plasmodium falciparum var genes. *Mol. Biochem. Parasitol.* 122, 111–115. [https://doi.org/10.1016/s0166-6851\(02\)00080-4](https://doi.org/10.1016/s0166-6851(02)00080-4)
- Salanti, A., Staalsoe, T., Lavstsen, T., Jensen, A.T.R., Sowa, M.P.K., Arnot, D.E., Hviid, L., Theander, T.G., 2003. Selective upregulation of a single distinctly structured var gene in chondroitin sulphate A-adhering Plasmodium falciparum involved in pregnancy-associated malaria. *Mol. Microbiol.* 49, 179–191. <https://doi.org/10.1046/j.1365-2958.2003.03570.x>
- Sampath, S., Brazier, A.J., Avril, M., Bernabeu, M., Vigdorovich, V., Mascarenhas, A., Gomes, E., Sather, D.N., Esmon, C.T., Smith, J.D., 2015. Plasmodium falciparum adhesion domains linked to severe malaria differ in blockade of endothelial protein C receptor. *Cell. Microbiol.* 17, 1868–1882. <https://doi.org/10.1111/cmi.12478>
- Sanchez, C.P., Karathanasis, C., Sanchez, R., Cyrklaff, M., Jäger, J., Buchholz, B., Schwarz, U.S., Heilemann, M., Lanzer, M., 2019. Single-molecule imaging and quantification of the immune-variant adhesin VAR2CSA on knobs of Plasmodium falciparum-infected erythrocytes. *Commun. Biol.* 2, 1–9. <https://doi.org/10.1038/s42003-019-0429-z>
- Sander, A.F., Salanti, A., Lavstsen, T., Nielsen, M.A., Magistrado, P., Lusingu, J., Ndam, N.T., Arnot, D.E., 2009. Multiple var2csa-type PfEMP1 genes located at different chromosomal loci occur in many Plasmodium falciparum isolates. *PloS One* 4, e6667. <https://doi.org/10.1371/journal.pone.0006667>
- Sanders, P.R., Dickerman, B.K., Charnaud, S.C., Ramsland, P.A., Crabb, B.S., Gilson, P.R., 2019. The N-terminus of EXP2 forms the membrane-associated pore of the protein exporting translocon PTEX in Plasmodium falciparum. *J. Biochem. (Tokyo)* 165, 239–248. <https://doi.org/10.1093/jb/mvy099>
- Sanders, P.R., Gilson, P.R., Cantin, G.T., Greenbaum, D.C., Nebl, T., Carucci, D.J., McConville, M.J., Schofield, L., Hodder, A.N., Yates, J.R., Crabb, B.S., 2005. Distinct protein classes including novel merozoite surface antigens in Raft-like membranes of Plasmodium falciparum. *J. Biol. Chem.* 280, 40169–40176. <https://doi.org/10.1074/jbc.M509631200>

- Sargeant, T.J., Marti, M., Caler, E., Carlton, J.M., Simpson, K., Speed, T.P., Cowman, A.F., 2006. Lineage-specific expansion of proteins exported to erythrocytes in malaria parasites. *Genome Biol.* 7, R12. <https://doi.org/10.1186/gb-2006-7-2-r12>
- Scherf, A., Hernandez-Rivas, R., Buffet, P., Bottius, E., Benatar, C., Pouvelle, B., Gysin, J., Lanzer, M., 1998. Antigenic variation in malaria: in situ switching, relaxed and mutually exclusive transcription of var genes during intra-erythrocytic development in *Plasmodium falciparum*. *EMBO J.* 17, 5418–5426. <https://doi.org/10.1093/emboj/17.18.5418>
- Schindelin, J., Arganda-Carreras, I., Frise, E., Kaynig, V., Longair, M., Pietzsch, T., Preibisch, S., Rueden, C., Saalfeld, S., Schmid, B., Tinevez, J.-Y., White, D.J., Hartenstein, V., Eliceiri, K., Tomancak, P., Cardona, A., 2012. Fiji: an open-source platform for biological-image analysis. *Nat. Methods* 9, 676–682. <https://doi.org/10.1038/nmeth.2019>
- Schneider, V.M., Visone, J.E., Harris, C.T., Florini, F., Hadjimichael, E., Zhang, X., Gross, M.R., Rhee, K.Y., Ben Mamoun, C., Kafsack, B.F.C., Deitsch, K.W., 2023. The human malaria parasite *Plasmodium falciparum* can sense environmental changes and respond by antigenic switching. *Proc. Natl. Acad. Sci.* 120, e2302152120. <https://doi.org/10.1073/pnas.2302152120>
- Schnider, C.B., Bausch-Fluck, D., Brühlmann, F., Heussler, V.T., Burda, P.-C., 2018. BioID Reveals Novel Proteins of the *Plasmodium* Parasitophorous Vacuole Membrane. *mSphere* 3, 10.1128/msphere.00522-17. <https://doi.org/10.1128/msphere.00522-17>
- Schulze, J., Kwiatkowski, M., Borner, J., Schlüter, H., Bruchhaus, I., Burmester, T., Spielmann, T., Pick, C., 2015. The *Plasmodium falciparum* exportome contains non-canonical PEXEL/HT proteins. *Mol. Microbiol.* 97, 301–314. <https://doi.org/10.1111/mmi.13024>
- Schureck, M.A., Darling, J.E., Merk, A., Shao, J., Daggupati, G., Srinivasan, P., Olinares, P.D.B., Rout, M.P., Chait, B.T., Wollenberg, K., Subramaniam, S., Desai, S.A., 2021. Malaria parasites use a soluble RhopH complex for erythrocyte invasion and an integral form for nutrient uptake. *eLife* 10, e65282. <https://doi.org/10.7554/eLife.65282>
- Sherling, E.S., Knuepfer, E., Brzostowski, J.A., Miller, L.H., Blackman, M.J., van Ooij, C., 2017. The *Plasmodium falciparum* rhoptry protein RhopH3 plays essential roles in host cell invasion and nutrient uptake. *eLife* 6, e23239. <https://doi.org/10.7554/eLife.23239>
- Silvestrini, F., Alano, P., Williams, J.L., 2000. Commitment to the production of male and female gametocytes in the human malaria parasite *Plasmodium falciparum*. *Parasitology* 121 Pt 5, 465–471. <https://doi.org/10.1017/s0031182099006691>
- Sinden, R.E., 1982. Gametocytogenesis of *Plasmodium falciparum* in vitro: an electron microscopic study. *Parasitology* 84, 1–11. <https://doi.org/10.1017/s003118200005160x>
- Sinha, A., Hughes, K.R., Modrzynska, K.K., Otto, T.D., Pfander, C., Dickens, N.J., Religa, A.A., Bushell, E., Graham, A.L., Cameron, R., Kafsack, B.F.C., Williams, A.E., Llinas, M., Berriman, M., Billker, O., Waters, A.P., 2014. A cascade of DNA-binding proteins for sexual commitment and development in *Plasmodium*. *Nature* 507, 253–257. <https://doi.org/10.1038/nature12970>
- Sinka, M.E., Bangs, M.J., Manguin, S., Coetzee, M., Mbogo, C.M., Hemingway, J., Patil, A.P., Temperley, W.H., Gething, P.W., Kabaria, C.W., Okara, R.M., Van Boeckel, T., Godfray, H.C.J., Harbach, R.E., Hay, S.I., 2010. The dominant Anopheles vectors of human malaria in Africa, Europe and the Middle East: occurrence data, distribution maps and bionomic précis. *Parasit. Vectors* 3, 117. <https://doi.org/10.1186/1756-3305-3-117>
- Sinka, M.E., Bangs, M.J., Manguin, S., Rubio-Palis, Y., Chareonviriyaphap, T., Coetzee, M., Mbogo, C.M., Hemingway, J., Patil, A.P., Temperley, W.H., Gething, P.W., Kabaria,

- C.W., Burkot, T.R., Harbach, R.E., Hay, S.I., 2012. A global map of dominant malaria vectors. *Parasit. Vectors* 5, 69. <https://doi.org/10.1186/1756-3305-5-69>
- Smith, J.D., 2014. The role of PfEMP1 adhesion domain classification in *Plasmodium falciparum* pathogenesis research. *Mol. Biochem. Parasitol.* 195, 82–87. <https://doi.org/10.1016/j.molbiopara.2014.07.006>
- Smith, J.D., Chitnis, C.E., Craig, A.G., Roberts, D.J., Hudson-Taylor, D.E., Peterson, D.S., Pinches, R., Newbold, C.I., Miller, L.H., 1995. Switches in Expression of *Plasmodium falciparum* var Genes Correlate with Changes in Antigenic and Cytoadherent Phenotypes of Infected Erythrocytes. *Cell* 82, 101–110.
- Smith, J.D., Craig, A.G., Kriek, N., Hudson-Taylor, D., Kyes, S., Fagan, T., Pinches, R., Baruch, D.I., Newbold, C.I., Miller, L.H., 2000. Identification of a *Plasmodium falciparum* intercellular adhesion molecule-1 binding domain: a parasite adhesion trait implicated in cerebral malaria. *Proc. Natl. Acad. Sci. U. S. A.* 97, 1766–1771. <https://doi.org/10.1073/pnas.040545897>
- Soldati, D., 1999. The apicoplast as a potential therapeutic target in and other apicomplexan parasites. *Parasitol. Today Pers. Ed* 15, 5–7. [https://doi.org/10.1016/s0169-4758\(98\)01363-5](https://doi.org/10.1016/s0169-4758(98)01363-5)
- Sommi Picenardi, G., 1888. Esumazione e ricognizione delle ceneri dei principi Medicei fatta nell' anno 1857: processo verbale e note. Direzione dell' Archivio Storico Italiano.
- Spielmann, T., Ferguson, D.J.P., Beck, H.-P., 2003. etramps, a new *Plasmodium falciparum* gene family coding for developmentally regulated and highly charged membrane proteins located at the parasite-host cell interface. *Mol. Biol. Cell* 14, 1529–1544. <https://doi.org/10.1091/mbc.e02-04-0240>
- Spielmann, T., Gardiner, D.L., Beck, H.-P., Trenholme, K.R., Kemp, D.J., 2006a. Organization of ETRAMPs and EXP-1 at the parasite-host cell interface of malaria parasites. *Mol. Microbiol.* 59, 779–794. <https://doi.org/10.1111/j.1365-2958.2005.04983.x>
- Spielmann, T., Gilberger, T.-W., 2015. Critical Steps in Protein Export of *Plasmodium falciparum* Blood Stages. *Trends Parasitol.* 31, 514–525. <https://doi.org/10.1016/j.pt.2015.06.010>
- Spielmann, T., Gilberger, T.-W., 2010. Protein export in malaria parasites: do multiple export motifs add up to multiple export pathways? *Trends Parasitol.* 26, 6–10. <https://doi.org/10.1016/j.pt.2009.10.001>
- Spielmann, T., Gras, S., Sabitzki, R., Meissner, M., 2020. Endocytosis in *Plasmodium* and *Toxoplasma* Parasites. *Trends Parasitol.* 36, 520–532. <https://doi.org/10.1016/j.pt.2020.03.010>
- Spielmann, T., Hawthorne, P.L., Dixon, M.W.A., Hannemann, M., Klotz, K., Kemp, D.J., Klonis, N., Tilley, L., Trenholme, K.R., Gardiner, D.L., 2006b. A cluster of ring stage-specific genes linked to a locus implicated in cytoadherence in *Plasmodium falciparum* codes for PEXEL-negative and PEXEL-positive proteins exported into the host cell. *Mol. Biol. Cell* 17, 3613–3624. <https://doi.org/10.1091/mbc.e06-04-0291>
- Spielmann, T., Montagna, G.N., Hecht, L., Matuschewski, K., 2012. Molecular make-up of the *Plasmodium parasitophorous* vacuolar membrane. *Int. J. Med. Microbiol. IJMM* 302, 179–186. <https://doi.org/10.1016/j.ijmm.2012.07.011>
- Spycher, C., Rug, M., Pachlatko, E., Hanssen, E., Ferguson, D., Cowman, A.F., Tilley, L., Beck, H.-P., 2008. The Maurer's cleft protein MAHRP1 is essential for trafficking of PfEMP1 to the surface of *Plasmodium falciparum*-infected erythrocytes. *Mol. Microbiol.* 68, 1300–1314. <https://doi.org/10.1111/j.1365-2958.2008.06235.x>
- Stäcker, J., 2021. Functional analysis of trophozoite- and schizont-exported proteins of the human malaria parasite *Plasmodium falciparum* (Welch 1897) (Dissertation). University of Hamburg.

- Stallmach, R., Kavishwar, M., Withers-Martinez, C., Hackett, F., Collins, C.R., Howell, S.A., Yeoh, S., Knuepfer, E., Atid, A.J., Holder, A.A., Blackman, M.J., 2015. Plasmodium falciparum SERA5 plays a non-enzymatic role in the malarial asexual blood-stage lifecycle. *Mol. Microbiol.* 96, 368–387. <https://doi.org/10.1111/mmi.12941>
- Stewart, L.B., Freville, A., Voss, T.S., Baker, D.A., Awandare, G.A., Conway, D.J., 2022. Plasmodium falciparum Sexual Commitment Rate Variation among Clinical Isolates and Diverse Laboratory-Adapted Lines. *Microbiol. Spectr.* 10, e02234-22. <https://doi.org/10.1128/spectrum.02234-22>
- Stirling, D.R., Swain-Bowden, M.J., Lucas, A.M., Carpenter, A.E., Cimini, B.A., Goodman, A., 2021. CellProfiler 4: improvements in speed, utility and usability. *BMC Bioinformatics* 22, 433. <https://doi.org/10.1186/s12859-021-04344-9>
- Stokes, B.H., Dhingra, S.K., Rubiano, K., Mok, S., Straimer, J., Gnädig, N.F., Deni, I., Schindler, K.A., Bath, J.R., Ward, K.E., Striepen, J., Yeo, T., Ross, L.S., Legrand, E., Arie, F., Cunningham, C.H., Souleymane, I.M., Gansané, A., Nzoumbou-Boko, R., Ndayikunda, C., Kabanywany, A.M., Uwimana, A., Smith, S.J., Kolley, O., Ndounga, M., Warsame, M., Leang, R., Nosten, F., Anderson, T.J., Rosenthal, P.J., Ménard, D., Fidock, D.A., 2021. Plasmodium falciparum K13 mutations in Africa and Asia impact artemisinin resistance and parasite fitness. *eLife* 10, e66277. <https://doi.org/10.7554/eLife.66277>
- Sturm, A., Amino, R., van de Sand, C., Regen, T., Retzlaff, S., Rennenberg, A., Krueger, A., Pollok, J.-M., Menard, R., Heussler, V.T., 2006. Manipulation of Host Hepatocytes by the Malaria Parasite for Delivery into Liver Sinusoids. *Science* 313, 1287–1290. <https://doi.org/10.1126/science.1129720>
- Su, X.Z., Heatwole, V.M., Wertheimer, S.P., Guinet, F., Herrfeldt, J.A., Peterson, D.S., Ravetch, J.A., Wellems, T.E., 1995. The large diverse gene family var encodes proteins involved in cytoadherence and antigenic variation of Plasmodium falciparum-infected erythrocytes. *Cell* 82, 89–100. [https://doi.org/10.1016/0092-8674\(95\)90055-1](https://doi.org/10.1016/0092-8674(95)90055-1)
- Suarez, C., Volkmann, K., Gomes, A.R., Billker, O., Blackman, M.J., 2013. The Malarial Serine Protease SUB1 Plays an Essential Role in Parasite Liver Stage Development. *PLOS Pathog.* 9, e1003811. <https://doi.org/10.1371/journal.ppat.1003811>
- Takano, R., Kozuka-Hata, H., Kondoh, D., Bochimoto, H., Oyama, M., Kato, K., 2019. A High-Resolution Map of SBP1 Interactomes in Plasmodium falciparum-infected Erythrocytes. *iScience* 19, 703–714. <https://doi.org/10.1016/j.isci.2019.07.035>
- Tarr, S.J., Moon, R.W., Hardege, I., Osborne, A.R., 2014. A conserved domain targets exported PHISTb family proteins to the periphery of Plasmodium infected erythrocytes. *Mol. Biochem. Parasitol.* 196, 29–40. <https://doi.org/10.1016/j.molbiopara.2014.07.011>
- Tawk, L., Lacroix, C., Gueirard, P., Kent, R., Gorgette, O., Thiberge, S., Mercereau-Puijalon, O., Ménard, R., Barale, J.-C., 2013. A Key Role for Plasmodium Subtilisin-like SUB1 Protease in Egress of Malaria Parasites from Host Hepatocytes. *J. Biol. Chem.* 288, 33336–33346. <https://doi.org/10.1074/jbc.M113.513234>
- Thomas, J.A., Collins, C.R., Das, S., Hackett, F., Graindorge, A., Bell, D., Deu, E., Blackman, M.J., 2016. Development and Application of a Simple Plaque Assay for the Human Malaria Parasite Plasmodium falciparum. *PLoS ONE* 11, e0157873. <https://doi.org/10.1371/journal.pone.0157873>
- Thomas, J.A., Tan, M.S.Y., Bisson, C., Borg, A., Umrekar, T.R., Hackett, F., Hale, V.L., Vizcay-Barrena, G., Fleck, R.A., Snijders, A.P., Saibil, H.R., Blackman, M.J., 2018. A protease cascade regulates release of the human malaria parasite Plasmodium falciparum from host red blood cells. *Nat. Microbiol.* 3, 447–455. <https://doi.org/10.1038/s41564-018-0111-0>

- Tibúrcio, M., Hitz, E., Niederwieser, I., Kelly, G., Davies, H., Doerig, C., Billker, O., Voss, T.S., Treeck, M., 2021. A 39-Amino-Acid C-Terminal Truncation of GDV1 Disrupts Sexual Commitment in *Plasmodium falciparum*. *mSphere* 6, e01093-20. <https://doi.org/10.1128/mSphere.01093-20>
- Toso, M.A., Omoto, C.K., 2007. Gregarina niphandrodes may lack both a plastid genome and organelle. *J. Eukaryot. Microbiol.* 54, 66–72. <https://doi.org/10.1111/j.1550-7408.2006.00229.x>
- Trager, W., Jensen, J.B., 1976. Human malaria parasites in continuous culture. *Science* 193, 673–675. <https://doi.org/10.1126/science.781840>
- Trager, W., Rudzinska, M.A., Bradbury, P.C., 1966. The fine structure of *Plasmodium falciparum* and its host erythrocytes in natural malarial infections in man. *Bull. World Health Organ.* 35, 883–885.
- Trimnell, A.R., Kraemer, S.M., Mukherjee, S., Phippard, D.J., Janes, J.H., Flamoe, E., Su, X., Awadalla, P., Smith, J.D., 2006. Global genetic diversity and evolution of var genes associated with placental and severe childhood malaria. *Mol. Biochem. Parasitol.* 148, 169–180. <https://doi.org/10.1016/j.molbiopara.2006.03.012>
- Turner, L., Lavstsen, T., Berger, S.S., Wang, C.W., Petersen, J.E.V., Avril, M., Brazier, A.J., Freeth, J., Jespersen, J.S., Nielsen, M.A., Magistrado, P., Lusingu, J., Smith, J.D., Higgins, M.K., Theander, T.G., 2013. Severe malaria is associated with parasite binding to endothelial protein C receptor. *Nature* 498, 502–505. <https://doi.org/10.1038/nature12216>
- Tyanova, S., Temu, T., Sinitcyn, P., Carlson, A., Hein, M.Y., Geiger, T., Mann, M., Cox, J., 2016. The Perseus computational platform for comprehensive analysis of (prote)omics data. *Nat. Methods* 13, 731–740. <https://doi.org/10.1038/nmeth.3901>
- Ukaegbu, U.E., Zhang, X., Heinberg, A.R., Wele, M., Chen, Q., Deitsch, K.W., 2015. A Unique Virulence Gene Occupies a Principal Position in Immune Evasion by the Malaria Parasite *Plasmodium falciparum*. *PLoS Genet.* 11, e1005234. <https://doi.org/10.1371/journal.pgen.1005234>
- Usui, M., Prajapati, S.K., Ayanful-Torgby, R., Acquah, F.K., Cudjoe, E., Kakaney, C., Amponsah, J.A., Obboh, E.K., Reddy, D.K., Barbeau, M.C., Simons, L.M., Czesny, B., Raiciulescu, S., Olsen, C., Abuaku, B.K., Amoah, L.E., Williamson, K.C., 2019. *Plasmodium falciparum* sexual differentiation in malaria patients is associated with host factors and GDV1-dependent genes. *Nat. Commun.* 10, 2140. <https://doi.org/10.1038/s41467-019-10172-6>
- Uwimana, A., Legrand, E., Stokes, B.H., Ndikumana, J.-L.M., Warsame, M., Umulisa, N., Ngamije, D., Munyaneza, T., Mazarati, J.-B., Munguti, K., Campagne, P., Criscuolo, A., Ariey, F., Murindahabi, M., Ringwald, P., Fidock, D.A., Mbituyumuremyi, A., Menard, D., 2020. Emergence and clonal expansion of in vitro artemisinin-resistant *Plasmodium falciparum* kelch13 R561H mutant parasites in Rwanda. *Nat. Med.* 26, 1602–1608. <https://doi.org/10.1038/s41591-020-1005-2>
- Uwimana, A., Umulisa, N., Venkatesan, M., Szigel, S.S., Zhou, Z., Munyaneza, T., Habimana, R.M., Rucogoza, A., Moriarty, L.F., Sandford, R., Piercefield, E., Goldman, I., Ezema, B., Talundzic, E., Pacheco, M.A., Escalante, A.A., Ngamije, D., Mangala, J.-L.N., Kabera, M., Munguti, K., Murindahabi, M., Brieger, W., Musanabaganwa, C., Mutesa, L., Udhayakumar, V., Mbituyumuremyi, A., Halsey, E.S., Lucchi, N.W., 2021. Association of *Plasmodium falciparum* kelch13 R561H genotypes with delayed parasite clearance in Rwanda: an open-label, single-arm, multicentre, therapeutic efficacy study. *Lancet Infect. Dis.* 21, 1120–1128. [https://doi.org/10.1016/S1473-3099\(21\)00142-0](https://doi.org/10.1016/S1473-3099(21)00142-0)
- Vaaben, A.V., 2018. Discovery and characterization of host-parasite interactions associated with severe malaria.

- van Ooij, C., Tamez, P., Bhattacharjee, S., Hiller, N.L., Harrison, T., Liolios, K., Kooij, T., Ramesar, J., Balu, B., Adams, J., Waters, A., Janse, C., Haldar, K., 2008. The Malaria Secretome: From Algorithms to Essential Function in Blood Stage Infection. *PLoS Pathog.* 4, e1000084. <https://doi.org/10.1371/journal.ppat.1000084>
- Venugopal, K., Hentzschel, F., Valkiūnas, G., Marti, M., 2020. Plasmodium asexual growth and sexual development in the haematopoietic niche of the host. *Nat. Rev. Microbiol.* 18, 177–189. <https://doi.org/10.1038/s41579-019-0306-2>
- Viebig, N.K., Levin, E., Dechavanne, S., Rogerson, S.J., Gysin, J., Smith, J.D., Scherf, A., Gamain, B., 2007. Disruption of var2csa gene impairs placental malaria associated adhesion phenotype. *PloS One* 2, e910. <https://doi.org/10.1371/journal.pone.0000910>
- Voss, T.S., Healer, J., Marty, A.J., Duffy, M.F., Thompson, J.K., Beeson, J.G., Reeder, J.C., Crabb, B.S., Cowman, A.F., 2006. A var gene promoter controls allelic exclusion of virulence genes in Plasmodium falciparum malaria. *Nature* 439, 1004–1008. <https://doi.org/10.1038/nature04407>
- Voss, T.S., Thompson, J.K., Waterkeyn, J., Felger, I., Weiss, N., Cowman, A.F., Beck, H.P., 2000. Genomic distribution and functional characterisation of two distinct and conserved Plasmodium falciparum var gene 5' flanking sequences. *Mol. Biochem. Parasitol.* 107, 103–115. [https://doi.org/10.1016/s0166-6851\(00\)00176-6](https://doi.org/10.1016/s0166-6851(00)00176-6)
- Voß, Y., Klaus, S., Guizetti, J., Ganter, M., 2023. Plasmodium schizogony, a chronology of the parasite's cell cycle in the blood stage. *PLOS Pathog.* 19, e1011157. <https://doi.org/10.1371/journal.ppat.1011157>
- Wahlgren, M., Goel, S., Akhouri, R.R., 2017. Variant surface antigens of Plasmodium falciparum and their roles in severe malaria. *Nat. Rev. Microbiol.* 15, 479–491. <https://doi.org/10.1038/nrmicro.2017.47>
- Waller, R.F., Reed, M.B., Cowman, A.F., McFadden, G.I., 2000. Protein trafficking to the plastid of Plasmodium falciparum is via the secretory pathway. *EMBO J.* 19, 1794–1802. <https://doi.org/10.1093/emboj/19.8.1794>
- Wang, C.W., Hermsen, C.C., Sauerwein, R.W., Arnot, D.E., Theander, T.G., Lavstsen, T., 2009. The Plasmodium falciparum var gene transcription strategy at the onset of blood stage infection in a human volunteer. *Parasitol. Int.* 58, 478–480. <https://doi.org/10.1016/j.parint.2009.07.004>
- Wang, C.W., Hviid, L., 2015. Rifins, rosetting, and red blood cells. *Trends Parasitol.* 31, 285–286. <https://doi.org/10.1016/j.pt.2015.04.009>
- Ward, P., Equinet, L., Packer, J., Doerig, C., 2004. Protein kinases of the human malaria parasite Plasmodium falciparum: the kinome of a divergent eukaryote. *BMC Genomics* 5, 79. <https://doi.org/10.1186/1471-2164-5-79>
- Warimwe, G.M., Keane, T.M., Fegan, G., Musyoki, J.N., Newton, C.R.J.C., Pain, A., Berriman, M., Marsh, K., Bull, P.C., 2009. Plasmodium falciparum var gene expression is modified by host immunity. *Proc. Natl. Acad. Sci. U. S. A.* 106, 21801–21806. <https://doi.org/10.1073/pnas.0907590106>
- Warncke, J.D., Vakonakis, I., Beck, H.-P., 2016. Plasmodium Helical Interspersed Subtelomeric (PHIST) Proteins, at the Center of Host Cell Remodeling. *Microbiol. Mol. Biol. Rev. MMBR* 80, 905–927. <https://doi.org/10.1128/MMBR.00014-16>
- Wassmer, S.C., Combes, V., Candal, F.J., Juhan-Vague, I., Grau, G.E., 2006. Platelets Potentiate Brain Endothelial Alterations Induced by Plasmodium falciparum. *Infect. Immun.* 74, 645–653. <https://doi.org/10.1128/IAI.74.1.645-653.2006>
- Waterkeyn, J.G., Wickham, M.E., Davern, K.M., Cooke, B.M., Coppel, R.L., Reeder, J.C., Culvenor, J.G., Waller, R.F., Cowman, A.F., 2000. Targeted mutagenesis of Plasmodium falciparum erythrocyte membrane protein 3 (PfEMP3) disrupts

- cytoadherence of malaria-infected red blood cells. *EMBO J.* 19, 2813–2823. <https://doi.org/10.1093/emboj/19.12.2813>
- Watermeyer, J.M., Hale, V.L., Hackett, F., Clare, D.K., Cutts, E.E., Vakonakis, I., Fleck, R.A., Blackman, M.J., Saibil, H.R., 2016. A spiral scaffold underlies cytoadherent knobs in *Plasmodium falciparum*-infected erythrocytes. *Blood* 127, 343–351. <https://doi.org/10.1182/blood-2015-10-674002>
- Weng, H., Guo, X., Papoin, J., Wang, J., Coppel, R., Mohandas, N., An, X., 2014. Interaction of *Plasmodium falciparum* knob-associated histidine-rich protein (KAHRP) with erythrocyte ankyrin R is required for its attachment to the erythrocyte membrane. *Biochim. Biophys. Acta* 1838, 185–192. <https://doi.org/10.1016/j.bbamem.2013.09.014>
- WHO, 2023. World malaria report 2023. URL <https://www.who.int/teams/global-malaria-programme/reports/world-malaria-report-2023> (accessed 15.02.24).
- WHO, 2020. WHO methods and data sources for country-level causes of death 2000-2019. <https://www.who.int/data/gho/data/themes/mortality-and-global-health-estimates/ghe-leading-causes-of-death> (accessed 15.02.2024)
- Wichers, J.S., Wunderlich, J., Heincke, D., Pazicky, S., Strauss, J., Schmitt, M., Kimmel, J., Wilcke, L., Scharf, S., von Thien, H., Burda, P.-C., Spielmann, T., Löw, C., Filarsky, M., Bachmann, A., Gilberger, T.W., 2021. Identification of novel inner membrane complex and apical annuli proteins of the malaria parasite *Plasmodium falciparum*. *Cell. Microbiol.* 23, e13341. <https://doi.org/10.1111/cmi.13341>
- Wickert, H., Göttler, W., Krohne, G., Lanzer, M., 2004. Maurer's cleft organization in the cytoplasm of *Plasmodium falciparum*-infected erythrocytes: new insights from three-dimensional reconstruction of serial ultrathin sections. *Eur. J. Cell Biol.* 83, 567–582. <https://doi.org/10.1078/0171-9335-00432>
- Wickert, H., Rohrbach, P., Scherer, S.J., Krohne, G., Lanzer, M., 2003. A putative Sec23 homologue of *Plasmodium falciparum* is located in Maurer's clefts. *Mol. Biochem. Parasitol.* 129, 209–213. [https://doi.org/10.1016/s0166-6851\(03\)00117-8](https://doi.org/10.1016/s0166-6851(03)00117-8)
- Wickham, M.E., Rug, M., Ralph, S.A., Klonis, N., McFadden, G.I., Tilley, L., Cowman, A.F., 2001. Trafficking and assembly of the cytoadherence complex in *Plasmodium falciparum*-infected human erythrocytes. *EMBO J.* 20, 5636–5649. <https://doi.org/10.1093/emboj/20.20.5636>
- Winter, G., Chen, Q., Flick, K., Kremsner, P., Fernandez, V., Wahlgren, M., 2003. The 3D7var5.2 (var COMMON) type var gene family is commonly expressed in non-placental *Plasmodium falciparum* malaria. *Mol. Biochem. Parasitol.* 127, 179–191. [https://doi.org/10.1016/s0166-6851\(03\)00004-5](https://doi.org/10.1016/s0166-6851(03)00004-5)
- Winter, G., Kawai, S., Haeggström, M., Kaneko, O., von Euler, A., Kawazu, S., Palm, D., Fernandez, V., Wahlgren, M., 2005. SURFIN is a polymorphic antigen expressed on *Plasmodium falciparum* merozoites and infected erythrocytes. *J. Exp. Med.* 201, 1853–1863. <https://doi.org/10.1084/jem.20041392>
- Yahata, K., Hart, M.N., Davies, H., Asada, M., Wassmer, S.C., Templeton, T.J., Treeck, M., Moon, R.W., Kaneko, O., 2021. Gliding motility of *Plasmodium* merozoites. *Proc. Natl. Acad. Sci. U. S. A.* 118, e2114442118. <https://doi.org/10.1073/pnas.2114442118>
- Ye, R., Zhang, D., Chen, B., Zhu, Y., Zhang, Y., Wang, S., Pan, W., 2015. Transcription of the var genes from a freshly-obtained field isolate of *Plasmodium falciparum* shows more variable switching patterns than long laboratory-adapted isolates. *Malar. J.* 14, 66. <https://doi.org/10.1186/s12936-015-0565-y>
- Yeh, E., DeRisi, J.L., 2011. Chemical rescue of malaria parasites lacking an apicoplast defines organelle function in blood-stage *Plasmodium falciparum*. *PLoS Biol.* 9, e1001138. <https://doi.org/10.1371/journal.pbio.1001138>

- Yeoh, S., O'Donnell, R.A., Koussis, K., Dluzewski, A.R., Ansell, K.H., Osborne, S.A., Hackett, F., Withers-Martinez, C., Mitchell, G.H., Bannister, L.H., Bryans, J.S., Kettleborough, C.A., Blackman, M.J., 2007. Subcellular discharge of a serine protease mediates release of invasive malaria parasites from host erythrocytes. *Cell* 131, 1072–1083. <https://doi.org/10.1016/j.cell.2007.10.049>
- Zhang, Q., Ma, C., Oberli, A., Zinz, A., Engels, S., Przyborski, J.M., 2017. Proteomic analysis of exported chaperone/co-chaperone complexes of *P. falciparum* reveals an array of complex protein-protein interactions. *Sci. Rep.* 7, 42188. <https://doi.org/10.1038/srep42188>
- Zhang, Q., Zhang, Y., Huang, Y., Xue, X., Yan, H., Sun, X., Wang, J., McCutchan, T.F., Pan, W., 2011. From in vivo to in vitro: dynamic analysis of *Plasmodium falciparum* var gene expression patterns of patient isolates during adaptation to culture. *PloS One* 6, e20591. <https://doi.org/10.1371/journal.pone.0020591>
- Zhang, X., Florini, F., Visone, J.E., Lionardi, I., Gross, M.R., Patel, V., Deitsch, K.W., 2022. A coordinated transcriptional switching network mediates antigenic variation of human malaria parasites. *eLife* 11, e83840. <https://doi.org/10.7554/eLife.83840>
- Zhang, Y., Jiang, N., Chang, Z., Wang, H., Lu, H., Wahlgren, M., Chen, Q., 2014. The var3 genes of *Plasmodium falciparum* 3D7 strain are differentially expressed in infected erythrocytes. *Parasite Paris Fr.* 21, 19. <https://doi.org/10.1051/parasite/2014019>
- Zhu, G., Marchewka, M.J., Keithly, J.S., 2000. *Cryptosporidium parvum* appears to lack a plastid genome. *Microbiol. Read. Engl.* 146 (Pt 2), 315–321. <https://doi.org/10.1099/00221287-146-2-315>

APPENDIX

Appendix A: Oligonucleotides

Appendix A.1

Oligonucleotides for cloning

Primer name	Direction	Sequence
3D7varUPSB6-HAendo	fw	AGCTgcgccgcTAA <u>ACCAGGTAGTCCTAAATATAAAAACGTTG</u>
	rv	GCTGGGTACCTATATTCATATATCTGATATAGGATATTC
3D7var2csa-HAendo	fw	GAACTATAGAATACTCAAGCTgcgccgcTAACGATAAATATATTTGGGACT TATCTTCC
	rv	GGAACATCGTATGGGTACATGGTGGTACCACAATTGTACGAATTTCCAT CTGATCG
3D7varUPSA1-HAendo	fw	CTCGgcgccgcTAA <u>GGATGTACCACAATATGATGTATCAAC</u>
	rv	TCCTGGTACCTATATTCATACATCCGATATAGG
3D7MEEDvarUPSA1-HAendo	fw	CTCGgcgccgcTAA <u>GGATGTACCACAATATGATGTATCAAC</u>
	rv	TCCTGGTACCTATATTCATACATCCGATATAGG
3D7rifA1-HAendo	fw	gacactatagaatactcgcgccgcTAAGTAAATACCCACAAAAACCACACACCAC AGCACGTC
	rv	GGAACATCGTATGGGTACATGGTGGTACCTTCTTTTAATAATTTTATGTAT TGTAATTTTTTGTTT
3D7rifA2-HAendo	fw	ggtgacactatagaatactcgcgccgcTAAGTTTCTCTAAAATTAATATATTGgtaacatta tgtg
	rv	GGAACATCGTATGGGTACATGGTGGTACCTTCTTTTAATAATTTTATATAT TGGAGTTTTTTC
3D7varUPSB6-mDHFR- HAendo	fw	AGCTgcgccgcTAA <u>ACCAGGTAGTCCTAAATATAAAAACGTTG</u>
	rv	<u>GCTGCCCCGGGTATATTCATATATCTGATATAGGATATTC</u>
3D7var2csa-mDHFR-HAendo	fw	GAACTATAGAATACTCAAGCTgcgccgcTAACGATAAATATATTTGGGACT TATCTTCC
	rv	GGAACATCGTATGGGTACATGGTGGTACCGTCCTTTTTTTCGTAAACCTCG AAC

Primer name	Direction	Sequence
IT4var66-HAendo	fw	gctatttaggtgacctatagaataactcaagctcgccgctaaCACATTAAGTGGTAATGAACATA TTG
	rv	GCGTAATCTGGAACATCGTATGGGTACATGGTGGTACCTATATTCCATATA TCCGCTATAGGATATTGC
IT4var2csa-HAendo	fw	gctatttaggtgacctatagaataactcgccgctTAATAAATATATTTGCGACTTATCTT CCTCTG
	rv	GTAATCTGGAACATCGTATGGGTACATGGTGGTACCCAAATTGTACGAAT TTCCACCTGATCGTC
IT4var02-HAendo	fw	gctatttaggtgacctatagaataactcgccgctTAAAATACAGAGGAAAACGGTACATTA CCTGAAG
	rv	GTAATCTGGAACATCGTATGGGTACATGGTGGTACCTATATTCCATACATC CGATATAGGAAATTCTGG
IT4var03-HAendo	fw	gctatttaggtgacctatagaataactcaagctcgccgctTAAGCAAAACGTCAAGTAGATATGA TACGG
	rv	GCGTAATCTGGAACATCGTATGGGTACATGGTGGTACCTATATTCCATAC ATCCGATATAGGAAATTG
IT4var06-HAendo	fw	gacctatagaataactcaagctcgccgctaaCGTTGAATACTAATAATGTTGATATATATG
	rv	GTAATCTGGAACATCGTATGGGTACATGGTGGTACCTATATCCATACATC TGCTATAGGATATTTCTCTTTCACCAATTTGG
IT4var07-HAendo	fw	gctatttaggtgacctatagaataactcaagctcgccgctTAAGGAATAAAACATCCAAAACATA CTAATACACACA
	rv	GCGTAATCTGGAACATCGTATGGGTACATGGTGGTACCTATATTCCATAC ATCCGATATAGGAAATTCTGGTTCCAAGG
IT4var08-HAendo	fw	gctatttaggtgacctatagaataactcaagctcgccgctTAAGGTAATGGTAACACACCAAGTA AGGG
	rv	GCGTAATCTGGAACATCGTATGGGTACATGGTGGTACCTATATTCCATAC ATCCGATATGGGAAATTCTGG
IT4var09-HAendo	fw	gctatttaggtgacctatagaataactcaagctcgccgctTAAAATATAAATATGGTTAATAATG ATATCCAATGAGTG
	rv	GCGTAATCTGGAACATCGTATGGGTACATGGTGGTACCTATATTCCATAC ATCTGATATAGGAAATTCTGGTTCCAAGG
IT4var16-HAendo	fw	CTCG gcccgcTAATAGTGGTAAGAACACAACAGCTAGTGGTAAAAAC

Primer name	Direction	Sequence
	rv	TCCTGGTACCTTTCTCTTTTCGCCATTTCTCCGTTCTTCACACTC
IT4var18-HAendo	fw	gtatttagtgacactatagaataactcaagctgcgccgcTAACAGATGAAGATAAATATGCATT TATGTC
	rv	GCGTAATCTGGAACATCGTATGGGTACATGGTGGTACCTATATTCCATAC ATCTGATATAGGAAATTCTGG
IT4var19-HAendo	fw	gtatttagtgacactatagaatactgcgccgc TAACTATGAATAAATTTACTGATGAGG AATGG
	rv	GTAATCTGGAACATCGTATGGGTACATGGTGGTACCTATATCCCATACATC CGATATAGGATATTTCTC
IT4var20-HAendo	fw	gtatttagtgacactatagaatactgcgccgcTAAGCAATCGTTATATCCCCTATGCTAGT GATCG
	rv	GTAATCTGGAACATCGTATGGGTACATGGTGGTACCTATATCCCATACATC TGCTATAGGATATTTCTC
IT4var22-HAendo	fw	gtatttagtgacactatagaataactcaagctgcgccgctaaCGAAGTGGTACTAGAACCTAGTG GTAACAAC
	rv	GCGTAATCTGGAACATCGTATGGGTACATGGTGGTACCTATATTCCATAC ATCCGATATAGGAAATTCTGG
IT4var35-HAendo	fw	gtatttagtgacactatagaataactcaagctgcgccgcTAAAAAAATTCAAATCGTCTGTGG ACTTGTG
	rv	GCGTAATCTGGAACATCGTATGGGTACATGGTGGTACCTTAAATGACACT GTTGTTGATGTAC
IT4var64-HAendo	fw	gtatttagtgacactatagaataactcaagctgcgccgcTAACTAGTGGAGATGAAGATAAATA TGC
	rv	GCGTAATCTGGAACATCGTATGGGTACATGGTGGTACCTATATTCCATAC ATCCGATATGGGAAATTCTGGTTCCAACGATCC
PTP1-TGD-GFP	fw	ctcgGCGGCCGctaaGTGAATAAAGATAAATAGG
	rv	tcctCGTACGCCTAGGGGTACCAAAGGAATCGTTATTTATC
IT4var01-BirA*Pos lendo	fw	same HR as IT4var1-HAendo
	rv	same HR as IT4var1-HAendo
IT4var01-BirA*Pos lendo 7xGGGS linker	fw	CTATCAAATAGATATGAATTCTAAACCTATTGGTACCGGAGGTGGAGGT AGTGGAGGCGGAGG
	rv	<u>GATTACGCTACGATGTACCCGTACGACGTGCCGGACTACGCGACTATGTA TCCATATGATGTTCCAGATTATGCT</u>

Primer name	Direction	Sequence
IT4var01-BirA*Pos1endo BirA*	fw	<u>ATCCAAATAGATATGAATTCTAAACCTATTGGTACCGGAGGTGGAGGTAG</u> <u>TGGAGGCGGAGGTAGCGGA</u>
	rv	<u>GATTACGCTACGATGTACCCGTACGACGTGCCGGACTACGCGACTATGTA</u> <u>TCCATATGATGTTCCAGATTATGCT</u>
IT4var01-BirA*Pos2endo	fw	ggtgacactatagaataactcaagctcgccgctaaTGTATACAGAATAGTGGAAATGAAA
	rv	GCGTAATCTGGAACATCGTATGGGTACATGGTGGTACCTTTGGTTTTTTct aaaaaaaaacg
IT4var01-BirA*Pos2endo BirA*	fw	GAGTTATTTTCGTAATAAGAAAAAACAAAGGTACCGGTGGAGGTGGAT CAGGTGGAGGTGGATCAATGAAAGATAATACAGTACC
	rv	ACGCGTACTTCCACTTCCACTTCCTTTTTTCAGCTGATCTTAATGATATTTT
IT4var01-BirA*Pos2endo recodized var01 rest position 2	fw	GAAAAAGGAAGTGGAAAGTGGAAAGTACGCGTAGCACAAATAGACTTACTTA GAGTAATAG
	rv	1.CACGTCGTACGGGTACATCGTAGCGTAATCTGGAACATCGTATGGGTAC ATGGTCCCGGGTATTGGCTTGCTGTTTCATGTCAATCTGTATG 2.GTCGACAGCATAATCTGGAACATCATATGGATACATAGTCGCGTAGTCC GGCACGTCGTACGGGTACATCGTAGCG 3.ACATGTTAATAAACTTCTCTTCTCCTCCGTCGACAGCATAATCTGGAA CATCATATG
IT4var01-BirA*Pos3endo	fw	ggtgacactatagaataactcaagctcgccgctaaGGAACATCTAAAAACATCATCTAATC
	rv	CCAGGACCAAAAGCACCAAAAAACGAGGTACCACCATGTACCCATACG ATGTTCCAGATTACGC
IT4var01-BirA*Pos3endo BirA*	fw	CCAAAACCAGGACCAAAAGCACCAAAAAACGAGGTACCGGAAGTGGAA GTGGAAGTATGAAAGATAATACAGTACC
	rv	ACGCGTTGATCCACCTCCACCTGATCCACCTCCACCTTTTTTCAGCTGATCT TAATGATATTTT
IT4var01-BirA*Pos3endo recodized var01 rest position 3	fw	GGTGGAGGTGGATCAGGTGGAGGTGGATCAACCGGTCAGCCTAGAGAGG TTACACACAG
	rv	GCGTAATCTGGAACATCGTATGGGTACATGGTCCCGGGTATTGGCTTGCT GTTTCATGTCAATC
TryThrA-Ty1	fw	aagctatttagtgacactatagaataactcGCGGCCGctaaGTTACTAGAGAAAACTCGAAT GGAAACATTG
	rv	GTCCAGGGGGTCTGGTTGGTGTGCACCTCCCTAGGAACATTAATTTTCATT TCCGTCATCATCAACTG
TryThrA-TGD-GFP	fw	ccaagctatttagtgacactatagaataactcGCGGCCGctaaAATTTAGAGCAGTTTAAAAAT ATAAACAAAG
	rv	TCCAGTGAAAAGTTCTTCTCCTTACTCATCGTACGATTTTTACTTTTACTA TTTTTTCTTTTAC
PTEF-Ty1	fw	aagctatttagtgacactatagaataactcGCGGCCGctaaATTATTATCCACATAATATGACA TTTGGAC

Primer name	Direction	Sequence
	rv	GTCCAGGGGGTCCTGGTTGGTGTGCACCTCCCTAGGTAATGCTTTGTTTGC ATTTGATTGTGGAAG
PTEF-TGD-GFP	fw	ccaagctatttaggtgacactatagaatactcGCGGCCGCtaaTTAAAGAAATATATTATATTA ATATATATACGG
	rv	TCCAGTGAAAAGTTCTTCTCCTTTACTCATCGTACGATAATTTAGTTGATC TTCTAAATCATCACTAC
C3-Ty1	fw	ccaagctatttaggtgacactatagaatactcGCGGCCGCtaaGCTTATCCTCTTTTAGAAGATG ACTTAAGATC
	rv	GTCCAGGGGGTCCTGGTTGGTGTGCACCTCCCTAGGTACATGAGCTTCATT AGTGTTTAAACCAGATACGC
C3-TGD-GFP	fw	ccaagctatttaggtgacactatagaatactcGCGGCCGCtaaGCTTATCCTCTTTTAGAAGATG ACTTAAGATC
	rv	TCCAGTGAAAAGTTCTTCTCCTTTACTCATCGTACGATTTCTTTTTTCAATT TCTTCAAATAATCC
PeMP2-Ty1	fw	ccaagctatttaggtgacactatagaatactcGCGGCCGCtaaAATAAAAAATCAATGCAAACCT AAGAACTTTTATC
	rv	TCCAGTGAAAAGTTCTTCTCCTTTACTCATCGTACGTTTATTTTTATTATAT ATCGATTTGGATGATACG
PeMP2-TGD-GFP	fw	ccaagctatttaggtgacactatagaatactcGCGGCCGCtaaAATAAAAAATCAATGCAAACCT AAGAACTTTTATC
	rv	TCCAGTGAAAAGTTCTTCTCCTTTACTCATCGTACGATTACAGATGTCAAG GTCTCTATCAGGATAATTAG
PTP7-TGD-GFP	fw	aagctatttaggtgacactatagaatactcGCGGCCGCtaaGCAAAAAGATAGTCAAAAAGAACT TGAATGTTTC
	rv	TCCAGTGAAAAGTTCTTCTCCTTTACTCATCGTACGATAAGGGTCATAATT TTCTTGAACCTTCATC

Appendix A.2

Oligonucleotides for diagnostic PCRs testing correct integration of SLI and SLI2 plasmids

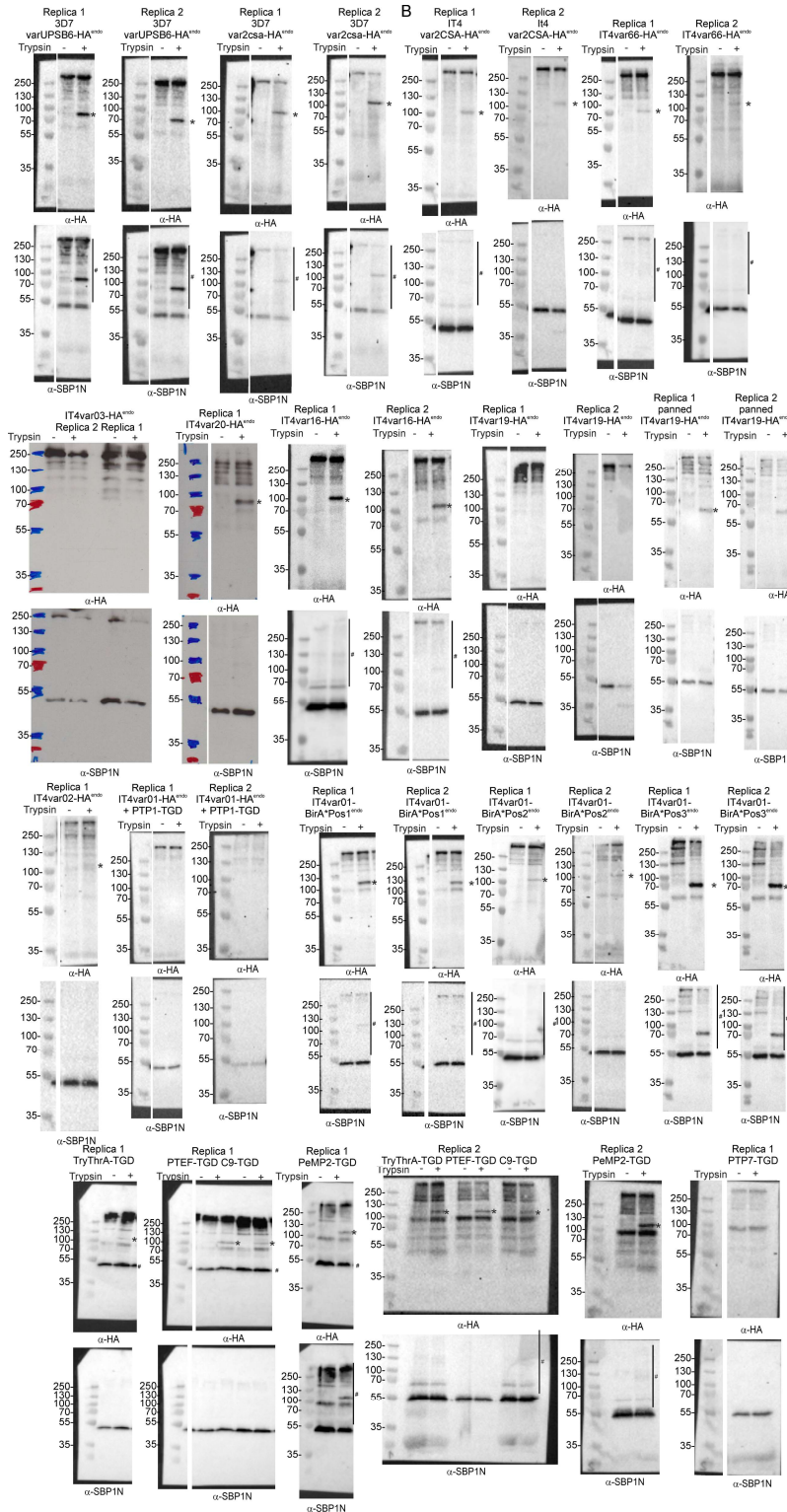
Tested cell line	Direction	Sequence
3D7varUPSB6-HAendo	fw	CCCCCAGTTCCTGCTCCAGCTGGTG
	rv	<u>CCTAATGCATATTATGAAATATCCAC</u>
3D7var2csa-HAendo	fw	<u>GGTGGGACATGAATAAATATCACATATGGG</u>
	rv	CTTCCATATATTTTATGCATTGCATTATTAG
3D7varUPSA1-HAendo	fw	GTAGATGAATGGATAAAGCTGAAAAAGG
	rv	CAAAAAATTATGAATCGAATATATTAG
3D7MEEDvarUPSA1-HAendo	fw	GTAGATGAATGGATAAAGCTGAAAAAGG
	rv	CAAAAAATTATGAATCGAATATATTAG
3D7rifA1-HAendo	fw	<u>GTTTATGTAAACATATTTGATGTATTTATAAC</u>
	rv	GCGCAAATAATTCATTCATTAATAACCTG
3D7rifA2-HAendo	fw	GTTATAGTTTTTATCATAAAATAATATACGTATCAC
	rv	CAGTACATGTACCAAACATCCTACCAACATCTAC
3D7varUPSB6-mDHFR-HAendo	fw	CCCCCAGTTCCTGCTCCAGCTGGTG
	rv	<u>CCTAATGCATATTATGAAATATCCAC</u>
3D7var2csa-mDHFR-HAendo	fw	<u>GGTGGGACATGAATAAATATCACATATGGG</u>
	rv	CTTCCATATATTTTATGCATTGCATTATTAG
IT4var66-HAendo	fw	TAATATGAGTACTAATAGTATGG
	rv	aaactccacataaaaaataaaaatcaaac
IT4var2csa-HAendo	fw	TAGATATATCCCCTATGTGAGTGATAC
	rv	ATATACACATATAAATCATCACC
IT4var02-HAendo	fw	AACTACATACATACATACATAAATATATAC
	rv	aattatattaaattatgaac
IT4var03-HAendo		CACAATATATACGTATAAATACGC

Tested cell line	Direction	Sequence
		ATTTAAATTATACAAATGAATATAC
IT4var08-HAendo		TTAATGATATATATCCCTACACG
		AAATATTATTATACAAATATTG
IT4var16-HAendo	fw	AGTCCTAAATATAAAACATTGATAGAAGTGG
	rv	aataaaaagaataataatatacg
IT4var19-HAendo	fw	ACATTGATAGAAGTGGTACTAGAACCATCG
	rv	aaaaaattcaacatatgtatatacatacg
IT4var20-HAendo; first primer pair	fw	AAATATTATTATACAAATATTG
	rv	ATACAAATAAAATCTAATATAATGC
Second primer pair	fw	ATACAAATAAAATCTAATATAATGC
	rv	TTAATTTAAACAAAAATACAACATATTCC
IT4var22-HAendo first primer pair	fw	AAAGTGAGTATGAAGAATTGGATATTAATG
	rv	aattatacaaatgaatatacaataaaaatg
Second primer pair	fw	ATCCACAAAGGAGATTATGGAATGCCTACG
	rv	caaattatatacaataatcaaatgtgc
PTP1-TGD-GFP	fw	TAGAATAACATATAAAAAATATGTATTCTG
	rv	TTAACTTTACAAATTCCTTTAATTTACG
IT4var01-BirA*Pos1endo, IT4var01-mTurbPos1endo IT4var01-FKBPPos1endo	fw	CGACAACCACGTGAAGTGACGCATTCCATAGTC
	rv	CTAATATAGTATCCATAGTAGAATTATCAGG
IT4var01-BirA*Pos2endo IT4var01-mTurbPos2endo IT4var01-FKBPPos2endo	fw	TTAAGGATGATTGTCGTAGTGACACCCAG
	rv	CTAATATAGTATCCATAGTAGAATTATCAGG
IT4var01-BirA*Pos3endo	fw	TTAAGGATGATTGTCGTAGTGACACCCAG

Tested cell line	Direction	Sequence
	rv	ttattcatttacgaaaacaccafftcac

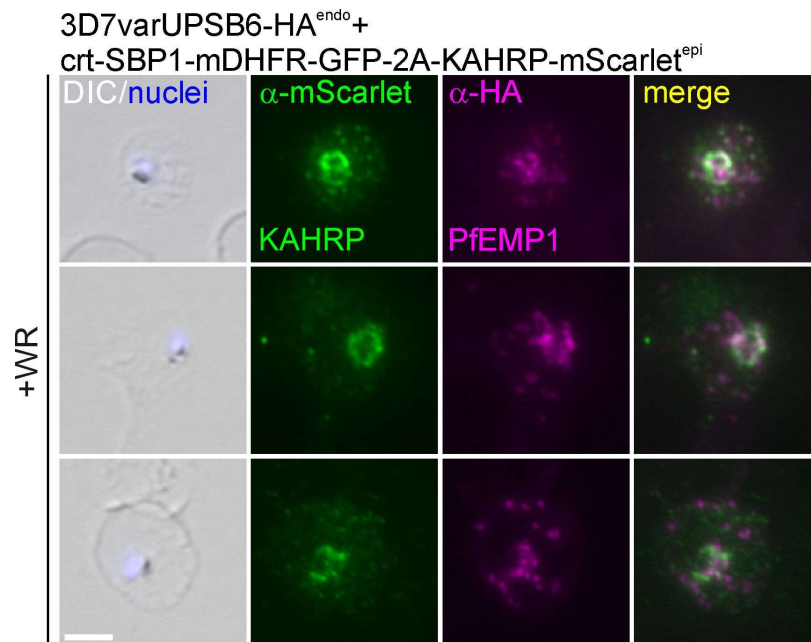
Appendix B – Full Western blots and replicates

Full Western blots and replicates of trypsin cleavage assays with parasites of the indicated cell lines (two independent experiments except for IT4var02-HA^{endo}, IT4var20-HA^{endo} and PTP7-TGD-GFP for which there is only one replicate). Asterisks show the protected PfEMP1 fragment indicative of surface exposure. Hash sign indicates signal from previous probing of the blot. α -SBP1-N: control for integrity of host cell (breach of ERYTHROCYTE membrane would result in a smaller SBP1 fragment). Marker in kDa.

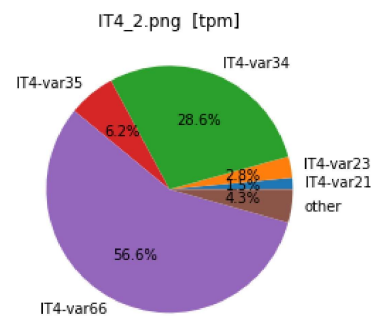


Appendix C – Partial co-block of HA-tagged PfEMP1

Fluorescence microscopy images show IFAs with acetone fixed 3D7varUPSB6-HA^{endo+} crt-SBP1-mDHFR-GFP-2A-KAHRP-mScarlet^{epi} parasites with the indicated antibodies. Nuclei: Hoechst 33342; DIC: differential interference contrast; size bars 5 μ m.

Appendix D – *var* gene expression pattern of a IT4 wildtype parasites population

Pie chart shows proportions of *var* gene transcripts determined by RNAseq and normalized to TPM of the utilized IT4 strain (RNAseq performed by Johannes Allweier).



Appendix E – Detailed results of the BioID for the SDS-samples

Majority protein IDs	Gene product	-Log Student's T-test p-value		Student's T-test Difference		-Log Student's T-test p-value		Student's T-test Difference		-Log Student's T-test p-value		Student's T-test Difference	
		pos1	control	pos1	control	pos2	control	pos2	control	pos3	control	pos3	control
PIT_110005700:PIT_080005100	rifin	2,72207	11,8572	0,721468	4,35419	1,15553	4,18287						
PIT_080005300	stevor	4,27988	11,3009	0,998502	2,62541	0,492964	-0,47193						
PIT_130076400	antigen 332, DBL-like protein	4,01628	11,2925	2,97999	9,3541	3,39789	9,19526						
PIT_060021400	erythrocyte membrane protein 1, P1EMP1	4,29439	10,9193	3,47746	9,99964	4,3084	9,57984						
PIT_130058600	membrane associated histidine-rich protein	2,1104	10,6495	1,84399	9,49409	1,87358	9,1579						
PIT_130075600	membrane associated histidine-rich protein	3,3941	9,89711	2,30934	8,98595	3,05468	8,75564						
PIT_090040600	ring-exported protein 1	2,76027	9,51928	2,1463	8,68814	2,57394	8,04273						
PIT_130039800	MSP7-like protein	1,77584	9,42992	1,48187	8,2884	1,5755	8,13408						
PIT_050006600	parasite-injected erythrocyte surface protein	3,8161	9,34966	2,5522	7,54478	3,23082	7,39491						
PIT_010017100:PIT_060035200	Pfmc-2TM Maurers cleft two transmembrane protein	4,80118	9,06526	NaN	0	NaN	0						
PIT_050006700	skeleton-binding protein 1	2,95695	8,56936	2,47615	7,63613	2,79928	8,00937						
PIT_080035300	Plasmodium exported protein (PHISTc), unknown function	4,01272	8,55172	3,56527	7,61853	2,96242	7,84711						
PIT_100005600	alpha/beta hydrolase, putative	3,10737	8,36858	3,94511	7,49142	2,2769	6,66319						
PIT_080037300	rifin	3,02958	8,11653	NaN	0	NaN	0						
PIT_040005500	rifin	2,89704	7,96811	0,366518	1,56311	0,069481	0,182953						
PIT_130076800	Plasmodium exported protein, unknown function	1,92403	7,7725	1,58941	7,86109	1,74797	4,94045						
PIT_070007300	small exported membrane protein 1	2,789	7,75365	1,64212	6,50396	1,96541	5,79244						
PIT_070035300	acyl-CoA synthetase	1,40637	7,56467	1,17072	6,3763	1,12677	5,8783						
PIT_100005800	alpha/beta hydrolase, putative	1,35579	7,32195	1,21396	6,3019	1,2576	6,3153						
PIT_100006100	Plasmodium exported protein (hyp16), unknown function	2,65276	7,31414	2,23122	6,99187	2,62208	6,50062						
PIT_020007000	EMPI-1 trafficking protein	2,82747	7,29186	1,13838	6,16186	1,32192	5,39491						
PIT_090007100	serine/threonine protein kinase, FIKK family	2,33518	7,23774	1,18846	5,53405	1,77636	5,16688						
PIT_120006300	acyl-CoA synthetase	5,72103	7,16762	0,623283	1,92255	2,62535	1,8954						
PIT_100006300	EMPI-1 trafficking protein	2,78775	7,05442	2,14858	6,60032	2,59528	5,78852						
PIT_060005700	conserved Plasmodium protein, unknown function	2,6582	6,91016	1,91658	5,70546	2,39746	6,01826						
PIT_100020500	serine/threonine protein kinase, FIKK family	1,63239	6,85818	1,34139	5,63409	1,35437	5,18276						
PIT_130058500	Plasmodium exported protein, unknown function	2,07819	6,84986	1,70036	6,07584	1,85403	5,87254						
PIT_080035200	tryptophan/threonine-rich antigen	1,93622	6,35775	1,4369	5,26704	1,76119	5,16717						
PIT_070007200	sporozoite threonine and asparagine-rich protein	3,20453	6,28405	1,54218	4,09163	1,31985	2,30237						
PIT_090006600	Plasmodium exported protein, unknown function	2,21047	6,2807	0,856456	4,91125	1,41409	4,09122						
PIT_100006200	Plasmodium exported protein (hyp2), unknown function	3,95778	6,2298	3,03789	5,79486	3,70965	6,11022						
PIT_070007400	Plasmodium exported protein (PHISTb), unknown function	1,55069	6,13065	1,38648	5,94862	1,42144	5,56928						
PIT_140083600	Plasmodium exported protein (PHISTb), unknown function	1,38553	6,12446	0,324334	1,79868	0,912813	3,96225						
PIT_050006400	Plasmodium exported protein, unknown function	2,75638	6,11883	1,59654	5,03564	2,27995	4,93272						
PIT_120006700	RESA-like protein with PHIST and DnaJ domains	1,63559	6,08536	1,30211	5,23919	1,13144	3,98216						
PIT_100037100	early transcribed membrane protein 10.2	2,65301	6,07983	1,24937	5,52524	2,4416	5,26026						
PIT_010016900	Plasmodium exported protein (hyp8), unknown function	2,10876	6,07598	1,25875	4,43821	0,583115	2,78791						
PIT_070034700	Plasmodium exported protein, unknown function	2,48387	6,07595	0,380617	2,91761	2,05469	5,21797						
PIT_060005100:PIT_000007900	Pfmc-2TM Maurers cleft two transmembrane protein	2,61369	6,07062	0,481865	3,041	0,580546	2,62802						
PIT_140067700	40S ribosomal protein S28e, putative	1,25623	6,04741	0,347912	3,66282	1,32	6,18874						
PIT_030006500	Plasmodium exported protein, unknown function	2,0397	5,81774	0,764195	3,49745	2,9258	5,21005						
PIT_110021000	dipeptidyl aminopeptidase 1	1,73792	5,46791	0,76707	3,47806	0,307442	1,48907						
PIT_120008500	high mobility group protein B1	0,711864	5,33914	0,715512	5,72554	0,762299	5,67						
PIT_120058000	Plasmodium exported protein (PHISTb), unknown function	2,56732	5,19142	0,771479	3,08441	1,35028	3,56039						
PIT_040006800	Plasmodium exported protein, unknown function	2,00034	5,10862	1,49077	4,58815	0,581663	2,21444						
PIT_070010600	40S ribosomal protein S29, putative	0,576916	5,02369	0,483236	4,33873	0,456959	4,07982						
PIT_120006500	Plasmodium exported protein (PHISTc), unknown function	3,01181	4,8885	1,97964	3,30568	0,768464	2,2002						
PIT_080036400	heat shock protein 70	1,9925	4,81819	1,47767	3,96315	1,57467	3,29095						
PIT_110024700	alpha/beta hydrolase fold domain containing protein, putative	1,52119	4,71957	0,994209	3,41613	1,31606	3,96179						
PIT_020022000	calcium-dependent protein kinase 1	0,991597	4,62524	0,766123	4,4013	0,996767	4,7111						
PIT_020006400	PHISTb domain-containing RESA-like protein 1	1,1417	4,61108	0,455204	-2,07798	0,597016	-2,60952						
PIT_030011700	40S ribosomal protein S23, putative	0,410284	4,59282	0,400836	4,52972	0,387711	4,37957						
PIT_070030000	Plasmodium exported protein, unknown function	1,68663	4,54814	0,497186	1,82765	0,567853	1,31733						
PIT_050023200	conserved protein, unknown function	1,24951	4,53836	0,655318	3,89236	1,43234	4,49058						
PIT_100037200	conserved Plasmodium protein, unknown function	1,24472	4,52548	1,0279	4,75	0,45435	3,12659						
PIT_130005900	inner membrane complex protein	0,9582	4,48065	1,02152	5,30819	0,882329	4,36743						
PIT_110039700	protein phosphatase PPM8, putative	1,02981	4,41429	0,775983	3,81115	1,00817	3,8173						
PIT_040029300	Plasmodium exported protein (PHISTa), unknown function	1,2955	4,39498	0,334453	-1,4159	1,28236	4,26192						
PIT_140026400	conserved Plasmodium protein, unknown function	1,3202	4,37541	0,239804	2,12113	1,51133	4,82181						
PIT_050031400	ADP-ribosylation factor GTPase-activating protein, putative	2,05712	4,3618	0,859804	3,72066	2,0556	4,27934						
PIT_130034400	myosin C	1,1233	4,34926	0,921292	4,53252	0,862206	3,5285						
PIT_130013400	40S ribosomal protein S27	0,6276	4,33953	0,654291	4,89341	0,66491	4,57884						
PIT_070020600	conserved Plasmodium protein, unknown function	1,22809	4,20592	1,07325	3,15593	1,06535	3,36885						
PIT_140049500	conserved Plasmodium protein, unknown function	2,27677	4,19827	1,05565	3,98342	1,87865	3,98585						
PIT_010016300	Plasmodium exported protein, unknown function	1,29799	4,16485	0,923585	3,29992	1,02685	3,12911						
PIT_130057100	conserved Plasmodium protein, unknown function	0,659881	3,98624	0,531503	3,57626	0,602335	3,67452						
PIT_040029200	Plasmodium exported protein (PHISTb), unknown function	1,98207	3,91981	NaN	0	0,541943	1,9461						
PIT_110036600	ubiquitin-like protein, putative	2,17086	3,83608	0,585774	3,08502	2,33964	3,48425						
PIT_100018900	conserved Plasmodium protein, unknown function	0,887362	3,79532	0,84716	4,08361	0,933177	3,92475						
PIT_030010400	AP endonuclease (DNA-[apurinic or apyrimidinic site] lyase), putative	1,18906	3,78639	1,12865	4,58284	1,43499	4,27552						
PIT_100028900	conserved Plasmodium protein, unknown function	0,876553	3,76515	0,482161	2,25069	0,491436	2,27481						
PIT_110032700	multi-protein bridging factor type 1, putative	1,00519	3,76502	0,529495	3,04326	0,910028	3,40561						
PIT_120042400	conserved Plasmodium protein, unknown function	1,36121	3,76333	0,655486	2,86781	0,966425	3,62228						
PIT_100030000	conserved Plasmodium protein, unknown function	0,673399	3,70903	0,636162	3,86625	0,637088	3,50939						
PIT_120050100	cytoplasmic translation machinery associated protein, putative	0,841111	3,69749	0,656997	3,35221	0,702728	3,15952						
PIT_100005900	Plasmodium exported protein (PHISTc), unknown function	0,853531	3,69422	0,574608	3,20721	0,845255	3,62452						
PIT_010019200	conserved Plasmodium protein, unknown function	0,900906	3,68793	1,03144	4,82031	0,9958	4,39263						
PIT_050014100	conserved Plasmodium protein, unknown function	0,982809	3,66749	0,846728	3,93509	0,807684	3,17881						
PIT_100030100	conserved Plasmodium protein, unknown function	1,15896	3,58158	1,13205	4,058	1,11681	3,48825						
PIT_070010400	inositol-phosphate phosphatase, putative	1,49847	3,52899	0,714819	1,91374	0,64827	1,59504						
PIT_130048600	conserved Plasmodium protein, unknown function	2,39947	3,51096	0,892798	2,71306	2,16575	3,46387						
PIT_050018700	deoxyribodipyrimidine photo-lyase, putative	1,25011	3,48927	0,828659	3,37413	1,04902	2,78877						
PIT_140016200	conserved Plasmodium protein, unknown function	1,31408	3,48242	0,843167	2,69291	0,961984	2,82134						
PIT_060015600	conserved Plasmodium protein, unknown function	0,681304	3,46358	0,733802	4,09805	0,652033	3,46226						
PIT_040015400	conserved Plasmodium protein, unknown function	1,24629	3,45981	0,761959	3,41467	1,05081	3,11947						
PIT_140056400	serine/threonine protein kinase, putative	0,936216	3,45535	0,341018	2,11871	0,447933	2,24077						
PIT_120033700	merozoite surface protein 9	2,29797	3,44804	1,93992	4,29076	2,45935	3,58264						
PIT_120012400	conserved Plasmodium protein, unknown function	1,15072	3,42897	0,665225	3,19819	0,974811	3,06469						
PIT_120035800	conserved Plasmodium protein, unknown function	1,0926	3,41946	0,224033	1,59067	0,337435	1,51127						
PIT_120048900	translation initiation factor SU11, putative	0,884572	3,41161	0,702525	3,82259	0,990837	3,83139						
PIT_060019700	RNA and export factor binding protein, putative	0,736791	3,3901	0,378212	2,34388	0,230155	1,57844						
PIT_120056400	coronin	0,707166	3,38544	0,95713									

PIT_03000900	EH domain-containing protein	0,988497	3,16733	0,45902	3,0783	0,820815	3,00703
PIT_130030700	conserved Plasmodium protein, unknown function	0,984384	3,16442	0,766293	3,47649	0,791878	3,30289
PIT_130046800	inner membrane complex suture component, putative	0,711556	3,14132	0,28335	2,14295	0,646099	2,87918
PIT_030023500	trophozoite stage antigen	0,61773	3,134	0,451123	2,59097	0,505101	0,389184
PIT_100030800	40S ribosomal protein S2	0,63727	3,09549	0,669386	3,77341	0,234671	1,57657
PIT_110020100	conserved Plasmodium protein, unknown function	0,968371	3,08345	0,444771	1,99451	0,73291	2,42188
PIT_030015100	phosphoglycerate mutase, putative	1,36319	3,06345	0,04449	3,85105	1,92801	3,58704
PIT_130018200	eukaryotic translation initiation factor 4 gamma	0,888224	3,06045	0,671183	3,97151	1,04078	3,57438
PIT_030009200	60S ribosomal protein L44	0,762402	3,0534	0,555965	2,61961	0,546514	2,39104
PIT_120043400	conserved Plasmodium protein, unknown function	0,338904	3,05104	1,2367	5,61865	0,259254	1,72581
PIT_130014600	H/ACA ribonucleoprotein complex subunit 1, putative	0,616671	3,0412	0,600063	3,03973	0,520205	2,74567
PIT_110033400	conserved Plasmodium protein, unknown function	0,627671	3,03572	0,665158	3,55349	0,565758	2,77286
PIT_110047600	translation initiation factor eIF-1A, putative	0,880016	3,01601	0,767238	3,92425	1,26622	4,46444
PIT_110045500	conserved Plasmodium protein, unknown function	0,749264	3,00955	0,537418	3,04177	0,888627	3,57125
PIT_070018800	transcription elongation factor s-II, putative	1,28127	3,00601	0,463874	2,40585	1,10898	3,08172
PIT_030026200	protein kinase, putative	0,792703	2,99663	0,223263	1,55131	0,813194	2,95594
PIT_070009200	conserved Plasmodium membrane protein, unknown function	0,967082	2,98492	0,699416	3,41085	1,06521	3,46354
PIT_110026800	conserved Plasmodium protein, unknown function	1,29722	2,98448	0,454376	2,09869	0,728753	1,90491
PIT_100020000	conserved Plasmodium protein, unknown function	0,537685	2,97869	0,586132	3,45099	0,649345	3,4506
PIT_130026000	conserved Plasmodium protein, unknown function	0,689356	2,9603	0,367184	2,46329	0,590322	2,57793
PIT_110024300	conserved Plasmodium protein, unknown function	0,984264	2,95003	0,890088	3,49748	0,925163	3,04003
PIT_050012100	rhomoid protease ROM4	0,685198	2,93174	0,490126	2,84365	0,781376	3,38082
PIT_070009000	conserved Plasmodium membrane protein, unknown function	0,612808	2,91733	0,445062	2,70763	0,520535	2,5997
PIT_060010700	coatamer alpha subunit, putative	0,939587	2,91536	1,09439	3,76941	1,15419	3,06455
PIT_100030700	conserved Plasmodium protein, unknown function	0,640528	2,90695	0,459971	2,63379	0,768658	3,22029
PIT_050034900	conserved Plasmodium protein, unknown function	1,07068	2,90323	0,606758	3,04364	0,728421	2,44928
PIT_120032700	cyclin related protein, putative	0,604883	2,89583	0,303397	2,12244	0,618949	2,8534
PIT_130045000	conserved Plasmodium protein, unknown function	1,50721	2,89224	1,11028	3,3241	1,21015	2,55012
PIT_140013900	pre-mRNA-splicing factor 38B, putative	0,680814	2,87382	0,482261	2,4721	0,577075	2,43878
PIT_120026000	heterochromatin protein 1	0,425264	2,8678	0,319334	2,61935	0,182653	1,66909
PIT_070034800	EMPI-trafficking protein	1,22004	2,86677	0,911404	3,12063	1,07573	2,62506
PIT_050029600	ribosome-interacting GTPase 1, putative	0,61651	2,86655	0,382636	2,18722	0,562035	2,63821
PIT_130076100	Plasmodium exported protein (PHISTc), unknown function	2,47846	2,85393	NaN	0	NaN	0
PIT_110049400	serine/threonine protein kinase, putative	2,08846	2,85043	0,702587	2,49808	1,31491	2,14049
PIT_050010100	conserved Plasmodium protein, unknown function	1,02452	2,7612	0,820692	3,421	0,967858	2,18022
PIT_120034800	myosin D	1,66586	2,70173	1,00537	3,73191	1,02975	2,42872
PIT_070010000	conserved Plasmodium protein, unknown function	0,661006	2,69487	0,689799	3,2791	0,714503	2,88918
PIT_040060700	reticulocyte binding protein homologue 1	1,35813	2,69178	0,630633	2,77164	1,22915	2,91948
PIT_100023100	eukaryotic translation initiation factor subunit eIF2A, putative	0,873752	2,68949	0,469793	2,27551	0,86675	2,75315
PIT_140032500	basic transcription factor 3b, putative	0,473275	2,68897	0,527064	3,26722	0,571473	3,16845
PIT_130038600	transmembrane protein Tmp21 homologue, putative	0,396078	2,68365	0,040524	0,390118	0,357804	2,3883
PIT_070012800	ribosomal protein S8e, putative	0,398118	2,67957	0,362217	2,57958	0,280401	1,96764
PIT_060006500	conserved Plasmodium protein, unknown function	1,27778	2,66308	0,344481	1,76257	1,246	2,96308
PIT_080022900	high mobility group protein B2	1,65162	2,65203	0,965432	3,5113	2,10973	3,43424
PIT_020024600	DnaJ protein, putative	1,51719	2,64165	1,06631	1,89516	0,194425	0,334915
PIT_110046300	conserved Plasmodium protein, unknown function	1,05372	2,64121	0,421992	2,34772	0,868021	2,27075
PIT_040029000	Plasmodium exported protein (PHISTb), unknown function	0,744919	2,61741	0,768257	2,82415	0,829977	2,85095
PIT_100031300	peroxiredoxin	0,947378	2,5997	0,766634	2,40328	0,661034	1,78624
PIT_020007300	early transcribed membrane protein 2	0,534046	2,57171	0,531876	2,71367	0,090405	0,741848
PIT_140065800	conserved Plasmodium protein, unknown function	1,17906	2,56623	1,21411	3,56276	3,05216	5,43835
PIT_140042000	conserved Plasmodium protein, unknown function	0,807519	2,54769	0,802275	3,8124	0,978571	3,78157
PIT_070026400	rhoGTPase-associated leucine zipper-like protein 1	0,961878	2,54166	0,615536	2,94439	1,04152	2,86096
PIT_070023900	40S ribosomal protein S10, putative	1,40003	2,53783	0,533496	1,91394	0,72991	1,71143
PIT_060021100	conserved Plasmodium protein, unknown function	1,56215	2,53304	0,785457	2,64987	1,59253	2,70559
PIT_030029400	stevor	1,49477	2,51988	1,26823	2,59286	2,30684	4,44971
PIT_080013100	conserved Plasmodium protein, unknown function	0,992415	2,51609	0,758557	2,13243	0,800454	2,05153
PIT_140072700	transcription factor with AP2 domain(s)	0,441337	2,5135	0,346134	2,21464	0,381926	2,26409
PIT_090017100	conserved Plasmodium protein, unknown function	0,798036	2,51289	0,640078	2,3563	0,741746	2,27987
PIT_140075500	shewanella-like protein phosphatase 1, putative	0,473108	2,50712	0,101259	0,885382	0,181001	1,391
PIT_110049600	dynamitin-like protein	1,06313	2,50024	0,377014	2,29085	0,760073	1,97112
PIT_080015200	protein phosphatase PPM5, putative	0,641	2,49483	0,231412	2,08653	0,872609	3,28231
PIT_130044000	conserved Plasmodium protein, unknown function	0,990559	2,48692	0,255641	1,35819	1,67074	2,34537
PIT_110019700	cysteine proteinase falcipain 3	0,40915	2,45671	0,515866	3,33841	0,513453	2,96029
PIT_010005700	ring-infected erythrocyte surface antigen	0,884333	2,44515	0,758475	2,6671	0,060296	0,22564
PIT_030017600	60S ribosomal protein L26, putative	0,575843	2,44468	0,515672	2,09564	0,533699	2,08035
PIT_040012400	conserved Plasmodium protein, unknown function	0,626496	2,44009	0,467339	2,36691	0,605866	2,41089
PIT_140024100	H/ACA ribonucleoprotein complex subunit 4, putative	0,42943	2,43843	0,310164	2,03736	0,418393	2,38986
PIT_130028700	60S ribosomal protein L23	1,09533	2,42608	0,875954	2,5546	0,664666	1,81269
PIT_050026600	FACT complex subunit SPT16, putative	0,658571	2,41542	0,629245	2,91381	0,36563	1,80933
PIT_070014600	lyso-phospholipase, putative	0,629428	2,40192	0,763986	3,38072	0,910775	3,35443
PIT_070012600	E3 ubiquitin-protein ligase, putative	0,983726	2,40104	0,260953	1,29019	0,757128	1,83292
PIT_130037100	60S ribosomal protein L23, putative	1,04685	2,40089	0,571255	1,79842	0,672607	1,66192
PIT_100026000	conserved Plasmodium protein (10b antigen), unknown function	1,6891	2,39876	0,783251	2,46882	1,62946	2,10997
PIT_030013500	conserved Plasmodium protein, unknown function	0,572722	2,39748	0,534015	2,85124	0,62013	2,75299
PIT_060010900	conserved Plasmodium protein, unknown function	0,786711	2,39525	0,393133	2,25417	0,80952	2,36937
PIT_090032100	conserved Plasmodium protein, unknown function	0,606544	2,39236	0,636364	3,01015	0,257759	1,39678
PIT_060007000	conserved Plasmodium protein, unknown function	0,421592	2,39226	0,496229	3,49316	0,754803	4,11525
PIT_020022300	40S ribosomal protein S26	0,682221	2,38145	0,549045	2,05626	0,582644	1,92052
PIT_060011600	spindle assembly abnormal protein 6, putative	0,775431	2,37589	0,638516	2,68773	0,589185	2,07612
PIT_040026900	40S ribosomal protein S19	1,12306	2,36858	0,687985	1,94548	1,07247	1,88738
PIT_060013750	conserved Plasmodium protein, unknown function	0,98578	2,35672	0,646054	3,36929	0,668565	2,36029
PIT_130042500	1-deoxy-D-xylulose 5-phosphate synthase	1,75116	2,35007	0,776284	2,25194	2,31846	3,00593
PIT_130066400	protein transport protein Sec24A	0,441484	2,31562	0,596299	3,61379	0,44641	2,45577
PIT_140055500	conserved Plasmodium protein, unknown function	0,855498	2,31406	0,577503	2,78291	1,01194	3,11846
PIT_080010000	GTPase-activating protein, putative	0,995379	2,31041	0,190143	1,20191	0,917225	2,18218
PIT_140068700	conserved Plasmodium protein, unknown function	1,19009	2,29721	0,606589	2,26559	1,81716	3,52771
PIT_010013900	transcription initiation factor TFIIB, putative	0,366763	2,29376	0,120086	0,998534	1,36585	4,09559
PIT_050006300	serine/threonine protein kinase, FIKK family	0,343555	2,2746	1,24073	4,98117	0,972308	3,6995
PIT_100025900	schizont egress antigen-1	1,68728	2,27028	0,351102	1,99814	0,519411	1,61856
PIT_050033900	nucleolar preribosomal GTPase, putative	1,35613	2,26666	0,224724	1,32177	0,355958	1,23295
PIT_130072200	conserved Plasmodium protein, unknown function	1,0532	2,26279	0,648881	2,14041	1,06731	2,25671
PIT_140042600	conserved Plasmodium protein, unknown function	0,635991	2,26067	0,637059	2,65067	0,723004	2,41259
PIT_030012300	conserved protein, unknown function	1,13139	2,23918	0,201951	1,14347	0,589139	1,65212
PIT_110012600	IWS1-like protein, putative	1,15346	2,23066	0,082823	0,58905	0,831769	1,60102
PIT_120050000	conserved Plasmodium protein, unknown function	0,425219	2,21756	0,550651	2,92865	0,580087	2,84089
PIT_020024100	replication factor C subunit 1, putative	1,9473	2,21498	0,672748	2,21584	1,44742	2,03011
PIT_050032200	DNA replication licensing factor MCM3, putative	1,79866	2,20652	0,758628	2,38825	1,55305	1,70223
PIT_100029100	formin 2, putative	0,903441	2,20603	0,382235	1,77952	0,882528	2,14509
PIT_140027850	40S ribosomal protein S25, putative	0,703825	2,20596	0,418446	1,54331	0,586769	1,73456
PIT_060010000	conserved Plasmodium protein, unknown function	1,54276	2,19581	0,340755	1,68622	1,03876	1,93583
PIT_090035700	elongation factor Tu, putative	1,74317	2,19498	0,39715	1,85129	0,554694	1,62082
PIT_020014700	60S ribosomal protein L37ac, putative	0,787355	2,19369	0,613786	2,02463	0,644744	1,70604
PIT_070016400	regulator of chromosome condensation, putative	1,27105	2,18701	0,476492	1,86849	1,60096	2,27398
PIT_120009300	nucleosome assembly protein	0,348835	2,17669	0,817392	4,22522	0,285408	2,17356
PIT_110022200	conserved Plasmodium protein, unknown function	0,600023	2,17375	0,424283	2,42086	0,608238	2,25742
PIT_120051000	epsin, putative	0,368565	2,17007	0,142744	1,24632	0,334097	1,99469
PIT_140020900	60S ribosomal protein L10, putative	0,639331	2,16765	0,347201	1,54488	0,326794	1,37183
PIT_110038300	conserved Plasmodium protein, unknown function	1,14536	2,16359	0,787172	1,74159	NaN	0
PIT_130037500	conserved Plasmodium protein, unknown function	0,673242	2,16137	0,523958	2,34223	0,535468	1,74595
PIT_140044900	metacaspase-like protein	0,665789	2,14265	0,502528	2,30958	0,686509	2,13613
PIT_080006400	Plasmodium exported protein (PHISTc), unknown function	0,784091	2,14193	0,348732	1,4834	0,579461	1,67623
PIT_100020400	glycophorin binding protein	1,61106	2,14126	0,582645	1,85102	1,59132	2,1901
PIT_030021600	40S ribosomal protein S15A, putative	1,122	2,12806	0,681106	1,9076	0,997457	1,78256
PIT_120050400	kinasin-13,						

PfIT_050024900	conserved Plasmodium protein, unknown function	0,737445	2,05938	0,619335	1,92226	0,609657	1,5438
PfIT_120051500	conserved Plasmodium protein, unknown function	0,932298	2,04493	0,435548	2,11958	0,362958	1,23699
PfIT_070028100	conserved Plasmodium protein, unknown function	0,798144	2,04026	0,134362	0,802258	0,690883	1,32099
PfIT_100036000	mRNA-decapping enzyme subunit 1, putative	1,48584	2,03804	0,468731	1,76642	1,34918	1,71442
PfIT_030007300	cytoadherence linked asexual protein 3.1	0,411824	2,0371	0,346531	1,84007	0,345509	1,78549
PfIT_090026490	ubiquitin-like protein, putative	0,784322	2,0316	0,168831	0,959146	0,451444	1,31352
PfIT_040021200	small GTP-binding protein sar1	0,42379	2,02173	0,577048	3,02584	0,550183	2,48958
PfIT_140066700	60S ribosomal protein L29, putative	1,62441	2,01249	0,827992	1,91997	1,10249	1,5056
PfIT_140007700	Plasmodium exported protein, unknown function	0,542365	2,00142	0,274586	-0,78894	0,367645	0,373104
PfIT_100028000	chromodomain-helicase-DNA-binding protein 1 homolog, putative	0,817377	2,00031	0,372168	1,67123	0,574402	1,39737
PfIT_030008900	inner membrane complex protein 1c, putative	0,448619	1,99346	0,324658	1,88896	0,526401	2,31086
PfIT_130020600	conserved Plasmodium protein, unknown function	0,330267	1,9917	0,426447	2,64702	0,17007	1,16016
PfIT_120011600	eukaryotic translation initiation factor 3 subunit C, putative	0,931542	1,98539	0,228316	1,38677	0,90844	2,49326
PfIT_080020800	vacuolar protein sorting-associated protein 9, putative	0,938029	1,96676	0,602147	3,04333	0,891176	2,85099
PfIT_090028400	RNA-binding protein, putative	0,788659	1,96564	0,44975	1,70756	0,809536	1,88966
PfIT_080022600	conserved Plasmodium protein, unknown function	0,475251	1,94745	0,577706	2,48428	0,536213	2,09751
PfIT_070011300	60S ribosomal protein L37	0,732371	1,93538	0,580116	1,68846	0,484776	1,21309
PfIT_110014800	asparagine-rich antigen	0,767151	1,93043	0,548044	1,7314	0,630576	1,58558
PfIT_010007800	ubiquitin carboxyl-terminal hydrolase 1, putative	0,689345	1,92781	0,189311	1,0653	0,302848	1,09247
PfIT_060008400	conserved Plasmodium protein, unknown function	1,15626	1,92194	0,528747	1,86354	1,09244	1,86595
PfIT_110011900	polyadenylate-binding protein-interacting protein 1, putative	1,30481	1,91621	0,450289	1,58202	1,12828	1,65436
PfIT_110038900	conserved Plasmodium protein, unknown function	0,68957	1,9149	0,471066	1,77258	1,16657	2,22481
PfIT_010011500	conserved Plasmodium protein, unknown function	1,24745	1,91023	0,51635	1,86152	1,13951	1,85367
PfIT_060016200	leucine-rich repeat protein	1,77007	1,9008	1,19541	2,78173	0,768834	1,86645
PfIT_010010100	ras-related protein Rab-5C	0,276628	1,87845	0,417266	2,69821	0,382857	2,56812
PfIT_120043000	calyculin binding protein, putative	0,451906	1,87694	0,667852	2,53427	0,519504	1,97266
PfIT_020018600	protein transport protein SEC31	0,898212	1,87526	0,485813	1,96389	0,86762	2,18099
PfIT_060033300	amino acid transporter, putative	0,41816	1,87469	0,404582	1,93189	0,261168	1,2306
PfIT_070015500	60S ribosomal protein L34	0,890241	1,86358	0,810298	1,70888	0,753055	1,53193
PfIT_130060300	conserved Plasmodium protein, unknown function	0,923152	1,85993	0,358842	1,75105	1,17864	2,3293
PfIT_070025800	40S ribosomal protein S5, putative	0,883398	1,85033	0,630065	1,56488	0,799287	1,41863
PfIT_090005300	rifin	0,798595	1,82835	2,708	9,50138	NaN	0
PfIT_080019000	60S ribosomal protein L13-2, putative	0,665846	1,82654	0,663332	1,73333	0,522113	1,19577
PfIT_110030700	40S ribosomal protein S18, putative	0,707854	1,82355	0,72378	1,97626	0,898472	2,11561
PfIT_130013000	tripartite motif protein, putative	0,50129	1,81901	0,449147	2,52881	0,019225	-0,14127
PfIT_080028200	RNA-binding protein, putative	2,09069	1,81617	0,633194	1,78686	1,87658	1,88697
PfIT_130020700	zinc finger (CCH type) protein, putative	1,66881	1,81261	0,679002	2,09521	1,74938	2,24828
PfIT_100007700	40S ribosomal protein S20c, putative	0,735201	1,80509	0,563203	1,7143	0,767876	1,73004
PfIT_100007800	inner membrane complex protein 1c, putative	0,242231	1,79424	0,344638	2,69072	0,34923	2,60547
PfIT_100010300	DNA/RNA-binding protein Alpha 3	0,160901	1,77374	0,173194	1,8526	0,48097	3,46938
PfIT_050037000	Plasmodium exported protein (PHISTb), unknown function	1,01588	1,75576	0,433952	1,20439	0,899538	1,50495
PfIT_140081100	trailer hitch homolog, putative	0,442026	1,75496	0,450993	1,65694	0,572011	1,9042
PfIT_020015500	conserved Plasmodium protein, unknown function	1,00449	1,75361	0,550328	1,50149	0,742272	1,11625
PfIT_040020300	60S ribosomal protein L15, putative	0,673477	1,75325	0,540661	1,4263	0,433921	1,0433
PfIT_140032400	60S ribosomal protein L21	0,597507	1,74531	0,542519	1,63499	0,543191	1,44488
PfIT_110014600	pre-mRNA-processing factor 6, putative	1,31663	1,74441	1,1152	2,16337	0,530683	0,942488
PfIT_120057300	rhopyr neck protein 3	0,465472	1,72793	0,445229	1,6766	0,489083	1,74338
PfIT_050034500	conserved Plasmodium protein, unknown function	1,01281	1,7132	0,291942	1,44072	1,02869	1,79568
PfIT_050020600	conserved Plasmodium protein, unknown function	0,88481	1,71302	0,356054	1,40095	1,8301	2,47268
PfIT_140026100	conserved Plasmodium membrane protein, unknown function	0,954785	1,71115	0,327306	1,3961	0,669017	1,22667
PfIT_080018900	40S ribosomal protein S16, putative	0,816597	1,70894	0,499003	1,29487	0,562463	1,12414
PfIT_100018100	conserved Plasmodium protein, unknown function	0,583061	1,69041	0,641866	2,73517	0,887486	2,44528
PfIT_080019200	DNA/RNA-binding protein Alpha 1	1,19038	1,68592	0,60207	1,09267	0,70179	0,929198
PfIT_030027700	40S ribosomal protein S3A, putative	0,877422	1,68488	0,571369	1,75213	0,923092	1,48563
PfIT_120018100	eukaryotic translation initiation factor 3 subunit A, putative	1,59953	1,67716	0,565548	1,39497	1,35305	1,55921
PfIT_050012900	nuclear protein localization protein 4, putative	0,474008	1,6673	0,100578	0,99374	2,16242	3,28719
PfIT_080017400	karyopherin alpha	1,01609	1,65973	0,549999	1,70686	1,07132	1,69171
PfIT_040027200	eukaryotic initiation factor 4A-III, putative	0,473234	1,65885	0,818479	2,80957	0,740537	2,50164
PfIT_110046700	60S ribosomal protein L28	0,874378	1,64398	0,801629	1,63695	0,817795	1,48878
PfIT_080025500	C-13 antigen	0,66169	1,64014	0,316243	1,46372	0,414052	1,2592
PfIT_030007800	N-ethylmaleimide-sensitive fusion protein	0,86223	1,62918	0,554595	2,27144	0,768466	1,63699
PfIT_130036100	conserved Plasmodium protein, unknown function	0,370677	1,61523	0,182005	0,952513	0,044869	0,245293
PfIT_090026400	conserved Plasmodium protein, unknown function	0,848236	1,61237	0,005169	-0,0408	0,23536	0,526438
PfIT_110042500	conserved Plasmodium protein, unknown function	0,6298	1,6118	0,549882	2,00602	0,618857	2,0607
PfIT_130039000	histone H3-like centromeric protein CSE4	0,809116	1,59563	0,538835	1,97041	0,885355	1,8707
PfIT_060018500	60S ribosomal protein L19	0,521292	1,59135	0,391568	1,05395	0,420063	0,882336
PfIT_070013900	chloroquine resistance transporter	0,241611	1,58964	0,038146	0,354243	0,217549	-1,68399
PfIT_060022100	60S ribosomal protein L27a, putative	0,516108	1,58792	0,483446	1,44324	0,319405	0,947721
PfIT_130023100	40S ribosomal protein S19	1,13133	1,5879	0,782408	1,49965	0,615593	0,969116
PfIT_100035200	conserved Plasmodium protein, unknown function	0,336708	1,58591	0,437887	1,98108	0,446808	2,05577
PfIT_140036200	coatamer beta subunit, putative	0,501069	1,58551	0,194525	1,02319	0,47204	0,728924
PfIT_120053900	conserved Plasmodium protein, unknown function	0,660892	1,55798	0,258691	1,2497	0,463267	1,14259
PfIT_130064200	40S ribosomal protein S15	1,11964	1,55091	0,703606	2,2475	1,85088	2,54083
PfIT_110035900	26S protease regulatory subunit 6A, putative	0,38925	1,54835	0,474452	2,26216	0,583886	2,20604
PfIT_110029400	60S ribosomal protein L5, putative	1,28502	1,53767	0,503336	1,36844	1,39802	1,56103
PfIT_110019600;PfIT_110020000	cysteine protease falcipain 2a	0,431088	1,53708	0,449861	2,46152	0,817461	2,7583
PfIT_110048000	tudor staphylococcal nuclease	0,652044	1,53008	0,595483	2,36688	1,08484	2,2953
PfIT_130071100;PfIT_120017200	ubiquitin-60S ribosomal protein L40	2,68831	1,52312	1,94741	2,14418	2,31368	1,5957
PfIT_030012900	conserved Plasmodium protein, unknown function	0,509245	1,52129	0,7667	2,39373	0,680144	1,70156
PfIT_060011000	translation initiation factor IF-2, putative	1,11944	1,49701	0,597541	2,11395	1,44263	1,99594
PfIT_110034600	60S ribosomal protein L38	1,051	1,49229	0,710786	1,95052	1,20083	1,64545
PfIT_140033700	conserved Plasmodium protein, unknown function	0,706361	1,48095	0,986881	2,30696	0,144992	0,582329
PfIT_140013700	rRNA 2-O-methyltransferase fibrillar, putative	1,45807	1,47178	0,537294	1,38886	1,24117	1,33692
PfIT_140055900	transcription factor with AP2 domain(s), putative	0,675328	1,46898	0,014647	-0,1105	0,366508	1,1569
PfIT_070028000	conserved Plasmodium protein, unknown function	0,266953	1,46807	0,351427	2,2721	0,498273	2,33524
PfIT_050025200	40S ribosomal protein S9, putative	0,520934	1,45863	0,273236	0,927258	0,96462	1,3793
PfIT_080018400	conserved Plasmodium protein, unknown function	1,06631	1,45639	0,498794	1,38662	1,02378	1,49378
PfIT_050022100	60S ribosomal protein L2	0,542415	1,45442	0,379048	1,1428	0,488775	1,21617
PfIT_140030200	conserved Plasmodium protein, unknown function	0,822722	1,45333	0,448646	1,47412	0,687216	1,39052
PfIT_050020200	pre-mRNA-splicing factor CWC2, putative	0,841314	1,45084	0,084975	0,698624	1,51593	2,12579
PfIT_130014200	60S ribosomal protein L24, putative	0,696976	1,44324	0,477608	1,17071	0,420587	1,11392
PfIT_090010100	high molecular weight rhopyr protein 3	0,448865	1,44128	0,303013	1,31025	0,223906	0,850565
PfIT_030012500	conserved Plasmodium protein, unknown function	0,611485	1,43722	0,468608	1,79987	0,38741	1,18581
PfIT_050008700	serine/arginine-rich splicing factor 12	0,565934	1,43555	0,323831	1,28928	0,262786	0,747527
PfIT_030025600	ATP-dependent RNA helicase DDX6	0,516009	1,4287	0,530999	1,60909	0,71836	1,50578
PfIT_120035700	protein transport protein SEC13	0,350088	1,42634	0,537995	2,40006	0,707414	2,55447
PfIT_060015700	60S ribosomal protein L39	0,535027	1,42239	0,511016	1,56785	0,316843	1,14005
PfIT_130067100	conserved Plasmodium protein, unknown function	0,470356	1,40731	0,58252	2,83286	1,32145	3,46999
PfIT_100010900	RNA-binding protein, putative	0,740843	1,4046	0,265119	0,703716	0,209948	0,399173
PfIT_120022200	DNA-binding chaperone, putative	0,860158	1,39155	0,234528	1,43894	0,650146	1,50986
PfIT_060014900	transcription elongation factor SPT5, putative	0,834235	1,39056	0,313725	1,06397	1,05534	1,12085
PfIT_050037100	lysine-rich membrane-associated PHISTb protein	0,611233	1,38887	0,269662	0,880983	0,411846	0,797611
PfIT_140084700	EMPI1-trafficking protein	0,550378	1,37867	0,263818	1,87701	0,709439	2,28286
PfIT_140054500	multidrug resistance protein 2	0,554776	1,37508	0,081838	0,538353	0,142867	0,601951
PfIT_100031800	60S ribosomal protein L3	0,480288	1,37298	0,406832	1,19277	0,28536	0,731619
PfIT_130007900	40S ribosomal protein S7, putative	3,43374	1,37021	0,664162	1,71308	1,77428	1,92822
PfIT_050012300	60S ribosomal protein L4	0,555349	1,36577	0,372607	0,95061	0,24744	0,618067
PfIT_100008200	60S ribosomal protein L13, putative	0,66921	1,36008	0,677307	1,59037	0,721908	1,26165
PfIT_080036100	Plasmodium exported protein, unknown function	0,493036	1,34661	1,19577	-4,15576	2,21385	-6,82844
PfIT_110021100	heat shock protein 101	0,311985	1,34535	0,133729	0,696573	0,969797	4,68387
PfIT_070008400	erythrocyte membrane-associated antigen	0,995191	1,33672	0,540131	1,39273	0,765572	1,22577
PfIT_060028400	SNF2 helicase, put						

PIT_08002790	conserved Plasmodium protein, unknown function	0,346276	1,26915	0,579366	2,46061	0,375362	1,82365
PIT_110014300	60S ribosomal protein L36	1,38121	1,26172	0,659318	1,94776	2,60932	1,85481
PIT_130047300	40S ribosomal protein S6	1,30347	1,26047	1,31623	1,51419	0,647334	0,982111
PIT_110023600	splicing factor UZAF small subunit, putative	0,41658	1,25269	0,106888	0,747628	1,01455	2,87273
PIT_100008600	RNA-binding protein, putative	0,641589	1,2492	0,105466	0,379555	0,304674	0,334997
PIT_140052190	conserved Plasmodium protein, unknown function	0,634845	1,24782	0,287311	0,855528	0,416951	0,795622
PIT_070026600	conserved Plasmodium protein, unknown function	3,57234	1,24292	0,137909	0,886284	0,417928	2,3022
PIT_070028800	protein kinase, putative	0,505074	1,22851	0,133564	0,665397	0,409117	0,964814
PIT_140044400	eukaryotic translation initiation factor eIF2A, putative	0,923616	1,22192	0,388472	1,34523	0,828431	1,18353
PIT_120034500	T-complex protein 1 subunit gamma	0,51374	1,21989	0,671411	2,82818	0,790221	2,3559
PIT_050031000	inner membrane complex protein Ig, putative	0,48147	1,20326	0,376973	1,37984	0,486337	1,31956
PIT_060021800	conserved Plasmodium membrane protein, unknown function	0,485864	1,20139	0,33595	1,64736	0,588225	1,51449
PIT_060017300	rhopty protein ROP14	0,447043	1,19645	0,389806	1,58206	0,53202	1,57967
PIT_130021900	cholesterol-phosphate cytidylyltransferase	0,314989	1,19415	0,070131	0,506481	0,211467	1,0994
PIT_110012400	transcription factor with AP2 domain(s)	1,87489	1,19182	0,378871	1,12421	2,1463	1,35411
PIT_090033800	RNA-binding protein, putative	0,741757	1,18741	0,595259	1,6249	0,845731	1,51189
PIT_020006600	knob associated heat shock protein 40	0,490266	1,18212	0,321904	1,15112	0,387341	0,984697
PIT_130061500	conserved Plasmodium protein, unknown function	0,584302	1,17803	0,616102	2,58736	1,36029	3,40177
PIT_050011100	small ubiquitin-related modifier	0,266185	1,17749	0,596207	2,42462	0,708405	1,68819
PIT_140053400	40S ribosomal protein S5	0,4952	1,17348	0,477337	1,16261	0,363484	0,778674
PIT_090034900	merozoite surface protein 1	0,2973	1,16112	0,649673	2,14146	0,643263	1,78417
PIT_100012400	26S protease regulatory subunit 4, putative	0,197855	1,15371	0,744533	4,0835	0,889802	4,14562
PIT_130037000	glutamine-tRNA ligase, putative	0,497608	1,14676	0,31932	1,29157	0,834633	1,29157
PIT_090008100	DEAD/DEAH box helicase, putative	0,218991	1,13496	0,536883	2,47594	0,189748	1,04173
PIT_140058400	rhopty neck protein 2	0,404659	1,12224	0,542782	2,42156	0,584629	2,1072
PIT_050022500	serine/arginine-rich splicing factor 1	0,785339	1,12111	0,663167	1,59511	0,353656	0,951011
PIT_130057700	conserved Plasmodium protein, unknown function	0,732854	1,11969	0,181011	0,64857	0,646113	1,00596
PIT_110043200	conserved Plasmodium protein, unknown function	0,396159	1,11786	0,170522	0,891706	0,511663	1,69811
PIT_080017500	RNA-binding protein, putative	0,471689	1,1172	0,043392	0,174279	0,169308	0,467363
PIT_130051600	DNA/RNA-binding protein Alba 2	0,926613	1,11185	0,65049	2,06503	1,55915	2,32183
PIT_100006600	RNA-binding protein, putative	0,3764	1,10705	0,299296	1,09563	0,352354	0,965406
PIT_080018000	conserved Plasmodium protein, unknown function	0,558908	1,10184	0,140558	0,65191	0,312055	0,635222
PIT_110026000	protein GCN20	0,486713	1,09018	0,104742	0,767204	0,821992	1,72328
PIT_060031600	acetyl-CoA synthetase, putative	0,428136	1,0706	0,148753	1,03608	0,501973	1,84428
PIT_110009600	histone H2B	0,601855	1,06985	0,488773	1,5457	0,670699	1,31081
PIT_050009100	60S ribosomal protein L31	1,23393	1,05391	0,829911	1,68962	1,246	0,99608
PIT_110013000	casein kinase 2, alpha subunit	0,710053	1,05266	0,684155	1,74429	0,841936	1,58809
PIT_110049300	coatomer subunit gamma, putative	0,497811	1,04245	1,47372	1,59491	1,46815	1,83285
PIT_050036000	formin 1	0,306615	1,0338	0,639017	1,81373	0,602052	1,76072
PIT_110008700	chromatin remodeling protein	0,343009	1,03107	0,489604	2,04906	1,06567	1,81442
PIT_030012000	60S ribosomal protein L7, putative	0,524335	1,02849	0,569925	1,55108	0,943878	1,58704
PIT_130064800	CUGBP Elav-like family member 1	0,624741	1,02828	0,418804	1,59791	0,36799	0,773298
PIT_130053900	conserved Plasmodium protein, unknown function	0,157097	1,02759	0,236702	1,51343	0,287419	1,80851
PIT_120027400	endoplasmic reticulum protein, putative	0,267565	1,02145	0,80955	2,30051	0,912015	2,57163
PIT_140074400	conserved Plasmodium protein, unknown function	0,760928	1,01915	0,451338	1,11618	0,835192	0,794313
PIT_130056700	60S ribosomal protein L17, putative	0,460963	1,0015	0,387329	0,927008	0,175855	0,358544
PIT_030022100	conserved Plasmodium protein, unknown function	0,340487	0,97823	1,02462	4,64414	0,812725	1,36353
PIT_140015200	40S ribosomal protein S8c, putative	0,557254	0,977404	0,353769	0,75458	0,606017	0,992561
PIT_130046500	60S ribosomal protein L18, putative	0,467649	0,976692	0,443176	1,05243	0,32185	0,644051
PIT_110048800	transcription initiation factor IIF subunit beta, putative	0,19076	0,971244	0,087388	0,858364	0,980934	3,2898
PIT_020017000	conserved Plasmodium protein, unknown function	0,524315	0,970165	0,627013	1,53541	1,13203	1,25229
PIT_080012700	conserved Plasmodium protein, unknown function	0,70005	0,969265	0,245717	0,560041	0,349792	0,484757
PIT_060009100	RNA-binding protein, putative	0,348918	0,963039	0,318323	1,48641	0,538422	1,69132
PIT_140067800	conserved Plasmodium protein, unknown function	0,556318	0,960097	1,22721	2,19004	0,68576	1,35314
PIT_130057000	inner membrane complex protein If, putative	0,213031	0,954571	0,320085	1,46385	0,299415	1,26261
PIT_040019900	nuclear cap-binding protein, putative	2,74829	0,949499	0,41201	1,36279	1,35168	1,11412
PIT_100016900	autophagy-related protein 18, putative	0,340623	0,936115	0,088606	0,515116	0,302594	0,650604
PIT_130061400	conserved Plasmodium protein, unknown function	0,298485	0,926248	0,408894	1,22134	0,369248	1,12193
PIT_140070200	conserved Plasmodium membrane protein, unknown function	0,514759	0,908329	0,526612	1,89664	0,701642	1,34811
PIT_020016800	peptide chain release factor subunit 1, putative	0,191237	0,907468	0,123085	0,704025	0,123308	0,576701
PIT_070009700	conserved Plasmodium protein, unknown function	0,210081	0,903639	0,212018	1,29215	0,312446	1,40209
PIT_130076500	Plasmodium exported protein, unknown function	0,192889	0,861709	0,616092	2,71744	1,21121	2,29792
PIT_140022700	protein SEY1, putative	0,21527	0,860335	0,11837	0,696647	0,466919	1,67964
PIT_100034100	conserved Plasmodium protein, unknown function	0,10908	0,852294	0,215475	1,73215	0,479681	2,96119
PIT_130057800	thioredoxin-related protein, putative	0,336711	0,84673	0,443602	1,31495	0,830399	1,57623
PIT_050017700	ras-related protein Rab-1B	0,309762	0,842764	0,331844	0,915652	0,388331	1,03362
PIT_110010000	40S ribosomal protein S4, putative	0,466897	0,838188	0,381602	0,945609	0,412433	0,717073
PIT_120024400	clathrin heavy chain, putative	0,224204	0,828487	0,523465	1,80503	0,352202	1,27031
PIT_130073500	ABC transporter E family member 1, putative	0,254537	0,816379	0,117373	0,781267	0,122054	0,652019
PIT_120023600	AP-2 complex subunit mu, putative	0,342793	0,811653	0,116145	0,415998	0,470661	1,00003
PIT_140030600	60S ribosomal protein L5, putative	0,563794	0,810172	0,579784	1,47122	0,771329	1,11025
PIT_140077600	diacylglycerol kinase, putative	0,291379	0,809177	0,13234	0,564536	0,295003	0,821429
PIT_130066200	polyadenylate-binding protein, putative	0,503637	0,793505	0,539895	1,32739	0,681621	1,14513
PIT_100038800	methionine-tRNA ligase	0,399257	0,786557	0,308304	1,18818	0,156284	0,501472
PIT_140052300	ATP-dependent RNA helicase DDX5, putative	0,700266	0,785149	0,278336	0,792462	0,976482	0,976034
PIT_120028500	phospholipid-transporting ATPase, putative	0,382309	0,78319	0,196699	0,79031	0,320597	0,679696
PIT_120048000	40S ribosomal protein S17, putative	0,527711	0,775483	0,480352	1,10272	0,897262	1,10609
PIT_070018500	conserved Plasmodium protein, unknown function	0,242402	0,766808	0,319032	1,21062	0,276708	0,8575
PIT_140030900	60S ribosomal protein L7-3, putative	0,779074	0,764072	0,504946	1,37426	0,778068	1,05218
PIT_110009500	histone H4	0,440214	0,760967	0,501523	1,10232	0,746431	0,930098
PIT_100012000	eukaryotic translation initiation factor 3 subunit D, putative	0,700419	0,756856	0,342967	0,875943	0,548353	0,806787
PIT_070033800	conserved Plasmodium protein, unknown function	0,546646	0,754767	0,372349	1,05876	0,522222	0,624894
PIT_140022000	conserved Plasmodium protein, unknown function	0,107335	0,745795	0,166413	0,972598	0,175944	1,03313
PIT_130014000	mRNA-decapping enzyme 2, putative	0,171428	0,7402	0,040414	0,322155	0,086136	0,414897
PIT_120028200	cAMP-dependent protein kinase regulatory subunit	0,242995	0,730196	0,385603	1,70276	0,549185	1,50211
PIT_030008000	HAD superfamily protein, putative	0,221913	0,728944	0,169447	1,05485	0,418262	1,32236
PIT_140023800	NOT family protein, putative	0,103041	0,721633	0,082624	0,710521	0,127617	0,871679
PIT_130031600	RNA-binding protein, putative	0,66413	0,712411	0,207682	0,587722	0,545943	0,641851
PIT_080012400	ras-related protein Rab-18	0,33485	0,710272	0,526372	1,09124	0,324401	0,762976
PIT_130059700	large subunit rRNA methyltransferase, putative	0,37038	0,706603	0,225772	0,890397	0,124173	-0,66149
PIT_040027800	conserved Plasmodium protein, unknown function	0,124369	0,702011	0,860546	3,54993	1,04644	3,51493
PIT_020015200	conserved Plasmodium protein, unknown function	0,160925	0,698314	0,46816	1,80304	0,298442	1,32663
PIT_140072200	40S ribosomal protein S3	0,30797	0,695913	0,647665	1,41121	0,429736	0,711808
PIT_140019100	actin II	0,131353	0,693698	0,146861	1,09452	0,044354	0,311767
PIT_020012200	serine repeat antigen 6	0,197463	0,686973	0,51615	1,99068	0,53989	1,59436
PIT_120044700	conserved Plasmodium protein, unknown function	0,387312	0,68157	0,342242	1,0058	0,530789	1,00492
PIT_130065000	conserved Plasmodium protein, unknown function	0,187204	0,677034	0,052742	-0,27883	0,069026	-0,25791
PIT_090009800	nucleoporin NUP100/NSP100, putative	0,210123	0,672997	0,079172	0,323207	0,115842	0,377654
PIT_090034000	high molecular weight rhopty protein 2	0,147856	0,669708	0,279775	1,37396	0,318117	1,29386
PIT_080032800	protein disulfide isomerase	0,431903	0,663534	0,915449	1,36726	1,26217	2,21333
PIT_050023700	ATP-dependent RNA helicase DDX23, putative	0,172954	0,65887	0,140577	0,683092	0,136945	0,441225
PIT_060021700	histone H3 variant, putative	0,322265	0,644587	0,448394	1,31166	0,542382	1,055
PIT_120032800	conserved Plasmodium protein, unknown function	0,183974	0,63969	0,002752	0,025345	0,452896	1,5289
PIT_030022400	40S ribosomal protein S11, putative	0,259759	0,636149	0,141937	0,353481	0,022499	0,056621
PIT_140021400	small nuclear ribonucleoprotein-associated protein B, putative	0,374591	0,634238	0,161098	-0,93241	0,537441	0,722500
PIT_120010900	zinc finger protein, putative	0,243456	0,631698	0,426063	1,45768	0,661381	1,40647
PIT_030025700	histone H2A variant, putative	0,327057	0,625125	0,58031	1,27409	0,500736	0,865339
PIT_060014300	histone H3	0,192678	0,624057	0,235018	1,12877	0,416302	1,26456
PIT_080022700	rhopty neck protein 5	0,139604	0,614274	0,475181	2,14926	0,564034	2,09678
PIT_130011500	26S protease regulatory subunit 10B, putative	0,158842	0,606558	0,703265	2,32366	0,401413	1,67039
PIT_110021700	conserved Plasmodium protein, unknown function	0,070301	0,60497	0,851491	4,05218	1,64438	6,03329
PIT_140038100	60S ribosomal protein L14, putative	0,191267	0,604378	0,6			

PfIT_120043700	glutyl-CoA synthetase	0,139473	0,54828	0,036687	0,330235	0,574732	1,99459
PfIT_010016100	lytic acid-rich protein	0,182481	0,539528	0,072311	0,32163	0,037374	-0,07911
PfIT_100012200	conserved Plasmodium protein, unknown function	0,137551	0,537017	0,173002	0,990271	0,199665	0,675285
PfIT_080023200	14-3-3 protein	0,352946	0,52905	1,39339	2,23361	1,56779	2,41971
PfIT_080023900	heat shock protein 70	0,317776	0,524783	0,462336	1,16646	0,58599	1,30645
PfIT_140022800	metacaspase-like protein	0,18128	0,52099	0,252344	1,38488	0,406924	1,29696
PfIT_140067100	60S ribosomal protein L27	0,521915	0,521915	0,464359	1,08073	0,875583	0,978377
PfIT_100016600	transcriptional coactivator ADA2	0,105342	0,519604	0,126605	0,696378	0,096347	0,529302
PfIT_000014600	eukaryotic translation initiation factor 2 beta subunit, putative	0,52103	0,516815	0,563191	1,45744	0,929496	1,05349
PfIT_140018900	nuclear transport factor 2, putative	0,063414	0,516485	0,052178	-0,55872	0,137468	1,12484
PfIT_070011400	conserved Plasmodium protein, unknown function	0,287085	0,505809	0,040102	0,201798	0,426612	0,778985
PfIT_020016600	conserved Plasmodium protein, unknown function	0,075797	0,484203	0,007185	0,055435	0,014859	0,100433
PfIT_130043500	60S ribosomal protein L6-2, putative	0,375325	0,483596	0,358466	1,02825	0,452692	0,6374
PfIT_110010200	translocon component PTEX88	0,151908	0,468346	0,429375	-1,45045	0,139057	-0,5255
PfIT_120029400	polyadenylate-binding protein, putative	0,354707	0,467704	0,373841	0,887047	0,468388	0,64545
PfIT_140038500	voltage-dependent anion-selective channel protein, putative	0,186233	0,463369	0,025117	-0,0697	0,146665	0,287537
PfIT_040006200	Plasmodium exported protein (PHISTb), unknown function	0,129247	0,461547	0,054392	0,187658	0,111282	0,358548
PfIT_100015800	PRE-binding protein	0,265761	0,456795	0,399251	1,25634	0,451684	1,02795
PfIT_140014500	plasmepsin II	0,237123	0,456739	0,4995	1,15044	0,57186	0,964988
PfIT_070023800	60S ribosomal protein L11a, putative	0,162509	0,452702	0,283552	0,697639	0,214227	0,513941
PfIT_020016300	asparagine-tRNA ligase	0,069535	0,448043	0,552498	2,72653	0,612459	2,51467
PfIT_040009400	dipeptidyl aminopeptidase 3	0,133924	0,44786	1,15187	3,04839	0,42093	1,78339
PfIT_130034800	conserved Plasmodium protein, unknown function	0,202432	0,44743	0,281424	-1,41683	0,398867	-0,8148
PfIT_140014600	plasmepsin II	0,172627	0,430679	0,380999	1,56335	0,34817	1,49684
PfIT_130017000	M1-family alanyl aminopeptidase	0,200095	0,422129	0,111975	-0,40267	0,257411	-0,6941
PfIT_050033300	AP-1 complex subunit beta, putative	0,146062	0,413207	0,435713	1,7162	0,830226	1,65336
PfIT_140014400	plasmepsin IV	0,113157	0,410482	0,649808	1,21657	0,20946	0,449209
PfIT_140074200	rab GTPase activator, putative	0,136739	0,407507	0,264137	1,0847	0,600342	1,4603
PfIT_110022800	box C/D snoRNP rRNA 2-O-methylation factor, putative	0,256487	0,390931	0,041959	0,250449	0,521259	0,948406
PfIT_100041000	ADP/ATP transporter on adenylate translocase	0,065054	0,388922	0,114135	0,600128	0,080948	0,418875
PfIT_050030300	acyl-CoA synthetase	0,307643	0,381883	0,369735	1,37433	0,951102	1,34556
PfIT_090007900	ras-related protein RAB7	0,186063	0,369269	0,626706	0,984105	0,370413	0,739676
PfIT_090023500	nucleosome assembly protein	0,131849	0,366782	0,394268	1,24545	0,625216	1,66589
PfIT_140017000	rhoptry-associated protein 1	0,083028	0,365667	0,091342	0,452318	0,23883	0,902146
PfIT_100026500	serine/arginine-rich splicing factor 4	0,418481	0,362501	0,440422	1,29356	0,416902	1,00934
PfIT_080016200	CCR4-associated factor 1	0,099586	0,359441	0,120578	0,446433	0,065184	0,266747
PfIT_100012800	nuclear protein 5, putative	0,156896	0,349287	0,045363	-0,37308	0,712778	1,24024
PfIT_140050700	1-acyl-sn-glycerol-3-phosphate acyltransferase, putative	0,034707	0,348891	0,022103	0,232118	0,257934	1,84682
PfIT_130008600	sodium/hydrogen exchanger, Na ⁺ , H ⁺ antiporter	0,09803	0,338291	0,067219	0,336023	0,251429	0,683291
PfIT_020016900	conserved Plasmodium membrane protein, unknown function	0,110352	0,321311	0,309065	1,06104	0,070332	-0,25092
PfIT_050011400	60S ribosomal subunit protein L24-2, putative	0,215971	0,3204	0,195106	0,480484	0,745447	-2,53178
PfIT_080015500	RNA helicase, putative	0,181305	0,31569	0,15123	0,404618	0,2541	0,394241
PfIT_140075100	splicing factor U2AF large subunit, putative	0,223105	0,307752	0,19393	0,761768	0,303716	0,442712
PfIT_140063700	conserved Plasmodium protein, unknown function	0,056657	0,289642	0,156849	0,949758	0,418988	1,65036
PfIT_090039600	cAMP-dependent protein kinase catalytic subunit	0,102537	0,286654	0,065174	0,41357	0,365386	0,738558
PfIT_090021300	RNA-binding protein musashi, putative	0,196631	0,279184	0,475044	1,35721	1,13649	1,26766
PfIT_050024600	40S ribosomal protein S24	0,887088	0,272214	0,645332	0,454419	0,213688	0,105799
PfIT_140014700	plasmepsin III	0,403074	0,246964	0,700057	3,03729	0,488014	2,26802
PfIT_070018300	histone H2B variant	0,108999	0,244424	0,202468	0,422047	0,347449	0,415734
PfIT_060023200	cell division cycle protein 48 homologue, putative	0,081415	0,239794	0,308044	1,31633	0,870327	1,61672
PfIT_030023000	DNA-directed RNA polymerase II subunit RPB1	0,053011	0,209305	0,789327	2,51413	0,21006	1,04217
PfIT_110041000	casein kinase 1	0,09912	0,207287	0,257423	0,788876	0,300008	0,711995
PfIT_130062200	serine/threonine protein kinase, putative	0,060176	0,206587	0,593927	2,53253	0,701245	1,85252
PfIT_140039700	chromatin assembly factor 1 P55 subunit, putative	0,03444	0,191767	0,24335	1,02715	0,158236	0,974768
PfIT_050016600	RNA pseudouridylate synthase, putative	0,080354	0,181238	0,051199	0,205953	0,234186	-0,4443
PfIT_110046800	60S ribosomal protein L35ae, putative	0,249187	0,170165	0,091995	0,193875	0,253908	0,293145
PfIT_110033500	spermidine synthase	0,031226	0,133677	0,333887	1,17084	0,208946	0,822519
PfIT_050026100	S-adenosyl-L-homocysteine hydrolase	0,045204	0,131476	0,415456	1,44422	0,326975	1,20518
PfIT_010006700	nucleoside transporter 4	0,033424	0,109615	0,177127	-0,85227	0,019045	-0,05746
PfIT_140072400	protein phosphatase containing kelch-like domains	0,038659	0,102342	0,164692	-0,36818	0,038459	-0,0906
PfIT_130015900	RNA-binding protein, putative	0,01955	0,096506	0,005362	-0,03394	0,133658	0,641744
PfIT_130069400	6-cysteine protein	0,023641	0,094503	0,230892	0,756143	0,018488	-0,07063
PfIT_100011800	transcription factor with AP2 domain(s)	0,020723	0,082503	0,220445	0,67942	0,153184	0,322652
PfIT_140076400	conserved Plasmodium protein, unknown function	0,020952	0,076368	0,06154	-0,20517	0,10135	-0,26201
PfIT_140044300	HSP40, subfamily A, putative	0,030517	0,073705	0,685574	1,54723	0,272334	0,755981
PfIT_090030400	conserved Plasmodium protein, unknown function	0,003621	0,038499	0,387947	2,34802	0,324541	1,9194
PfIT_140069200	glyceraldehyde-3-phosphate dehydrogenase	0,01275	0,038041	0,456163	1,22176	0,281847	0,791044
PfIT_090022500	heat shock protein 70	0,000278	0,000881	0,186386	0,482733	0,211033	0,610998
PfIT_140041200	mitochondrial acidic protein MAM33, putative	0,009444	-0,02713	0,004677	0,013439	0,392499	0,75153
PfIT_100012700	tubulin beta chain	0,017849	-0,05558	1,13619	2,83585	0,964697	2,27018
PfIT_050028200	multidrug resistance protein 1	0,022671	-0,07243	0,078219	0,302662	0,006505	-0,02344
PfIT_040023000	regulator of chromosome condensation, putative	0,177873	-0,08449	0,328253	-0,54821	0,08127	0,057485
PfIT_080026000	conserved Plasmodium protein, unknown function	0,044115	-0,1063	0,297623	0,749038	0,186913	0,443934
PfIT_050007900	rhoptry-associated protein 2	0,022341	-0,12181	0,044597	0,243084	0,092589	0,466035
PfIT_140057500	elongation factor 2	0,062457	-0,1223	0,380475	1,05984	0,32875	0,851671
PfIT_130068000	conserved Plasmodium protein, unknown function	0,072913	-0,13885	0,533057	1,05884	0,088516	0,314092
PfIT_110040400	3-oxo-5-alpha-steroid 4-dehydrogenase, putative	0,029414	-0,14135	0,327602	-1,36138	0,094824	0,433337
PfIT_030019900	eukaryotic translation initiation factor 4E	0,100099	-0,1438	0,069806	0,145369	0,12762	0,217544
PfIT_090040500	cytoadherence linked asexual protein 9	0,048053	-0,15716	0,12862	0,625216	0,182116	0,631285
PfIT_100041200	dynamitin-like protein	0,034332	-0,16125	0,208553	1,40098	0,407505	1,7637
PfIT_110030000	small nuclear ribonucleoprotein Sm D1, putative	0,16197	-0,16168	0,250114	-1,63881	0,32592	-1,17477
PfIT_060012900	ornithine aminotransferase	0,088857	-0,1694	0,380792	1,42138	0,49783	1,30668
PfIT_110022000	GTP-binding nuclear protein RAN/GC4	0,084514	-0,17776	0,354666	0,772296	0,234485	0,58907
PfIT_100025000	ADP-ribosylation factor	0,042848	-0,20268	0,473658	1,36678	0,334535	1,1855
PfIT_130011000	conserved Plasmodium protein, unknown function	0,141301	-0,21022	0,397856	1,07129	0,167096	0,551561
PfIT_060012800	T-complex protein 1 subunit zeta	0,061698	-0,21537	0,114543	0,462784	0,583671	1,16693
PfIT_030025900	conserved Plasmodium protein, unknown function	0,183777	-0,21829	0,335728	0,579822	0,530024	-1,22019
PfIT_090030600	protein kinase, putative	0,053516	-0,21883	0,407284	-1,34633	0,545633	-1,87265
PfIT_020014500	ATP-dependent RNA helicase UAP56	0,08205	-0,22049	0,025582	0,162286	0,304934	0,747911
PfIT_110039400	coatamer subunit delta	0,159342	-0,23678	0,394636	0,609756	0,269429	0,749147
PfIT_110041300	DnaI protein, putative	0,09304	-0,2418	0,174407	-0,86503	0,329769	0,76887
PfIT_140067000	inner membrane complex sub-compartment protein 3	0,033061	-0,24415	0,607458	3,29003	0,837054	3,72544
PfIT_100023500	60S ribosomal protein L30e, putative	0,104718	-0,2537	0,18491	0,516513	0,00318	0,010268
PfIT_040010100	pre-mRNA-processing-splicing factor 8, putative	0,234365	-0,26513	0,260454	0,991598	0,17263	0,29024
PfIT_130029000	glicodeome associated protein with multiple membrane spans 1	0,135971	-0,26579	0,411346	0,65538	0,226172	0,610567
PfIT_110024400	phosphoglycerate mutase, putative	0,112277	-0,27242	0,05618	-0,3425	0,070382	0,247802
PfIT_140047600	60S ribosomal protein L1, putative	0,118937	-0,29524	0,282213	0,564007	0,043988	0,066026
PfIT_130048300	phosphoethanolamine N-methyltransferase	0,218894	-0,31279	0,455044	1,15395	0,273133	0,914226
PfIT_090022600	glicodeome-associated protein 50	0,074244	-0,32923	0,12925	0,488846	0,306368	1,04763
PfIT_030023600	triosephosphate isomerase, putative	0,148502	-0,33862	0,106485	0,249727	0,304644	-0,61471
PfIT_140054100	conserved Plasmodium protein, unknown function	0,093811	-0,34113	0,3832	-1,99568	0,026687	-0,07998
PfIT_060030600	pyruvate kinase	0,058526	-0,34887	0,209451	1,20067	0,378502	1,78857
PfIT_120051400	actin I	0,200648	-0,37095	0,152685	0,39275	0,128809	0,29623
PfIT_090011300	zinc finger protein, putative	0,080924	-0,37222	0,194279	-0,95099	0,443103	-1,92626
PfIT_120036100	ras-related protein Rab-2	0,124495	-0,38479	0,078213	0,260646	0,119715	0,360369
PfIT_090009300	ubiquitin specific protease, putative	0,500015	-0,39204	0,752478	1,64711	0,498845	0,461385
PfIT_010009600	calcium-transporting ATPase	0,182132	-0,40455	0,147481	0,41511	0,004955	0,016195
PfIT_140016000	conserved Plasmodium membrane protein, unknown function	0,093451	-0,41431	0,177504	0,608842	0,251754	0,887382
PfIT_110020700	guanine nucleotide-exchange factor SEC12	0,219315	-0,41452	0,137578	0,284562	0,164824	0,460987
PfIT_070025600	conserved Plasmodium protein, unknown function	0,049741	-0,42674	0,080127	0,794463	0,129126	1,17008
PfIT_08003							

PfIT_140043600	ribonucleoside-diphosphate reductase, large subunit, putative	0,109683	-0,60078	0,631637	2,6835	0,092376	0,64453
PfIT_130052800	DNA/RNA-binding protein Alba 4	0,389737	-0,61245	0,308406	-0,50759	0,192382	-0,32206
PfIT_120011200	high mobility group protein B3, putative	0,420837	-0,62236	0,120474	-0,21581	0,167782	-0,37875
PfIT_130049000	kelch protein K13	0,290251	-0,62709	0,084797	0,255354	0,094307	0,234292
PfIT_100037500	haloacid dehalogenase-like hydrolase	0,082066	-0,63154	0,121933	1,14273	0,505624	3,14626
PfIT_130016700	26S protease regulatory subunit 7, putative	0,170624	-0,63707	0,570843	2,27691	0,431889	1,65094
PfIT_090025300	inosine-5-monophosphate dehydrogenase	0,242407	-0,71029	0,096381	0,355762	0,142639	0,508553
PfIT_110010300	rRNA-splicing ligase RclB, putative	0,155457	-0,72084	0,217493	1,27819	0,410335	1,63506
PfIT_090019000	conserved Plasmodium protein, unknown function	0,094882	-0,73544	0,395409	2,76582	0,588447	2,59775
PfIT_070021100	eukaryotic translation initiation factor 3 subunit I, putative	0,376267	-0,74875	0,12568	-0,23234	0,094688	-0,22416
PfIT_140075000	eukaryotic initiation factor 4A	0,337876	-0,75712	0,068003	0,227475	0,021349	0,076253
PfIT_130030200	L-lactate dehydrogenase	0,211171	-0,776	0,253218	1,00447	0,277623	1,04378
PfIT_130043600	elongation factor 1-gamma, putative	0,478023	-0,81616	0,265618	0,69091	0,133639	0,499461
PfIT_060016900	nucleolar GTP-binding protein 1, putative	0,305615	-0,83117	0,118757	-0,60989	0,276978	0,309378
PfIT_090017800	elongation factor I-beta	0,187206	-0,83507	0,021641	-0,16861	0,385519	1,04562
PfIT_130006200	Plasmodium exported protein (hyp12), unknown function	0,223085	-0,84513	1,21466	5,45594	0,094515	0,568691
PfIT_120016800	heat shock protein DNAJ homologue Pfj4	0,597962	-0,84667	0,036195	-0,06068	0,091643	-0,228
PfIT_010006400	aspartate--tRNA ligase	0,568663	-0,91855	0,203095	0,750796	0,578376	0,94028
PfIT_060013100	conserved Plasmodium protein, unknown function	0,400784	-0,93449	0,405598	1,19712	0,447933	-1,05012
PfIT_030011000	activator of Hsp90 ATPase	0,418137	-0,94027	0,282566	0,840644	0,12847	0,486763
PfIT_060033000	DnaJ protein, putative	0,201117	-0,94646	0,104167	-0,51854	0,051991	0,304394
PfIT_080007100	mannose-6-phosphate isomerase, putative	0,372992	-0,9943	0,093352	0,341258	0,063559	-0,20793
PfIT_090027000	phosphoglycerate kinase	0,451975	-0,99858	0,13263	0,439732	0,054613	0,203178
PfIT_140046300	vesicle-associated membrane protein, putative	0,863653	-1,06127	0,225766	-0,66085	0,028502	-0,0824
PfIT_130069500	conserved Plasmodium protein, unknown function	0,269959	-1,0836	0,004811	-0,02513	0,065107	-0,27994
PfIT_130054500	glutamate--tRNA ligase, putative	0,349578	-1,08822	0,125389	0,778794	0,090306	0,40078
PfIT_140017200	eukaryotic translation initiation factor 2 gamma subunit, putative	0,588528	-1,13695	0,008788	0,033935	0,145249	-0,45717
PfIT_090009500	replication protein A1, small	0,348229	-1,28338	0,199833	0,797932	0,16992	0,682244
PfIT_110031200	autophagy-related protein 23, putative	0,174391	-1,31997	0,582849	4,66996	0,329183	2,31549
PfIT_090008400	alpha tubulin 2	0,518713	-1,33425	0,822257	2,0636	0,911396	2,3168
PfIT_040006400	Plasmodium exported protein (PHISTa), unknown function	0,71901	-1,36483	1,76057	4,87226	2,3638	4,90077
PfIT_110038600	heat shock protein 70	0,348059	-1,38817	0,020511	-0,17191	0,250643	1,16565
PfIT_060031300	protein Df-1	0,416368	-1,483	0,028777	-0,17139	0,104111	0,406299
PfIT_050025600	conserved Plasmodium protein, unknown function	0,384398	-1,49726	0,090998	-0,35979	0,200695	-0,61949
PfIT_120054100	26S protease regulatory subunit 8, putative	1,2493	-1,73955	0,316565	0,720402	0,010174	-0,03761
PfIT_070026600	GTP-binding protein, putative	0,413609	-1,7561	0,222581	0,85837	0,102746	0,578436
PfIT_080018300	conserved Plasmodium protein, unknown function	0,95715	-1,82479	0,049555	0,203449	0,443391	1,13879
PfIT_030025100	T-complex protein 1 subunit epsilon	0,604341	-1,98066	0,023859	0,141189	0,048377	-0,26442
PfIT_020010700	26S proteasome regulatory subunit RPN1, putative	0,596421	-2,04876	0,311584	0,887602	0,00616	0,032151
PfIT_050028300	mitochondrial processing peptidase alpha subunit, putative	0,453904	-2,16701	0,212724	-0,91075	0,323498	-1,60468
PfIT_080020600	eukaryotic translation initiation factor 3 subunit G, putative	0,563181	-2,24269	0,310723	0,971717	0,209649	-0,1906
PfIT_060033200	RNA-binding protein, putative	0,472405	-2,2548	0,41224	-2,26345	0,200828	-0,70366
PfIT_030013400	pre-mRNA-processing factor 19, putative	2,22209	-5,00947	0,614668	-2,06101	0,398839	-2,07104

Appendix F – Abbreviations of candidate from the proxime of PfEMP1

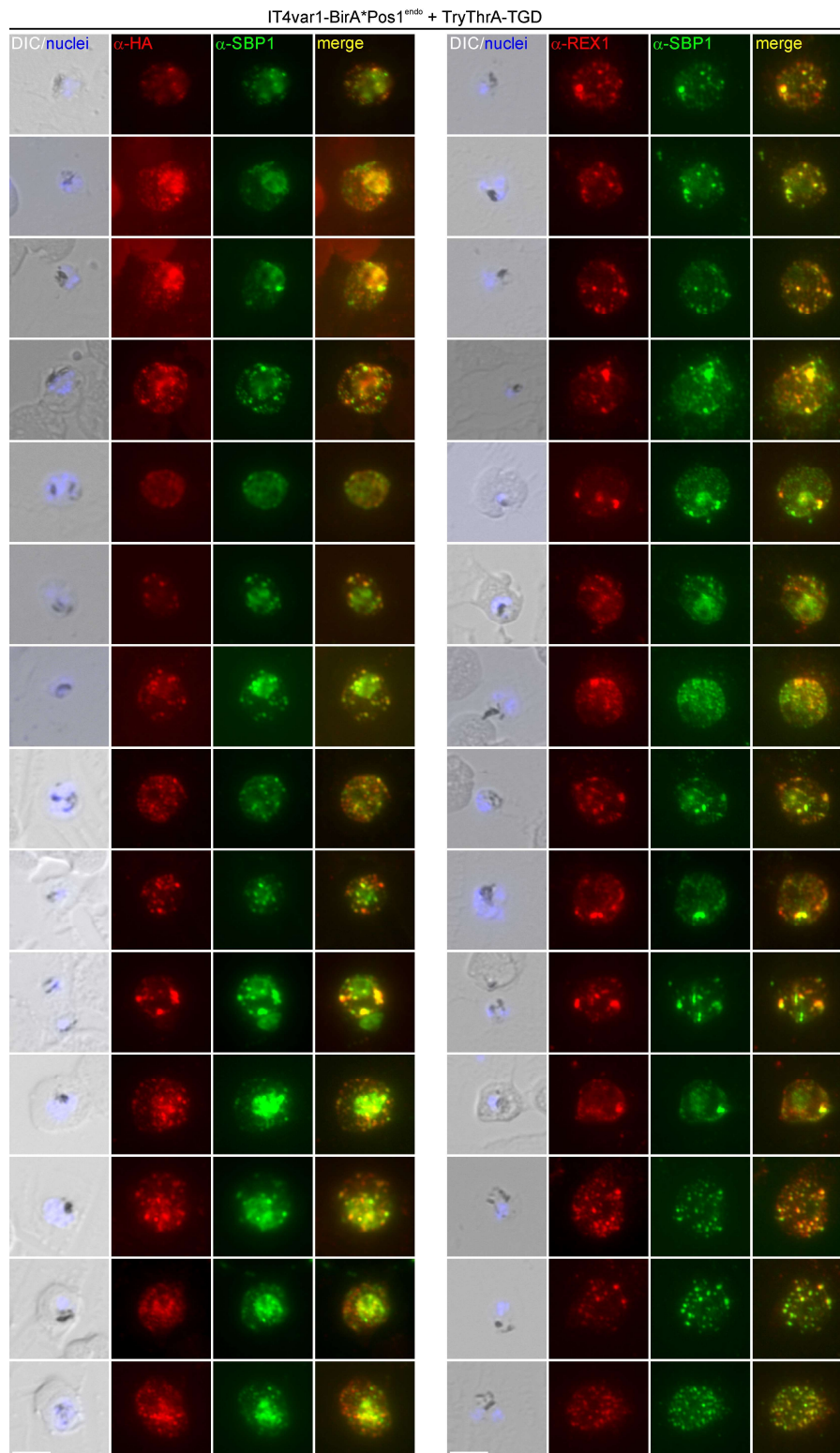
abbreviations and accession numbers for exported proteins with unknown function (green) and PHISTs (beige)

Uncharacterized exported proteins	Accession number IT4	Accession number 3D7
EMPIC1	PfIT_130058500	PF3D7_1353100
EMPIC2	PfIT_100006200	PF3D7_1002000
EMPIC3	PfIT_070007400	PF3D7_0702500
EMPIC4	PfIT_070030000	PF3D7_0726100
EMPIC5	PfIT_010016300	PF3D7_0113200
EMPIC6	PfIT_130006200	PF3D7_1301400

PHIST abbreviation	Accession number IT4	Accession number 3D7
P1	PfIT_080035300	PF3D7_0830600
P2	PfIT_120006500	PF3D7_1200900
P3	PfIT_120058000	PF3D7_1252700
P4	PfIT_120006700	PF3D7_1201100
P5	PfIT_140083600	PF3D7_1477500
P6	PfIT_040029200	PF3D7_0424800
P7	PfIT_130076100	PF3D7_1148700
P8	PfIT_040006400	PF3D7_0402000

Appendix G – TryThrA-TGD-GFP parasites exhibit a Maurer's cleft phenotype

IFA images of TryThrA-TGD-GFP showing Maurer's clefts structure defect. Fluorescence microscopy images show IFAs with acetone fixed parasites probed with α -HA (detection of PfEMP1), α -SBP1 (detection of Maurer's clefts marker SBP1) and α -REX1 (detection of another Maurer's cleft marker REX1) antibodies. Nuclei: Hoechst 33342; DIC: differential interference contrast; size bars 5 μ m.



PUBLICATIONS

Kimmel, J., Schmitt, M., Sinner, A., Jansen, P. W. T. C., Mainye, S., Ramón-Zamorano, G., Toenhake, C. G., Wichers-Misterek, J. S., Cronshagen, J., Sabitzki, R., Mesén-Ramírez, P., Behrens, H. M., Bártfai, R., & Spielmann, T. (2023). Gene-by-gene screen of the unknown proteins encoded on *Plasmodium falciparum* chromosome 3. *Cell systems*, 14(1), 9–23.e7. <https://doi.org/10.1016/j.cels.2022.12.001>

Bachmann, A., Metwally, N. G., Allweier, J., Cronshagen, J., Del Pilar Martinez Tauler, M., Murk, A., Roth, L. K., Torabi, H., Wu, Y., Gutschmann, T., & Bruchhaus, I. (2022). CD36-A Host Receptor Necessary for Malaria Parasites to Establish and Maintain Infection. *Microorganisms*, 10(12), 2356. <https://doi.org/10.3390/microorganisms10122356>

Cronshagen, J., Allweier, J., Mesén-Ramírez, P., Stäcker, J., Vaaben, A. V., Ramón-Zamorano, G., Naranjo, I., Ofori, S., Jansen, P. W. T. C., Hornebeck, J., Murk, A., Castro-Peña, C., Kieferle, F., Brehmer, J., Bártfai, R., Lavstsen, T., Bruchhaus, I., Spielmann, T. (unpublished). A system for functional studies of the major virulence factor of malaria parasites.

DANKSAGUNG

An dieser Stelle möchte ich allen danken, die meine Doktorarbeit möglich gemacht haben, sei es durch fachliche oder anderweitige Unterstützung.

Ein besonderer Dank gilt Dr. Tobias Spielmann, der mir ermöglicht hat, sowohl meine Masterarbeit als auch meine Dissertation in seiner Arbeitsgruppe zu verfassen. Für die intensive Betreuung und Unterstützung, die ich als außergewöhnlich empfunden habe, bin ich sehr dankbar. Ich denke, dass ich eine Menge bei dir gelernt habe. Ebenso danke ich Prof. Dr. Iris Bruchhaus herzlich, die mich stets unterstützt, mir mit Rat zur Seite stand und in ihrer Arbeitsgruppe willkommen geheißen hat. Vielen Dank für nochmal Tobi und Iris.

Weiterhin danke ich meinen Co-Betreuern Prof. Dr. Tim Gilberger und Dr. Maria Rosenthal. Ein Dank geht zudem an die Joachim Herz Stiftung, die diese Arbeit finanziell unterstützt hat.

Ich möchte auch allen Mitgliedern der Arbeitsgruppen Spielmann, Bruchhaus und Gilberger für teamorientierte, produktive und unterstützende Zusammenarbeit danken. Ein besonderer Dank gilt Carolina Castro, Jessica Kimmel, Ulrike Fröhlke, Susann Ofori, Jana Brehmer, Johannes Allweier, Paolo Mesén-Ramírez, Isabelle Henshall, Sheila Mainye, Gala Ramón Zamorano, Stephan Wichers-Mistereck, Hannah Behrens, Andrés Guillén Samander, Lea Sophie Panitzsch, Joelle Hornebeck, Agnes Murk, Florian Kieferle und Jan Stäcker, für ihre Hilfe bei diesem Projekt sowie für die fachliche und moralische Unterstützung. Ohne eure Hilfe wäre diese Arbeit nicht möglich gewesen.

Meine Familie hat mich ständig unterstützt, wofür ich mich ganz herzlich bedanken möchte. Vielen Dank für alles was ihr für mich getan hab Udo, Elke, Merle, Melanie, Gunter und ganz besonders Caro, dafür, dass du mich immer in dieser schwierigen Zeit unterstützt und mich immer wieder aufgerichtet hast. Ebenso geht ein besonderer Dank an meine Freunde, die mir immer zur Seite standen und mir geholfen haben, diese Zeit zu erleichtern. Obwohl ich in den letzten Jahren kaum Zeit für euch hatte, wart ihr immer für mich da. Ein spezieller Dank gilt Jasper, Felix, Marci, Andrey, Manu, Malika, Stance, Marco und Heiner.